INVESTIGATING THE ROLES OF THE N-DEGRON PATHWAY IN REGULATING THE CROSSTALK BETWEEN HYPOXIA AND INNATE IMMUNE RESPONSES

CATHERINE DOORLY

This Thesis is submitted to Maynooth University for the Degree of Doctor of Philosophy

Supervisor: Dr. Emmanuelle Graciet

Head of Department: Prof. Paul Moynagh

Department: Biology

September 2024

Declaration

Acknowledgements

Thank you to Dr. Emmanuelle Graciet and Prof. Frank Wellmer for starting me on my academic journey. For confirming my interests in pursuing science and guiding me from my week-long work experience at age 16, through my bachelor's degree in Genetics at Trinity and during my PhD. Emmanuelle has been a wonderful PhD supervisor to me and has been an absolute role model for the scientist I want to be - intelligent, diligent, thorough, a great teacher, and kind. I cannot thank her enough for all her guidance and support.

I would like to thank my colleagues in the Plant Biochemistry Lab, Dr. Alexandra Miricescu, Dr. Brian Mooney, Dr. Ailbhe Brazel, Dr. Shree Singh, Pablo Garcia, and Gabin Dajoux, and the Comparative Developmental Genetics group members, Dr. Diarmuid O'Maoileidigh and Niranjana Manoj. I have created lovely memories and have learned a lot from them. I would like to thank Dr. Maud Sorel, a previous postdoc in the lab who came before me and whose work laid the groundwork for the JAZ project. I would like to thank my PhD committee members, Dr. Jackie Nugent and Dr. Joanne Masterson for their feedback and suggestions on my work. I would also like to thank the ARM lab for always greeting me with a friendly face, and the Biology Badminton Buds for a bit of craic and exercise on Fridays! I would like to thank each and every one of you for supporting me and my experiments and for making Maynooth such a wonderful place to work for the last four years.

I would like to acknowledge the contribution of my collaborators Dr. Eoin McNamee, Dr. Ailbhe Brazel, Prof. Alain Goossens, and Dr. Elia Lacchini. Thank you for your generosity in your time and help with experiments, providing reagents and for the insightful discussions. I would also like to offer my gratitude to Dr. Chris Brower, Dr. Marion Butler, and Prof. Silke Robatzek for gifting reagents for use in my Ph.D. projects.

A big thank you to the Irish Research Council and the Kathleen Lonsdale Institute for Human Health Research for funding my work.

I wish to thank my family for their constant love and support. I would like to thank my parents for providing so much for me. Their time, supporting my education, hobbies, and nurturing my love for science since I was small. They have also instilled values in me that drive me and is why I do what I do today - from dad bringing me along to marches and campaigns organised by his

work at Concern including Ending World Hunger and mum's role as a nurse - together they have laid out a path for me in which I hope I may make a positive difference as they have. To Coman and Laura for being a source of laughter and fun and supplying me with lots of little treats and encouragement throughout. To my dog, Snickers, who has been a great study buddy while writing this thesis.

I would like to thank my friends for always being there for me with open ears, open arms, and cups of tea! I would like to particularly mention Becky, Simone, Laura, Ping, and Ciara.

To David for bringing me happiness and ease and being with me through every step of the way. Thank you for all the shows of support both small and grand - driving me home and food deliveries on late nights in the lab, being there for me or giving me space as I needed it, reassuring me, motivating me, and enriching my life in every way. I appreciate all you have done and continue to do. I love you so much and I look forward to seeing where the road takes us!

Publications and Presentations

Research Publications

Mooney BC*, **Doorly CM***, Mantz M, García P, Huesgen PF, Graciet E. Hypoxia represses pattern-triggered immune responses in Arabidopsis. Plant Physiology. 2024 Aug 19:kiae432.

Miricescu A*, Byrne T*, **Doorly CM**, Ng CK, Barth S, Graciet E. Experimental comparison of two methods to study barley responses to partial submergence. *Plant methods*. 2021 Dec;17(1):1-5.

* *indicates co-first authorship*

Review Publications

Doorly CM, Graciet E. Lessons from Comparison of Hypoxia Signaling in Plants and Mammals. *Plants.* 2021 May;10(5):993.

Conference presentations

09/2023 Jasmonate Meeting, Halle (Germany)

Talk

"*Investigating the molecular and biochemical links between the N-degron pathway and jasmonic acid signalling"*

08/2023 Plant Molecular Mechanisms, Maynooth (Ireland)

Talk

"Investigating the molecular and biochemical links between the N-degron pathway and jasmonic acid signalling"

06/2022 EMBO Workshop – Protein Termini: From Mechanisms to Biological Impact Conference, Bergen (Norway)

Poster

"Investigation of the N-degron pathway in the regulation of the crosstalk between hypoxia response and immunity."

Table of Contents

Abstract

How plants integrate and respond to multiple simultaneous or consecutive stresses is an increasingly pressing question with the advent of Climate Change. Presented in this Ph.D. thesis is an exploration of the crosstalk between hypoxia and immune responses and the role of the N-degron pathway in its regulation. Transcriptomic analyses using RNA-Seq facilitated dissection of Arabidopsis responses to combined hypoxia and flg22, uncovering interactions between responses to these stresses. It was discovered that hypoxia represses flg22-induced responses at the gene level and also dampens cellular immune responses (e.g. MAPK signalling and callose deposition). This work also found combined hypoxia/flg22 treatments induce novel responses which may point towards pathways that antagonise multi-stress resistance but also those which lie at the intersection of multiple stresses. One pathway which was particularly enriched under combined treatments was jasmonic acid (JA) signalling. The phytohormone JA is well known for its involvement in plant stress responses and this study further highlighted its role as a potential point of intersection for hypoxia and flg22 responses. Further, a potential role for the N-degron pathway in the removal of repression of JA signalling by the repressor protein, JASMONATE ZIM-DOMAIN 8 (JAZ8), was proposed by this work, with an N-degron pathway component, ARGINYL-TRANSFERASE 1 (ATE1), binding JAZ8 and mediating its destabilization. This further supports JA as a point of crosstalk between hypoxia and flg22 responses with the N-degron pathway potentially playing a regulatory role. Similar work to that in plants was attempted in mammals to allow direct comparison of conserved roles of the N-degron pathway in innate immunity and its role in the interplay between hypoxia and immunity. Aims to generate ATE1 knockout RAW264.7 macrophages were however unsuccessful, halting this work.

Abbreviations List

A. tumefaciens	*Agrobacterium tumefaciens*
ABA	Abscisic acid
ACX	ACYL-COA-OXIDASE
ADH1	ALCOHOL DEHYDROGENASE 1
ADO	CYSTEAMINE (2-AMINOETHANEDIOL) OXYGENASE
AlaAT1	Alanine AMINOTRANSFERASE 1
ALS	amyotrophic lateral sclerosis
AOC	ALLENE OXIDE CYCLASE
AOP2	ALKENYL HYFROXALKYL PRODUCING 2
AOS	ALLENE OXIDE SYNTHASE
Arabidopsis	*Arabidopsis thaliana*
AT5MAT	MALONYL-COA:AMTHOCYANIDIN 5-O-GLUCOSIDE-6”-O-MALONYLTRANSFERASE
ATE1	ARGINYL-TRANSFERASE 1
ATE2	ARGINYL-TRANSFERASE 2
B. cinerea	*Botrytis cinerea*
BAK1	BRI1-ASSOCIATED RECEPTOR KINASE 1
BIK1	BOTRYTIS-INDUCED KINASE 1
BPM	BTB/POZ-MATH
BSK1	BRASSINOSTEROID-SIGNALLING KINASE 1
CAMTA	CALMODULIN-BINDING TRANSCRIPTIONAL ACTIVATOR
Caspase	Cysteine-dependent aspartate-specific proteases
CAT	CATALASE
CDPK	Calcium-dependent protein kinase
CERK1	CHITIN ELICITOR RECEPTOR KINASE 1
CIR	Core immunity response
CLD	Compact letter display
CML38	CALMODULIN-LIKE 38
CNGC in plants; CNG in mammals	CYCLIC NUCLEOTIDE-GATED CHANNELS
CO8	chitooctaose
COI1	CORONATINE INSENSITIVE1
Col-0	Columbia
COP1	CONSTITUTIVE PHOTOMORPHOGENIC 1
CPK5	CALCIUM-DEPENDENT KINASE 5
CRK17	CYSTEINE-RICH KINASE 17
crRNA	CRISPR RNA
CYP83B1	CYTOCHROME P450 FAMILY 83 SUBFAMILY B
DAMP	Damage-associated molecular pattern
DEG	Differentially expressed gene
Degrons	Degradation signals
DFR	DIHYDROFLAVONOL REDUCTASE
dls1	delayed leaf senescence 1
DOC1	DARK OVER-EXPRESSION OF CAB 1
DREB26	DEHYDRATION RESPONSE ELEMENT-BINDING PROTEIN 26
DSBs	double-strand breaks
E. coli	*Escherichia coli*
EAR	ERF-associated amphiphilic repression
EBF1	EIN3 BINDING F-BOX PROTEIN 1

ECD	Extracellular domain
EFR	ELONGATION FACTOR-TU RECEPTOR
EGL3	ENHANCER OF GLABRA 3
EIL1	ETHYLENE INSENSITIVE 3 LIKE 1
EIN3	ETHYLENE INSENSITIVE 3
elf18	peptide of bacterial EF-Tu
EPO	ERYTHROPOIETIN
ERF	ETHYLENE RESPONSE FACTOR
ERFVII	Group VII ETHYLENE RESPONSE FACTORS
ERK	EXTRACELLULAR SIGNAL-REGULATED KINASE
ETI	Effector-triggered immunity
EXPA10	EXPANSIN 10
FAO	Food and Agriculture Organization
FIH	FACTOR INHIBITING HIF
Flg22	22-amino acid residue peptide of flagellin
FLS2	FLAGELLIN-INSENSITIVE 2
FTLD	frontotemporal lobar dementia
GAI	GIBERELLIC ACID INSENSITIVE
GL3	GLABRA 3
GLR2.7	GLUTAMATE RECEPTOR 2.7
GLR2.9	GLUTAMATE RECEPTOR 2.9
GNAT	GCN5-related N-acetyl transferase
GO	Gene ontology
gRNA	guide RNA
GSL	GLUCAN SYNTHASE-LIKE
GSNO	S-nitrosoglutathione
GSNOR	S-NITROSOGLUTATHIONE REDUCTASE
GS-ox1	GLUCOSINOLATE S-OXYGENASE
GSSG	Glutathione disulphide
H3K27me3	Histone 3 lysine 27 trimethylation
HDA6	HISTONE DEACETYLASE 6
HF	Hypoxia/flg22
HF v NM	Hypoxia/flg22 v normoxia/mock
HIF1ß	HYPOXIA-INDUCIBLE FACTOR1ß
HIF1α	HYPOXIA-INDUCIBLE FACTOR1α
HM	Hypoxia/mock (dH_2O)
HM v NM	Hypoxia/mock v normoxia/mock
HRE1	HYPOXIA RESPONSIVE ETHYLENE RESPONSE FACTOR 1
HRE2	HYPOXIA RESPONSIVE ETHYLENE RESPONSE FACTOR 2
HSCs	Haematopoietic stem cells
ICE	INDUCER OF CBF EXPRESSION
IFN-γ	Interferon gamma
IL	Interleukin
Indels	insertions/deletions
IP	Immunoprecipitation
IRAK	INTERLEUKIN-1 RECEPTOR ASSOCIATED KINASE
JA	Jasmonic acid
JA-Ile	Jasmonyl-L-isoleucine
JAM	JASMONATE-ASSOCIATED MYC2-LIKE
JAR1	JASMONATE RESISTANT 1
JAZ	JASMONATE ZIM-DOMAIN
JNK	c-Jun N-terminal kinase
K. lactis	*Kluyueromyces lactis*

KAT	L-3-KETOACYL-COA-THIOLASE
KD	Knock down
KEG	KEEP ON GOING
KO	Knock out
LBD41	LOB DOMAIN-CONTAINING PROTEIN 41
LDC	Least developed country
LDOX	LEUCOANTHOCYANIDIN DIOXYGENASE
LF	Anthrax lethal factor
LHP1	LIKE HETEROCHROMATIN PROTEIN 1
Ll	Llagostera
LMIC	Lower-middle-income country
LOX	LIPOXYGENASE
LPS	Lipopolysaccharide
LRR	Leucine-rich repeat
LYK4	LYSM-CONTAINING RECEPTOR-LIKE KINASE 4
LYK5	LYSM-CONTAINING RECEPTOR-LIKE KINASE 5
MAM1	METHYLTHIOALKYLMALATE SYNTHASE 1
MAPK/MPK	Mitogen-activated protein kinase
MAPKKK	Mitogen-activated protein kinase kinase kinase
MDAR3/MDHAR3	MONODEHYDROASCORBATE REDUCTASE 3
MEF	Mouse embryonic fibroblast cells
MeJA	Jasmonic acid methyl ester
MFPs	THE MULTIFUNCTIONAL PROTEINS
MHC	Major histocompatibility complex
MKK	Mitogen-activated protein kinase kinase
MMP9	MATRIX METALLOPEPTIDASE 9
MYB51	MYB DOMAIN PROTEIN 51
MyD88	MYELOID DIFFERENTIATION PRIMARY RESPONSE 88
N. benthamiana	*Nicotiana benthamiana*
NF	Normoxia/flg22
NF v NM	Normoxia/flg22 v normoxia/mock
NF-κB	NUCLEAR FACTOR KAPPA B
NHEJ	non-homologous end joining
NIA1	NITRATE REDUCTASE 1
NIA2	NITRATE REDUCTASE 2
NINJA	NOVEL INTERACTOR OF JASMONATE ZIM-DOMAIN
NI-NOR	Nitrite-NO reductase
NLR	Nucleotide-binding leucine-rich repeat protein
NM	Normoxia/mock (dH_2O)
NO	Nitric oxide
NOA1	NO ASSOCIATED 1
NOI	Nitrate-induced
NOS	Nitric oxide synthase
NOX	NADPH oxidase
NPR1	NONEXPRESSOR OF PATHOGENESIS-RELATED GENES 1
NR	Nitrate reductase
NTAN1	N-TERMINAL ASPARAGINE AMIDOHYDROLASE 1
NTAQ1	N-TERMINAL GLUTAMINE AMIDOHYDROLASE 1
NTCs	Non-targeting controls
ONOO-	Peroxynitrite
OPDA	12-oxophytodienoic acid
OPR3	12-OXOPHYTODIENOIC ACID REDUCTASE
ORA59	OCTADECANOID-RESPONSIVE ARABIDOPSIS AP2/ERF 59

OSCA	REDUCED HYPEROSMOLARITY-INDUCED CALCIUM INCREASE
P. aeruginosa	Pseudomonas aeruginosa
P. rapae	*Pieris rapae*
PAM	protospacer adjacent motif
PAMP	Pathogen-associated molecular pattern
PAP1	PRODUCTION OF ANTHOCYANIN PIGMENT 1
PCA	Principal Component Analysis
PCO	PLANT CYSTEINE OXIDASE
PDC	PYRUVATE DECARBOXYLASE
PDF1.2	PLANT DEFENSIN 1.2
Pepper	Xinyou No.5 wrinkled skin pepper
PFKFB3	6-PHOSPHOFRUCTO-2-KINASE/FRUCTOSE-2,6-BISPHOSPHATASE 3
PGB1/HB1	PHYTOGLOBIN 1/HEMOGLOBIN 1
PHD	PROLYL HYDROXYLASE
PlantPAN	Plant promoter analysis navigator
PlcS	Phospholipase C
PR	PDF1.2, PATHOGENESIS RELATED
PRC2	Polycomb repressive complex 2
PRR	Pattern recognition receptor
PRT1	PROTEOLYSIS 1
PRT6	PROTEOLYSIS 6
***Pst* DC3000**	*Pseudomonas syringae pathovar tomato* DC3000
PTI	Pattern-triggered immunity
PUB10	PLANT U-BOX PROTEIN 10
PUB26	PLANT U-BOX 26
RAP2.12	RELATED TO APETALA2.12
RAP2.2	RELATED TO APETALA2.2
RAP2.3	RELATED TO APETALA2.3
RBOH	RESPIRATORY BURST OXIDASE HOMOLOGUES
RGA	REPRESSOR OF GIBBERELLIC ACID
RGS4	REGULATOR OF G PROTEIN SIGNALLING 4
RGS5	REGULATOR OF G PROTEIN SIGNALLING 5
RK	Receptor kinase
RLCK	Receptor-like cytoplasmic kinases
RLP21	RECEPTOR LIKE PROTEIN 21
RNA-Seq	RNA-sequencing
RNS	Reactive nitrogen species
ROS	Reactive oxygen species
RP	Receptor protein
S. cerevisiae	*Saccharomyces cerevisiae*
S. exigua	*Spodoptera exigua*
S. pyogenes	*Streptococcus pyogenes*
SA	Salicylic acid
SAR	Systemic acquired resistance
SCF	Skp1/Cullin/F-box E3 ubiquitin ligase complex
SEN4	SENESCENCE 4
SGT1B/EDM1	ENHANCED DOWNY MILDEW 1
SKIP31	S PHASE KINASE-ASSOCIATED PROTEIN 1-INTERACTING PARTNER 31
SNO	S-nitrosothiols
SNP	Sodium nitroprusside
SOD	SUPEROXIDE DISMUTASE

SUS	SUCROSE SYNTHASE
TDP43	TAR DNA-binding protein 43
TGFß	Transforming growth factor beta
TIDE	Tracking of Indels by Decomposition
TIR	Toll-like receptor/interleukin
TIR3	TRANSPORT INHIBITOR RESPONSE 3
TLR5	TOLL-LIKE RECEPTOR 5
TNF	Tumour necrosis factor
TOE	TARGET OF EAT
ToxA	Endotoxin A
TPL	TOPLESS
tracrRNA	trans-activating CRISPR RNA
TRX	Thioredoxin
TSS	Transcriptional start site
TT7	TRANSPARENT TESTA 7
TT8	INDUCER OF CBF EXPRESSION TRANSPARENT TESTA 8
UBR	UBIQUITIN AMINO-END RECOGNISING PROTEIN
UF3GT	UDP-GLC:FLAVONOID 2-O-GLUCOSYLTRANSFERASE
UPS	Ubiquitin-proteasome system
VEGF	VASCULAR ENDOTHELIAL GROWTH FACTOR
VHL	VON HIPPEL-LINDAU
VRN2	VERNALIZATION2
VSP	VEGETATIVE STORAGE PROTEIN
WAKL10	WALL-ASSOCIATED KINASE-LIKE 10
XOR	Xanthine oxidoreductase
XT1	XYLOSYLTRANSFERASE 1
XTHs	Xyloglucan endotransglucosylases
Y2H	Yeast-two-hybrid
ZPR2	LITTLE ZIPPER2

Chapter 1: An overview of the roles of the N-degron pathway and nitric oxide in plant and mammal innate immune responses and oxygen sensing

Some of the following sections contain passages/sections/figures which have been taken from two manuscripts; one review (Doorly and Graciet, 2021) and a recently published research article (Mooney et al., 2024).

1.1. Overview of the research questions and relevance

In response to danger, organisms fight to survive. Animals induce a fight or flight response, but for plants which are sessile organisms, survival requires perception of environmental signals (including stresses) and induction of cellular mechanisms that relieve the stress or lead to acclimation to the environmental conditions. Both plants and mammals experience either sequentially or simultaneously abiotic and biotic stresses, with biotic stresses being those inflicted by another living organism (e.g. microbes), while abiotic stresses are a result of changes in the physical and chemical environments. In the case of plants, these include external factors such as flooding, drought, extreme temperatures and UV, but also internal factors such as nutrient imbalances, oxygen or carbon dioxide level changes, or variation in osmotic pressure. Global climate change results in an increased occurrence of extreme weather events, as well as changes in the geographical distribution and/or preponderance of different pathogens and pests (Bebber et al., 2013; Burdon and Zhan, 2020; Kocmánková et al., 2009), all of which increase the frequency and amplitude of (a)biotic stresses that can affect plant survival in the wild, as well as crop yields in agricultural systems.

The Food and Agriculture Organization (FAO) of the United Nations recently reported on the leading causes of crop and livestock loss between 2008 and 2018. The data indicate that water-related stresses (e.g. drought and flooding) are among the most frequent threats to agriculture, with flooding accounting for $21 billion-worth of losses or 19% loss of total production in least developed and lower-middle-income countries (LDCs and LMICs, respectively) (FAO, 2021). Some abiotic stresses are particularly complex, because they result in a combination of different

stresses. For example, flooding is a so-called compound stress, because it induces multiple simultaneous stresses in plants. Limited gas exchange imposed by flood water results in a depletion of oxygen (hypoxia or anoxia if no oxygen) in the plants environment (Sasidharan et al., 2018), but at the same time, submerged plants experience reduced light levels because the flood water tends to be muddy. These combined factors (hypoxia and low light) are responsible for starvation stress, which results from the ensuing energy and carbohydrate crises (Sasidharan et al., 2018). Indeed, under normal oxygen conditions (normoxia), oxidative phosphorylation (with oxygen as the final electron acceptor) is the primary pathway through which aerobic organisms generate cellular ATP. In contrast, under hypoxic conditions, less oxygen is available to maintain oxidative phosphorylation, and cells instead rely on glycolysis for ATP production and on fermentative pathways to regenerate the NAD+ that is needed to sustain glycolysis (Bailey-Serres et al., 2012; Cho et al., 2021; Lee et al., 2020; Voesenek and Bailey-Serres, 2015). Glycolysis is also highly dependent on sugar levels. Due to lower carbon dioxide levels and reduced light, flooded plants cannot replete the sugar levels through photosynthesis or produce their own oxygen. If hypoxia persists, decreased sugar level availability can lead to carbon starvation, thus triggering additional changes, such as reduced energy consumption and an increase in catabolic metabolism (Cho et al., 2021). In addition, to the above-mentioned stresses, heavy metals can leach from the soil during flooding and expose plants to toxic levels of manganese, iron and sulfides (e.g. H_2S, HS^-, S^{2-}) (Voesenek and Bailey-Serres, 2015).

Pests and pathogens are also among the leading causes of crop and livestock loss, accounting for 9% of total production loss in LDCs and LMICs (FAO, 2021). Both plants and animals are intertwined in an on-going arms-race with microbial pathogens. In this continuous 'battle', pathogens have evolved mechanisms to penetrate hosts, evade detection by the immune system and manipulate the host cellular pathways to favour pathogen fitness and virulence. To combat pathogens, host organisms have had to continuously evolve elaborate mechanisms of detection and defence responses, which can in turn also be overcome by pathogens as they evolve and adapt. For example, plant and animal pathogenic bacteria employ type III secretion systems, which permit secretion of effectors into plant and animal cells (Staskawicz et al., 2001). These effectors have roles in allowing pathogens to evade the immune system by targeting and inhibiting important defence pathways and responses. As well as this, some bacterial species are capable of infecting both animal and plant hosts. These include some of the *Pseudomonas, Erwinia, Rhizobium, Salmonella* and *Enterococcus* bacterial species as well as the fungal *Fusarium oxysporum* pathogen (Kim et al., 2020; Ortoneda et al., 2004; Rahme et al., 1995; Rahme et al., 2000). *Pseudomonas aeruginosa (P. aeruginosa)*, for example, is a soil-borne pathogen. The *P.*

aeruginosa strain UCBPP-PA14 was found to induce chlorosis and soft-rot on leaves in the Columbia (Col-0) and Llagostera (Ll) accessions of the model plant *Arabidopsis thaliana* (henceforth referred to as Arabidopsis) (Rahme et al., 1995). The same study showed that this strain also caused local tissue invasiveness and high mortality (≥77%) in a mouse model. Three *P. aeruginosa* genes that were previously shown to be important during infection of mammals (exotoxin A (ToxA), phospholipase C (PlcS)) and infection of plants (GacA) were mutated. These single mutants resulted in reduced or eliminated pathogenesis in Arabidopsis Ll and in the mouse model, thus highlighting how pathogenic bacteria can evolve conceptually similar mechanisms to increase virulence in both plants and animals. Despite these similarities, colonization and acquisition of nutrients from plant and mammal cells can differ significantly. In general, plant pathogens live extracellularly in the apoplast and manipulate the plant to transport nutrients, while mammalian pathogens invade cells and manipulate the host cell using intracellular mechanisms (Staskawicz et al., 2001). In contrast to animal pathogens, plant pathogens are also grouped depending on whether they feed off living plant tissue (biotrophs) or dying/dead tissue (necrotrophs), with hemibiotrophs exhibiting sequentially biotrophic and necrotrophic lifestyles over the course of infection.

Importantly, the FAO, 2021 report highlights how abiotic and biotic stresses may actually co-occur in the context of global climate change, with important consequences (FAO, 2021 https://www.fao.org/3/cb3673en/cb3673en.pdf). For example, changes in water availability including higher rainfall and flooding can produce an environment which facilitates growth, spread and colonization of plants by pathogens, as these may come more easily into contact with plant hosts *via* moisture in the air and soil (Anderson et al., 2020; Martínez-Arias et al., 2022; Velásquez et al., 2018). Furthermore, the decreased oxygen availability caused by flooding means that plants may simultaneously experience hypoxia and pathogen infection, which could affect their ability to trigger an efficient defence response. Such combination of hypoxic conditions and immunogenic stress/infection are encountered by both plants and mammals and are not necessarily caused by the external environment (e.g. they could be the result of a physiological condition). For example, hypoxia and infection can co-occur within infected tissues where both the host and pathogen use up oxygen through respiration, leading to lower levels of oxygen in these tissues (Chung and Lee, 2020; Kempf et al., 2005; Valeri et al., 2021). In mammals, immune cells responsible for the destruction of tumours need to induce an immune response within the hypoxic environment that the tumour imposes (Taylor and Colgan, 2017). Hence, there is a strong overlap and potential for crosstalk between the signalling and response pathways to these two stresses in both plants and mammals. In line with this, studies in plants

and mammals have shown that hypoxia can affect both pathogen virulence and host immune responses to pathogens resulting in increased or reduced resistance (Chung and Lee, 2020). While in mammals the crosstalk between hypoxia and immunity is well established (reviewed in Taylor and Colgan, 2017), further research is needed to dissect the mechanisms underlying the crosstalk in plants, which this Ph.D. work has explored.

Comparison of signal transduction pathways involved in the response to different abiotic and biotic stresses may reveal important common regulators of stress responses. For example, many stress response pathways across eukaryotes relay signals through the use of post-translational modifications, which can alter target protein activity, stability, localization, and interactions with other proteins. These modifications can also be reversible, providing flexibility and allowing for quick turning on/off of signalling pathways in response to various external and internal stimuli. This Ph.D. work focused on two core signalling pathways which are highly conserved in both mammals and plants, are known to be interconnected, and have established roles in regulating responses to abiotic and biotic stress: (1) the ubiquitin proteasome system (UPS, in particular, a protein degradation pathway called the N-degron pathway; see section 1.2.2.) and (2) nitric oxide (NO) signalling. Studies have shown that both of these signalling pathways play key roles in oxygen sensing, in the activation of hypoxia response, as well as in the regulation of responses to immunogenic factors such as pathogen-associated molecular patterns (PAMPs) and pathogens, as outlined in detail below. There is also a significant interaction and crosstalk between these two signalling pathways, as NO-mediated post-translational modifications can promote or inhibit the ubiquitylation of protein targets (Pande et al., 2022; Rizza et al., 2014). NO signalling is also mediated in part *via* its link with the UPS by regulating the stability of target proteins through the aforementioned N-degron pathway. Further, NO can also regulate ubiquitin proteasome components' activity by post-translationally modifying them. A known example of this includes NO-induced post-translational modification of the core protease of the human 26S proteasome in vascular smooth muscle cells at 10 different cysteine residues, which inhibits proteasomal degradation (Kapadia et al., 2009).

Caution is also needed when identifying core stress regulators from individual stress treatments, as previous studies in plants have shown that combined stresses can produce entirely novel effects that cannot be predicted by comparing responses to the individual stresses alone (Rasmussen et al., 2013; Tan et al., 2023). For example, in studies of Arabidopsis accessions treated with individual and combined abiotic stresses, 61% of genes followed a transcriptional

behaviour which could not be predicted by studying the gene expression profiles in response to the individual stresses (Rasmussen et al., 2013). In addition, the number of differentially expressed genes (DEGs) was higher in plants treated with combined stresses compared to the corresponding individual stresses. Transcriptomic analyses have further shown that the outcome of combined stresses can elicit multiple different transcriptional behaviours, including: (1) similar gene expression in combined and corresponding individual stresses; (2) the transcriptional response to combined stress could be similar to one of the individual stresses but not to the other one, because one stress is prioritized over another, or only one stress regulates specific sets of genes, or because the expression of genes with opposite behaviour in response to the single stresses is cancelled out under combined stress; and (3) a transcriptional programme may be unique to combined stress treatment because of the involvement of a different set of transcription factors (Pandey et al., 2015; Prasch and Sonnewald, 2013; Rasmussen et al., 2013; Rizhsky et al., 2004; Shaar-Moshe et al., 2017; Zandalinas et al., 2020; Zandalinas et al., 2021). The unpredictability of transcriptional responses to combined stresses compared to the single stresses can be a problem for plant breeders, as target genes shown to provide tolerance to one stress could cause susceptibility to another (Atkinson and Urwin, 2012). Genes with more pleiotropic functions are therefore now being proposed as targets for crop improvement.

This Ph.D. work explored several of the open questions and gaps of knowledge outlined above. First, the potential connections between hypoxia response and immunity were explored and established in plants, with the core finding being that hypoxia supresses innate immunity in plants (Chapter 3). Second, this Ph.D. work sought to dissect the roles of NO signalling and the UPS-dependent N-degron pathway in the regulation of the crosstalk between hypoxia and immune responses in plants (Chapter 3), but also to some extent in mammals (Chapters 5). Third, results obtained in Chapter 3, opened new questions that led to the exploration of the roles of an important UPS-regulated and immunity-related phytohormone signalling pathway (jasmonic acid (JA) signalling) in hypoxia response (Chapter 4).

1.2. N-terminal amino acid residues as degradation signals for the UPS-dependent N-degron pathways

1.2.1 Overview of the UPS

The 76 amino acid protein, ubiquitin, is present in all eukaryotes with few amino acid substitutions across species, as plant, human and yeast ubiquitin differ by as little as 3 amino acids (Zuin et al., 2014). The conjugation of ubiquitin to its target proteins acts as a post-translational modification which is mainly associated with regulating the stability of proteins by targeting them to the 26S proteasome for degradation. A proteome study of ubiquitin targets in Arabidopsis showed that out of 971 detected substrates, 471 were only present upon MG132 (proteasome inhibitor) treatment. Further, 100 of 366 substrates, which were detected in the presence or absence of MG132, increased in abundance with MG132 treatment supporting ubiquitin's role in targeting substrates for proteasomal degradation (Kim et al., 2013). However, further studies have also identified non-proteolytic roles of ubiquitin in plants and mammals. In mammals, non-proteolytic roles of ubiquitin include DNA replication and repair, transcription, mRNA processing and regulating inflammatory responses. In plants, ubiquitin acts in translation, protein trafficking, DNA repair, iron deficiency responses and regulation of immunity (Komander and Rape, 2012; Ma et al., 2021; Mukhopadhyay and Riezman, 2007; Romero-Barrios and Vert, 2018). The conjugation of ubiquitin to its target proteins requires a cascade of reactions which are mediated by E1 ubiquitin activating, E2 ubiquitin conjugating, and E3 ubiquitin ligase proteins (reviewed in (Callis, 2014; Marshall and Vierstra, 2019; Miricescu et al., 2018; Vierstra, 2009)). E3 ubiquitin ligases are responsible for the specific recognition of degradation signals (degrons) in target proteins. In addition, together with an E2 conjugating enzyme, the E3 ligase conjugates ubiquitin to the substrate protein singly (mono-ubiquitination) or to another ubiquitin that was previously attached to the target protein to form poly-ubiquitin chains. Ubiquitin has a conserved C-terminal glycine residue that is crucial for its conjugation to target proteins *via* the formation of an isopeptide bond between this last glycine residue and the ε amino group of a lysine residue on the target protein or on a previously conjugated ubiquitin in the case of poly-ubiquitin chain formation (reviewed in (Callis, 2014; Marshall and Vierstra, 2019; Miricescu et al., 2018; Vierstra, 2009)). Ubiquitin has seven lysine residues (Lys-6, Lys-11, Lys-27, Lys-29, Lys-33, Lys-48, Lys-63) which can be used to form chains (homotypic, mixed/heterotypic, or branched) (Komander and Rape, 2012) with studies showing a preference for Lys-48 chains followed by Lys-63 and Lys-11 chains in Arabidopsis (Kim et al., 2013). Together with the reversible nature of ubiquitination due to the activity of specific deubiquitinating enzymes (Isono et al., 2014), this post-translational

modification contributes to rapidly changing the protein landscape and governing fast fine-tuning of multiple biological processes.

1.2.2. The N-degron pathways

The N-degron pathways, formerly the N-end rule pathways, are a subset of the UPS. An N-degron is a degradation signal which is recognized by components of the N-degron pathway. Characteristics of an N-degron include a destabilizing amino acid residue at the N-terminus and an internal lysine(s), which facilitates polyubiquitylation (Varshavsky, 2019). Since the initial discovery by the Varshavsky group that different N-terminal amino acids confer different half-lives to a ß-galactosidase reporter protein in the yeast *Saccharomyces cerevisiae* (*S. cerevisiae*) (Bachmair et al., 1986), the N-degron pathway was shown to be widely spread across eukaryotes, as well as prokaryotes (with the exception of archaea) (Gonda et al., 1989; Graciet et al., 2006; Graciet et al., 2010), and several additional branches of the N-degron pathway that target proteins for degradation based on the post-translational modification of N-terminal residues (e.g. acetylation) were discovered, thus resulting in a complex set of pathways that regulate protein stability based on N-degrons (Heo et al., 2023; Holdsworth et al., 2020; Varshavsky, 2019). These different branches include the Arg/N-degron pathway (the focus of this work and referred to as the N-degron pathway for the remainder of the work; see below for more details) (Bachmair et al., 1986), the Pro/N-degron pathway (targets proteins for degradation via N-terminal proline) (Chen et al., 2017), and the Ac/N-degron pathway (based on acetylation of N-terminal residues) in eukaryotes (Hwang et al., 2010), the fMet/N-degron pathway in eukaryotes and bacteria (depending on formyl-methionine) (Piatkov et al., 2015), the Leu/N-degron pathway in bacteria (Tobias et al., 1991) (also reviewed in Varshavsky, 2019), and a more recently discovered Gly/N-degron pathway in humans based on the presence of an N-terminal glycine (Timms et al., 2019). The eukaryotic N-degron pathways involve conserved E3 ubiquitin ligases, termed N-recognins, which recognize and bind N-degrons of substrate proteins. Long-lived intracellular proteins/peptides generally possess stabilizing N-terminal residues (Bachmair et al., 1986; Berezovsky et al., 1999; Lange et al., 2014), so cleavage of these N-degron pathway substrates by exopeptidases (e.g. methionine amido-peptidase) or endoproteases (e.g. cysteine-dependent aspartate-specific proteases (caspases), calpains, cathepsins, etc.) is necessary to expose neo-N-degrons which are recognized by N-degron pathway components including N-recognins and targeted for degradation via the 26S proteasome (Dissmeyer et al., 2018). The components of the N-degron pathway are mostly conserved in plants and mammals, so much so that it has been suggested that this pathway and its components evolved in a common ancestor before their divergence (Graciet et al., 2010).

The N-degron pathway has a hierarchical organisation. Tertiary N-terminal destabilizing residues include cysteine (C), asparagine (N) and glutamine (Q) (Figure 1.1.). These must be first modified before they can be recognized by an N-recognin and the protein can be targeted for degradation. In mammals and plants, deamidation of asparagine and glutamine is carried out by two separate enzymes, N-TERMINAL ASPARAGINE AMIDOHYDROLASE 1 (NTAN1) and N-TERMINAL GLUTAMINE AMIDOHYDROLASE 1 (NTAQ1), resulting in proteins starting with the secondary N-terminal destabilizing residues aspartic acid (D) and glutamic acid (E), respectively (Figure 1.1.) (Grigoryev et al., 1996; Graciet et al., 2010; Stewart et al., 1994; Wang et al., 2009). The tertiary N-terminal destabilizing residue cysteine is converted to cysteine sulfinic acid, through its enzymatic oxidation by PLANT CYSTEINE OXIDASE (PCO) enzymes in plants (Weits et al., 2014; White et al., 2017) in the presence of NO and oxygen (Gibbs et al., 2015). A mammalian equivalent of PCOs has only recently been identified and is known as the enzyme CYSTEAMINE (2-AMINOETHANEDIOL) OXYGENASE (ADO) (Masson et al., 2019) (Figure 1.1.). ADO also oxidizes the N-terminal cysteine of its protein substrates in an oxygen-dependent manner, and NO has also been shown to be involved in cysteine oxidation in mammals (Hu et al., 2005). Whether this occurs non-enzymatically or in conjunction with ADO requires further study. The post-translational modifications catalysed by NTAN1, NTAQ1, PCO/ADO all generate secondary destabilizing residues which act as a signal for the conjugation of arginine (arginylation) to the N-terminus of substrate proteins by arginyl-transferases.

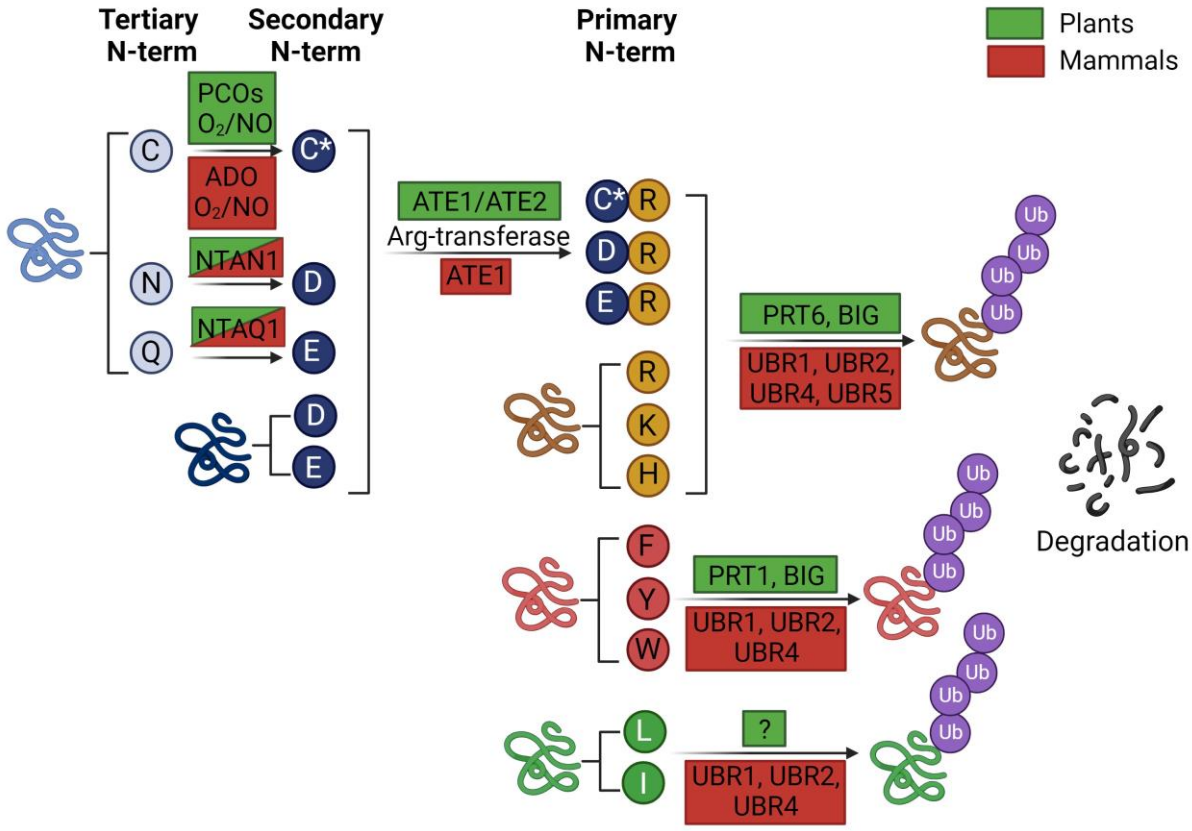

Figure 1.1. The N-degron pathway and its enzymatic components in plants and mammals. The figure depicts the destabilizing N-terminal residues that act as N-degrons through the N-degron pathway and showcases its hierarchical organisation, with the steps necessary for the modification and degradation of target proteins (including cysteine oxidation; asparagine and glutamine deamidation; arginylation; and ubiquitination). The evolutionary conservation of this pathway in mammals (enzymes denoted in red) and plants (enzymes denoted in green) is apparent with the tertiary, secondary and primary destabilizing N-terminal residues being the same across the two kingdoms, and with its enzymatic components being largely conserved, with a notable exception being the E3 ligase PRT1, which is plant specific (Bachmair et al., 1993; Potuschak et al., 1998; Stary et al., 2003). N-terminal amino acid residues are presented using single-letter abbreviations; Ub stands for ubiquitin. Created using BioRender.com.

Arginyl-transferase proteins across eukaryotes contain two conserved PFAM domains, which have ~55% identity between Arabidopsis and mammalian arginyl-transferases (Domitrovic et al., 2017). Recent elucidation of the crystal structures of *S. cerevisiae* and *Kluyveromyces lactis* (*K. lactis*) ARGINYL-TRANSFERASE 1 (ATE1)s has shown the structural conservation of the predicted substrate binding domain and of the GNAT fold, where the charged Arg-tRNA binds. These domains appear to fold in on each other allowing for the transfer of arginine to ATE1 substrates (Kim et al., 2022; Van et al., 2022). In mammals, a single arginyl-transferase, *ATE1*, is encoded in the genome. However, higher eukaryotes possess multiple ATE1 splicing isoforms (e.g. there are six main mouse MsATE1 isoforms) (Hu et al., 2006). These different isoforms are expressed in

different tissues, but reports differ in their abundance and localisation (Hu et al., 2006; Rai and Kashina, 2005). While generally it is thought that these isoforms act in a semi-redundant manner, reports also differ on the specificity of these isoforms for both canonical and non-canonical residues at N-termini, as well as internal aspartic acid and glutamic acid residues (Wadas et al., 2016; Wang et al., 2011; Wang et al., 2018a). Indeed, some studies have shown that mouse ATE1 also arginylates internal aspartic acid and glutamic acid residues in a variety of proteins, including neurotensin (Wang et al., 2014; Wong et al., 2007). The Arabidopsis genome codes for two arginyl-transferases, *AtATE1* and *AtATE2*, which act in a functionally redundant manner. Interestingly, AtATE1 contributes about 95% of the total arginyl-transferase activity in seedlings, and while these two enzymes display similar expression patterns, there are some minor differences in their tissue distribution in plants (Graciet et al., 2009). The addition of arginine, a primary N-terminal destabilizing residue, to the substrate proteins of arginyl-transferase enzymes enables their direct recognition by N-recognins (E3 ubiquitin ligases of the N-degron pathway).

In general, all primary N-terminal destabilizing residues (including N-terminal arginine (R), lysine (K), histidine (H), phenylalanine (F), tyrosine (Y), tryptophan (W), leucine (L) and isoleucine (I)) are directly recognized by N-recognins. In mammals, the N-recognins UBIQUITIN AMINO-END RECOGNISING PROTEIN 1 (UBR1), UBR2, UBR4 and UBR5 work semi-redundantly to ubiquitylate and target for degradation proteins starting with primary N-terminal destabilizing residues. Studies have shown that UBR1, 2 and 4 bind all primary N-degrons, while UBR5 binds only basic N-terminal destabilizing residues (R, K and H). Furthermore, UBR1 and UBR2 have preferences for bulky hydrophobic amino acids (F, Y, W, L, and I) (Taskai et al., 2005; Tasaki et al., 2009) (Figure 1.1.). In plants, PROTEOLYSIS 6 (PRT6), which was identified because of its sequence similarity to yeast and mammalian UBR1, is involved in the recognition of basic N-terminal destabilizing residues (R, K, H; Figure 1.1.) (Garzón et al., 2007). However, unlike UBR1, PRT6 does not appear to bind hydrophobic N-terminal destabilizing residues. PROTEOLYSIS 1 (PRT1), which has no homology to yeast or mammalian UBR proteins and is found in plants only, binds primary N-terminal destabilizing aromatic residues (F, Y and W) (Figure 1.1.) (Bachmair et al., 1993; Potuschak et al., 1998; Stary et al., 2003). More recently, the plant protein called BIG (also known as DARK OVER-EXPRESSION OF CAB 1 (DOC1) or TRANSPORT INHIBITOR RESPONSE 3 (TIR3), and a homolog of mammalian UBR4 (Tasaki et al., 2005)) was shown to contribute to the degradation of proteins with both basic and aromatic N-terminal destabilizing residues (Figure 1.1.) (Zhang et al., 2023). While a *big* mutant is unable to stabilize proteins with primary N-terminal destabilizing residues, double mutants *prt6 big* or *prt1 big* show enhanced stabilization of the

respective substrates of PRT6 and PRT1, compared to single *prt6* or *prt1* mutants. This suggests that BIG works alongside PRT1 and PRT6 to degrade N-degron pathway substrates (Zhang et al., 2023). Further plant N-recognins remain to be identified, as leucine and isoleucine are N-terminal destabilizing residues (Graciet et al., 2010), but the E3 ubiquitin ligase responsible for their degradation is yet to be discovered.

1.2.3. Functions of the N-degron pathway

The arginylation branch of the N-degron pathway, which is the focus of this Ph.D. work, is arguably the branch that is best understood, and for which many substrates with a wide range of functions have been identified both in plants and in mammals. These substrates are generally not conserved between plants and mammals, yet, some of the physiological processes that are regulated by the plant and mammal N-degron pathway are conserved. This is the case for the regulation of hypoxia and immune/defence responses, for example, which are discussed in more detail in sections 1.5.1. and 1.4.4., respectively. In mammals, the use of mutant mouse strains for the different enzymatic components of the N-degron pathway has revealed roles in the regulation of many developmental processes, with *ubr1*$^{-/-}$ *ubr2*$^{-/-}$ double mutant and *ate1*$^{-/-}$ single mutant mice showing embryo lethality (Kwon et al., 2002; Tasaki et al., 2005). More specific examples of developmental processes affected in the N-degron pathway mutants include spermatogenesis (Kwon et al., 2003), cardiovascular development and angiogenesis (Kwon et al., 2002). The latter defects were shown to result from the stabilization of G protein subunits, which are substrates of the N-degron pathway (Lee et al., 2005). The pathway also regulates essential cellular processes such as apoptosis by targeting for degradation pro-apoptotic fragments generated by caspase cleavage (Gubina et al., 2020; Piatkov et al., 2012), and plays important roles in the regulation of inflammation, as highlighted more in detail in section 1.4.4.

In plants, most of the substrates identified to date are degraded in an oxygen-dependent manner because of the requirement for the activity of PCOs. These substrates are presented and discussed in more detail in section 1.5.1., but the most notable substrates are 5 members of the group VII ETHYLENE RESPONSE FACTOR transcription factors (ERFVIIs), which act as the master regulators of the transcriptional changes that accompany the onset of hypoxia response in plants. Other known substrates of the N-degron pathway in plants include a nitrate-induced (NOI)-domain family of proteins involved in plant immunity. These proteins are known to be cleaved by a pathogenic protease, which produces fragments that start with secondary

destabilizing residues, and whose stability then depends on ATE1/2 and PRT6 (Goslin et al., 2019).

A conserved feature of the N-degron pathway substrates in plants and mammals is the dependency on oxygen and NO for the degradation of targets that start with N-terminal cysteine. Because of this connection, the N-degron pathway is often referred to as a pathway that may act to sense either oxygen or NO (Gibbs et al., 2014; Hu et al., 2005), and hence connections between NO signalling and the N-degron pathway have been an active area of research. This link between hypoxia, NO signalling and the N-degron pathway underlies many of the questions addressed in this work because of its potential relevance to the regulation of the crosstalk between hypoxia and immunity in both plants and mammals. The following sections aim at providing more details on (1) NO signalling, (2) plant immunity and (3) hypoxia response with the aim of supporting their interconnections and relevance to mechanisms regulated by the N-degron pathway.

1.3. NO Signalling and the N-degron pathway

NO is a gaseous signalling molecule that is key to the regulation of a multitude of developmental and stress response pathways in plants and mammals. NO is produced by oxidative as well as reductive pathways in both organisms (Astier et al., 2018; Chamizo-Ampudia et al., 2017; Jansson et al., 2008; Yu et al., 2014). In plants, the main source of NO originates from the reductive pathway. This involves the reduction of nitrate to nitrite and then the reduction of nitrite to NO in the presence of NAD(P)H (Gupta et al., 2005). Nitrate reductase (NR) enzyme(s) are involved in these reduction reactions of the NO biosynthesis pathway (Figure 1.2). In many plant species, there are two isoforms of NRs. In Arabidopsis, these are encoded by the genes NITRATE REDUCTASE 1 (*NIA1*) and *NIA2*. The NIA1 and NIA2 proteins both form homodimers but differ in their activity. Specifically, these isoforms have different preferences for the reducing reactions with NIA2 more efficiently reducing nitrate to nitrite while NIA1 reduces nitrite to NO with higher efficiency (Mohn et al., 2019). Nitrite reduction is also performed by a root plasma membrane-bound protein, which is referred to as nitrite-NO reductase (NI-NOR) (Figure 1.2) (Stöhr et al., 2001). Nitrite can also be reduced by complexes III and IV of the mitochondrial electron transport chain (Figure 1.2); however, this only appears to occur in roots under hypoxic conditions (e.g. soil waterlogging) (Gupta et al., 2005; Stoimenova et al., 2007). While there has been some evidence for the presence of an oxidative mechanism for the generation of NO from L-arginine in plants similar to that in mammals (described below), little is known about this mechanism in plants and the players involved (Astier et al., 2018; Corpas et al., 2009).

In mammals, when oxygen is available, NO is produced via the oxidation of L-arginine in the presence of NADPH and other co-factors to form NO and citrulline (Figure 1.2). NO synthases (NOSs) are particularly important for this oxidative NO biosynthesis pathway. There are three NOS isoforms in mammals, endothelial (eNOS), neuronal (nNOS), and inducible (iNOS), all of which function as homodimers in order to produce NO in different cell types and in response to different conditions (reviewed in Förstermann and Sessa, 2012) (Figure 1.2). While NOS enzymes require oxygen for NO production via the oxidative pathway, eNOS has been shown to possess nitrite reductase activity and can reduce nitrite into NO under acute hypoxic or anoxic conditions (Gautier et al., 2006; Vanin et al., 2007) (Figure 1.2). The presence of NOS in plants is still debated and remains an important open question. While NOS-like activity has been detected in plants (Corpas et al., 2009), the specific protein(s) which mediates plant NOS activity has yet to be isolated, and analyses of plant genomes have so far not led to the identification of plant homologs to the mammalian NOSs (Astier et al., 2018; Yu et al., 2014). Mammals also possess a xanthine oxidoreductase (XOR) which has nitrite reductase activity (Jansson et al., 2008; Mikula et al., 2009; Vanin et al., 2007) (Figure 1.2). Furthermore, XOR is capable of reducing nitrate to nitrite in normoxic and hypoxic conditions (Jansson et al., 2008) (Figure 1.2). Interestingly, plants also have a XOR found in the peroxisome, which is capable of reducing nitrite to NO during hypoxia (Yu et al., 2014) (Figure 1.2). Lastly, as in plants, complex III and IV of the mammalian mitochondrial electron transport chain produces NO through reduction of nitrite in hypoxia (Castello et al., 2006; Kozlov et al., 1999) (Figure 1.2). In sum, apart from the absence of known NOSs in plants so far, direct parallels can be drawn for other NO-producing pathways in plants and mammals.

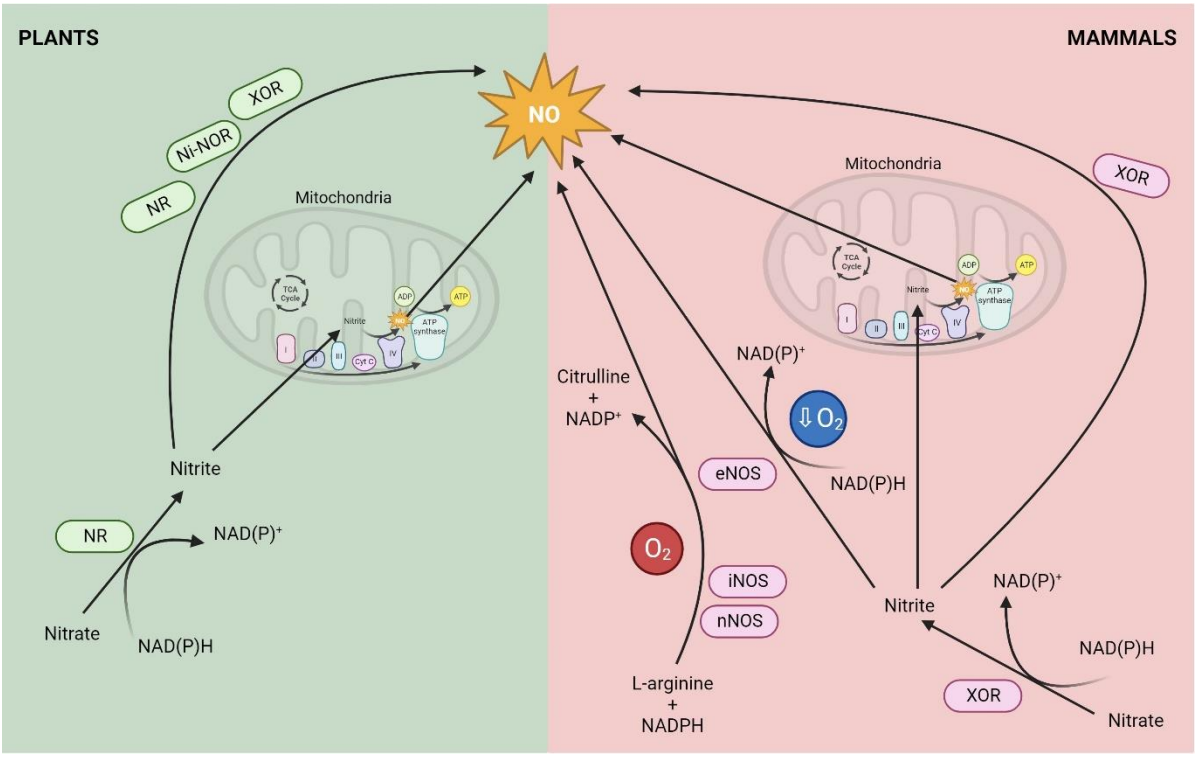

Figure 1.2. Comparison of NO biosynthesis pathways in plants and mammals. In plants, NR catalyses the first step of NO biosynthesis turning nitrate into nitrite. Nitrite can then be reduced to NO by NR, NI-NOR, XOR, and complexes III and IV of the mitochondrial electron transport chain. The latter results from the use of nitrite as a terminal electron acceptor. In mammals, NOS enzymes (eNOS, iNOS and nNOS) produce NO *via* oxidative mechanisms in the presence of oxygen. eNOS generates NO through reductive mechanisms under reduced oxygen conditions. XOR is also capable of reducing nitrite to NO, as is complex III and IV of the mitochondrial electron transport chain. Based on figure from Doorly and Graciet, 2021. Created using BioRender.com.

NO and its derivatives include NO radical, NO^-, NO^+, NO_2, NO_3, N_2O_3, N_2O_4, S-nitrosothiols (SNO) (e.g. S-nitrosoglutathione (GSNO), and peroxynitrite ($ONOO^-$), and are collectively referred to as reactive nitrogen species (RNS). RNS are labile molecules which are unlikely to be directly recognized by receptors to facilitate NO signalling (Bogdan, 2001). Instead, NO-mediated changes in gene expression and interaction with other signalling pathways, such as phytohormone signalling, regulation of reactive oxygen species (ROS), etc. are largely attributed to the direct modification of targets through NO-induced post-translational modifications. The main modifications include S-nitrosylation, tyrosine nitration and metal nitrosylation (reviewed in Astier and Lindermayr, 2012), with S-nitrosylation being the most well-studied, in particular for its role in stress responses (reviewed in Borrowman et al., 2023; Feng et al., 2019). S-nitrosylation involves the addition of NO to the thiol group on cysteine residues, resulting in the formation of a SNO. This covalent modification permits rapid detection and signalling responses

based on the redox environment of the cell (Hess et al., 2005; Yu et al., 2014). Similarly to most post-translational modifications, S-nitrosylation impacts target protein activity, localization, stability, and protein/protein interactions (Hess et al., 2005; Yu et al., 2014). In addition, this modification is reversible through both enzymatic and non-enzymatic de-nitrosylation (Bogdan, 2001). One method of S-nitrosylation regulation is through the enzyme GSNO REDUCTASE (GSNOR) which maintains the SNO-protein levels by converting GSNO, with the use of NADH, to glutathione disulphide (GSSG) and ammonia (Borrowman et al., 2023). In comparison, thioredoxins (TRXs) directly de-nitrosylate target proteins. In plants, this denitrosylation has been found to occur through trans-nitrosylation of the SNO from its substrate to one of the cysteine residues on the TRX, which leads to the generation of a free NO radical (e.g. denitrosylation of NONEXPRESSOR OF PATHOGENESIS-RELATED GENES 1 (NPR1) by TRX-5h) (Kneeshaw et al., 2014). While this method of denitrosylation is not ruled out in mammals, studies of TRX-mediated denitrosylation in mammals suggest a mechanism based on the formation of a mixed disulphide which involves the formation of a disulphide bridge between TRX and substrate protein which releases the nitroxyl group (NO^-) (e.g. denitrosylation of Caspase-3 by TRX1) (Benhar et al., 2009; Ben-Lulu et al., 2014). TRX-mediated denitrosylation provides more selectivity to the reversibility of this post-translational modification important in some biological processes e.g. immunity and apoptosis (Benhar, 2015; Benhar et al., 2009; Ben-Lulu et al., 2014; Kneeshaw et al., 2014; Mata-Pérez and Spoel, 2019).

As outlined above, the N-degron pathway is often qualified as a NO sensing pathway (Gibbs et al., 2014; Hu et al., 2005). In fact, it has been suggested that the N-degron pathway might have initially evolved to sense NO, but that as a result of increasing atmospheric oxygen levels with the evolution of photosynthetic organisms, sensing of NO and oxygen might have been linked *via* the oxidation of N-terminal cysteine residues and subsequent degradation by the N-degron pathway (Holdsworth and Gibbs, 2020). NO may also directly regulate N-degron pathway components, as one study listed PRT6 as a potential S-nitrosylation target (Zarban et al., 2019); however this has not yet been verified *in vitro* or *in vivo*. In addition, NO may further regulate signalling through the N-degron pathway by regulating protease activity and therefore coordinating the exposure of N-terminal destabilizing residues by protease cleavage. For example, several caspases and calpains have been confirmed as being S-nitrosylated (Dimmeler et al., 1997; Li et al., 1997; Marino and Gladyshev, 2010), which was shown to have an inhibitory effect on caspase function (Dimmeler et al., 1997; Li et al., 1997).

The ubiquitous roles of NO in the regulation of stress response pathways have been explored in detail in both plants and animals, where the role of this gaseous molecule has been identified as essential in the onset of immune responses.

1.4. Plant and mammal innate immunity

Innate immunity in plants and mammals facilitates the perception of pathogen invaders and the initiation of signalling pathways which lead to clearance of these invaders. The structure of innate immune signalling pathways in plants and mammals exhibit a striking resemblance, with the similarities being most notable when considering: 1) how pathogens are perceived *via* highly conserved motifs across commensal and pathogenic microbes termed PAMPs; 2) which downstream signal transduction pathways are deployed in response to PAMP recognition; 3) the genome-wide reprogramming of gene expression; and 4) the involvement of the UPS. Plant and mammal innate immunity is thought to have arisen through convergent evolution, which highlights the similar selective pressures exerted by pathogens on hosts and the constraints imposed on the evolution of mechanisms for an effective immune response (Ausubel, 2005). However, this also explains the many differences between the innate immune responses of these two kingdoms. These differences include the cells capable of mounting immune responses with mammals having specialized immune cells, while it is thought that all plant cells are capable of eliciting immune responses. As well, while the structure and many of the signal transduction pathways are common, many of the key players and final defence outputs are not. As the focus of my Ph.D. thesis lies mainly on plant innate immunity and its crosstalk with hypoxia while looking to the mammalian kingdom for conserved pathways and core elements in this crosstalk, this section will detail the plant innate immune system and will refer to similarities in the mammalian innate immune system where applicable.

Plants have a two-tier innate immune response comprised of pattern-triggered immunity (PTI) and effector-triggered immunity (ETI) (Jones and Dangl, 2006; Ngou et al., 2022a). PTI is induced upon recognition of conserved non-self molecules (PAMPs) or exposure to host damage signals (damage-associated molecular patterns (DAMPs)) (De Lorenzo et al., 2018). These molecules are recognized by direct binding to transmembrane pattern recognition receptors (PRRs), thus triggering an array of signalling pathways, including redox changes, calcium signalling, mitogen-activated protein kinase (MAPK) phosphorylation, and phytohormone signalling. These pathways promote genome-wide gene expression changes and defence mechanisms, which include the production of molecules with antimicrobial activities and callose deposition (Ngou

et al., 2022b). Some pathogens have evolved to subvert these responses and dampen PTI through the use of effector proteins. Adapted hosts possess intracellular receptors, called nucleotide-binding leucine-rich repeat proteins (NLRs), which detect specific effectors either directly or indirectly through detecting modifications of effector targets (Jones and Dangl, 2006; Ngou et al., 2022a). This branch of immunity relies on PTI and induces similar signalling pathways and downstream target genes but at a higher level and often results in a form of programmed cell death termed the hypersensitive response (Ngou et al., 2021; Yuan et al., 2021).

This Ph.D. work exclusively studied PTI responses with experiments looking into the crosstalk between hypoxia and innate immunity employing the use of the PAMP, flagellin. Flagellin is the conserved protein of the bacterial flagellum and PAMP-mediated responses induced by flagellin were studied in the presence and absence of hypoxia. Hence, the following discussion of plant innate immunity will revolve solely around PTI-mediated responses.

1.4.1. How pathogens are perceived via PAMPs

Pathogen recognition by transmembrane PRRs is essential for the initiation of innate immune responses in plants and mammals. PAMPs and DAMPs are recognized by PRRs located exclusively at the plasma membrane in plants, whereas in mammals PRRs are also present on intracellular membranes e.g. at the lysosome, endosome or endoplasmic reticulum (Duan et al., 2022). In plants, PRRs are generally receptor kinases (RKs) or receptor proteins (RPs). RKs possess an extracellular domain (ECD) responsible for ligand binding, a transmembrane domain and a cytosolic kinase domain for relaying signals intracellularly. RPs are similar apart from the absence of the intracellular kinase domain and so these require a RK co-receptor for full PAMP-induced signalling (DeFalco and Zipfel, 2021; Ngou et al., 2022a). Most PRRs possess leucine-rich repeats (LRRs) in their ECDs which are referred to as LRR-RKs e.g. FLAGELLIN-SENSITIVE 2 (FLS2) and ELONGATION FACTOR-TU RECEPTOR (EFR). Other ECD binding domains also exist including lysine-motif containing RKs e.g. CHITIN ELICITOR RECEPTOR KINASE 1 (CERK1) and LYSM-CONTAINING RECEPTOR-LIKE KINASE 4/5 (LYK4 and LYK5) (DeFalco and Zipfel, 2021).

Flagellin sensing in plants and mammals is mediated by PRRs with extracellular LRR domains (Gómez-Gómez and Boller, 2000; Mizel et al., 2003; Sun et al., 2013 Yoon et al., 2012). In plants, the PRR, FLS2, is responsible for the binding of a 22-amino acid residue peptide of flagellin (noted flg22) (Chinchilla et al., 2006; Gómez-Gómez and Boller, 2000; Felix et al., 1999), while TOLL-LIKE

RECEPTOR 5 (TLR5) in mammals recognizes a different region of flagellin, at its N-terminus, as well as conserved motifs in the C-terminus of this bacterial protein (Smith et al., 2003) (Figure 1.3). The LRR domain of FLS2 is not only responsible for flg22 binding, it is also important for the formation of a complex with the co-receptor BRI1-ASSOCIATED RECEPTOR KINASE 1 (BAK1), in which the C-terminal segment of flg22 acts as a molecular glue for the dimerization of FLS2 and BAK1 (Figure 1.3) (DeFalco and Zipfel, 2021; Gómez-Gómez and Boller, 2000; Sun et al., 2013). FLS2-BAK1 interaction occurs rapidly upon flg22 treatment (Chinchilla et al., 2007) and leads to trans-phosphorylation of the intracellular signalling domain (DeFalco and Zipfel, 2021). This initiates a series of signal transduction cascades culminating in PTI through the activation of receptor-like cytoplasmic kinases (RLCKs) (detailed in section 1.4.2.) such as BOTRYTIS-INDUCED KINASE 1 (BIK1), PBL1, PBL27 and BRASSINOSTEROID-SIGNALLING KINASE 1 (BSK1). These kinases promote MAPK-phosphorylation cascades which phosphorylate targets (e.g. WRKY transcription factors), resulting in defence gene expression (Figure 1.3) (Ngou et al., 2022a). TLR5 has 22 LRRs (Matsushima et al., 2007), which are responsible for flagellin binding and complex assembly (Mizel et al., 2003; Yoon et al., 2012). Similar to plants, TLR5 interacts with a co-receptor upon flagellin binding, which in this case, is a second flagellin-bound TLR5 (Figure 1.3) (Yoon et al., 2012). Like other members of the TLR family, homodimerization of flagellin-bound TLR5 receptors leads to interaction of the intracellular domains which instead of kinase domains in plants, TLRs have toll-like receptor/interleukin (TIR) domains, which recruit proteins such as MYELOID DIFFERENTIATION PRIMARY RESPONSE 88 (MyD88) and INTERLEUKIN-1 RECEPTOR ASSOCIATED KINASE (IRAK) kinase family members to facilitate activation of downstream signalling pathways including phosphorylation cascades which activate MAPK and NUCLEAR FACTOR KAPPA B (NF-κB) signalling leading to induction of cytokine and pro-inflammatory gene expression (Figure 1.3) (DeFalco and Zipfel, 2021; Narayanan and Park, 2015).

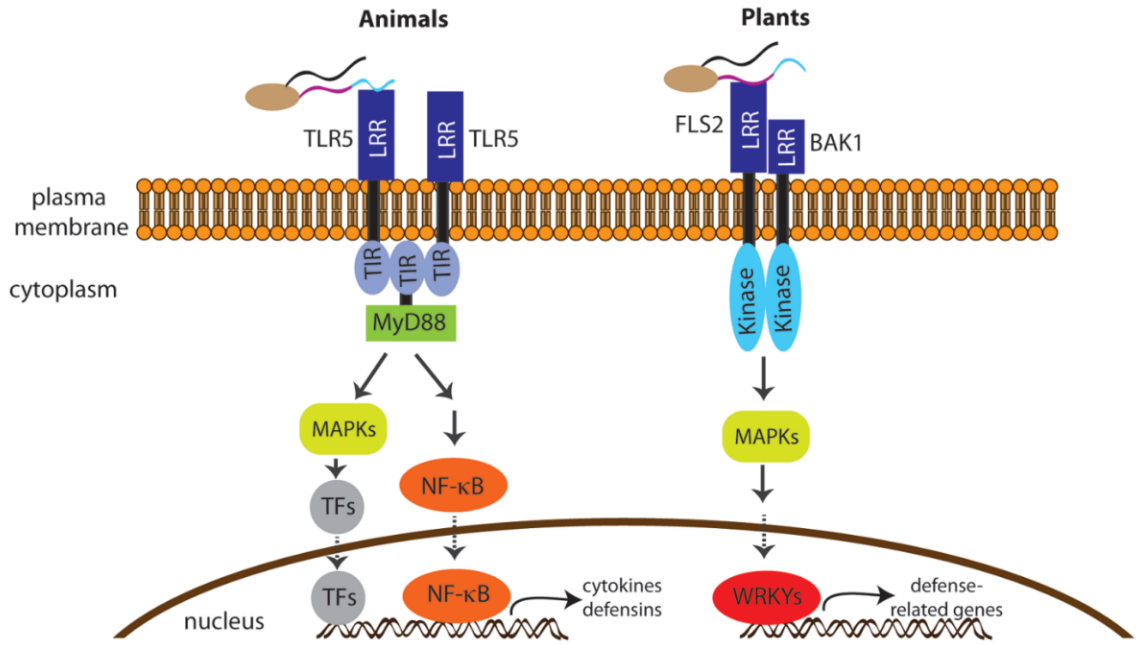

Figure 1.3. Comparisons of PTI signalling pathways in plants and mammals. The figure showcases the similarities between the signalling pathways employed in plants and mammals after PRR binding to its PAMP. Here, different epitopes of flagellin bind to TLR5 and FLS2 in mammals and plants, respectively. This results in dimerization of the PRRs which facilitates binding of the intracellular domains, TIR domains in mammals and kinase domains in plants. This leads to activation of proteins which lead to MAPK signalling and activation of defence-related transcription factors, inducing widespread transcriptional changes. In mammals, PAMP-binding also initiates a signalling pathway absent in plants called the NF-κB pathway which results in the de-inhibition of the NF-κB transcription factor, which translocates to the nucleus and induces pro-inflammatory genes. Figure taken from Haney et al., 2014.

1.4.2. Downstream signal transduction pathways deployed in response to PAMP recognition

The early signalling events downstream of PAMP recognition by a PRR are highly conserved across eukaryotes and include: (i) MAPK-phosphorylation cascades; (ii) calcium signalling; and (iii) redox changes as a result of increased ROS and RNS (Figure 1.4). In plants, the link between pathogen recognition by PRRs and the activation of these conserved signalling events are RLCKs (Bi et al., 2018; Hailemariam et al., 2024; Rao et al., 2018). RLCKs are protein kinases. There are 149 RLCKs in Arabidopsis and are organised into 17 subfamilies (Hailemariam et al., 2024). In particular, the RLCK subfamily VII has been implicated in regulating many PTI responses. For example, the extensively studied RLCK, BIK1, which interacts with and acts downstream of many PRRs (e.g. FLS2, EFR, CERK1, and PEPR1/2), and has roles in pathogen resistance through the induction of Ca^{2+} influx (Thor et al., 2020) and ROS generation (Kadota et al., 2014), is a member of this RLCK VII subfamily (Hailemariam et al., 2024; Rao et al., 2018). Further highlighting the importance of this subfamily in PTI, the use of RLCK VII subgroup (1-9) higher order mutants has

identified roles for members of the RLCK VII subgroups -5, -7 and -8, the latter group containing BIK1, in acting downstream of multiple PRRs and regulating ROS production (Rao et al., 2018), as well as implicating RLCK VII subgroup -4 members in the activation of the ROS burst and MAPK signalling in response to chitin treatment (Bi et al., 2018; Rao et al., 2018).

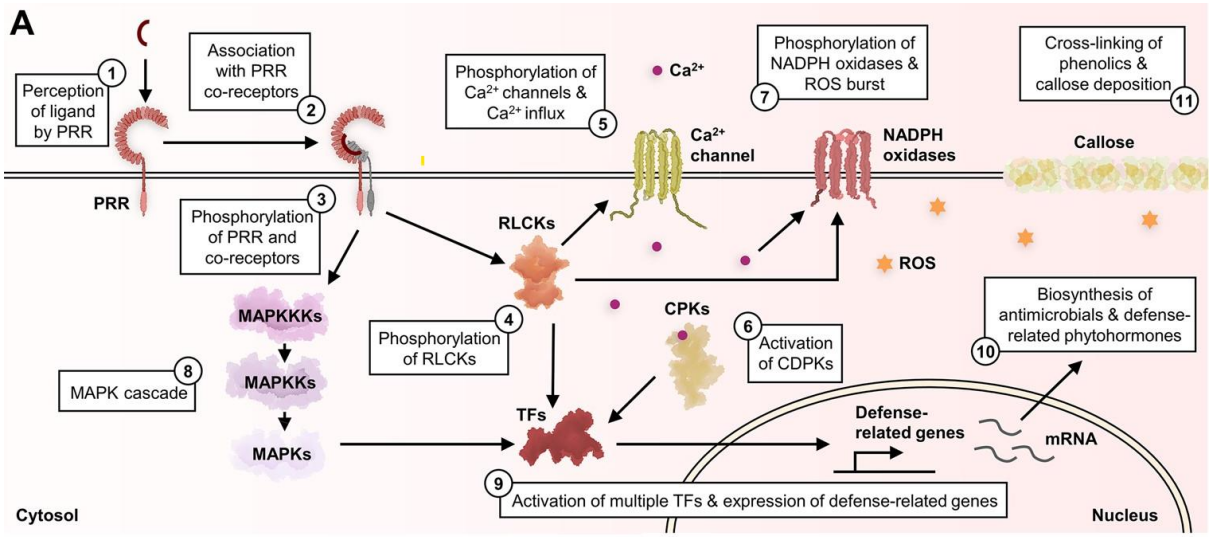

Figure 1.4. Signal transduction pathways involved in plant PTI. PAMP-binding to PRRs (1,2) activates a number of signal transduction pathways, including MAPK signalling (3,8), activation of RLCKs (4) which phosphorylate calcium channels (5) and NADPH oxidases (7). These play a role in the regulation of intracellular calcium levels and activation of calcium-dependent protein kinases (CDPKs) (6) and oxidative burst, respectively. The signal transduction pathways culminate in the genome-wide rewiring of gene expression (9) and physiological responses to pathogens, e.g. production of antimicrobial compounds, phytohormone signalling (10) and callose deposition (11). Figure taken from Ngou et al., 2022a.

1.4.2.1. MAPK phosphorylation signal transduction cascades.

MAPK signalling is a conserved pathway in developmental and stress responses in plants and mammals. Activation of this signalling pathway is mediated through a phosphorylation cascade, which results in the activation of different kinases: first with the phosphorylation and activation of MAPK kinase kinases (MAPKKK), which then phosphorylate and activate MAPK kinases (MKK) e.g. MPK3 and MPK6 activation lies downstream of the MAPKKK3/MAPKKK5 – MKK4/MKK5 – MPK3/MPK6 cascade (Zhang and Zhang, 2022). MAPK proteins are phosphorylated at a conserved TxY motif (Kalapos et al., 2019). In mammals, the identity of the middle amino acid in this conserved motif denotes MAPK function. TEY containing MAPKs are involved in EXTRACELLULAR SIGNAL-REGULATED KINASE (ERK)-pathway mediated processes including cell cycle and development. TGY and TPY containing MAPKs are involved in stress responses and include p38 and c-Jun N-terminal kinase (JNK) family MAPKs, respectively. Plants, on the other

hand, lack these distinct groupings and instead harbour an expansion of the ERK-like MAPKs containing T[E/D]Y motifs. In plants, these MAPKs have roles in both cell cycle and responses to (a)biotic stress (Kalapos et al., 2019). Target substrates include transcription factors which contribute to the genome-wide expression changes that occur during PTI including WRKY33 (WRKYs detailed below in section 1.4.3.) and PRODUCTION OF ANTHOCYANIN PIGMENT 1 (PAP1; also known as MYB75) (detailed in section 4.1.1.2.). MAPKs also target enzymes involved in diverse functions including 1-aminocyclopropane-1-carboxylic acid synthase (ACS)2/6 which are involved in the biosynthesis of the phytohormone, ethylene (Sun and Zhang et al., 2022).

Activated by PAMP-induced RLCKs, MAPK signalling involves three major MAPKs, MPK3, MPK4 and MPK6 (DeFalco and Zipfel, 2021). These kinases act semi-redundantly and have major roles in plant immunity with *mpk3, mpk4* and *mpk6* single mutants having impacted responses to flg22 (Li et al., 2016), and with *mpk3 mpk6* double mutants showing dysfunctional PTI responses, e.g. reduced biosynthesis of important secondary metabolite, camalexin (detailed in section 1.4.2.4), and inhibition of PAMP-induced stomatal closure (Ren et al., 2008; Su et al., 2017; Zhang and Zhang, 2022).

1.4.2.2. Calcium signalling

Under homeostasis, cytosolic levels of calcium are low with stores of calcium existing extracellularly, as well as intracellularly in vacuoles, the endoplasmic reticulum, mitochondria and chloroplasts. PRR binding to its ligand results in rapid opening of calcium channels and an influx of calcium ions into the cytosol. While plants have fewer calcium channels than mammals, their calcium channels have homology to mammalian ones including, CYCLIC NUCLEOTIDE-GATED CHANNELS (CNGCs in plants; CNGs in mammals) and REDUCED HYPEROSMOLARITY-INDUCED CALCIUM INCREASE (OSCA) channels (Luan and Wang, 2021). In plants, calcium channels of these families (CNGC2-4 and OSCA1.3), have been implicated with mediating PAMP-triggered influx of calcium which leads to activation of calcium signalling through CDPKs and downstream induction of key immune signalling and physiological responses (Luan and Wang, 2021; Ngou et al., 2022a; Thor et al., 2020). These include the induction of the ROS burst with both cytosolic calcium and CDPKs binding to and regulating the activity of the main ROS producing enzyme in plant immunity, RESPIRATORY BURST OXIDASE HOMOLOGUE D (RBOHD) (RBOHD discussed in section 1.4.2.3.). For example, the CDPKs, CPK4/5/6/11, have been shown to phosphorylate RBOHD which, along with BIK1 phosphorylation, activates it (Dubiella et al., 2013; Kadota et al., 2014). CPK5 has also been found to phosphorylate the transcription factors WRKY33 (WRKYs detailed below in section 1.4.3.) and CALMODULIN-BINDING PROTEIN 60-LIKE

G (CBP60g) implicating calcium signalling in defence-related transcriptomic changes (Sun et al., 2022; Zhou et al., 2020). Calcium influx mediated by OSCA1.3 and OSCA1.7 was also found to regulate PAMP-induced stomatal closure (Thor et al., 2020). For more in-depth discussions of calcium channels in immunity please refer to these reviews (Luan and Wang, 2021; Xu et al., 2022).

1.4.2.3. Redox changes and role of ROS and RNS in immunity

ROS and RNS are rapidly induced upon pathogen perception in both plants and mammals, resulting in oxidative and nitrosative bursts, respectively (Bleau and Spoel, 2021; Borrowman et al., 2023). The changes in the redox environment by these molecules induce signalling pathways which mediate many immune-related processes. In plants, these redox molecules lead to strengthening of the cell wall through cross-linking of glycoproteins and callose deposition. They also have direct and indirect cytotoxic effects on pathogens (Bleau and Spoel, 2021; Borrowman et al., 2023; Ngou et al., 2022a).

ROS are synthesized by the conserved enzymes NADPH oxidases (NOXs) in plants and mammals. In plants, these proteins are called RBOHs. There are 10 RBOH proteins encoded in the Arabidopsis genome, which localize to the plasma membrane and generate apoplastic ROS (Bleau and Spoel, 2021; Torres and Dangl, 2005). RBOHD and RBOHF are the predominant NOXs responsible for apoplastic ROS production in response to pathogens and/or PAMPs in Arabidopsis (Bleau and Spoel, 2021). In mammals, NOXs bear a resemblance to the plant NOXs structure and function in ROS production. In particular, the C-terminal region containing the FAD and NADPH domains show high homology between plant and mammalian NOXs (Torres and Dangl, 2005).

iNOS activity is induced in immune cells in mammals early in pathogen infection in response to PAMPs and cytokines e.g. interferon-gamma (IFN-γ) and TNF-α (Bogdan et al., 2000; Bogdan, 2015; Salim et al., 2016). As stated in section 1.3, the presence of a NOS-like enzyme in plants is controversial and it is thought that NO synthesis in plants is generated primarily by a NR-dependent reductive pathway (e.g. NIA1 and NIA2 in Arabidopsis) (Borrowman et al., 2023; Gupta et al., 2005; Mohn et al., 2019). Mutants of the *NIA1* and *NIA2* genes in Arabidopsis show defects in important immunity-related processes, including reduced signalling by the phytohormone salicylic acid (SA), dampened defence-gene expression, dysregulated ROS

signalling, and reduced stomatal closure (Borrowman et al., 2023; Hao et al., 2010; Vitor et al., 2013; Zhao et al., 2016).

S-nitrosylation has become a well-established post-translational modification in plant and mammal immune responses. With the nitrosative burst in response to PAMPs and pathogens comes an increase in the cellular level of GSNO which facilitates S-nitrosylation of target proteins (Bleau and Spoel, 2021). Balancing SNO levels is important for proper immune function. For immune-related SA signalling, both GSNO and TRXs are required. TRX-5h is involved in de-nitrosylating the SA signalling master regulator, NPR1 under SA-treatment, allowing its monomerization and translocation to the nucleus. On the other-hand, GSNO-facilitated S-nitrosylation of NPR1 mediates its oligomerization which restricts NPR1 to the cytosol and prevents SA-induced signalling but also acts to replenish and sustain NPR1 protein levels (Tada et al., 2008). The relevance of balancing the redox levels is further emphasized by the role of GSNOR (Borrowman et al., 2023). In plants, over-accumulation of SNO levels in *gsnor1-3* mutants leads to increased pathogen susceptibility. In contrast, *gsnor1-1* mutants, which have lower SNO levels have increased resistance to *Pseudomonas syringae pathovar tomato* DC3000 (*Pst* DC3000) (Feechan et al., 2005). Balancing GSNO levels is also important in mammalian immunity. A key component of the pro-inflammatory NF-κB pathway is S-nitrosylated, which inhibits its activity and reduces inflammatory responses (Reynaert et al., 2004).

ROS and RNS also regulate each other's activity. For example, NO has been shown to repress RBOHD activity through its S-nitrosylation at Cys890 (Yun et al., 2011). NO has also been shown to negatively regulate the activity of human NOXs 1-5 (Qian et al., 2012). In line with plant and mammal NOXs being homologous, the Cys890 site from RBOHD is conserved in human NOX5 and NOX2 at Cys694 and Cys537, respectively, which has also been shown to be S-nitrosylated and has been implicated in reducing ROS production (Castro et al., 2021; Yun et al., 2011; Qian et al., 2012). These mechanisms highlight a NO-mediated negative feedback loop for ROS signalling.

1.4.2.4. Phytohormone signalling during plant immunity

Part of the responses to PAMPs is the induction of phytohormones. SA and JA are among the main phytohormones in plant immunity along with ethylene and abscisic acid (ABA). JA is known for mediating defences against necrotrophic and hemibiotrophic pathogens, as well as insect pests (Lorenzo et al., 2004; Song et al., 2014; Verhage et al., 2011; Zhu et al., 2011). On the other

hand, SA-mediated responses are deployed against biotrophic pathogens. Notably, JA and SA mediated responses are largely antagonistic (Li et al., 2016). Some aspects of the work carried out focused on JA, whose role in plant immunity is therefore discussed in more detail here and in Chapter 4.

Wounding, herbivory or the detection of PAMPs/DAMPs (e.g. chitosan and oligogalacturonides) trigger JA signalling (Doares et al., 1995; Denoux et al., 2008). JA signalling is particularly important because of its role in activating the biosynthesis of species specific secondary metabolites, which are vital for defence (reviewed in De Geyter et al., 2012; Lacchini and Goossens, 2020; Wasternack and Strnad, 2019). These include camalexins, indole glucosinolates, and anthocyanins in Arabidopsis (De Geyter et al., 2012). JA, ethylene and MAPK signalling pathways act synergistically to regulate the biosynthesis of camalexins in response to *Botrytis cinerea* (*B. cinerea*) infection. These pathways lead to the induction of ETHYLENE RESPONSE FACTOR 1 (ERF1) and WRKY33 transcription factors (WRKYs detailed below in section 1.4.3.) which form a complex in the nucleus and regulate camalexin biosynthesis genes (Zhou et al., 2022). The accumulation of camalexins during infection cause damage to bacterial and fungal cell membranes and inhibits their growth (Nguyen et al., 2022). Glucosinolates have roles in preventing entry of microbial invaders and are metabolised by myrosinases in response to infection, releasing biproducts with anti-microbial and anti-herbivore activities (Bednarek et al., 2009; Sugiyama and Hirai, 2019). They can also contribute to aspects of PTI, such as callose deposition (Clay et al., 2009; Millet et al., 2010). Anthocyanins are flavonoids which are responsible for some plant pigments. These compounds are induced by developmental, sugar and external stimuli including pathogen and herbivore attack and they have been shown to have anti-microbial and anti-herbivore properties (Shan et al., 2009).

JA has also been implicated in systemic acquired resistance (SAR) with elevated JA levels being detected by 6 hours after inoculation with *Pst* DC3000 (*AvrRpm1*) in systemic leaves. Further, mutants for JA biosynthesis and signalling resulted in reducesd SAR response against *Pst* DC3000 (*AvrRpm1*). A JA responsive gene, *SGT1B* (also refered to as *ENHANCED DOWNY MILDEW 1* (*EDM1*)) appeared to be required for SAR and it was suggested that this protein may act in perceiving the signal to induce SAR (Truman et al., 2007).

1.4.3. Genome-wide reprograming of gene expression

In plants, despite the PRR/ligand diversity, the downstream transcriptional responses are remarkably similar irrespective of the source or biochemical nature of the PAMPs (Bjornson et al., 2021). This highlights the similarity of responses to different pathogens at early timepoints and that complexity/specificity of responses is likely to arise at a later stage.

WRKY transcription factors constitute one of the largest families of transcription factors in plants and have major roles in developmental processes, as well as responses to (a)biotic stresses (Mohanta et al., 2016; Wani et al., 2021). These transcription factors possess a WRKY domain with a highly conserved N-terminal WRKYGQK motif and a C-terminal zinc finger motif. They bind the so-called W-box (TTGACC/T) in the promoters of their target genes (Mohanta et al., 2016; Wani et al., 2021). WRKYs are activated downstream of ligand binding to PRRs. In Bjornson et al., 2021, a large number of WRKY transcription factors were found to be induced by all PAMPs at 10-30 minutes after treatment. One of the WRKY transcription factors present in this analysis is WRKY33, a well-known and key regulator of plant immune responses (Saha et al., 2024). WRKY33 has been previously shown to be activated by phosphorylation at N-terminal Ser residues (Ser-54, Ser-59, Ser-65, Ser-72, Ser-85) by MPK3 and MPK6 (Mao et al., 2011; Zhou et al., 2020), and at Thr-229 by the calcium dependent kinases CALCIUM-DEPENDENT KINASE 5 (CPK5) and CPK6 (Zhou et al., 2020). The MAPKs and CDPKs also additively impact WRKY33 activity (and camalexin production) in response to *B. cinerea* infection (Zhou et al., 2020).

Another family of transcription factors, the CALMODULIN-BINDING TRANSCRIPTIONAL ACTIVATORs (CAMTAs) were also highly represented in response to all PAMPs tested in Bjornson et al., 2021. These were induced after 5- or 10-minute treatments and have been previously associated with general stress responses (Benn et al., 2014; Bjornson et al., 2014; Iqbal et al., 2020), suggesting a role for these transcription factors in the more general, early responses to danger seen with all PAMP treatments.

This study by Bjornson et al. was also key in identifying 39 genes which are only induced in responses to PAMPs (e.g. they do not appear to be regulated in response to abiotic stresses). These genes are referred to as 'core immunity response' (CIR) genes, and include the calcium channels GLUTAMATE RECEPTOR (GLR)2.7 and GLR2.9, the kinases CYSTEINE-RICH KINASE 17 (CRK17), WALL-ASSOCIATED KINASE-LIKE 10 (WAKL10), RECEPTOR LIKE PROTEIN 21 (RLP21), as well as the NAC transcription factor 61 and MYB98 to name a few (Bjornson et al., 2021).

1.4.4. Roles of the UPS-dependent N-degron pathway as a regulator of defence responses

In plants, the UPS is responsible for the regulation of every aspect of PTI, from the abundance of PRRs at the plasma membrane, to the regulation of hormone signalling pathways and of transcriptional regulators (Adams and Spoel, 2018; Linden and Callis, 2020; Ma et al., 2021; Miricescu et al., 2018; Nagels et al., 2016; Pauwels et al., 2015; Wang et al., 2022). The N-degron pathway has also been implicated in the regulation of mammal innate immune responses, as well as defence responses in plants. However, its potential roles in PTI have only been recently studied in parallel to the work conducted here (Mooney et al., 2024).

The N-degron pathway regulates the inflammatory response in mammalian immune cells through the activation of pro-inflammatory factors *via* a proteasome-dependent mechanism (Chui et al., 2019; Sandstrom et al., 2019; Xu et al., 2019). The pathway also functions in the suppression of inflammation as many pro-inflammatory factors are activated by caspase cleavage e.g. the inflammatory cytokine IL-1ß. This cleavage reveals neo-N-degrons, which target the protein for degradation and contributes to a dampening of the immune response after the infection has been resolved (Leboeuf et al., 2020a).

In plants, the inoculation of N-degron pathway mutants with a range of pathogens with different lifestyles has highlighted functions of this pathway in plant defence, with varying susceptibility/resistance phenotypes (de Marchi et al., 2016; Gravot et al., 2016; Till et al., 2019; Vicente et al., 2019). The *ate1 ate2* and *prt6* mutants were found to be more susceptible to clubroot gall caused by the biotrophic protist pathogen *Plasmodiophora brassicae* and this susceptibility was dependent on the accumulation of the ERFVIIs in the N-degron pathway mutant backgrounds (Gravot et al., 2016). This points to a potential double role of ERFVIIs in the regulation of hypoxia response and plant defences against pathogens, but the role of these transcription factors in plant innate immune pathways or in the crosstalk between hypoxia response and plant immunity have not been explored in detail. This dual role of the N-degron pathway and its ERFVII substrates in hypoxia and defence in plants and their role in the crosstalk between these stress pathways is a main focus of this Ph.D. work. The following section describes the similarities and differences between plant and mammalian hypoxia responses including a discussion of the role of the N-degron pathway in oxygen and NO sensing.

1.5. Plant and mammal hypoxia response

With the evolution of photosynthetic organisms, cells adapted to the resulting increase in oxygen in the atmosphere. Living organisms developed mechanisms to sense oxygen levels and respond to fluctuations while also becoming reliant on oxygen for biochemical reactions or as the final electron acceptor in the mitochondrial electron transport chain to generate energy for cellular functions (reviewed in (Hammarlund et al., 2020; Holdsworth and Gibbs, 2020)). As dependence on oxygen evolved, hypoxia (or reduced oxygen availability) became a stress that affected survival if prolonged. For example, in plants, including in many staple crops, hypoxia reduces growth and productivity, and can negatively affect the responses to other stresses (Fukao et al., 2019). Both plants and mammals experience hypoxia and its negative effects. Notably, both have evolved conceptually similar molecular mechanisms to sense and respond to hypoxia stress, making it interesting to draw parallels between hypoxia-related signalling and responses in plants and mammals (see also (Doorly and Graciet, 2021; Hammarlund et al., 2020; Holdsworth and Gibbs, 2020).

1.5.1. N-degron pathway function in oxygen sensing and in downstream signal transduction

Oxygen-sensing mechanisms in both plants and mammals rely on the activity of oxygen-dependent enzymes that post-translationally modify master regulators of hypoxia response when oxygen is available. While these enzymes and their substrates differ in plants and mammals, the downstream effects are conceptually and functionally strikingly similar. Indeed, in both plants and mammals, the master regulators of hypoxia responses are transcription factors that are (i) modified by oxygen-dependent enzymes; (ii) rapidly degraded in normoxia and (iii) stabilized under hypoxic conditions resulting in the subsequent activation of the hypoxia response program (Figure 1.5.).

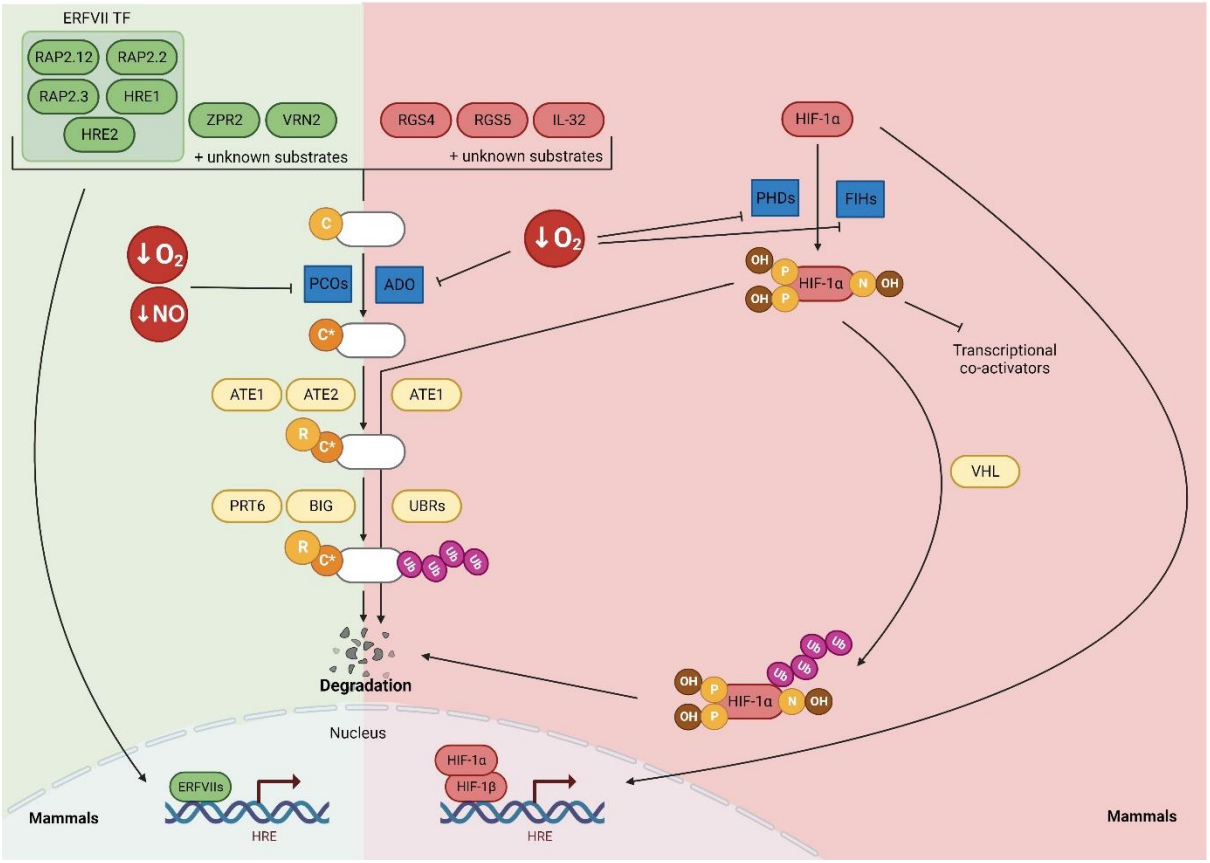

Figure 1.5. Oxygen sensing pathways in plants and mammals. Oxygen sensing is mediated by oxygen-dependent enzymes (PCOs in plants, and ADO, PHDs, and FIHs in mammals) that regulate cellular responses to oxygen (denoted O_2) levels. These enzymes contribute to the regulation of the stability of transcription factors that act as master regulators of hypoxia response genes (e.g., ERFVIIs in plants and HIF1α in mammals). Oxidation of N-terminal cysteine residues by PCOs and ADO (in plants and mammals, respectively) results in the degradation of target proteins *via* the evolutionarily conserved N-degron pathway. In plants, this includes the ERFVII transcription factors, following their arginylation by arginyl-transferase enzymes and ubiquitination by the N-recognin PRT6. In mammals, PHDs and FIHs hydroxylate specific proline and asparagine residues, respectively, on HIF1α, which can then be ubiquitinated by the E3 ubiquitin ligase VHL. Hydroxylation of proline residues on HIF1α also promotes arginylation and ubiquitination by the N-degron pathway facilitating its degradation. Based on figure from Doorly and Graciet, 2021. Created using BioRender.com.

In plants, an important and conserved oxygen-sensing mechanism depends on the oxygen-dependent activity of a family of Fe(II)-dependent thiol dioxygenases known as PCO enzymes of the N-degron pathway, with five members being present in Arabidopsis (Weits et al., 2014; White et al., 2017). An important feature of PCO enzymes in oxygen sensing is the dependency of their activity on oxygen levels (White et al., 2018) and the fact that the expression of some of the Arabidopsis PCOs is hypoxia dependent, while other family members are expressed

constitutively (Weits et al., 2014). Although the full complement of proteins modified by PCO enzymes is still unknown, several substrates with diverse physiological and developmental roles have been identified e.g. VERNALIZATION2 (VRN2) which is involved in the control of flowering, LITTLE ZIPPER2 (ZPR2) which regulates the activity of the shoot apical meristem (Gibbs et al., 2018; Weits et al., 2019), and the set of conserved ERFVII transcription factors (Weits et al., 2014; White et al., 2017). An important common feature of ERFVIIs, e.g. Arabidopsis RELATED TO APETALA2.2 (RAP2.2), RAP2.3, RAP2.12, HYPOXIA RESPONSIVE ERF1 (HRE1) and HRE2, is the presence of a cysteine residue at position 2 after the initial methionine residue of the protein (Gibbs et al., 2011; Gibbs et al., 2015; Licausi et al., 2011a). However, this cysteine residue becomes N-terminal following removal of the initial Met residue by methionine aminopeptidases and can then be oxidized into cysteine sulfinic acid by PCO enzymes (Weits et al., 2014; White et al., 2017). Based on genetic evidence, as well as *in vitro* biochemical assays, the degradation of ERFVIIs downstream of PCO modification occurs through the N-degron pathway and also requires arginylation by ATE1 and ATE2, followed by recognition and ubiquitination by the E3 ubiquitin ligase PRT6 (Gibbs et al., 2011; Licausi et al., 2011a; Weits et al., 2014; White et al., 2017) (Figure 1.5). Under hypoxic conditions, PCO-mediated oxidation of the N-terminal cysteine residue of ERFVII transcription factors is limited due to decreased oxygen availability, so that N-degron-dependent degradation is hindered (Gibbs et al., 2011). As a result, ERFVIIs accumulate in the cell, translocate to the nucleus and regulate the expression of hypoxia-response genes (Licausi et al., 2011a; Schmidt et al., 2018) (Figure 1.5).

ADO, the mammalian equivalent of the PCOs, also oxidizes the N-terminal cysteine of its protein substrates in an oxygen-dependent manner and facilitates subsequent degradation through the N-degron pathway. Proteins which are degraded through this ADO-mediated and oxygen-dependent mechanism include the pro-inflammatory cytokine INTERLEUKIN-32 (IL-32) (Masson et al., 2019), as well as regulator of G protein signalling 4 (RGS4) and RGS5 (Hu et al., 2005; Lee et al., 2005; Masson et al., 2019) (Figure 1.5). The latter have been previously shown to be involved in angiogenesis and the cardiovascular development (Albig and Schiemann, 2005; Jaba et al., 2013; Lee et al., 2005). Similarly to PCOs, the full complement of ADO substrates is not known, so that additional (still unknown) substrates may also play a role in the response of animals to hypoxia response.

A major mechanism by which mammals respond to hypoxia is through the degradation of the alpha subunit (HIF1α) of the heterodimeric transcription factor HYPOXIA-INDUCIBLE FACTOR

(HIF; the second subunit is known as HIF1β and is constitutively expressed). Similar to plant ERFVIIs, HIF1α is unstable under normoxia (Huang et al., 1998; Maxwell et al., 1999; Tanimoto et al., 2000) due to the activity of oxygen-dependent Fe(II), 2-oxoglutarate enzymes, including PROLYL HYDROXYLASES (PHDs) (Ivan et al., 2001; Jaakkola et al., 2001) and FACTOR INHIBITING HIF (FIH) enzymes (Hewitson et al., 2002; Lando et al., 2002a; Lando et al., 2002b; McNeill et al., 2002) (Figure 1.5). Specifically, in normoxia, two proline residues of HIF1α are hydroxylated by PHDs in an oxygen-dependent reaction. PHD-dependent HIF1α hydroxylation serves as a degradation signal that is recognized/bound by the VON HIPPEL-LINDAU (VHL) protein as part of the multi-subunit cullin2/elongin-based E3 ligase resulting in its ubiquitination and degradation (Ivan et al., 2001; Jaakkola et al., 2001; Maxwell et al., 1999; Tanimoto et al., 2000) (Figure 1.5). In addition, oxygen-dependent FIH hydroxylates an asparagine residue of HIF1α, this time hindering the recruitment of transcriptional co-activators by HIF1 (Lando et al., 2002a; Lando et al., 2002b). During hypoxia, PHD-mediated hydroxylation of HIF1α does not occur, resulting in HIF1α stabilization, as well as translocation to the nucleus and regulation of its target genes. The ubiquitin/proteasome-mediated regulation of HIF1α is hence conceptually very similar to that of the ERFVII transcription factors in plants.

A recent paper has identified a link between the HIF oxygen sensing pathway and the N-degron pathway in mammals (Moorthy et al., 2022) (Figure 1.5). Specifically, HIF1α is stabilized in ATE1 knockout (KO) mouse embryonic fibroblast cells (MEFs), with a corresponding increase in expression of known HIF1 targets including VASCULAR ENDOTHELIAL GROWTH FACTOR A (VEGFA), ERYTHROPOIETIN (EPO) and 6-PHOSPHOFRUCTO-2-KINASE/FRUCTOSE-2,6-BISPHOSPHATASE 3 (PFKFB3). This cell line also showed an induction of aerobic glycolysis or glycolysis (pathway for ATP generation employed when oxygen levels are insufficient for oxidative phosphorylation) in the presence of normal oxygen conditions. This suggests that hypoxia responses are induced in the ATE1 KO MEFs even when oxygen is present. Notably, HIF1α was found to be arginylated by mammalian ATE1 in normoxic conditions, but not during hypoxia. This led to the discovery that HIF1α arginylation is dependent on PHD activity. This arginylation resulted in HIF1α degradation which did not rely on VHL but rather was dependent on the UBR N-recognins (Moorthy et al., 2022).

In sum, while mammals have a separate oxygen sensing mechanism found only in metazoans, it is apparent that the N-degron pathway may have been the primary/ancestral oxygen sensing mechanism shared by higher eukaryotes (Gibbs and Holdsworth, 2020).

1.5.2 The role of NO in oxygen sensing and downstream signal transduction

NO production rapidly increases in response to hypoxia in both plants and mammals (Gautier et al., 2006; Gibbs et al., 2014; Mikula et al., 2009; Mugnai et al., 2012; Vanin et al., 2007) and plays a role in the sensing of oxygen/hypoxia and downstream signalling events. For example, the NO producing enzyme NR was previously shown to be important for plant survival under hypoxia (Allegre et al., 2004). NO production in roots is an important component of hypoxia tolerance, as the application of NO scavengers reduces plant survival in hypoxic stress (Mugnai et al., 2012). NO-mediated effects include the induction of genes coding for enzymes such as ALCOHOL DEHYDROGENASE 1 (ADH1) and PYRUVATE DECARBOXYLASE (PDC) (Mugnai et al., 2012; Wany et al., 2018; Zhan et al., 2018), as well as the regulation of genes necessary to shift ATP generation to oxygen-independent mechanisms and reduce oxidative stress in response to low oxygen (Gupta et al., 2020; Wany et al., 2018). In mammals, NO also contributes to the regulation of oxygen sensing mechanisms (see below), while also facilitating vasodilation, anti-thrombotic effects, and angiogenesis to increase oxygenated blood getting to hypoxic tissues (Förstermann and Sessa, 2012; Krumenacker et al., 2004; Lei et al., 2021). This latter effect is comparable to the role of NO in plants in facilitating the transport of oxygen to hypoxic tissues through the formation of aerenchyma, which facilitates gas exchange in waterlogged plants (Wany et al., 2017).

In plants, reduced levels of NO prior to hypoxia can prime plant responses to this stress and increase their survival (Hartman et al., 2019). This initial depletion of NO is likely the result of elevated ethylene levels in submerged tissue, which induces the up-regulation of HEMOGLOBIN1 (HB1; also known as PHYTOGLOBIN1 (PGB1)) (Hartman et al., 2019), a known scavenger of NO during hypoxia (Hebelstrup et al., 2012; Perazzolli et al., 2004). Up-regulation of HB1 allows the stabilization of the ERFVII transcription factors, thus promoting hypoxia tolerance (Hartman et al., 2019). Notably, the stabilization of N-degron pathway substrates, including the ERFVII transcription factors, leads to NO induction. Hence, the early suppression of NO at the onset of hypoxia not only allows stabilization of the ERFVIIs, but may also contribute to inducing the NO burst in response to hypoxia (Gibbs et al., 2014).

Similarly to the regulation of ERFVIIs by NO, the regulation of the mammalian HIF1-dependent oxygen-sensing pathway by NO has also been proposed during hypoxia, although this remains controversial. Indeed, reports have shown conflicting roles for NO in regulating HIF1 activity, with studies showing both positive (Brüne et al., 2001) as well as negative (Agani et al., 2002; Hagen

et al., 2003) effects on HIF1α accumulation. Mateo et al., 2003 proposed that these results are NO concentration dependent. High concentrations of NO (>1 μM) have a positive effect on HIF1α stability, while low NO concentrations (<400 nM) destabilize HIF1α. This concentration-dependent effect of NO on HIF1α stabilization occurs in high (21%) as well as low oxygen (3%) conditions. It was also shown that the destabilizing effect of low NO concentrations on HIF1α during hypoxia was dependent on the mitochondrial electron transport chain, while the stabilizing effect of high NO concentrations was not (Agani et al., 2002; Hagen et al., 2003; Mateo et al., 2003). The repression of HIF1α was proposed to stem from the redistribution of the limited oxygen within the cell from the mitochondrial electron transport chain to be used for other oxygen-dependent processes. Interestingly, this inhibition of mitochondrial complexes by NO in order to redistribute oxygen for other oxygen-dependent processes as well as reducing the rate of oxygen consumption has also been found in plants (Gupta et al., 2020).

As mentioned above, the effects of NO are also mediated by its post-translational modification of proteins. In both plants and mammals, the NO burst during hypoxia coincides with an increase in protein S-nitrosylation (Chen et al., 2008; Zhan et al., 2018). The level of GSNO, a stable source of intracellular NO, mediates protein S-nitrosylation. The increase in S-nitrosylation during hypoxia stems from the autophagic degradation of the inhibitor of GSNO, GSNOR1 in plants (Zhan et al., 2018). Mammalian GSNOR is conserved at the ATG8 recognition site and S-nitrosylated amino acid residue in plants, which suggests that a similar S-nitrosylation-dependent mechanism for the regulation of GSNOR during hypoxia may exist in mammals (Zhan et al., 2018).

While all three mammalian NOS isoforms have important physiological roles in both homeostasis as well as stress conditions, of particular importance in mammalian tolerance to hypoxia is the constitutively expressed eNOS. NO production by eNOS (especially in vascular endothelial cells) during hypoxia and anoxia allows vasodilation, angiogenesis, and wound repair (Förstermann and Sessa, 2012; Gautier et al., 2006; Lei et al., 2021). It has also been shown that eNOS has protective effects in ischaemic brain injury and strokes (Mikula et al., 2009). Oxidation of L-arginine to NO by eNOS requires oxygen. Depending on the severity of hypoxia, there may be sufficient oxygen to allow eNOS to continue to oxidize L-arginine to NO. However, in acute hypoxia and anoxia, eNOS has nitrite reductase activity and can reduce nitrite into NO (Gautier et al., 2006; Vanin et al., 2007). This dual activity probably explains why eNOS was found to be the only NOS isoform capable of significant NO production from normoxia to anoxia (Mikula et

al., 2009). In sum, NO plays a central role in the regulation of the oxygen-sensing pathways and promotes hypoxia survival in plants and mammals.

1.6. Project objectives and aims

1.6.1. Investigating the crosstalk between hypoxia and immunity in Arabidopsis.

As outlined above, in nature, plants are confronted with a multitude of abiotic and biotic stresses, either sequentially or simultaneously. Although the last decades have led to major advances in the understanding of the molecular and biochemical mechanisms that underpin how plants respond to individual stresses, studies have also highlighted the limitations of this approach. Indeed, plant responses to combined stresses appear to be quite different from their respective individual stresses. In addition, previous stresses can affect how plants respond to future stresses with sequential stresses having both positive and antagonistic effects on plant survival (Atkinson and Urwin, 2012). Hence, investigating how combined stresses and the response to these stresses are integrated to trigger a specific output that promotes plant survival remains a key open question.

Hypoxia and immunogenic stresses frequently occur together. While much is known about the mechanisms by which plants sense and promote tolerance against either hypoxia or immunogenic factors, little is known about how hypoxia and the onset of the hypoxia response affect the ability of plants to trigger innate immunity and establish defence responses. Here, combined treatments of hypoxia and the PAMP flg22 were used to (1) determine whether hypoxia affected PTI; (2) the nature of the response to combined hypoxia/flg22; and (3) some of the molecular mechanisms underlying the crosstalk between hypoxia signalling and PTI.

Through the use of RNA sequencing (RNA-seq), it was aimed to characterise responses to individual and combined treatments of hypoxia and flg22 in Arabidopsis seedlings. This dataset would then allow exploration of the impact these stresses have on one another, with the objective to identify key pathways that are regulated by both stresses and what may lie at their intersection. The impact of hypoxia on diverse aspects of PTI - from signalling pathways (e.g. PRR expression and MAPK-phosphorylation) to downstream physiological responses (e.g. root growth, callose deposition) were also explored.

After establishing that there are interactions between hypoxia signalling and PTI, I asked if the N-degron pathway could mediate the crosstalk between hypoxia and PTI through its roles in NO signalling. To answer this question, mutants of Arabidopsis N-degron pathway enzymatic components and NO biosynthesis enzymes were characterized under combined hypoxia/flg22, as well as individual stresses.

1.6.2. Exploring the role of JA signalling in the crosstalk between hypoxia and PTI

Continuing the work detailed in 1.6.1., in the search for common mechanisms in plant hypoxia and immune responses which may regulate the crosstalk between hypoxia and immunity, the phytohormone JA was put forward as a potential point of intersection for these responses. As specified above, JA is one of the main immune hormones in plants which also has roles in responses to abiotic stresses including hypoxia. Some studies have suggested a role for JA in hypoxia: (i) JA levels have been shown to be induced early in hypoxia treatments (Arbona and Gómez-Cadenas, 2008; Shukla et al., 2020; Ullah et al., 2017; Yuan et al., 2017); (ii) JA responses have been shown to be responsible for hypoxia-induced root growth inhibition (Shukla et al., 2020) and (iii) JA has been implicated in mediating tolerance to re-oxygenation after hypoxia treatment (Yuan et al., 2017). However, uncovering the mechanisms underlying the role of JA in hypoxia responses requires further study. One possible connection between JA signalling and hypoxia responses could be through the N-degron pathway (deMarchi et al., 2016). Indeed, N-degron pathway mutants have reduced JA levels and JA signalling (deMarchi et al., 2016) however, the mechanism underlying this link is currently unknown. It was the aim of this work to investigate the mechanistic link between JA signalling, the N-degron pathway and hypoxia responses. One hypothesis tested was whether N-degron pathway mutants have an over-accumulation of the so-called JASMONATE ZIM-DOMAIN (JAZ) proteins, which play key roles in JA signalling. In the experiments carried out, one particular candidate, *JAZ8*, appeared to be linked to both the N-degron pathway and hypoxia, so that its putative function in hypoxia response was also investigated.

1.6.3. Exploring a potential role of the N-degron pathway in mammalian innate immunity.

Given the role of the N-degron pathway in the regulation of plant defences against pathogens (de Marchi et al., 2016; Gravot et al., 2016; Till et al., 2019; Vicente et al., 2019) and the high level of conservation of this protein degradation pathway across eukaryotes, I asked whether the N-degron pathway could also have roles in the regulation of mammalian innate immunity. Some recent studies have shown that the N-degron pathway has roles in the induction and suppression

of the inflammatory response in mammals (Chui et al., 2019; Leboeuf et al., 2020a; Sandstrom et al., 2019; Xu et al., 2019), however, further work is needed to characterise the role of the N-degron pathway in innate immune cells. In order to investigate this, I aimed to generate clustered regularly interspaced short palindromic repeats (CRISPR)/CRISPR associated 9 (Cas9) (CRISPR/Cas9)-mediated stable ATE1 KOs for the mouse innate immune cell line RAW264.7 macrophage and characterise the immune responses in these lines.

Chapter 2: Materials and Methods

2.1. Materials

2.1.1. Plant lines

Arabidopsis thaliana (Arabidopsis) Col-0 accessions (Table 2.1) and *Nicotiana benthamiana* (*N. benthamiana*) were used in this work.

Table 2.1. Arabidopsis lines used in studies.

Line	Description	Reference
Col-0	Wild-type Columbia-0 accession	
ate1ate2	SALK_023492 x SALK_040788	Graciet et al., 2009
prt6-1	SAIL-1278-H11	Garzón et al., 2007
prt6-5	SALK-051088	Graciet et al., 2009
rap2.2/3/12	SAIL_184_G12 x SAIL _1031_D10 x GK_503A1_11	Gibbs et al., 2014
hre1/2	SALK_039484 x SALK_052858	Gibbs et al., 2014
erfVII	Quintuple mutant for RAP2.2/3/12 and HRE1/2	Abbas et al., 2015
prt6-1rap2.2/3/12	Quadruple mutant for PRT6 and RAP2.2/3/12	Gibbs et al., 2014
prt6-1hre1/2	Triple mutant for PRT6 and HRE1/2	Gibbs et al., 2014
prt6-1erfVII	Sextuple mutant for PRT6 and ERFVIIs	Abbas et al., 2015
gsnor1-3	GK-315D11.03	Feechan et al., 2005; Lee et al., 2008
hb1 (pgb1-1)	SALK_058388	Hartman et al., 2019
noa1	SALK_047882	Guo et al., 2003
jaz1-1	SALK_011957C	Sharma et al., 2022

jaz8	SALK 200208c	This study
ate1ate2jaz8	Triple mutant for ATE1, ATE2 and JAZ8	This study
prt6-5jaz8	Double mutant for PRT6 and JAZ8	This study
Col-0 *FLS2pro:FLS2-3xmyc-GFP*	Agrobacterium containing FLS2-3xmyc-GFP expressed by FLS2 endogenous promoter transformed Col-0	Robatzek et al., 2006
Col-0 *35S:Met-Ala-HRE1-FLAG* lines #1.1; 5.2; 10.4	Col-0 was transformed with agrobacterium containing pKG35 (pML-BART *35S:Met-Ala)-HRE1-FLAG*) (Goslin, 2019) using the floral dip method.	A. Brazel
Col-0 *35S:Met-Ala-HRE2-HA*		Gibbs et al., 2011
Col-0 *35S:GFP-JAZ1*	Agrobacterium transformed Col-0 with *35S:GFP-JAZ1*.	Grunewald et al., 2009
Col-0 *35S:JAZ8-YFP*	Agrobacterium containing *35S:JAZ8-YFP* transformed Col-0	Shyu et al., 2012

2.1.2. Bacterial strains

The following bacterial strains (Table 2.2) were employed in these studies.

Table 2.2. Bacterial strains used in studies.

Strain	Genotype	Reference
Escherichia coli (*E. coli*) strain stbl2	F–, mcrA, Δ(mcrBC-hsdRMS-mrr), recA1, endA1, gyrA96, thi-1, supE44, relA1, λ-, Δ(lac-proAB)	Thermo Fisher

Agrobacterium tumefaciens (*A. tumefaciens*) strain C58 pGV2260		McBride and Summerfelt, 1990

2.1.3. Mammalian cell lines

Two different mammalian cell lines were used in this project (Table 2.3).

Table 2.3. Mammalian cell lines used in Chapter 5.

Cell Line	Description	Reference	Source
HEK293T	Human embryonic kidney cells immortalized using adenovirus and expressing the simian virus 40 (SV40) T-antigen.	DuBridge et al., 1987	Gifted from Marion Butler stocks.
RAW264.7	Mouse macrophage line immortalized using Abelson Leukemia Virus.	Raschke et al., 1978	Gifted from Eoin McNamee stocks.

2.1.4. Oligonucleotides

Oligonucleotides were designed for genes of interest and the OligoAnalyzer tool from IDT was used to verify oligonucleotide melting temperatures, as well as identify any predicted hairpin formation, self-dimerization and hetero-dimerization problems. Stock solutions of oligonucleotides were prepared in dH_2O at a concentration of 100 µM. Oligonucleotides designed for Arabidopsis line genotyping (Table 2.4, 2.5 and 2.6), RT-qPCR analysis (Table 2.7) and for the generation and screening of plasmid constructs (Table 2.8) are presented below.

Table 2.4. Oligos used for genotyping – wild type reactions.

Line	Oligo name	Sequence (5’ -> 3’)
ate1-2	At1	GTGCAGCCCAGGGAACAAAGAGGTG
	At2-3	GAGAGGAGATCAATGATAAACTAAGGCATAG
ate2-1	At3	GCGAAGCCGAGTGAGCAGACAGA

	At4-2	CCACAAAGAGGAATCTTTTCTTCATCATCAT
prt6-1 and *prt6-5*	At120	AAAATTGATCCTTTCCATGCC
	At121	CAACATAAGAATCTGCGGGAG
rap2.2-1	MS47	ATGACAACATTGGGATGCAAC
	MS48	TTTCTTGGCATATGCTGAACC
rap2.3-1	MS43	ATGTGTGGCGGTGCTATTATT
	MS44	TTACTCATACGACGCAATGAC
rap2.12-4	MS45	CTCAGCTGTCTTGAACGTTCC
	MS46	TGGCTACTCCTGAATGCAAAC
hre1	At482	GGTGAATAAGCCAACCATTACTATAGG
	At483	CTTCTTCAGCTGTGTTGAAAGTCC
hre2	MS41	AAGAAAGCGTTATGGTTCAAATG
	MS42	CGACGGTGTTTAGTGTGTTTG
hb1 (pgb1-1)	KD2	ATGAAGAGTTTGAGACCTAATTCAGC
	KD3	GTGATTGAAGATGGAGAAGCACG
gsnor1-3	BM117	TTTCTTCCTGCGTCAATGGC
	BM118	CACAGCCTCAAATTGATTCACTAA
	BM106	ATAATAACGCTGCGGACATCTACATTTT
noa1	KD70	AGATTATTGCACGGAAAGTTGTTGA
	KD71	ACCACCAACTGCTGTAATCATATGT
jaz1-1	KD77	TCTCAAACTGCACCATTGACTAT
	KD78	ACCTACCTACTAACTCATAATTCACG
jaz8	BM160-up	GCACAAATGTAAGTGTGGAAAA
	MS66	TTCAAAATCGATCTTCGGATG

Table 2.5. Oligos used for genotyping – TDNA reactions.

Line	Oligo name	Sequence (5’ -> 3’)
ate1-2	At1	GTGCAGCCCAGGGAACAAAGAGGTG
	LB2	CCAAACTGGAACAACACTCAACCCTATCTC
ate2-1	At3	GCGAAGCCGAGTGAGCAGACAGA
	LB2	CCAAACTGGAACAACACTCAACCCTATCTC
prt6-1	LB_SAIL	GCTTCCTATTATATCTTCCCAAATTACCAATACA
	At121	CAACATAAGAATCTGCGGGAG
prt6-5	LB2	CCAAACTGGAACAACACTCAACCCTATCTC

	At121	CAACATAAGAATCTGCGGGAG
rap2.2-1	MS47	ATGACAACATTGGGATGCAAC
	LB_SAIL	GCTTCCTATTATATCTTCCCAAATTACCAATACA
rap2.3-1	MS43	ATGTGTGGCGGTGCTATTATT
	LB_SAIL	GCTTCCTATTATATCTTCCCAAATTACCAATACA
rap2.12-4	MS45	CTCAGCTGTCTTGAACGTTCC
	GK8760	GGGCTACACTGAATTGGTAGCTC
hre1	LB2	CCAAACTGGAACAACACTCAACCCTATCTC
	At483	CTTCTTCAGCTGTGTTGAAAGTCC
hre2	MS41	AAGAAAGCGTTATGGTTCAAATG
	LB2	CCAAACTGGAACAACACTCAACCCTATCTC
hb1 (pgb1-1)	LB2	CCAAACTGGAACAACACTCAACCCTATCTC
	KD3	GTGATTGAAGATGGAGAAGCACG
gsnor1-3	BM118	CACAGCCTCAAATTGATTCACTAA
	BM106	ATAATAACGCTGCGGACATCTACATTTT
noa1	LB2	CCAAACTGGAACAACACTCAACCCTATCTC
	KD71	ACCACCAACTGCTGTAATCATATGT
jaz1-1	KD77	TCTCAAACTGCACCATTGACTAT
	LB2	CCAAACTGGAACAACACTCAACCCTATCTC
jaz8	LB2	CCAAACTGGAACAACACTCAACCCTATCTC
	MS66	TTCAAAATCGATCTTCGGATG

Table 2.6. Oligos used for genotyping – overexpression/tagged lines.

Line	Oligo name	Sequence (5’ -> 3’)
35S:JAZ8-YFP	KD7	GGTAGCTCAGGTAGTGGTTGTCG
	KD9	GCACCATCTTCTTCAAGGACGACG
35S:GFP-JAZ1	KD5	CGACCACATGAAGCAGCACGAC
	KD8	GCGGATCTTGAAGTTCACCTTGATGC
35S:ATE1-HA	qPCR126	TACAAGGAAATGCGGCAGATC
	qKD32-lo	AGAAGCGTAATCTGGAACGTCATA

Table 2.7. Oligos used for RT-qPCRs.

Oligo name	Gene	Sequence (5’ -> 3’)

qKD49 MON1_REF_up	*MON1*	AACTCTATGCAGCATTTGATCCACT
qKD49 MON1_REF_lo		TGATTGCATATCTTTATCGCCATC
qBM81-up	*HB1*	TGTCATGTGTTGTGAATCAGCAGTACA
qBM82-lo		GCCACCTCAAAGTGTTCGTCAAC
qPCRBM3-up	*WRKY33*	GGAGTGAACCTGAAGCAAAGAGATGGAA
qPCRBM4-lo		CGTTGTCTGCACTACGATTCTCGGC
qBM175-up	*BIK1*	CATGTCATCAGGTCACTTGAATGCAAG
qBM176-lo		CGGTCTGTTATGATCCAACGCTCG
qKG5	*ADH1*	AAGTACATGAACAAGGAGCTGGAGC
qKG6		TGGTGATGATGCAACGAATACTCTCTCC
qPCRBM25-up	*FLS2*	GCCAGCTAATATACTCCTTGACAGTGACC
qPCRBM26-lo		TTCCTCATATAAGCAAACTCTGGAGCTAAGT
qKD20-up	*EFR*	CTAGACGATGATCTGACTGCTCATGT
qKD20-lo		TTGCTGCCTCCACTGCTCGT
qPCRBM5-up	*MPK3*	CTGTTGAACAAGCTCTGAATCACCAGT
qPCRBM6-lo		GTGCTATGGCTTCTTGGTAGATCATCTC
PG-29	*MPK4*	CGCTTATGGAATTGTCTGTGCTGCT
PG-30		TCATTGAAGTTCTCTCTCTGCGGTGG
qBM49-up	*MPK6*	GCTCATAGGAACTCCATCAGAAGAAGAGC
qBM50-lo		GCCAATGCGTCTAAAACTGTGATTCTC
qBM31-up	*MYB51*	TTCACGGCAACAAATGGTCTGC
qBM32-lo		CCCTTGTGTGTAACTGGATCAATACCTTT
qBM29-up	*CYP83B1*	GCCATGATATTGGATATTGTTGTGCCG
qBM30-lo		CCTATCACACTCCTCACTTCGTCTTGA
qCQ2-up	*JAZ8-MYC*	GATGTTACCCATCTTCAGGCAAGATC
qKD33-lo		AAGTCCTCTTCAGAAATGAGCTT
qPCR5-up	*LOX2*	ACGGAGGTGGAATCATTGAGACTTGTT
qPCR6-lo		CGGTCTTATCTTCCTCAGCCAACC
Q-MS-19 REV	*VSP2*	CACGAGACTCTTCCTCACCTTTGACT
Q-MS-20-FWD		AAGCTGCTGGCGTGACCTAC
Q-MS-82	*ORA59*	CGCTTTGAAAGGCAGCCTCG
Q-MS-83		TCTAGGACGGTTTCTCATGGAGTGT
Q-MS-21-REV	*PDF1.2A*	ATGTCCCACTTGGCTTCTCGC
Q-MS-22-FWD		CTTTCGACGCACCGGCAATG

qKD55-up	*SEN4*	TCATATTGACCGTCGATGACACACC
qKD55-lo		TCTAGCTTGGCTTGTTGAATCCATTTCT
Q-MS-66	*JAZ1*	GGAATGTTCTGAGTTCGTCGGTAGC
Q-MS-67		CTCATGGTTGTTGTCGGCTGACG
qKD24-up	*JAZ3*	ACGGTTCCTCTATGCCTCAAGTCTT
qKD24-lo		CCAGAGGTAATGCCACTGTTGGA
qCQ2-up	*JAZ8*	GATGTTACCCATCTTCAGGCAAGATC
qCQ2-lo		CGTGAATGGTACGGTGAAGTAGCTTG
qKD8-up	*SUS1*	GGTGTCACTCAGTGTACCATTGCTC
qKD8-lo		AGCTCCTCGATCTCAGAGTGGAAC
qBM73-up	*HRE2*	CCGTCTCAGTGAGTGAAGAAAGAGATGG
qBM74-lo		CTCCGCTGCCCATTTGCC
qBM71-up	*HRE1-FLAG*	GCTTCAGGCTCAGCATCAGATGG
KG76		CGTCATCATCCTTATAGTCtgcg
qBM73-up	*HRE2-HA*	CCGTCTCAGTGAGTGAAGAAAGAGATGG
qKD32-lo		AGAAGCGTAATCTGGAACGTCATA

Table 2.8. Oligos used for cloning and screening plasmid constructs.

Oligo name	Sequence (5’ -> 3’)	Description
KD40	ACTATCATATGCTTACCGTAACTTGA	Forward primer in U6 promoter to validate + sequence LentiCRISPRv2
KD41	CTTAGGAACAAGTGGTGGAGT	Reverse primer in LentiCRISPRv2 in ~2 kb region cut out by *Bsm*BI
KD42	TTCATGCAGGATCAAATTCTGG	Forward primer in LentiCRISPRv2 in ~2 kb region cut out by *Bsm*BI
KD43	GGACTAGCCTTATTTTAACTTGCTAT	Reverse primer in gRNA scaffold of LentiCRISPRv2
KD44	ACCGTATATAAGTGCAGTAGTCG	Forward primer in EF-1a core promoter of LentiCRISPRv2
KD45	TGGTGTATCTTCTTCTGGCG	Reverse primer at 200 bp in Cas9 of LentiCRISPRv2

KD46	AGTGCTGTCCGCCTAC	Forward primer at 3867 bp in Cas9 of LentiCRISPRv2
KD47	AGCCTGTCCAGCCTTC	Reverse primer in NLS of LentiCRISPRv2
KD76	TTCTTGCAGCTCGGTGA	Reverse primer in puromycin resistance gene of LentiCRISPRv2. To be used with KD46.
CB431 (Kasu et al., 2018)	CACCGTATCAGGATCTTATAGACCG	Forward primer to be used with CB432 to generate double-strand oligomer = gRNA for MsATE1 (exon 2)
CB432 (Kasu et al., 2018)	AAACCGGTCTATAAGATCCTGATAC	Reverse primer to be used with CB431 to generate double-strand oligomer = gRNA for MsATE1 (exon 2)
KD50	caccgGCGAGGTATTCGGCTCCGCG	Forward primer to be used with KD51 to generate ctrl double-strand oligomer that doesn't target mouse genome = non-targeting gRNA (NTC1)
KD51	aaacCGCGGAGCCGAATACCTCGCc	Reverse primer to be used with KD50 to generate ctrl double-strand oligomer that doesn't target mouse genome = non-targeting gRNA (NTC1)
KD52	caccgACCCATCCCCGCGTCCGAGA	Forward primer to be used with KD53 to generate ctrl double-strand oligomer that doesn't target mouse genome = non-targeting gRNA (NTC2)
KD53	aaacTCTCGGACGCGGGGATGGGTc	Reverse primer to be used with KD52 to generate ctrl double-strand oligomer that doesn't

		target mouse genome = non-targeting gRNA (NTC2)
KD59	TGACTCCACCATCTGACTCCACAT	Forward primer to be used with KD65 to do T7 endonuclease I assay to screen for ATE1 KO (heteroduplex DNA)
KD65	AGAATATCCTGAGGGCAATTCTCACT	Reverse primer to be used with KD59 to do T7 endonuclease I assay to screen for ATE1 KO (heteroduplex DNA)
KD12	tctagaATGTCGAGTTCTATGGAATG	Forward primer to clone JAZ1 into pBJ36 (add XbaII restriction site (tctaga)) used with KD14 and KD19.
KD19	cttcagaaatgagcttttgctcgcctgatccTATTTCAGCTGCTAAACC	Reverse primer to clone JAZ1 into pBJ36 (and be used in conjunction with KD12 and KD14 to add a myc tag to JAZ1)
KD14	TCTAGATCACAAGTCCTCTTCAGAAATGAGCTTTTGC	Reverse primer to clone JAZ1 into pBJ36 (and be used in conjunction with KD12 and KD19 to add a myc tag to JAZ1)
KD15	tctagaATGAAGCTACAGCAA	Forward primer to clone JAZ8 into pBJ36 (add XbaII restriction site (tctaga)) used with KD20.
KD20	ttgctcgcctgatccTCGTCGTGAATGGTACG	Reverse primer to clone JAZ8 into pBJ36 (and be used in conjunction with KD15 to add a myc tag to JAZ8)

KD17	TCTAGaTTAcaagtcctcttcagaaatgagcttttgctcgcctgatcc	Reverse primer to clone JAZ8 into pBJ36 (and be used in conjunction with KD15 to add a myc tag to JAZ1)
KD21	TTCTGAGTTCGTCGGTAGC	Forward primer to check JAZ1-myc construct in pJET and pBJ36 by using with pJET1.2 rev and 3'ocs_lo, respectively
KD22	aTCAcaagtcctcttcagaa	Reverse primer to check JAZ1-myc construct in pJET and pBJ36 by using with pJET1.2 fw and 35S_up, respectively
KD23	AATTGTGACTTGGAACTTCGTCT	Forward primer to check JAZ8-myc construct in pJET and pBJ36 by using with pJET1.2 rev and 3'ocs_lo, respectively
KD24	ATGGTACGGTGAAGTAGCTTGAA	Reverse primer to check JAZ8-myc construct in pJET and pBJ36 by using with pJET1.2 fw and 35S_up, respectively.
35S-up	GAAAAAGAAGACGTTCCAACCAC	Oligo to sequence for presence of inserts in plasmids with 35S promoters.
3’ocs-lo	GGTAAGGATCTGAGCTACACATGCTC	Reverse oligo in 3’ocs for sequencing.
pJET1.2 fw	CGACTCACTATAGGGAGAGCGGC	Thermo Fisher
pJET1.2 rev	AAGAACATCGATTTTCCATGGCAG	Thermo Fisher

2.2. Methods

2.2.1. Plant techniques

2.2.1.1. Plant growth conditions

Arabidopsis and *N. benthamiana* plants were grown on autoclaved soil comprising 5:3:2 ratio of compost:vermiculite:perlite in 4-cell pots. For MeJA treatment experiments, Arabidopsis was grown for 4-weeks on Jiffy pots (section 2.2.8.1.). For experiments requiring sterile conditions, seedlings were grown in Petri dishes containing 0.5x Murashige and Skoog (MS) medium (pH 5.7) and 6 g/L agar with 0.5% sucrose (w/v). Seeds were sterilized as described in section 2.2.1.2. before sowing. Trays or plates were stratified at 4°C for 3 days before transferring to growth rooms.

2.2.1.2. Seed sterilization

Arabidopsis seeds were sterilized according to the vapor-phase sterilization method (Lindsey III et al., 2017). Briefly, an aliquot of seeds, transferred to an Eppendorf tube and tubes with lids open, were placed in a dessicator in a fume hood. A beaker with 100 mL of bleach was placed in the dessicator. 3 mL of 37% HCl was added to the bleach. The dessicator was closed and seeds were sterilized for 3 hours. Sterilized seeds were then sown on the same day.

2.2.2. Microbiology techniques

2.2.2.1. Bacterial growth media

E. coli and *A. tumefaciens* were grown on LB medium (1% (w/v) tryptone, 0.5% (w/v) yeast extract, 1% (w/v) NaCl) in liquid culture or on LB media supplemented with 15 g/L agar for plates. Appropriate antibiotics were added to select for the strain and/or plasmids. *E. coli* cells were grown at 37°C. *A. tumefaciens* was grown at 28°C.

2.2.2.2. Preparation of *E. coli* competent cells

Competent stbl2 *E. coli* cells were produced following the protocol outlined in Inoue et al., 1990. A loopful of stbl2 glycerol stock was streaked onto an LB plate and incubated at 37°C overnight. A loopful of the stbl2 cells from this LB plate were used to inoculate 2 mL of LB liquid medium and this was incubated with constant shaking (200-250 rpm) at 37°C overnight. 200 µL of this starter culture was added to 250 mL SOB medium (2% (w/v) tryptone, 0.5% (w/v) yeast extract, 0.05% (w/v) NaCl, 10 mM $MgSO_4$, 10 mM $MgCl_2$). Cells were grown on a shaker (200-250 rpm) at 18-20°C until the culture density achieved an OD_{600} of 0.7. The culture was then placed on ice. The cooled culture was transferred to a sterile centrifuge flask and spun down at 4,000xg for 10 minutes at 4°C. The supernatant was discarded, and the cell pellet was resuspended in 80 mL of ice-cold transformation buffer (TB) (10 mM PIPES/KOH pH 6.7, 15 mM $CaCl_2$, 250 mM KCl, 55 mM $MnCl_2$). The cells were centrifuged (4,000xg for 10 minutes at 4°C), the supernatant was discarded, and the pellet was resuspended in 20 mL TB. DMSO was added to a final concentration of 7% (v/v) with constant swirling. Cells were incubated on ice for 10 minutes and 100 – 500 µL aliquots were made-up. Aliquots were frozen in liquid nitrogen and stored at 80°C.

2.2.2.3. Transformation of *E. coli*

Transforming competent stbl2 cells with plasmid DNA or ligation reaction was done using heat shock. A 10 µL ligation reaction or a volume containing ~5 ng plasmid DNA was added to 100 µL of stbl2 competent cells. After gentle mixing, the cells were transferred to 42°C for 1 minute. The transformed cells were then incubated on ice for 1-5 minutes. 1 mL of LB medium was added, and the transformation reaction was incubated at 37°C for 1 hour. For plasmid transformation, a 100 µL aliquot was directly plated on LB agar with appropriate antibiotic(s). For ligation reaction transformation, the transformation reaction was spun down (≥ 14,000 rpm for 1 minute), 700-800 µL of supernatant was discarded, the pellet was resuspended and 100 µL aliquot was pipetted onto LB agar plate with appropriate antibiotic(s).

2.2.2.4. Transformation of *A. tumefaciens*

A 100 µL aliquot of *A. tumefaciens* C58 pGV2260 was thawed at room temperature and added to a cryotube containing 2-5 µL of plasmid. The cells were placed in liquid nitrogen for 5 minutes and were subsequently thawed at room temperature, followed by addition of 1 mL LB medium and incubation at 28°C for 4 hours. The cells were pelleted by centrifuging at 4,000 rpm for 5 minutes at room temperature. 500 µL of supernatant was removed and the cells were

resuspended in the remaining supernatant. A 100 µL aliquot was pipetted onto a LB agar plate with appropriate antibiotics. Glycerol stocks were made by inoculating a 2 mL aliquot of LB medium with appropriate antibiotics with a colony from the LB agar plate and incubating with constant shaking (200-250 rpm) overnight. 500 µL of the overnight culture was added to 500 µL 50% glycerol in a cryotube. The stock was mixed and placed in liquid nitrogen. The glycerol stocks were stored at -80C.

2.2.3. Mammalian cell techniques

2.2.3.1. Cell culture

HEK293T cells were cultured using growth medium containing Dulbecco's Modified Eagle's Serum (DMEM) - high glucose (Sigma), 10% foetal bovine serum (FBS), and 2 mM L-glutamine.

RAW264.7 cells were cultured using growth medium containing DMEM - high glucose, 10% FBS, and 1% Penn/Strep (penicillin/streptomycin).

Growth medium for each cell line was changed every two days. Cells were generally grown in T25 and T75 flasks and treated in 6- or 96- well plates and cells were split upon reaching 70% confluency.

2.2.3.2. Splitting cells

HEK293T cells were rinsed with phosphate buffered saline (PBS) and 1x trypsin was added until all adherent cells had lifted from bottom of well/flask. Growth medium was added to neutralize the trypsin. Cells were diluted 1:10 into new plates/flasks.

RAW264.7 cells were resuspended through the use of a cell scraper. Cells were pipetted up and down to remove cell clumps. Cells were split 1:3 into new plates/flasks.

2.2.3.3. Freezing down stocks

Upon reaching ~70% confluency, cells were split as usual. Cells were counted using a hemocytometer and an appropriate volume of cell suspension was spun down to ensure 2 million cells per vial. Growth medium was removed and freezing solution (90% FBS, 10% DMSO) was used to resuspend cells. Cells were aliquoted into cryotubes and placed in a Mr. Freezy at -80°C overnight. Cells were stored in a box in -80°C.

2.2.3.4. Transformation of HEK293T cells for lentiviral production

HEK293T cells were seeded into a 6 well plate ($7.5x10^5$ cells per well) the night before and incubated at 37°C, 5% carbon dioxide. The following day, growth medium was aspirated and replaced with medium containing 25 µM chloroquine diphosphate. Cells were incubated for 5 hours at 37°C, 5% carbon dioxide. A 1:1:1 mixture of the packaging (psPAX2), envelope (pMD2.G) and targeting (pKD11; pKD12; or pKD13) plasmids (Table 2.9.) was prepared. At the same time, a solution of OptiMEM and Lipofectamine2000 was mixed and incubated at room temperature for 5 minutes. The two solutions were combined and incubated at room temperature for 20 minutes before adding to the cells. The cells were incubated overnight at 37°C, 5% carbon dioxide. The medium was changed the next day. On the second day, lentivirus was harvested by collecting the cell medium. The lentiviral supernatant was centrifuged (405xg for 5 minutes) 2-3 times to pellet and remove any HEK293T cells. The lentivirus supernatant was collected in 50 mL falcon tubes and stored at -20°C.

Table 2.9. Plasmids used for lentiviral production.

Plasmid number	Plasmid name	Description	Source
	psPAX2	Packaging plasmid	Gifted by Dr. Marion Butler (MU)
	pMD2.G	Viral envelope plasmid	Gifted by Dr. Marion Butler (MU)
	LentiCRISPRv2	Lentiviral backbone containing Cas9, guide RNA scaffold, and puromycin resistance gene.	Sanjana et al., 2014

pKD11	ATE1 gRNA LentiCRISPRv2	CB431 and CB432 oligos were made into double stranded oligomers using T4 ligation buffer and were heated in thermocycler at 95°C for 5 minutes and allowed to cool in the block for 2 hours. LentiCRISPRv2 was digested with *Bsm*BI for 6 hours at 37°C. Double stranded oligomer was ligated into *Bsm*BI-digested LentiCRISPRv2.	This study
pKD12	NTC1 gRNA LentiCRISPRv2	KD50 and KD51 were used to generate double stranded oligomer for non-targeting gRNA insert into *Bsm*BI-digested LentiCRISPRv2.	This study
pKD13	NTC2 gRNA LentiCRISPRv2	Similar to pKD13 but KD52 and KD53 oligos were used to generate the non-targeting gRNA insert.	This study

2.2.3.5. Lentiviral transduction

The lentiviral transduction method was based on a protocol in Giuliano et al., 2019. RAW264.7 cells ($1.5x10^5$ per well) were seeded into a 6-well plate the day before lentiviral transduction, so they would be 50% confluent. Growth medium was aspirated and replaced with fresh medium

supplemented with 8 µg/mL polybrene and an appropriate concentration of lentivirus (0 (untreated), 1:10, 1:100, 1:1000, 1:10,000). Cells were incubated overnight at 37°C, 5% carbon dioxide. The medium was then removed and replaced with fresh growth medium supplemented with 5 µg/mL puromycin to select transduced cells. Puromycin selection was carried out until untreated cells were all dead. Puromycin-resistant lentiviral transduced cells were grown and stocks were frozen as described in Section 2.2.3.3.

2.2.4. Molecular biology methods

2.2.4.1. Genomic DNA extraction from Arabidopsis

Genomic DNA was extracted from plants based on the protocol from (Edwards et al., 1991). Briefly, plant tissue was ground in lysis solution (200 mM Tris-HCl pH 7.5-8.0, 250 mM NaCl, 25 mM EDTA, 0.5% (w/v) SDS) and plant debris were spun down. Isopropanol was added to the supernatant in a 1:1 (v/v) ratio and spun down. The pellet was rinsed with 70% ethanol and allowed to air-dry. 70-100 µL dH_2O was added. Genomic DNA was stored at -20°C.

2.2.4.2. Genomic DNA extraction from mammalian cells

Cells were grown in 96 well plates to over-confluence. Genomic DNA was extracted using a protocol adapted from the McManus lab website (https://mcmanuslab.ucsf.edu/protocol/dna-isolation-es-cells-96-well-plate). The medium was aspirated and cells were washed twice with PBS followed by the addition of 50 µL Bradley lysis buffer (10 mM Tris HCl (pH 8), 10 mM EDTA, 0.5% SDS, 10 mM NaCl, 1 mg/mL proteinase K) to each well and incubation overnight at 60°C in a humidified oven. The plate was removed from the oven and allowed to cool to room temperature. Ice cold DNA precipitation solution (98.5% ethanol, 7.5 mM NaCl) was added and incubated for 30 minutes at room temperature. The DNA was pelleted by centrifugation (3,000 rpm for 10 minutes at room temperature). The DNA pellet was rinsed twice using 70% ethanol and the pellet was air-dried. The genomic DNA was resuspended in warm TE buffer (10 mM Tris-HCl, pH 8, 1 mM EDTA, pH 8) and incubated at 56°C for 10 minutes and stored at -20°C.

2.2.4.3. DNA extraction from *E. coli*

Plasmid DNA was extracted from *E. coli* with the use of the E.Z.N.A. plasmid mini kit (Omega Bio-Tek) and stored at -20°C.

2.2.4.4. T7 endonuclease I assay

To determine the presence of heteroduplex DNA, a 300-600 bp genomic DNA region containing CRISPR-Cas9 targeted region was amplified by PCR. Two reactions were set up to reanneal the PCR products (using the thermocycler program: 95°C for 5 minutes, then sample left in block to cool for 2 hours). After reannealing, T7 endonuclease I (NEB) was added to one of the reactions, while dH_2O was added to the other. The samples were returned to the thermocycler at 37°C for 20 minutes. The endonuclease reaction was stopped by adding 0.5M EDTA to a final concentration of 0.02M EDTA and samples were loaded on a 3% agarose gel to visualize bands.

2.2.4.5. RNA extraction from plants

Frozen plant tissue was ground on liquid nitrogen and RNA was extracted using the protocol and solutions from the Spectrum Total RNA Kit (Merck). RNA concentration and quality (260/230 = 2.0-2.2 and 260/280 ≈ 2.0 values) were determined using a nanodrop (DeNovix). RNA samples were stored at -80°C.

2.2.4.6. RT-qPCR

1 µg of RNA extracted according to 2.2.4.5. was reverse transcribed to cDNA by adding a reverse transcription mastermix of RevertAid Reverse Transcriptase (Thermo Fisher), RiboLock RNase inhibitor (Thermo Fisher), oligo(dT)18 (IDT) and 1 mM dNTP mixture and placing in a thermocycler at 42°C for 45 minutes. cDNA was diluted 1:1 with nuclease-free dH_2O. To each well of a LightCycler 480 96-well plate (Roche), 10 µL of reaction mixture comprising: 1 µL of this diluted cDNA, 1 µL of a primer pair mixture (1 µM final concentration each primer), 5 µL 2X SYBR green master mix (Roche) and nuclease-free water was added. A LightCycler 480 instrument (Roche) was used for qPCR. Crossing point (Cp) values were retrieved by the LightCycler 480 software which determined the Cp values based on the Absolute Quantification/Second Derivative Maximum method. Using the delta Ct method, gene expression was normalized to a reference gene according to the following calculation ($Cp_{reference\ gene} - Cp_{gene\ of\ interest}$ = deltaCp). For Arabidopsis samples, the reference gene used was *MON1* (AT2G28390). For *N. benthamiana*

samples, the reference gene used was *EF-1α*. The relative expression was determined as $2^{deltaCp}$ based on the assumption that the PCR products double each cycle. Microsoft Excel and GraphPad Prism were used to calculate, graph, and conduct statistical analyses on the relative expression values.

2.2.4.7. RNA-Seq and bioinformatic analysis

This section has been directly taken from Mooney et al., 2024.

For the RNA-seq experiment, samples from three biological replicates were sent for sequencing. Nine-day old seedlings (grown under continuous light conditions at 20°C) were transferred to 0.5xMS liquid medium in 35 mm x 10 mm dishes and placed on a shaker at 120 rpm overnight in continuous light. On day 10, seedlings were treated +/- hypoxia (anaerojars) +/- 100 nM flg22 (mock = dH_2O) for 1 hour. Seedlings were collected on liquid nitrogen. Total RNA was extracted as described in 2.2.4.5. and RNA integrity was assessed using an Agilent 2100 Bioanalyzer (Agilent). All RNA samples had RNA integrity (RIN) values >7.0. Library preparation and paired-ended 100 bp next-generation sequencing was performed by BGI (Hong Kong) using the BGI-seq PE100 platform. Data processing was carried out by BGI using the filtering software SOAPnuke (including removal of reads containing the adaptor; removal of reads whose N content is greater than 5%; and removal of low-quality reads). The Hierarchical Indexing for Spliced Alignment of Transcripts (HISAT) software was then used for mapping clean reads to the reference genome. Differential gene expression was determined using DESeq2. Cut-offs of adj. p-value<0.05 and $|\log_2(\text{fold-change})|>0.585$ were applied to determine differentially expressed genes (DEGs). Significant enrichment analysis of GO function on DEGs was carried out using the BiNGO plug-in in Cytoscape (Maere et al., 2005) or the ShinyGO GO enrichment analysis software (Ge et al., 2020). Overlap between datasets was determined using InteractiVenn (Heberle et al., 2015), and statistical significance of the overlap between datasets was calculated using http://nemates.org/MA/progs/overlap_stats.html.

RNA-seq data have been deposited with the Gene Expression Omnibus (GEO) repository (at http://www.ncbi.nlm.nih.gov/) under GSE246848.

2.2.5. Biochemical methods

2.2.5.1. Transient protein expression in *N. benthamiana*

A. tumefaciens C58 pGV2260 was transformed (according to protocol 2.2.2.4) with pML-BART backbone plasmids listed in Table 2.10 which contained the tagged proteins of interest, including ATE1-HA6, ATE2-HA6, JAZ8-MYC and JAZ1-MYC under the control of the constitutive cauliflower mosaic virus (CaMV) 35S promoter. Glycerol stocks were streaked out on LB agar plates supplemented with 50 mg/L rifampicin, 100 mg/L carbenicillin, 100 mg/L spectinomycin and the bacteria were grown for 2 days at 28°C. 2 mL of infiltration solution medium (10 mM MES pH5.5, 10 mM $MgCl_2$, 150 µM acetosyringone) was used to lift the bacterial cells into solution. The bacterial suspension was diluted with infiltration solution to an OD_{600} of 0.8 for all constructs, except 35:ATE1-HA6 and 35S:JAZ1-MYC, which were diluted to an OD_{600} of 0.3 and 1.0, respectively. The night before agroinfiltration, 4–5-week-old *N. benthamiana* plants grown in continuous light (20°C) were watered heavily to promote opening of stomata. A blunt 1 mL syringe was used to infiltrate the bacterial suspensions into *N. benthamiana* leaves. Plants were returned to continuous light (20°C) for 2 days. After the 2 days, infiltrated leaves were collected and frozen in liquid nitrogen. Tissue was harvested, frozen in liquid nitrogen and stored at -80°C until RNA and/or protein extraction.

Table 2.10. Plasmids used to transform *A. tumefaciens* for transient protein expression in *N. benthamiana.*

Plasmid number	Plasmid name	Description	Source
pEG345	pML-BART 35S:ATE1-HA6	Plasmid generated by E. Graciet	E. Graciet
pEG346	pML-BART 35S:ATE2-HA6	Plasmid generated by E. Graciet	E. Graciet
pKD14	pJET JAZ1-MYC	Using a cDNA library and primers KD12, KD19 and KD14, PCR was used to amplify the *JAZ1* coding sequence, add a C-terminal MYC-tag and	This study

		*Xba*I restriction sites. The PCR product was blunt cloned into pJET.	
pKD30	pBJ36 35S:JAZ1-MYC	The *JAZ1-MYC* sequence was digested out of pKD14 using *Xba*I/*Xho*I. The fragment of interest was blunted using T4 DNA polymerase and ligated into *Sma*I-digested and dephosphorylated pBJ36-35S.	This study
pKD32	pML-BART 35S:JAZ1-MYC	pKD30 was digested with *Not*I to clone the 35S:JAZ1-MYC fragment into *Not*I digested and dephosphorylated pML-BART. This plasmid was used for *A. tumefaciens* transformation.	This study
pKD15	pJET JAZ8-MYC	Two sequential PCR reactions were run using an Arabidopsis cDNA library to add a MYC tag and cloning *Xba*I restriction sites to the *JAZ8* coding sequence. Specifically, the first PCR was run using primers	This study

		KD15/KD20 and the product was used in a 2nd PCR with KD15/KD17. The PCR product was then ligated into pJET.	
pKD16	pBJ36 35S:JAZ8-MYC	pKD15 was digested with *Xba*I and the JAZ8-MYC insert was cloned into the *Xba*I-digested and dephosphorylated pBJ36-35S plasmid.	This study
pKD29	pML-BART 35S:JAZ8-MYC	pKD16 was digested using *Not*I to clone the 35S:JAZ8-MYC fragment into *Not*I digested and dephosphorylated pML-BART. This construct was used for *A. tumefaciens* transformation.	This study

2.2.5.2. Nuclei extraction for co-immunoprecipitation (co-IP)

All steps, unless explicitly stated, were conducted at 4°C. Diagenode Plant ChIP kit reagents for extraction of the soluble nuclear protein fraction were supplemented with 1:100 plant protease inhibitor cocktail (Sigma) and 5 mM ß-mercaptoethanol as specified by the manufacturer's instructions. 1 g of *N. benthamiana* agroinfiltrated leaves (see section 2.2.5.1) was ground using a cooled mortar and pestle in 4 mL extraction buffer 1. The extract was filtered through miracloth twice. 100 µL of this extract was kept to load on an SDS-PAGE gel as a 'total protein' fraction. The extract was centrifuged (1,000xg for 20 minutes) and 100µL of the supernatant was kept to load

on an SDS-PAGE gel as the 'cytosol' fraction. The pellet (nuclei fraction) was washed by adding 1.5 mL extraction buffer 2, resuspending the pellet by gentle shaking and spinning down (1,000xg for 10 minutes) 5 times. The pellet was then washed once with 1.5 mL extraction buffer 3 similar as indicated above. The pellet was then resuspended in 100 µL co-IP buffer (50 mM Tris-HCl, pH 7.5, 100 mM NaCl, 10% (v/v) glycerol, 0.1% Tween-20) supplemented with 1 mM PMSF and 1:100 plant protease inhibitor cocktail (Sigma)). The samples were sonicated using the Bioruptor (Diagenode) for 10 cycles of 30 seconds ON/30 seconds OFF. Sonicated samples were transferred to 1.5 mL Eppendorf tubes and centrifuged (12,000xg for 10 minutes). The soluble nuclear fraction in the supernatant was collected for co-IP and 20 µL was set aside for SDS-PAGE. The pellet (insoluble nuclear fraction) was resuspended in 2xSDS loading dye to extract insoluble proteins for the SDS-PAGE gel. 2xSDS loading dye was also added 1:1 to the samples collected above for loading on the SDS-PAGE gel including total protein, cytosolic protein, soluble nuclear fraction. These proteins were all denatured by boiling at 95°C for 5 minutes before running on an SDS-PAGE gel.

2.2.5.3. Co-IP using anti-HA resin

All steps, unless explicitly stated, were conducted at 4°C. Before performing the co-IP, the soluble nuclear fraction extracted from *N. benthamiana* leaves transiently expressing ATE1-HA6 and the fraction extracted from JAZ8-MYC expressing leaves were mixed together 1:1 and left on ice for 1 hour. A 20 µL aliquot was taken as the 'input' fraction and 2xSDS loading dye was added and the protein sample was boiled. Remaining ATE1-HA and JAZ8-MYC mixture (as well as empty vector (EV; pML-BART) and JAZ8-MYC alone controls) were added to a 30 µL aliquot of anti-HA resin (Sigma #E6779) which had been previously equilibrated with co-IP buffer (50 mM Tris-HCl, pH 7.5, 100 mM NaCl, 10% (v/v) glycerol, 0.1% Tween-20). The volume added to the resin was topped up to 750 µL using co-IP buffer and this was incubated at 4°C with constant rotation. The resin was centrifuged (8,200xg for 30 seconds) and the supernatant was collected for the 'flow through' fraction and 2xSDS loading dye was added and the protein was denatured by boiling. The resin was washed by adding 750 µL co-IP buffer, vortexing the sample and incubating it at 4°C with constant rotation. The resin was centrifuged (8,200xg for 30 seconds) and the supernatant was collected as the 'wash' fraction and 2xSDS loading dye was added and the protein was boiled. This was repeated a further two times. 50 µL 2xSDS loading dye was added to the resin and it was boiled at 95°C for 5 minutes to denature the protein and was centrifuged at 8,200xg for 30 seconds. The supernatant 'elution' fraction was collected.

2.2.5.4. Protein extraction from Arabidopsis seedlings

Frozen tissue was ground on liquid nitrogen, samples were quickly weighed and protein extraction buffer (2xSDS loading dye) was added to the ground tissue in a 1:1 volume (µL):weight (mg) ratio. The tissue was mixed and protein samples were then denatured by heating at 95°C for 5 minutes, followed by centrifugation at ≥14,000xg for 10 minutes at room temperature. The protein lysate was transferred to a fresh tube and protein was quantified using the amido black protein quantification method (Popov et al., 1975; Schaffner and Weissmann, 1973).

2.2.5.5. Immunoblots

This section has been directly taken from Mooney et al., 2024.

Protein samples were loaded on a SDS-PAGE gel and run through the gel using 1x running buffer (25 mM Tris base, 192 mM glycine, 0.1% SDS, pH 8.3) at 60 volts through the stacking gel and 120 volts through the separating gel.

Separated proteins were transferred to PVDF membrane. Equal protein loading was assessed through Ponceau S staining (0.4% (w/v) Ponceau S, 10% (v/v) acetic acid in water) of the PVDF membrane. After removal of Ponceau staining, the membrane was blocked with 5% milk in PBS-T or TBS-T (containing 0.05% (v/v) Tween-20). Blots were incubated overnight at 4°C with appropriate primary antibody (listed in table 2.11) with constant rotation. Blots were washed with PBS-T or TBS-T for 3 x 5 minutes before and after incubation of blots with appropriate secondary antibody (listed in table 2.12) for 2 hours at room temperature. WesternBright ECL substrate (Advansta) was used and immunoblots were imaged using the G:BOX gel documentation system and the GeneSys software.

Table 2.11. Primary antibodies used for immunoblots.

Antibody	Serial ID	Dilution
Anti-MAPK-phosphorylation (Phospho-p44/p42)	Cell Signalling #4370S	1:2,000
Anti-GFP	Merck #1181446001	1:1,000
Anti-eGFP/eYFP	Abcam #Ab290	1:2,500

Anti-HA (mouse)	Merck #H3663	1:4,000
Anti-HA (rabbit)	Invitrogen #71-5500	1:3,000
Anti-MYC (mouse)	Merck #M5546	1:1,500
Anti-MYC (rabbit)	Merck #PLA0001	1:5,000

Table 2.12. Secondary antibodies used for immunoblots.

Antibody	Serial ID	Dilution
Anti-rabbit HRP	Merck #A0545	1:50,000
Anti-mouse HRP	Merck #A9044	1:10,000

2.2.6. Plant immune response assays

2.2.6.1. Flg22 growth and root inhibition assays

This section has been directly taken from Mooney et al., 2024.

Seedlings were grown on 0.5xMS agar plates supplemented with 0.5% sucrose in continuous light at 20°C.

For seedling growth inhibition assays: individual 5.5-day old seedlings were transferred to one well of a 48-well plate containing 1 mL of liquid 0.5xMS medium supplemented with 100 nM flg22 (or equivalent volume of water (mock). For each condition and genotype, 8 seedlings were used in a given biological replicate. Seedlings were then grown with mild shaking (120 rpm) in continuous light (20°C) for 7 days. All 8 seedlings for a given genotype and condition were harvested, dried on a paper towel and weighed together.

For root growth inhibition assays: 5.5-day old seedlings were transferred to 0.5xMS with 1% agar plates that contained either a mock solution (water) or 500 nM flg22 and grown vertically for 3 days in continuous light (20°C). Root elongation during this 3-day period was measured using Image J (Schneider et al., 2012).

For root growth inhibition assays under combined hypoxia/flg22: 5.5-day old seedlings were transferred to 0.5xMS with 1% agar plates that contained either a mock solution (water) or 500 nM flg22, followed by vertical growth in short-day conditions (8 hours light; 16 hours dark) for 48 hours under normal oxygen conditions. Hypoxia treated seedlings were kept at 0.5% oxygen (applied using PhO2X Box (Baker Ruskinn)); plates kept vertical) for 48 hours in short day conditions. Normoxia-treated seedlings were kept under normoxic and short-day conditions for 48 hours. After this 48-hour hypoxia/normoxia treatment, all seedlings were kept vertical for an additional 3 days in short-day conditions and normoxia (i.e. recovery period). Root elongation during the 3-day recovery period was determined using ImageJ.

2.2.6.2. Determining levels of FLS2 protein and MAPK-phosphorylation after flg22 treatment

This section has been directly taken from Mooney et al., 2024.

Seedlings grown on 0.5xMS agar plates supplemented with 0.5% sucrose for 9 days in continuous light (20°C) were transferred to 3 mL 0.5xMS liquid medium in 35 mm x 10 mm dishes so that there were 10-15 seedlings per genotype per treatment in each dish. These dishes were returned to continuous light on a shaker at 120 rpm overnight. On day 10, seedlings were treated +/- 100 nM flg22 (mock: PBS) +/- hypoxia in anaerojars (normoxia: ambient oxygen levels) for 30 minutes for MAPK-phosphorylation immunoblots and 1 hour for FLS2-GFP immunoblots. Seedlings were collected on liquid nitrogen and protein was extracted as specified in section 2.2.5.4. 30 µg of protein was loaded per well on 12% SDS-PAGE gels for MAPK-phosphorylation immunoblots, and 100 µg of protein was loaded per well on 10% SDS-PAGE gels for FLS2-GFP immunoblots. The protocol for immunoblotting described in section 2.2.5.5. was followed.

2.2.6.3. Callose deposition

This section has been directly taken from Mooney et al., 2024.

Seedlings were grown on 0.5xMS agar with 0.5% sucrose plates for 9 days under short-day light conditions (8 hours light; 16 hours dark) at 20°C. After 9 days of growth, 5 seedlings per genotype per treatment were transferred to 3 mL 0.5xMS liquid medium in 35 mm x 10 mm petri dishes. These were placed on a shaker at 120 rpm in short-day conditions before the dark period. On day 10, seedlings were treated for 24 hours as follows: NM = normoxia (ambient oxygen) and

mock treatment (addition of a volume of PBS equivalent to that of the flg22 solution); NF = normoxia (ambient oxygen) and flg22 (1 µM; prepared in PBS); HM = hypoxia (5% oxygen) and mock treatment; HF = hypoxia (5% oxygen; applied using PhO2X Box (Baker Ruskinn)) and 1 µM flg22. After 24 hours, treatment solutions were aspirated, 100% ethanol was added and samples were returned to short days on a shaker at 120 rpm. After 24 hours, the ethanol was removed and seedlings were washed with 0.07 M potassium phosphate buffer (pH 9). Seedlings were stained using 0.01% (w/v) aniline blue in 0.07 M potassium phosphate buffer (pH 9) for 2 hours with constant agitation at 120 rpm. Cotyledons were mounted on slides using 50% (v/v) glycerol and imaged using a fluorescent microscope under the DAPI filter. Quantitation of callose deposits was done as detailed in Mason et al., 2020. Briefly, the Trainable Weka Segmentation (TWS) plugin on Fiji (Arganda-Carreras et al., 2017) was used to identify callose deposits while excluding background fluorescence (e.g. vasculature or edges of tissue), by manually training the plugin using a set of callose deposition pictures. Once trained, all pictures obtained were analysed using the plugin and the results depicting the identified puncta were quantified using the Analyze Particles tool in Fiji (Schindelin et al., 2012).

2.2.7. Plant hypoxia response assays

2.2.7.1. Hypoxia survival

Vapour-phase sterilized seeds were sown on 0.5xMS agar plates and after a 3-day stratification at 4°C, plates were transferred to short day conditions (8 hours light/16 hours dark; 20°C). After 9 days of growth, the plates were placed in an anaerojar for the duration of the dark phase (5 pm – 9 am). Plates were removed from the anaerojar and returned to normoxia in the short-day room for 3 days when pictures were taken of the plates, followed by chlorophyll extraction as described in section 2.2.7.2 below.

2.2.7.2. Chlorophyll extraction and quantification

The method employed to extract and determine chlorophyll content of seedlings collected in Section 2.2.7.1. was based on the protocol described in Sumanta et al., 2014. All steps were carried out at 4°C. The fresh weight of the collected seedlings was determined, and the volume of chlorophyll extraction buffer (80% acetone) added so that seedlings were 5% (w/v) (e.g. 0.5 g seedlings in 10 mL 80% acetone). The seedlings were ground in the chlorophyll extraction buffer using a TissueLyzer (2 minutes, frequency 30/s). Tissue debris were spun down by centrifuging

samples at 10,000 rpm for 15 minutes at 4°C. The supernatant was transferred to a cuvette and absorbance readings were taken at 646 nm and 663 nm.

Chlorophyll-a content was determined using the equation: Chlorophyll-a = $12.25Abs_{663} - 2.79Abs_{646}$.

Chlorophyll-b levels were calculated as follows: Chlorophyll-b = $21.5Abs_{646} - 5.1Abs_{663}$.

2.2.7.3. Dark submergence

Seeds were sterilized and sown on soil. The dark submergence protocol was based on Bui et al., 2020. Plants were grown for 5 weeks in short day conditions (8 hours light/16 hours dark; 20°C). Treatments were started at the beginning of the dark phase. Photos of the plants were taken at t0 and then the plants were transferred to dark or dark and submerged in dH_2O (5 cm above rosette surface) for four days. Plants were imaged and returned to short day conditions for a one-week recovery period, at the end of which photos were taken and fresh weights measured.

2.2.8. Plant MeJA response assays

2.2.8.1. MeJA induced gene expression

Sterilized seeds were sown on Jiffy pots and stratified at 4°C for 3 days. Trays were transferred to a short-day growth room (8 hours light/16 hours dark; 20°C) and plants were grown for 30 days. On day 30, the plants were sprayed with 20 µM MeJA (in 0.1% ethanol and 0.05% Silwett) or a mock solution containing 0.1% ethanol and 0.05% Silwett. The plants were returned to the short-day room for 3 hours. The fifth leaf was harvested from each plant and leaf tissue from 8-9 plants was pooled in one cryotube per genotype per treatment (one replicate). RNA was extracted followed by RT-qPCR.

2.2.8.2. Anthocyanin production

Methods used to germinate seeds on MeJA containing medium to test anthocyanin accumulation in different mutant seedlings were based on Shan et al., 2009. Seeds were sterilized and sown on 25 µM MeJA or mock (0.12% ethanol) 0.5xMS supplemented with 1% (w/v) sucrose and 6 g/L agar. 120 mm square plates were used with 30 seeds sown per 1/6 section of the plate. Plates were placed at 4°C for 3 days and transferred to short day room (8

hours light/16 hours dark; 20°C). Seedlings were grown for 12 days, when fresh weight was measured, and seedlings were frozen in liquid nitrogen. Anthocyanin content was determined using a protocol based on Nakata and Ohme-Takagi, 2014 by grinding tissue in 250 µL anthocyanin extraction buffer (45% ethanol, 5% acetic acid) for the 30 seedlings. The value for 'volume extraction buffer' in the equation below was adjusted based on the fresh weight of the seedlings. Plant debris were spun down three times (12,000 x g for 5 minutes at room temperature), placing supernatant in fresh tube each time. The supernatant was then pipetted into a cuvette and absorbance was measured at 530 nm and 657 nm using a spectrophotometer. Anthocyanin content per grams of fresh weight was calculated according to the following equation:

Anthocyanin/g F.W. = $[Abs_{530} - (0.25 \times Abs_{657})] \times$ volume extraction buffer.

Chapter 3: Repression of PTI by hypoxia

3.1. Introduction

Aspects of this work have been published along with the work of fellow colleagues (Mooney et al., 2024). Some of the writing and figures in the following sections have been directly taken from this paper.

3.1.1. Background information

As stated in the Introduction, by comparing stress pathways across kingdoms, insight into conserved elements or mechanisms in eukaryotic stress responses may be identified. In mammals, immune cells and immune responses are both positively and negatively impacted by hypoxia. Hypoxia occurs naturally in many tissues which are responsible for generating immune cells (e.g. bone marrow), or for training the immune system and detecting pathogens (e.g. in the intestine). In these contexts, hypoxia plays a beneficial part by maintaining the stem cell like nature of haematopoietic stem cells (HSCs), which are responsible for the production of immune cells in the bone marrow and by maintaining the epithelial barrier of the intestinal lumen (Taylor and Colgan, 2017). Hypoxia also occurs in pathological immune settings within tumours and during infection and inflammation. Unlike the physiological hypoxia mentioned above, hypoxia induced in these tissues is aberrant and tends to have a steeper oxygen gradient making it more severe (Taylor and Colgan, 2017). Within infected tissues, hypoxia has context-dependent roles, however, previous studies have shown that generally hypoxia is a hallmark for poor infection prognosis (Thompson et al., 2017). Hypoxia results in reduced immune cell migration (Cramer et al., 2003), as well as macrophage and neutrophil infiltration into infected tissues (Thompson et al., 2017). Oxygen is also required for iNOS activity, with this enzyme having a high K_m (Michaelis constant) for oxygen of ~130 µM (Abu-Soud et al., 2001; McCormick et al., 2000), indicating that iNOS has a low affinity for oxygen and that reduced oxygen levels impact its activity faster than an enzyme with high oxygen affinity. Hence, while hypoxia induces iNOS gene expression, low oxygen tension inhibits its activity resulting in lower NO levels and reduced bacteria-killing capacity (Hayek et al., 2021; Jennewein et al., 2015; McCormick et al., 2000). This all culminates in higher mortality and disease scores which worsen with more severe hypoxia (Thompson et al., 2017). For example, mice treated with *Staphylococcus pneumoniae* under acute hypoxia exhibited 100% mortality at 24 hours post-inoculation compared to the 50% mortality displayed

in mice infected under normoxic conditions (Thompson et al., 2017). Hypoxia can also increase the inflammatory response due to increased cytokine release (Lewis et al., 1999; Rahat et al., 2011), which may increase tissue damage (Taylor and Colgan, 2017). However, hypoxia has also been shown to prime the immune system. A low oxygen pre-treatment rescues the hypoxia-related pathology associated with infection (Thompson et al., 2017). It was shown that the positive effect of prior hypoxia treatment was a result of reducing leukocyte metabolism through the glycolytic pathway and lowering glucose use, thus rescuing these immune cells from carbohydrate crisis (Thompson et al., 2017).

In plants, studies have shown that some pathogens can trigger hypoxia at the site of infection. For example, *B. cinerea* reduces oxygen levels in infected leaf tissue as a result of increased plant cell respiration in these regions and also due to the water soaking of these infected tissues (Valeri et al., 2021). Gall forming pathogens (e.g. *A. tumefaciens*) also induce hypoxic environments within these structures through an increase in the rate of host cell respiration (Kerpen et al., 2019). Despite these observations, the role that hypoxia plays in plant immunity is not well understood and plant responses to combined hypoxia and elicitor treatment in plants have not been studied.

In the pursuit of potential common regulators of hypoxia response and immunity, in mammals, the HIF transcription factors (see also section 1.5.1.), which are the master regulators of hypoxia response, are also well known as regulators of mammalian immunity and of inflammatory responses (Taylor and Colgan, 2017). In macrophages, which are central mediators of innate immunity, loss of HIF1α causes defects in core immune responses including inflammation, induction of glycolysis and generation of ATP, migration and bactericidal activity (Cramer et al., 2003; Hayek et al., 2021). Murine macrophage phagocytosis also increases during hypoxia in a HIF1α-dependent mechanism (Anand et al., 2007; Hayek et al., 2021). On the other hand, loss of HIF1α reduced disease symptoms upon combined treatment of mice with the bacterial pathogen *Staphylococcus aureus* and acute hypoxia (Thompson et al., 2017). While plants do not possess orthologs to HIF proteins, the ERFVII transcription factors act as the main regulators of the transcriptional response to hypoxia in plants (Licausi et al., 2011a; Schmidt et al., 2018). As stated in section 1.4.5., ERFVIIs have been associated with conflicting roles in plant resistance to pathogens (Gravot et al., 2016; Zhao et al., 2012). This, along with the finding that the ERFVII transcription factor HRE2 can bind to the promoters of many genes induced by flg22 (Lee and Bailey-Serres, 2019; Mooney et al., 2024), points potentially to a converging role of the ERFVIIs

in hypoxia response, as well as in plant defences against pathogens, which is akin to that of the HIFs in mammals. Furthermore, the N-degron pathway regulates the stability of both ERFVIIs and HIF proteins in plants and mammals, respectively, thus providing another point of similarity across kingdoms (Moorthy et al., 2022; Weits et al., 2014; White et al., 2017).

3.1.2. Aims of the work presented in this chapter

The aim of this project was to better understand the connections between hypoxia and plant immunity, uncover pathways that may have roles in both hypoxia and immunity, and pinpoint potential regulators of combined hypoxia/immunity. As hypoxia and immunity initiate many of their effects through large-scale transcriptional changes, a transcriptomic approach was first employed to identify common molecular aspects of plant responses to hypoxia and flg22, while also finding points of crosstalk and cross-regulation between plant responses to these treatments. The effects of hypoxia on essential immune pathway components such as PRRs and MAPK signalling, as well as on important aspects of PTI (e.g. callose deposition) were also tested.

Considering that N-degron pathway mutants are affected for their defences against a range of pathogens in both plants and mammals (Chui et al., 2019; de Marchi et al., 2016; Gravot et al., 2016; Leboeuf et al., 2020a; Till et al., 2019; Vicente et al., 2019; Xu et al., 2019), one question is whether the N-degron pathway may be a conserved regulator of hypoxia and immunity across kingdoms. Hence, this work also aimed to uncover whether the N-degron pathway may act as a regulator of the crosstalk between hypoxia and immunity in plants and whether this role is dependent on its function in regulating ERFVII stability. Furthermore, as stated in section 1.4.2.3. and 1.5.2., NO is an important signalling molecule in hypoxia and immune responses in both plants and mammals with perception of these stresses resulting in a nitrosative burst. Considering the roles of the N-degron pathway as a NO sensing pathway and the connections between NO and ERFVII stability (see sections 1.3 and 1.5.2.), an additional question I aimed to explore was whether NO may regulate the crosstalk between hypoxia and immune responses in Arabidopsis, possibly through a mechanism that would also be linked to the N-degron pathway.

3.2. Results

3.2.1. Generation and validation of RNA-Seq datasets to monitor the response to combined hypoxia/flg22

3.2.1.1. Identification of experimental conditions for hypoxia/flg22 combined treatments

To examine the potential crosstalk between hypoxia and flg22 responses, the genome-wide expression changes that occur under individual hypoxia (HM: hypoxia/mock) or flg22 (NF: normoxia/flg22) treatments, and combined hypoxia/flg22 (HF: hypoxia/flg22) compared to a normoxia/mock control (NM) were determined in wild-type Col-0 Arabidopsis seedlings. Both experimental conditions and timepoints were first optimized by treating 14-day old Col-0 seedlings with 100 nM, 500 nM flg22 or water (mock) in an anaerojar (hypoxia) or in ambient oxygen (normoxia) for 1 hour, 2 hours or 6 hours (Figure 3.1A), followed by monitoring the expression of hypoxia (*HRE2; ADH1; HB1*) and immunity (*FLS2; BIK1; WRKY33*) marker genes using RT-qPCR (Figure 3.1B). The anaerojars induce hypoxia response genes at all timepoints confirming that this is an appropriate method of inducing hypoxia for these experiments. Both 100 nM and 500 nM flg22, but not mock-treated samples, induced immune genes under hypoxic and normoxic conditions (Figure 3.1B). As 100 nM flg22 concentration was sufficient to induce immune response genes, it was chosen over the 500 nM flg22 concentration as to not saturate the system and overpower crosstalk between flg22 and hypoxia. For example, at 1 hour, the difference in *WRKY33* expression between NF and HF samples is smaller in 500 nM flg22 treated seedlings, compared to 100 nM flg22 treated ones (Figure 3.1B). The timepoint that allows comparison of hypoxia and immune responses, as well as potentially differential responses in combined treatment was then determined. The peak of immune gene expression appeared to be at 1 hour for most genes tested (Figure 3.1B), while hypoxia response gene expression appeared to increase from 1 hour, with longer treatments further increasing differential expression and the highest expression being reached at 6 hours of treatment. Previous studies have shown an early response (by 30 minutes) to moderate hypoxia which involves the differential expression of a small but specific set of genes (Cho et al., 2021; Licausi et al., 2011b; van Dongen et al., 2009), so the 1-hour hypoxia treatment was deemed sufficient to induce important early-response genes. Notably, at the 1-hour timepoint, the hypoxia/flg22 treated samples showed differences in expression compared to each of the individual treatments (hypoxia/mock and normoxia/flg22). For example, *WRKY33* expression appears higher in

hypoxia/flg22 treated samples compared to flg22 alone but this difference was less striking at later timepoints (Figure 3.1B and 3.1C). Importantly, hypoxia response genes were not induced at any timepoint in the normoxia/mock control conditions, indicating that keeping the seedlings in the liquid medium overnight on a shaker did not generate a hypoxic stress.

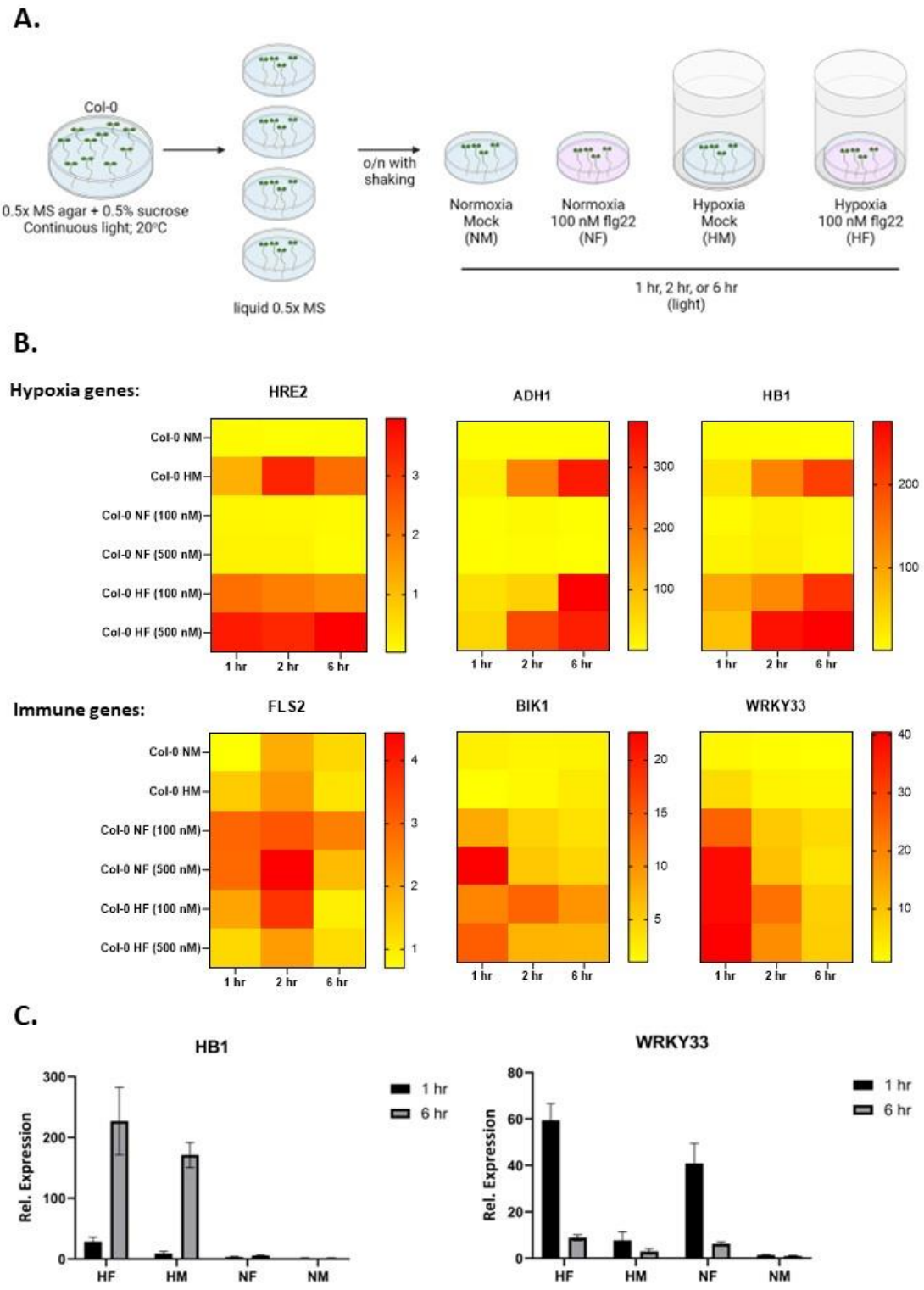

Figure 3.1. Optimization of hypoxia and flg22 treatments. A. A depiction of the methodology used to treat seedlings: Col-0 seedlings grown under continuous light were transferred to 0.5xMS liquid medium and placed on a shaker in continuous light overnight. The following morning, seedlings were treated to normoxia/mock (NM); normoxia/flg22 (NF); hypoxia/mock (HM) or hypoxia/flg22 (HF) for 1, 2 or 6 hours. This was followed by the collection of seedlings in liquid nitrogen and RNA extraction. **B.** RT-qPCR results of 14-day old seedlings treated with normoxia/mock (NM); normoxia/flg22 (NF); hypoxia/mock (HM) or hypoxia/flg22 (HF) for 1, 2 or 6 hours. Flg22 concentration = 100 or 500 nM. This data was exploratory, so one biological replicate with 5 seedlings is presented. **C.** RT-qPCR results for a representative hypoxia marker gene (*HB1*) and immunity gene (*WRKY33*) gene for 10-day old seedlings treated to individual and combined hypoxia and flg22 for 1 and 6 hours. Mean and SEM of 5 biological replicates are shown.

To be in-keeping with previous datasets generated in the lab, which were generated using 10-day old seedlings and to allow direct comparison, I generated samples for RNA-Seq transferring seedlings to liquid medium on day 9 and treating on day 10 +/- 100 nM flg22 +/- hypoxia in anaerojars (Figure 3.1A). To ensure that the results were similar between day 14 and day 10 treated samples and to confirm that that the experimental design optimized above was appropriate at this earlier developmental timepoint/on these younger seedlings, the expression of *HB1* and *WRKY33* was tested after 1- and 6-hour treatments in the 10-day old seedlings (Figure 3.1C). The results showed a similar pattern of expression in *HB1* and *WRKY33* for seedlings treated on day 10 or 14. Based on the preliminary data obtained, it was decided to treat 10-day old Col-0 seedlings with 100 nM flg22 (or dH_2O, mock) in an anaerojar (or at ambient oxygen conditions) for 1 hour to compare the genome-wide gene expression changes in response to individual treatments and combined hypoxia/flg22. In addition, a previous study showed significant transcriptional overlaps between RNA-Seq datasets obtained at early timepoints (ranging from 5 minutes to 3 hours) in response to PAMPs (e.g. flg22, elf18), and different abiotic stresses, including cold, drought, salt and wounding (Bjornson et al., 2021), thus suggesting that an early timepoint might be more suitable to detect early cross-regulatory events between hypoxia and flg22 responses. Finally, as I also aimed to study the role of NO as a regulator of the crosstalk between hypoxia and immunity, it was reasoned that an early timepoint would detect more direct roles of NO, as the NO burst is an early response in response to either flg22 or hypoxia (Bleau and Spoel, 2021).

3.2.1.2. Validation of RNA-Seq datasets

Samples undergoing 1 hour treatment as highlighted above (Figure 3.1A and section 2.2.4.7.) from three biological replicates were generated, followed by total RNA extraction, next-generation sequencing and initial bioinformatic analysis (both performed by BGI). Reads were measured using the DNBSEQ platform. Low quality reads and those containing contaminating adapter sequences or high levels of unknown bases were removed and the high-quality reads were aligned to the Arabidopsis thaliana TAIR 10.1 genome (https://www.ncbi.nlm.nih.gov/datasets/genome/GCF_000001735.4/). There was high read alignment to the reference genome with an average of 98.34% alignment ratio per sample.

Assessing variability between replicates and treatments was done using Pearson's correlation and Principal Component Analysis (PCA) on the total read counts *per* sample in each replicate. Pearson's correlation finds the linear relationship between gene expression between two samples, with correlation coefficients close to 1 suggesting high similarity in gene expression between the samples. High correlation coefficients (>0.85) were found between all samples (Figure 3.2A). Replicates in general correlated well with each other, with some deviation in some samples. Replicate 1 was not as closely related to replicates 2 and 3 for HM, NF and NM samples, while replicates 1 and 3 were quite similar, with replicate 2 being less so for HF samples. All samples treated with flg22 also had high correlation, while all mock samples clustered together. These findings are confirmed by the PCA which uncovered flg22 as the major contributing factor accounting for the differences between the groups (Figure 3.2B). The lack of the contribution of hypoxia to differences in these groups may be due to the short hypoxia treatment not inducing a large number of hypoxia response genes (Figure 3.3).

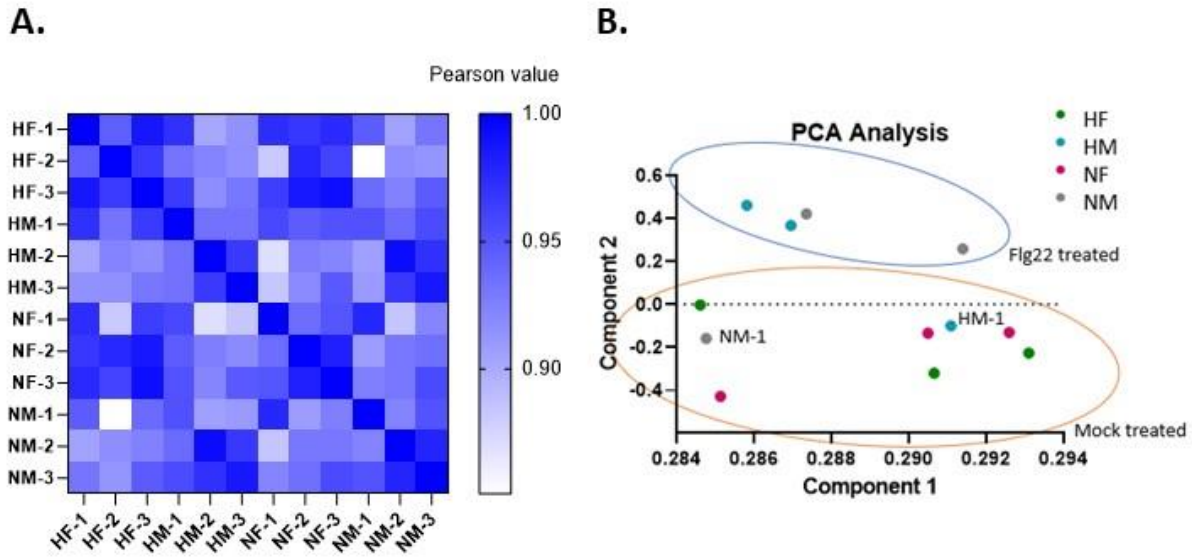

Figure 3.2. Variability between samples and replicates. Pearson's Correlation (A.) and PCA (B.) were conducted by BGI genomics and results were graphed using GraphPad Prism.

The DEGs (cut-offs: adj. *p*-value<0.05 and $|\log_2(FC)|>0.585$) identified under individual hypoxia (HM v NM) or flg22 (NF v NM) and combined (HF v NM) treatments compared to untreated seedlings all showed a higher number of up-regulated genes compared to down-regulated genes. Hypoxia treatment alone (no flg22) exhibited the lowest number of DEGs (HM v NM; 145 DEGs) (Figure 3.3), presumably due to the early timepoint. Flg22 treatment alone resulted in a high level of gene expression changes (NF v NM; 1906 DEGs) (Figure 3.3). The combined HF treatment showed an increase in the number of DEGs with higher number of up- and down-regulated DEGs than the sum of the individual stresses (HF v NM; 2612 DEGs) (Figure 3.3). This is most striking for the downregulated DEGs, suggesting that inhibition may play an important role in the adaptation and survival to these stresses.

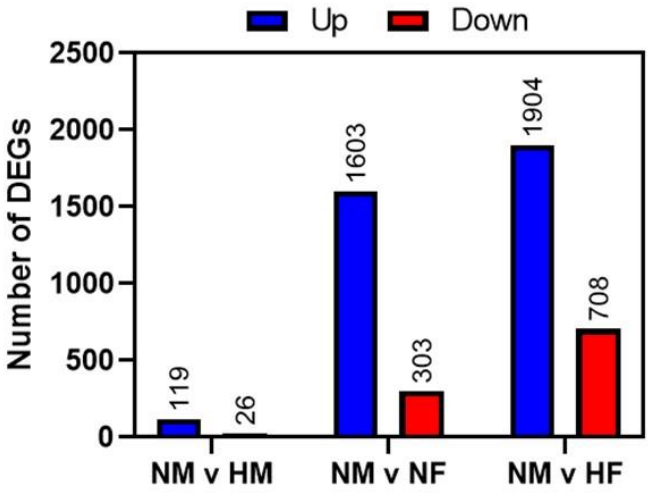

Figure 3.3. Number and directionality of DEGs for each of the RNA-Seq datasets. The number of up-and down-regulated genes in HM v NM: hypoxia/mock v normoxia/mock; NF v NM: normoxia/flg22 v normoxia/mock; and HF v NM: hypoxia/flg22 v normoxia/mock datasets.

In order to validate the datasets, the genes which were differentially expressed by the individual treatments (HM v NM and NF v NM) were examined against previously published datasets (Denoux et al.,2008; Lee and Bailey-Serres, 2019) (Figures 3.4A and 3.5A), and a gene ontology (GO) analysis was also performed to identify enrichment for genes associated with different functional categories (Figures 3.4B and 3.5B). Specifically, for the NF v NM dataset, expected GO terms including response to chitin, bacterium and defence responses were significantly enriched in the list of DEGs (Figure 3.4B). The NF v NM dataset was compared against the transcriptomic dataset published in Denoux et al., 2008 where 8-day old seedlings were treated +/- 1 µM flg22 for 1 hour. The overlap of DEGs between these datasets was significant (Figure 3.4A) and the directionality of expression of these common 1253 DEGs was similar (Figure 3.4C). Higher log_2FC values seen in Denoux et al., 2008 and only moderate correlation (R^2 = 0.3) for expression of these common DEGs as well as the higher number of total DEGs are likely accounted for by the higher concentration of flg22 used during treatment for this dataset (1 µM flg22 compared to 100 nM flg22 in our case). Similar expression responses were seen for representative immunity genes, such as *BIK1* (Figures 3.4D and 3.4E) and *WRKY33* (Figure 3.1C and 3.4E) by RT-qPCR and RNA-Seq, respectively. Taken together, these analyses validate the dataset obtained.

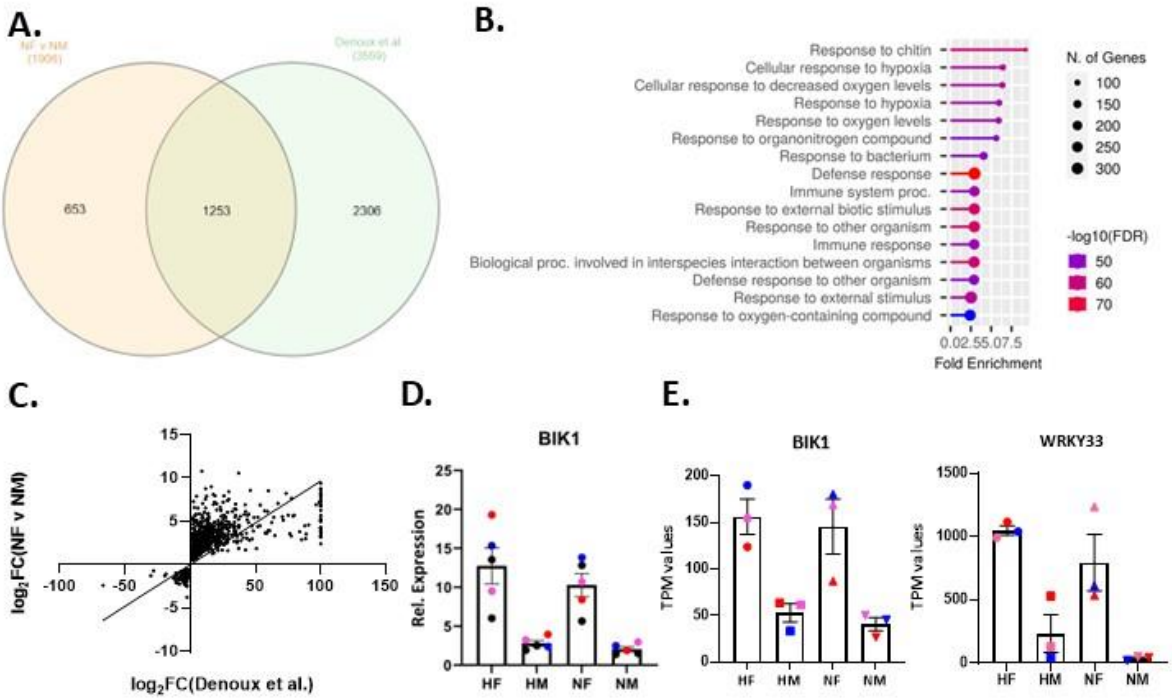

Figure 3.4. Validation of NF v NM dataset. A. Overlap of DEGs from NF v NM dataset and microarray dataset for Arabidopsis seedlings treated to 1-hour flg22 (1 µM) compared with untreated samples (Denoux et al., 2008). **B.** Top 20 significant GO terms associated with the NF v NM dataset. GO analysis was conducted using ShinyGO software with FDR < 0.05. **C.** XY plot of the log2 fold-changes for NF v NM dataset vs Denoux et al., 2008 dataset for the 1253 DEGs found in overlap. **D.** Results of RT-qPCRs for *BIK1* using the same RNA samples as those sent for RNA-Seq. Mean and SEM of the relative expression to the reference gene, *MON1*, are shown. **E.** RNA-Seq results for *BIK1* and *WRKY33*. The mean TPM values and SEM are shown.

Similar analyses were performed for the HM v NM dataset. Again, expected GO terms, such as cellular response to hypoxia and cellular response to stress, were retrieved. A significant overlap was obtained when comparing DEGs for HM v NM dataset and a dataset obtained by Lee and Bailey-Serres, 2019, in which 7-day old seedlings were treated to 2 hours of hypoxia by placing seedlings in a sealed chamber flushed with argon. The directionality of these common DEGs had moderate positive correlation (R^2 = 0.66). Again, differences in the number of DEGs between datasets may be accounted for by the differences in the duration of treatment (1 hour vs 2 hours) and methods of hypoxia treatment (anaerojar vs argon chamber). The typical hypoxia response marker gene *ADH1* (Figure 3.5D and 3.5E) and *HB1* (Figure 3.1C and 3.5E) showed similar pattern of expression in RNA-Seq and RT-qPCR analyses, respectively.

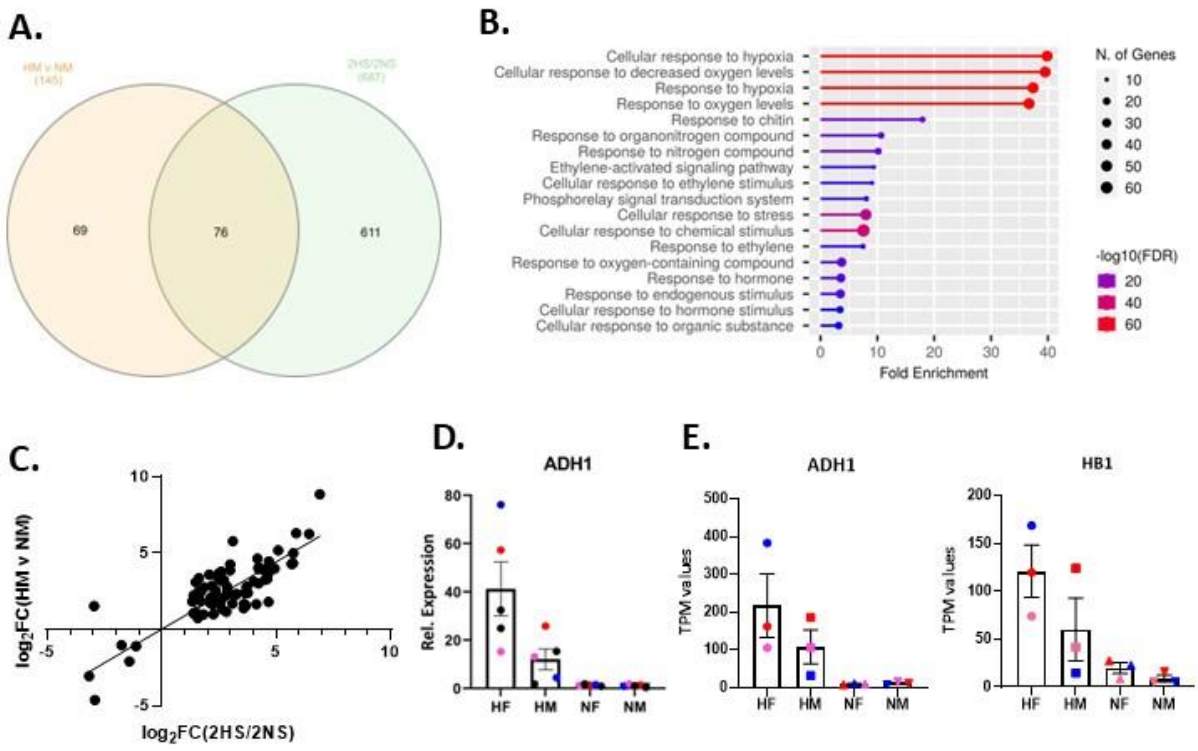

Figure 3.5. Validation of HM v NM dataset. A. Overlap of DEGs from HM v NM dataset and previously published RNA-Seq dataset obtained by treating 7-day old seedlings with 2-hour hypoxia (2HS/2NS; Lee and Bailey-Serres, 2019). **B.** Top 20 GO terms enriched for the HM v NM dataset. GO analysis was conducted using ShinyGO software, with FDR < 0.05. **C.** XY plot of the log2 fold-changes for common DEGs found between HM v NM dataset vs Lee and Bailey-Serres, 2019 dataset. **D.** RT-qPCR results for *ADH1* using the same RNA samples as those sent for RNA-Seq. Mean and SEM of the relative expression to the reference gene, *MON1*, are shown. **E.** RNA-Seq results for *ADH1* and *HB1*. The mean TPM values and SEM are shown.

Taken together, the initial analyses of the RNA-Seq datasets obtained served to validate the experimental approach used and indicated that the treatments used worked.

3.2.2. Investigating the interactions between hypoxia and flg22 response at the transcriptional level

To further analyse the RNA-Seq datasets with the aim of characterising the crosstalk between hypoxia and flg22 responses, I used three metrics established to study the crosstalk between the transcriptional programs to combined abiotic stresses in *Marchantia polymorpha* (Tan et al., 2023) (see also Figure 3.6A for calculations). Specifically, these metrics allow the quantification of (i) shared aspects of the transcriptional response programs (similarity score ranges from 0 to 1, with 1 corresponding to identical response programs), (ii) novel components of combined treatments (novel interaction score; varies between 0 and 1, with 1 indicating that combined stresses results in an entirely new transcriptional program), and (iii) stress dominance (suppression score varies between −1 and 1, with a negative score indicating a suppression of flg22 response by hypoxia) (Tan et al., 2023). Upon conducting these calculations, a low level of similarity for hypoxia and flg22-induced responses for both up- and down-regulated genes (0.031 and 0.006, respectively) was found (Figure 3.6E). The novel interaction score presenting the proportion of unique response genes to combined hypoxia/flg22 was high, particularly for down-regulated genes indicating that the repression of specific genes under combined hypoxia/flg22 might be an important aspect of the unique response to this combined stress (Figure 3.6E). For both up- and down-regulated genes, the negative suppression score obtained suggests that the hypoxia response program represses flg22 response at the transcriptional level (Figure 3.6E).

A.

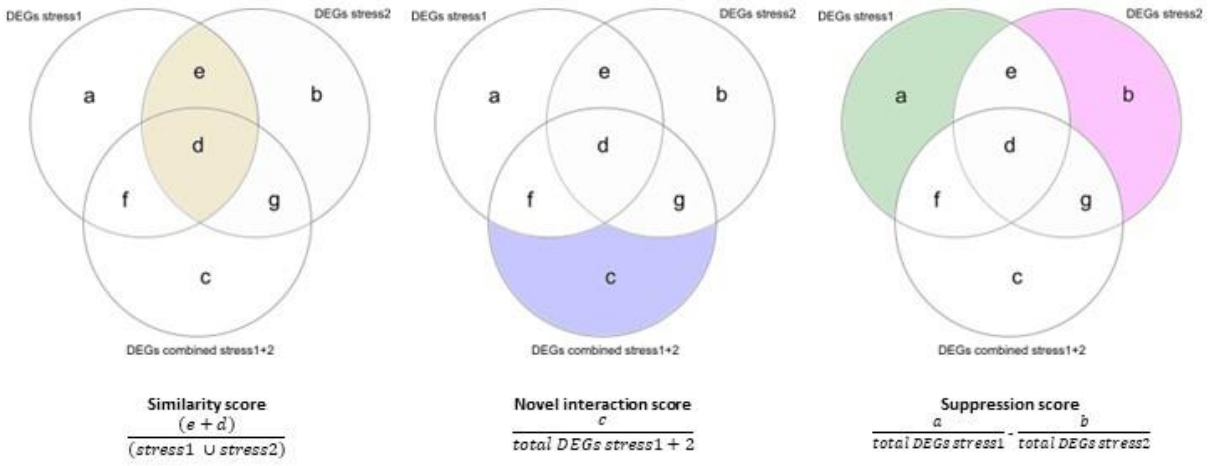

B.

C.

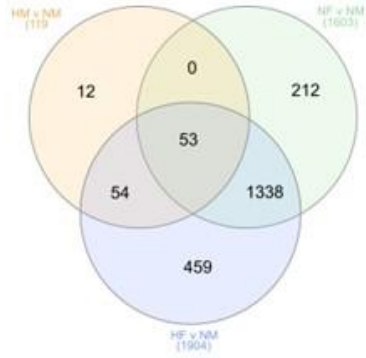

D.

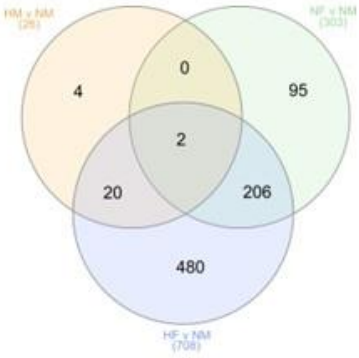

E.

Metric	Up	Down
Similarity	0.031	0.0061
Novel Interaction	0.241	0.678
Suppression	-0.031	-0.16

Figure 3.6. Analysis of similarity, uniqueness and dominance of hypoxia and flg22-induced responses. **A.** Calculation of metrics to characterise the transcriptional response to combined stresses, as outlined in (Tan et al., 2023). Single letters in the different sections of the Venn diagrams correspond to the number of DEGs in that particular section. Stress1 U stress2: total number of DEGs in stress1 and stress2. **B.**, **C.** and **D.** show the overlaps of the total (**B.**), up-regulated (**C.**) and down-regulated (**D.**) DEGs in the NF v NM, HM v NM and HF v NM datasets. **E.** Similarity, novel interaction and suppression scores calculated for up-regulated and down-regulated DEGs.

The following sections will analyse in detail similarities, novel interactions and suppression effects between the transcriptional responses to hypoxia and flg22 when both treatments are combined.

3.2.2.1. Investigating the similarity in hypoxia and flg22 responses

While the calculations suggest low similarity between hypoxia and flg22 responses with only 0.031 as a similarity score for up-regulated DEGs and an even lower similarity score (0.0061) for down-regulated genes (Figure 3.6E), a small overlap of 59 DEGs between the three datasets was identified (Figure 3.6B). The over-represented GO terms for these common DEGs included cellular response to hypoxia, ethylene-activated signalling pathway, and several terms related to cell wall biogenesis and metabolism (Figure 3.7A).

There was an enrichment for genes associated with the GO term 'response to hypoxia' amongst the 59 common DEGs. A similar enrichment was found when analyzing different transcriptomics datasets generated upon treatment with flg22 alone (Mooney et al., 2024), thus suggesting that this may be an important feature of the flg22 response program. The 59 DEGs common to NF v NM and HM v NM datasets comprise 10 'core hypoxia response genes' including *RBOHD*, *LOB DOMAIN-CONTAINING PROTEIN 41* (*LBD41*), *Alanine AMINOTRANSFERASE 1* (*AlaAT1*) and *CALMODULIN-LIKE 38* (*CML38*), which were up-regulated in the NF v NM dataset. These genes are also all upregulated in HF v NM dataset. In addition, *LBD41* and *CML38* are upregulated in HM v NM. However, hypoxia response genes that are necessary for the metabolic changes that accompany plant responses to hypoxia (e.g. *ADH1*, *PDC*s, *SUCROSE SYNTHASES* (*SUS*s)) were not induced in the NF v NM dataset. Hypoxia and flg22 responses thus appear to share common regulated genes, which have a broader role in stress response (e.g. *RBOHD* is involved in ROS signalling). These results also suggest that flg22 treatment does not induce a hypoxic environment which is in line with the results of Valeri et al., 2021.

GO terms associated with cell wall integrity and remodelling were also significantly enriched among the DEGs common to all treatments. This is of interest considering that the cell wall is an important player in response to biotic and abiotic stresses. Previous studies show that environmental conditions impact cell wall composition (Le Gall et al., 2015; Novaković et al., 2018). In plant defences against pathogens, the cell wall is the first barrier against pathogens. The importance of the cell wall in defense against pathogens is highlighted by the use of cell wall degrading enzymes and induction of other cell wall modifications by the pathogen in order to facilitate host colonization (Kubicek et al., 2014). Plants further employ the use of cell wall polymers in plant defence during infection by depositing callose (1,3 ß-glucan) which blocks pathogen entry by accumulating at the cell wall and prevents cell to cell movement of the pathogen by depositing at plasmodesmata (Cui and Lee, 2016; Ellinger et al., 2013; Xiao et al.,

2018). Abiotic stresses such as flooding also results in cell wall changes. Proteomic studies in wheat roots have shown that flooding leads to a reduction of cell-wall metabolism proteins, which are thought to contribute to flooding-induced reduced growth (Le Gall et al., 2015; Kong et al., 2010). It has also been suggested that cell wall remodeling and degradation may be important for the generation of aerenchyma (channel-like structures involved in flooding tolerance) in flooded tissues of legume species (Pegg et al., 2020). In the current work, four genes associated with cell wall metabolic processes were up-regulated under hypoxia and/or flg22 treatments. These genes include *XYLOSYLTRANSFERASE 1* (*XT1*) and three xyloglucan endotransglucosylases (XTHs); *XTH18, XTH22*, and *XTH23*. XTHs function in remodeling cell walls and have been previously shown to be upregulated at the transcriptional level in Arabidopsis under submergence. *XTH18* was shown to be upregulated under submergence; *XTH22* was upregulated under hypoxia; and *XTH23* was upregulated under both (Lee et al., 2011). *XTH22* has also been up-regulated downstream of hormone signalling pathways (e.g. brassinosteroids and auxin, as well as a range of environmental stimuli including touch, temperature and darkness (Iliev et al., 2002) suggesting a potential role for cell wall remodeling under multiple stresses in Arabidopsis. A literature search suggests that these genes have so far not been identified as being involved in flg22 responses. However, they may act as susceptibility factors in some pathosystems (Wang et al., 2017a).

Ethylene is an important phytohormone which has been implicated in both responses to biotic and abiotic stresses. During flooding, ethylene accumulates within submerged tissues and has been shown to be important for ERFVII stabilization (Hartman et al., 2019). Ethylene has also been shown to work alongside JA in inducing immune responses and increasing resistance to necrotrophic pathogens (Zhu, 2014; Zhu et al., 2011). The ethylene signalling pathway genes regulated under all treatments include *DEHYDRATION RESPONSE ELEMENT-BINDING PROTEIN 26* (*DREB26)*, *ERF6*, *ERF13* and *ERF105*, all of which are transcription factors. *DREB26* is of particular interest as it is one of the few DEGs with opposite directionality of expression depending on the treatment, with it being down-regulated in NF v NM and up-regulated in HM v NM and HF v NM. This opposite behaviour is found with other stresses, as *DREB26* is upregulated in response to dehydration and touch, while it is downregulated upon heat or freezing treatments (Krishnaswamy et al., 2011; Urano et al., 2017). The other above-mentioned ERF transcription factors have also been shown to have roles in abiotic as well as biotic stress responses (Bolt et al., 2017; Huang et al., 2016; Miyamoto et al., 2019; Sewelam et al., 2013). These results suggests that some ethylene response transcription factors could be important in combined stress responses, as well as individual stresses.

The majority of DEGs common to hypoxia, flg22 and hypoxia/flg22 showed largely similar pattern of expression (53 DEGs out of 59; Figure 3.7B). For the 53 genes that were up-regulated in all conditions (Figure 3.6C), the combined hypoxia/flg22 treatment enhanced the amplitude of up-regulation compared to the individual stresses (Figure 3.7C). While there were only 2 common genes being down-regulated (Figure 3.6D), the same trend was observed, so that combined hypoxia/flg22 resulted in a stronger repression of these 2 genes compared to hypoxia or flg22 alone (Figure 3.7D).

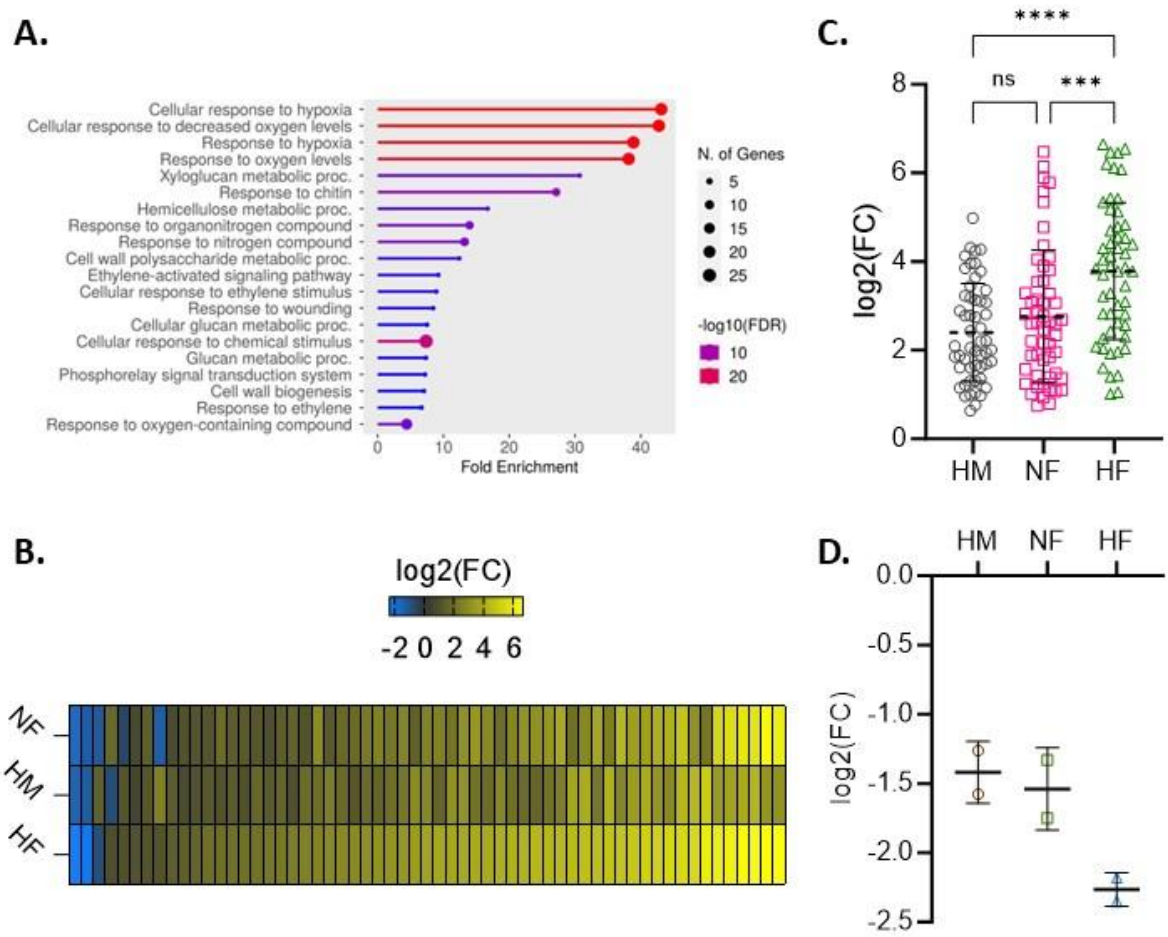

Figure 3.7. Analysis of similarity between hypoxia and flg22 responses. A. GO enrichment of the 59 DEGs found in the overlap between NF v NM, HM v NM, and HF v NM datasets. Top 20 GO categories are shown. Analysis was conducted using ShinyGO software, with FDR < 0.05. **B.** Heatmap showing log_2FC expression of the common DEGs in the NF v NM, HM v NM, and HF v NM datasets. **C.** and **D.** Log2 of gene expression fold-changes in NF v NM, HM v NM, and HF v NM datasets for common up-regulated (**C.**) and down-regulated (**D.**) DEGs. Mean values and standard deviations are shown. One-way ANOVA statistical test conducted on data in C.

In sum, the datasets obtained show that (1) flg22 and hypoxia responses share common components that play broad roles in plant responses to both biotic and biotic stresses, with a particular emphasis on genes involved in hypoxia signalling, ethylene signalling and cell wall modifications; and (2) combined hypoxia/flg22 treatment elicits a stronger transcriptional response of these genes compared to the individual treatments.

3.2.2.2. Investigating novel aspects of the transcriptional response to combined hypoxia/flg22.

As indicated above by the novel interaction score and the comparison of DEGs in the different RNA-Seq datasets (Figure 3.6E), unique features associated with the response of wild-type seedlings to combined hypoxia/flg22 emerged. 939 unique DEGs were identified upon hypoxia/flg22 treatment, compared to hypoxia or flg22 treatments alone (Figure 3.6B), including 459 upregulated and 480 downregulated genes. Additionally, the novel interaction score obtained for downregulated genes upon combined hypoxia/flg22 was higher than those calculated for the range of 18 combined abiotic stresses in *Marchantia polymorpha* (Tan et al., 2023), thus suggesting that the repression of specific sets of genes is an important and unique feature of plant responses to combined hypoxia/flg22. GO analysis of the 939 unique DEGs to combined hypoxia/flg22 revealed expected GO terms such as response to hypoxia, response to stress and signal transduction were upregulated. There were however several GO terms associated with plant responses to phytohormones in general, but also more specifically plant responses to auxin and to JA (Figure 3.8A). It appears that combined hypoxia/flg22 leads to the repression of developmental processes by downregulating genes involved in 'response to auxin stimulus' (Figure 3.8A), which could correlate with a resource/allocation problem and potential energy crisis that is typical of hypoxia stress.

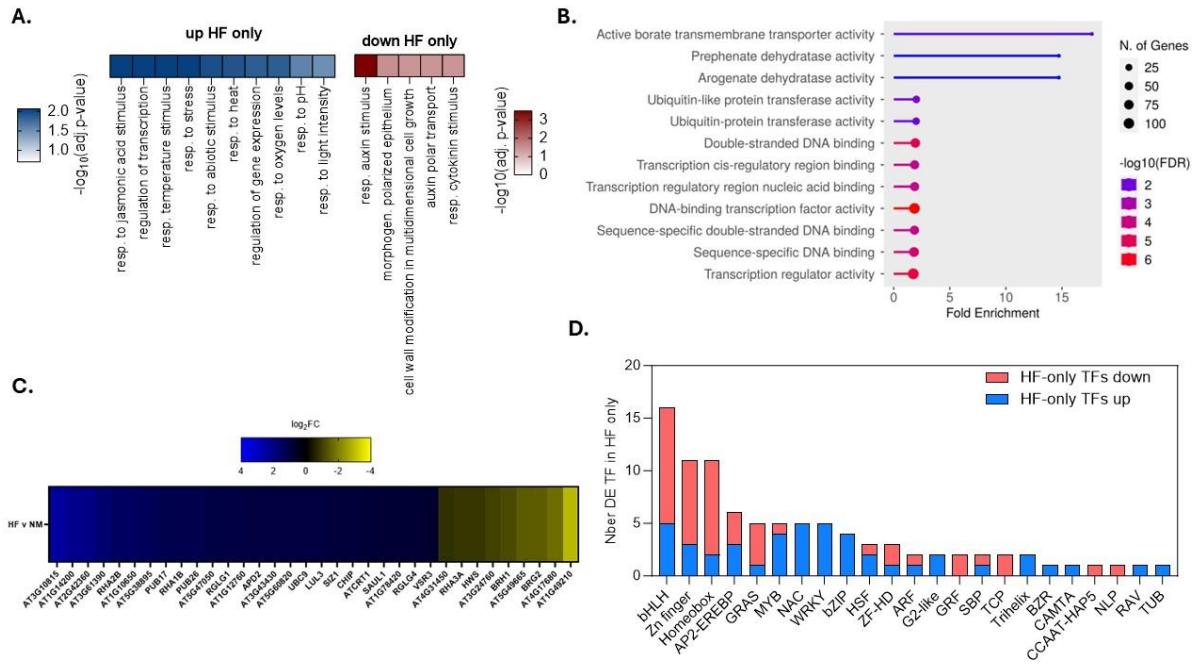

Figure 3.8. Novel expression in response to combined hypoxia/flg22. A. Selected GO terms enriched (corrected p-value<0.05) amongst uniquely up- and down-regulated DEGs upon combined hypoxia/flg22 analysed by BiNGO feature of Cytoscape software. **B.** Top 20 GO terms for Molecular Function of 939 DEGs unique to the HF v NM dataset analysed by ShinyGO with FDR<0.05. **C.** log2 of the fold change of genes in the 'ubiquitin-like transferase activity' GO term. **D.** Transcription factor families up- and down-regulated in HF v NM dataset only.

To determine whether specific type of signalling components may be enriched among the 939 unique DEGs upon combined treatment, an additional GO analysis was carried out, focusing on molecular function instead of biological function (Figure 3.8B). This analysis revealed two interesting features of the unique transcriptional response to combined hypoxia/flg22 treatment: (1) the enrichment for genes associated with ubiquitin and ubiquitin-like transferase activity (34 DEGs) and (2) an over-representation of transcriptional regulators (92 DEGs). Both are relevant considering the fundamental roles that the UPS and transcriptional regulation play in the onset and regulation of plant responses to stresses. Out of 34 DEGs associated with the UPS, 25 were upregulated (Figure 3.8C), with many of these being already known for their roles in the regulation of plant responses to stress, including responses to abiotic stress, immunity, phytohormone signalling, and cell death (Al-Saharin et al., 2022; McLellan et al., 2020; Zhang et al., 2012; Zhang et al., 2015). Of note is the E3 ubiquitin ligase *PLANT U-BOX 26* (*PUB26*) which is up-regulated under combined hypoxia/flg22 treatment and mediates the degradation of BIK1, a key regulator of PTI (Wang et al., 2018b). These data suggest that the UPS has important roles

in the regulation of plant responses to multiple stresses and supports the further study of UPS-related in regulation to combined stresses.

As indicated above, another unique feature of the combined hypoxia/flg22 response was the over-representation of genes associated with transcription factors, with some families being up-regulated (NAC, WRKY, bZIP), while others tended to be predominantly down-regulated (bHLH, Zn finger, homeobox) (Figure 3.8D). Altogether, the data suggest that the coordination of plant responses to combined hypoxia/flg22 requires the orchestration of gene expression changes under the control of specific transcription factor families. Notably, some of the up-regulated transcription factor families, such as NAC or WRKY, are typically associated with stress responses (Shao et al., 2015), while some of the transcription factor families that are mostly repressed (*e.g.* homeobox transcription factors) are generally associated with developmental processes (Jeong et al., 2012). This suggests again an increased need to regulate resource allocation under combined stress, with a stronger prioritization of stress response pathways as opposed to developmental processes. The core findings with combined hypoxia/flg22 (*e.g.* the preponderance of a novel transcriptional response, the relevance of transcription factors and the stronger prioritization of stress responses) are reminiscent of previous findings in studies with combined abiotic/biotic stresses (Atkinson and Urwin, 2012; Pandey et al., 2015; Prasch and Sonnewald, 2013; Rasmussen et al., 2013; Saijo and Loo, 2020; Suzuki et al., 2014; Zhang and Sonnewald, 2017). However, such studies have thus far focused on combinations between pathogens and abiotic stresses such as heat and drought and have not included hypoxia.

Because of the important role of JA in plant defence against pathogens as well as in response to hypoxia, a more detailed analysis was performed for genes found in this GO category. The role of JA in both PTI and hypoxia response is also evidenced here by the fact that the 'response to JA' GO term was enriched in transcriptomics datasets obtained upon flg22 treatment (e.g. the NF v NM dataset generated here and in Denoux et al., 2008), as well as in the 2-hour hypoxia dataset presented in Lee and Bailey Serres, 2019 (2HS/2NS) (Figure 3.9A). This term was not present in the GO analysis of the HM v NM dataset obtained here, possibly due to the short timepoint used to generate the samples. In line with this, none of the JA signalling genes were differentially expressed in the HM v NM dataset, while all JA signalling DEGs were upregulated in the HF v NM dataset, and some were induced also in the NF v NM dataset (Figures 3.9B). JA-associated genes specific to the combined hypoxia/flg22 treatment included several *JAZ* genes (*JAZ3*, *JAZ6* and *JAZ8*) which code for transcriptional repressors of JA response genes. Notably,

MYC2 which acts as the master regulator of JA response genes, is upregulated upon combined hypoxia/flg22 treatment specifically (Figure 3.9C). To obtain a better understanding of the potential contribution of MYC2 in the combined stress response, DEGs unique to HF v NM were compared to a MYC2 ChIP-Seq dataset (Zander et al., 2020), and this analysis identified an overlap (Figure 3.9D). The genes whose promoter might be bound by MYC2 and that responded to combined hypoxia/flg22 treatment were either up- or downregulated. As expected, a number of these DEGs were JA response genes (depicted in orange; Figure 3.9E), most of which were upregulated with the exception of *REPRESSOR OF GIBBERELLIC ACID* (*RGA)* and *GIBERELLIC ACID INSENSITIVE* (*GAI)* which were downregulated by hypoxia/flg22 treatment.

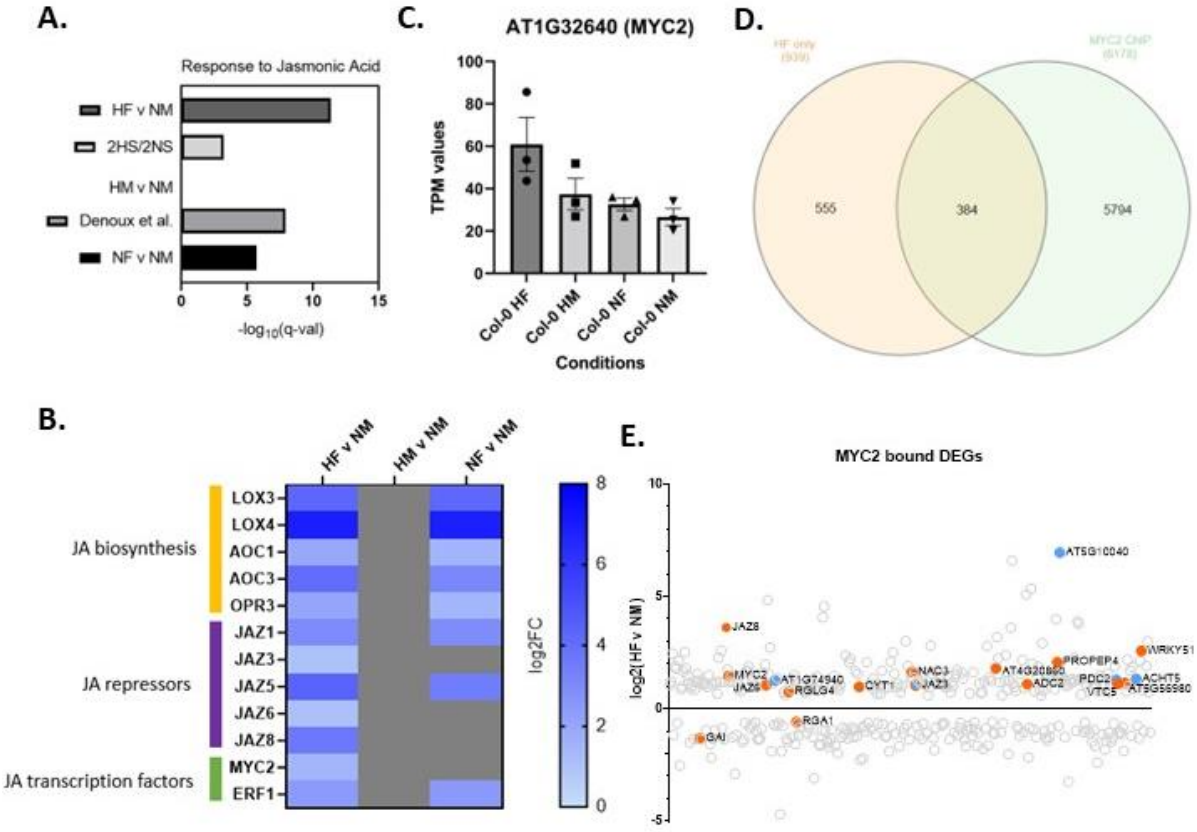

Figure 3.9. Role of MYC2 in combined stress response. **A.** Enrichment for the 'response to JA' GO term in flg22, hypoxia and hypoxia/flg22 datasets. The -log10 of the q-value are shown. **B.** Gene expression fold changes (log_2FC) for known JA biosynthesis, repressors and transcription factors in HF v NM, HM v NM and NF v NM datasets. **C.** Gene expression (TPM values) of *MYC2* across HF, HM, NF, and NM samples. Plotted on graph are means and SEMs. **D.** Overlap between the 939 DEGs unique to HF v NM and genes with a MYC2 binding site in a ChIP-seq dataset (Zander et al., 2020). **E.** Expression of the 384 genes bound by MYC2 and uniquely differentially expressed during hypoxia/flg22 combined treatment. Orange: JA response genes; blue: hypoxia response genes.

In sum, novel responses in combined hypoxia/flg22 responses include the differential expression of a number of ubiquitin transferase genes highlights the role of the UPS as a regulator of stress responses. As well, a range of different families of transcription factor were also induced by hypoxia/flg22 treatments. The effect of the induction or suppression of these transcriptional regulators will require further study. One transcription factor induced under hypoxia/flg22 treatments alone is the JA-master regulator, MYC2. Response to JA is a significant GO term in HF only suggesting that JA responses may be important for coordinating responses to these two stresses. In line with stress/growth trade-offs, genes involved in developmental processes e.g. response to auxin stimuli, are downregulated.

3.2.2.3. Investigating the repressive effect of hypoxia on flg22-induced responses

The negative suppression scores (Figure 3.6E) suggest that hypoxia represses some aspects of the transcriptional response to flg22. Examination of the 304 DEGs (Figure 3.6B) identified only after flg22 treatment (e.g. these genes no longer respond to flg22, when combined with hypoxia) showed an enrichment for molecular functions associated with phosphorylation ('protein phosphorylation' and 'cell surface receptor signalling pathway') (Figure 3.10). Notably, genes in the latter GO category included PRRs such as *FLS2* and *EFR*. Hence, the data suggest that one particular aspect of the repression of flg22 response by hypoxia could occur at the level of PRR expression.

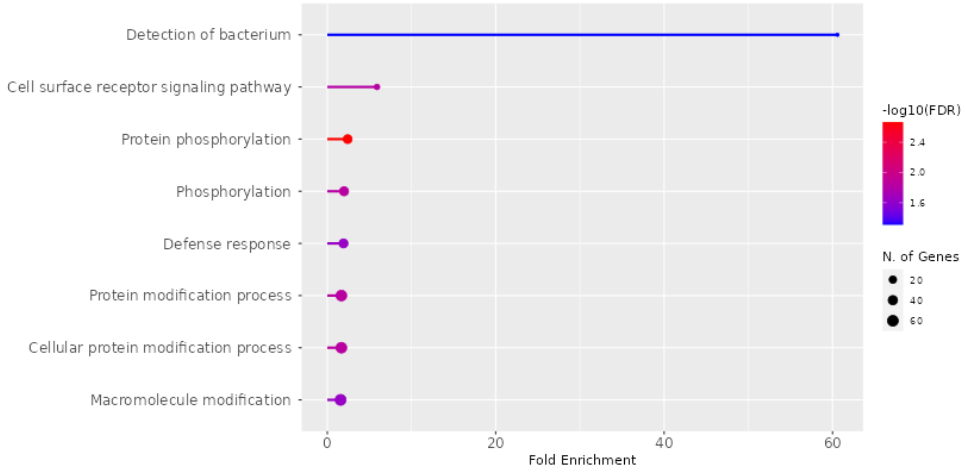

Figure 3.10. GO analysis of flg22 induced DEGs only. GO enrichment of the 304 DEGs found in NF v NM dataset only. The top 20 GO categories are shown. GO analysis was conducted using ShinyGO software with FDR<0.05.

Screening of the RNA-Seq datasets for differential expression of PRRs detected differences in expression between treatments for *FLS2*, *EFR* and *LYK4*. These PRRs function by recognizing different PAMPs with EFR recognizing the elf18 peptide of bacterial EF-Tu and LYK4 binding to chitooctaose (CO8), a component of the fungal cell wall. These PRRs were shown to have reduced expression in hypoxia/flg22 treatments compared to flg22 alone, with *FLS2* and *LYK4* being significantly downregulated in the combined treatment (Figure 3.11A). However, immunoblot analysis of FLS2 protein levels using seedlings of a *FLS2$_{pro}$:FLS2-3xmyc-GFP* line (Robatzek et al., 2006) suggested that FLS2 protein levels are unchanged after 1 hour of combined hypoxia/flg22 treatment compared to individual treatments (Figure 3.11B), perhaps because a longer timepoint would be needed to detect changes in protein abundance.

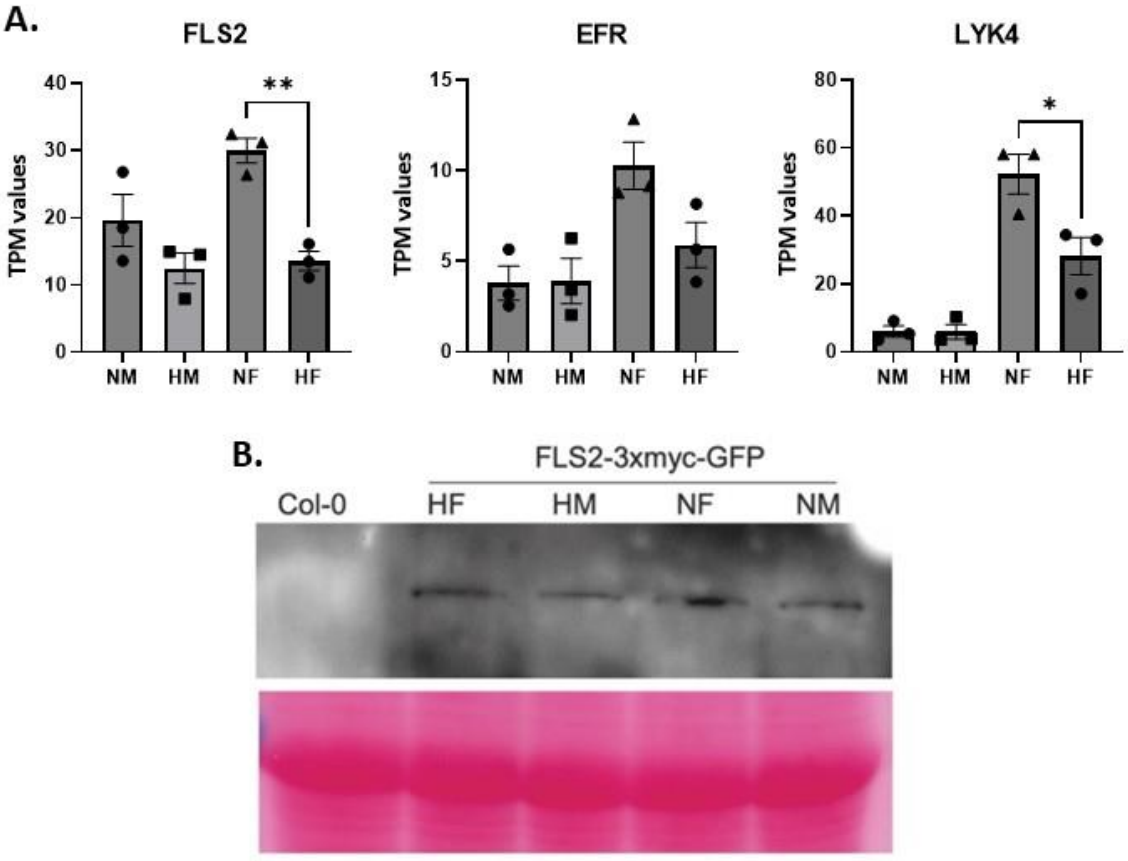

Figure 3.11. Expression of PRRs under combined and individual hypoxia and flg22 treatment. A. TPM values of the PRR genes, *FLS2*, *EFR* and *LYK4*, are shown with means and SEM plotted using GraphPad Prism. The results of statistical tests (one-way ANOVA with Tukey test) for relevant comparisons are shown. B. Anti-GFP immunoblot for accumulation of FLS2-3xmyc-GFP protein upon 1 hour treatment of HF, HM, NF, and NM.

3.2.3. Investigating the repression of PTI by hypoxia and potential underlying mechanisms

The transcriptomic analysis of plant responses to combined hypoxia/flg22 indicates that hypoxia suppresses part of the flg22 response programme, at least at the transcriptional level. Here, I tested whether different aspects of PTI were also repressed by combined hypoxia/flg22 as opposed to flg22 or hypoxia treatments alone. In addition, I sought to identify potential molecular mechanisms. Due to the role of ERFVII transcription factors as master regulators of the hypoxia response as well as conflicting roles in susceptibility to various plant pathogens, I investigated the role of the ERFVIIs in regulating the hypoxia-mediated suppression of flg22 responses. In addition, as outlined in the introduction (sections 1.3, 1.4.2.3, and 1.5.2), NO signalling is a key player in the regulation of plant responses to hypoxia and to flg22, and this signalling molecule is also tightly linked to the N-degron pathway via the degradation of the ERFVIIs. Hence, I also investigated a potential role of NO signalling in the regulation of plant responses to combined hypoxia/flg22.

3.2.3.1. Effect of combined hypoxia/flg22 in root inhibition assays

A typical test to assess the ability of plants to trigger PTI involves monitoring either seedling survival or the inhibition of root elongation during prolonged exposure to flg22, with the idea being that mutants that are insensitive to flg22 or that are affected for their ability to trigger PTI will survive and will continue to grow despite the presence of flg22. In the field of hypoxia research, the inhibition of root elongation by hypoxia treatment is also often used to determine plant tolerance to low oxygen and their ability to survive this stress. Hence, monitoring the inhibition of root elongation in the presence of individual hypoxia or flg22 treatments and comparing it to combined hypoxia/flg22 is a suitable approach to detect any additional repressive effects that might result from the combined treatment. As expected, either flg22 (NF) or hypoxia (HM) treatments resulted in decreased root elongation compared to the same genotype in control conditions (normoxia/mock (NM)), with hypoxia having a stronger inhibitory effect than flg22 (Figure 3.12). Combined hypoxia/flg22 (HF) did not enhance the inhibitory effects of hypoxia on the inhibition of root elongation in wild-type Col-0.

To test the contribution of ERFVII transcription factors in root growth inhibition to hypoxia/flg22 combined or single treatments, *erfVII* quintuple mutants were used. Analyses with the *erfVII* mutant were complemented by using the N-degron pathway mutant, *ate1 ate2*, because of its constitutive accumulation of the ERFVIIs. The *ate1 ate2* mutant showed similar results to Col-0

for all treatments, but the *erfVII* quintuple mutant was more severely affected by the combined stress (Figure 3.12), thus suggesting that expression of ERF-VIIs in the wild type may contribute to protecting the root meristem under combined hypoxia/flg22 treatment, but that their accumulation in *ate1 ate2* is not sufficient to protect the meristem. However, one possibility is that the hypoxia treatment used was too severe (0.5% O_2 for 48 hours). A milder treatment may have allowed for additive effects of the combined hypoxia and flg22 to be identified in other genotypes.

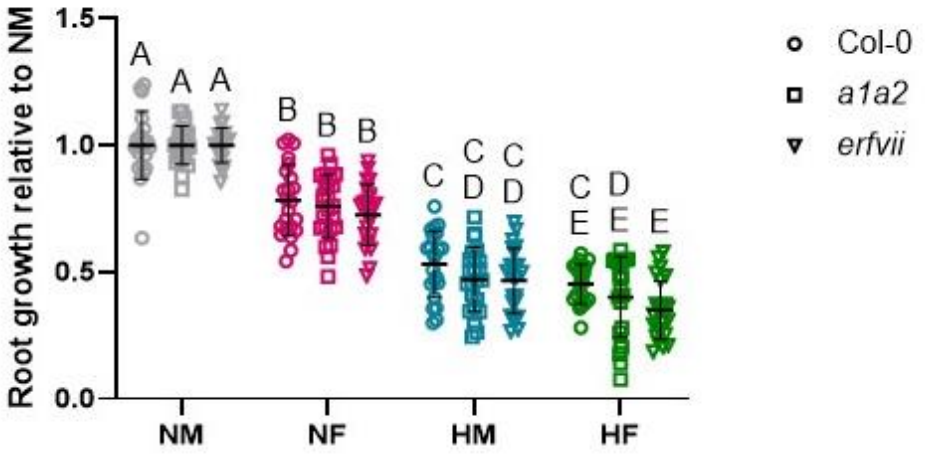

Figure 3.12. Individual and combined hypoxia and flg22 treatment on root growth of Col-0 and erfVII seedlings. Root growth inhibition assays with Col-0, *ate1 ate2* (a1a2) and *erfVII* (erf) mutant seedlings under combined hypoxia/flg22 treatment, and control conditions (NM) or individual hypoxia (HM) and flg22 (NF) treatments. Means relative to NM and standard deviations of four biological replicates with five-six seedlings/genotype/condition in each biological replicate are shown. The results of statistical tests (two-way ANOVA with Tukey test) are presented in a compact letter display (CLD) format.

3.2.3.2. Effect of hypoxia/flg22 on PRR expression

As outlined in section 3.2.2.3, hypoxia/flg22 treatment is sufficient to dampen the upregulation of PRR expression compared to flg22 treatment. Here, I investigated whether the ERFVIIs and NO signalling could play a role in mediating this reduced PRR expression upon combined treatment. Like 3.2.3.1. above, *erfVII* and the N-degron pathway mutant, *prt6-5,* were employed to test the role of the ERFVIIs in the repression of PTI. To study the contribution of NO, I made use of mutants that are affected for their NO levels, including a mutant for *HB1* (SALK_058388, noted *hb1*), whose function as a NO scavenger is impaired (Hartman et al., 2019). A mutant for *NO ASSOCIATED 1* (*NOA1*) (SALK_047882, noted *noa1*), which has been implicated in NO synthesis through the oxidative process was also used, with this mutant producing lower NO

levels (Lozano-Juste and Leon, 2010). Finally, the *gsnor1-3* (GK-315D11.03) which has higher GSNO levels and subsequent S-nitrosylation of target proteins was also used (GSNOR1 is involved in reducing GSNO levels) (Feechan et al., 2005).

Expression analysis by RT-qPCR confirmed that hypoxia dampens the upregulation of PRR-coding genes such as FLS2 and EFR (Figure 3.13A), through mechanisms that appear to be mostly independent from the ERF-VIIs as both *erfVII* and *prt6-5* mutants behave similarly to WT (Col-0). The data presented with the NO mutants remains preliminary because of the variation and additional replicates are needed for a better statistical analysis. Conclusions are difficult to draw, but NO does not appear to play a major role in the dampening of *FLS2* and *EFR* expression during combined stress (Figure 3.13B).

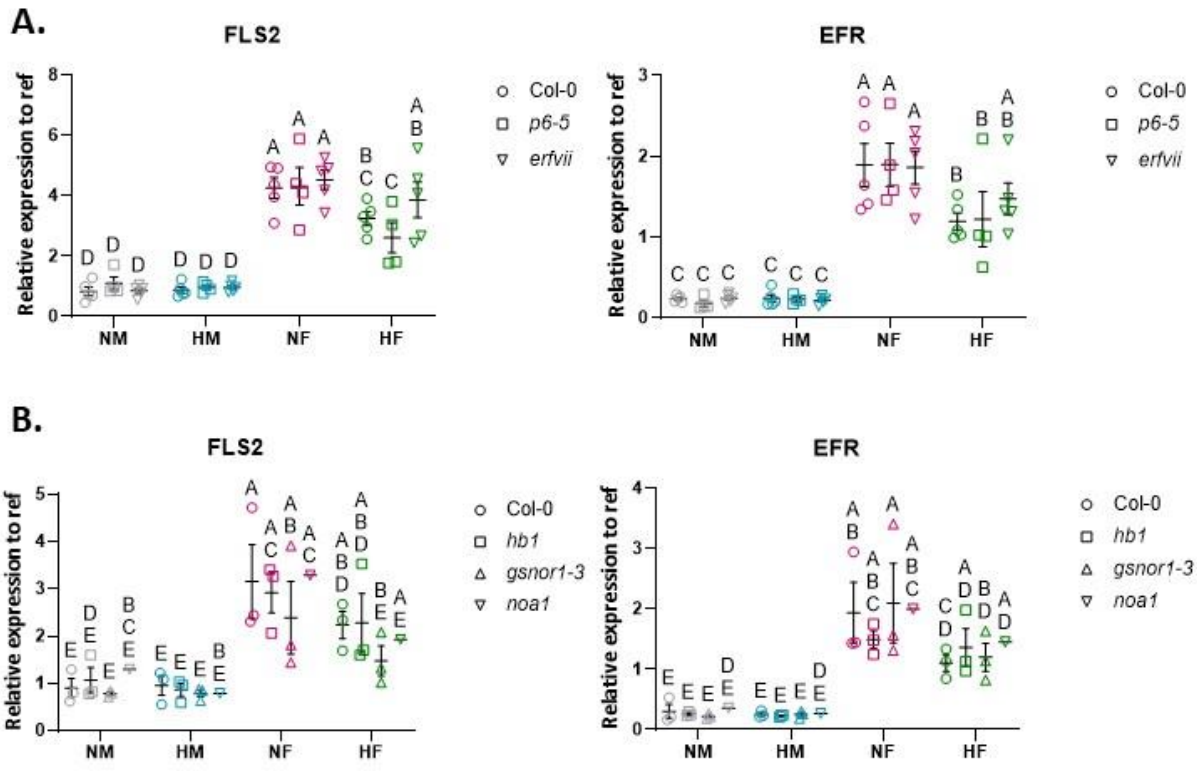

Figure 3.13. Role of the N-degron pathway and NO signalling on hypoxia-reduced PRR expression. A. RT-qPCR expression analysis of *FLS2* and *EFR* using the genotypes: Col-0, *prt6-5* and *erfVII*, treated to HF, HM, NF and NM. **B.** Similar RT-qPCR analysis of *FLS2* and *EFR* expression using the genotypes Col-0, *gsnor1-3*, *hb1* and *noa1*. Mean and SEM are shown. The results of statistical test results (two-way ANOVA with Fisher's test) are displayed in CLD format.

3.2.3.3. MAPK signalling

Activation of MAPK signalling downstream of PRR activation by PAMP binding is a key early event in the onset of PTI (see section 1.4.2.1.). Nine-day old seedlings, grown in continuous light, were transferred to 0.5xMS medium and placed on a shaker overnight. The following day, the seedlings were treated with 100 nM flg22 (or mock = PBS) in anaerojars (hypoxia) or under ambient oxygen conditions (normoxia) for 30 minutes. Immunoblots with anti-phosphorylated MPK antibodies indicated that the phosphorylation of MPK3 and MPK6 is reduced in Col-0 seedlings under combined hypoxia/flg22 treatment compared to flg22 treatment (Figure 3.14A). A reduction in MPK3/6 phosphorylation was also observed with the *erfVII* mutant (Figure 3.14A). Similar results between Col-0 and *erfVII* mutants for this repressive effect of hypoxia on flg22-mediated MAPK phosphorylation suggests that this process is independent of the ERFVII transcription factors (Figure 3.14B). In contrast, *MPK3/4/6* expression was not repressed under hypoxia/flg22 compared to flg22 treatment alone (Figure 3.14C), suggesting that post-transcriptional or post-translational mechanisms downstream of FLS2 are likely responsible for the decreased MAPK signalling activation.

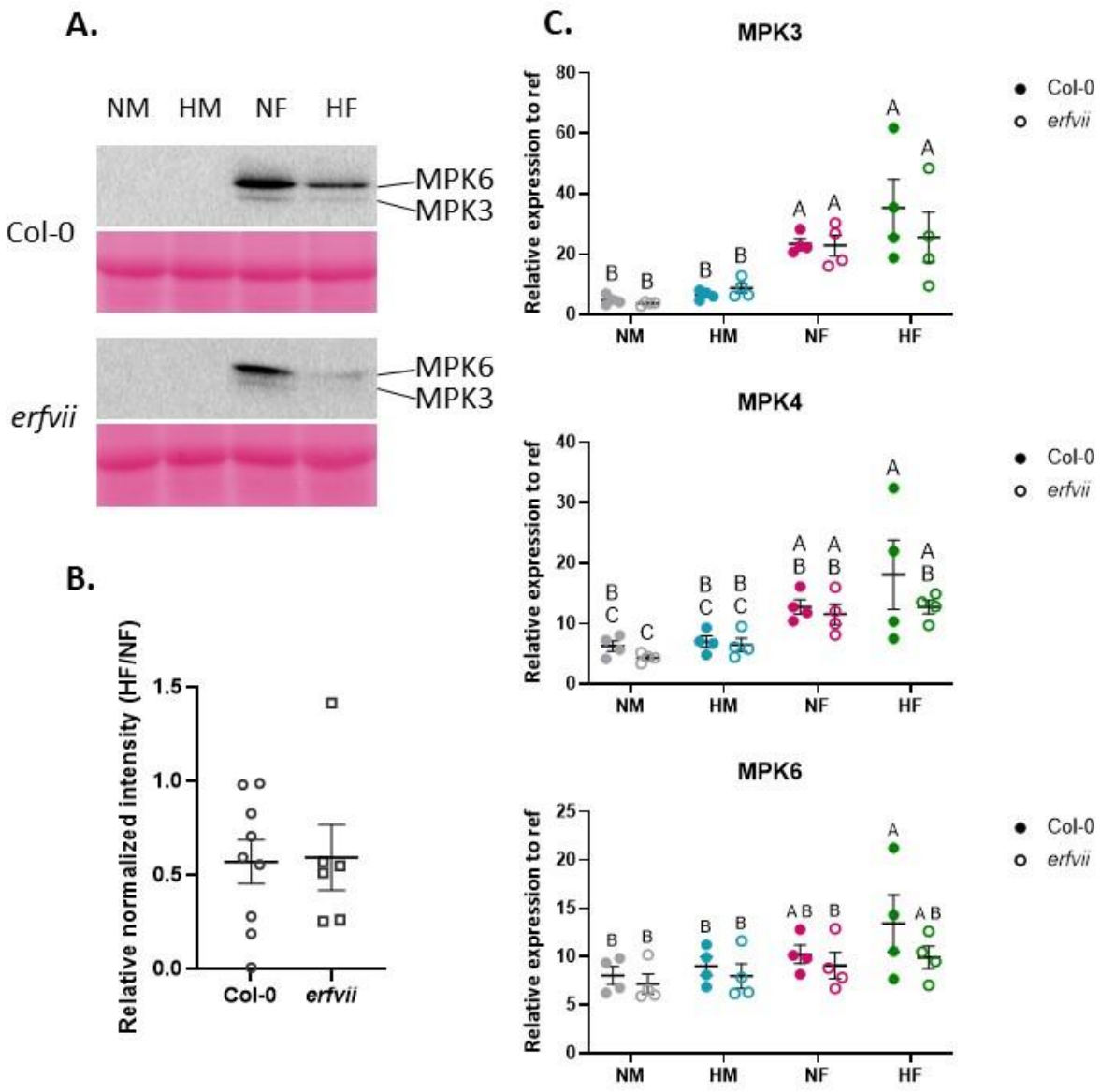

Figure 3.14. Impact of hypoxia and ERFVIIs on flg22-induced MAPK-phosphorylation. A. Anti-phosphorylated MPK immunoblots using Col-0 and *erfVII* mutant seedlings. **B.** Relative intensity of MPK signals under combined hypoxia/flg22 compared to normoxia/flg22 after normalization with Ponceau intensity. Mean and SEM are shown. Nine biological replicates are presented for Col-0 and six biological replicates are presented for *erfVII*. **C.** RT-qPCR results for expression of *MPK3*, *MPK4* and *MPK6* relative to a reference gene (*MON1*) in Col-0 and *erfVII* seedlings treated with HF, HM, NF and NM. Mean and SEM of four biological replicates are shown. The results of statistical test results (two-way ANOVA with Fisher's test) are displayed in CLD format.

3.2.3.4. Callose deposition

Callose deposition is another hallmark of PTI which could be affected by the combined hypoxia/flg22 treatment considering the identification of cell wall related GO terms identified as enriched in the transcriptomic datasets. I hence tested whether callose deposition was affected upon combined hypoxia/flg22 compared to individual treatments. Ten-day old seedlings, grown under short-day light conditions were treated +/- 1 µM flg22 under hypoxic (5% oxygen; 0% carbon dioxide) applied using PhO2X Box (Baker Ruskinn)) or normoxic (ambient oxygen) conditions for 24 hours. Callose deposits are visible as bright puncta after staining with 0.01% aniline blue (Figure 3.15A). Callose deposition was visually lower in hypoxia/flg22 treated samples compared to treatment with flg22 alone (Figure 3.15A). To quantify the callose deposition in response to each treatment condition, the Fiji plugin Weka Segmentation classifier, was trained to identify the callose puncta and ignore other structures such as the veins. Quantification results show significantly decreased callose deposition under combined hypoxia/flg22 conditions in Col-0 compared to treatment with flg22 alone (Figure 3.15B).

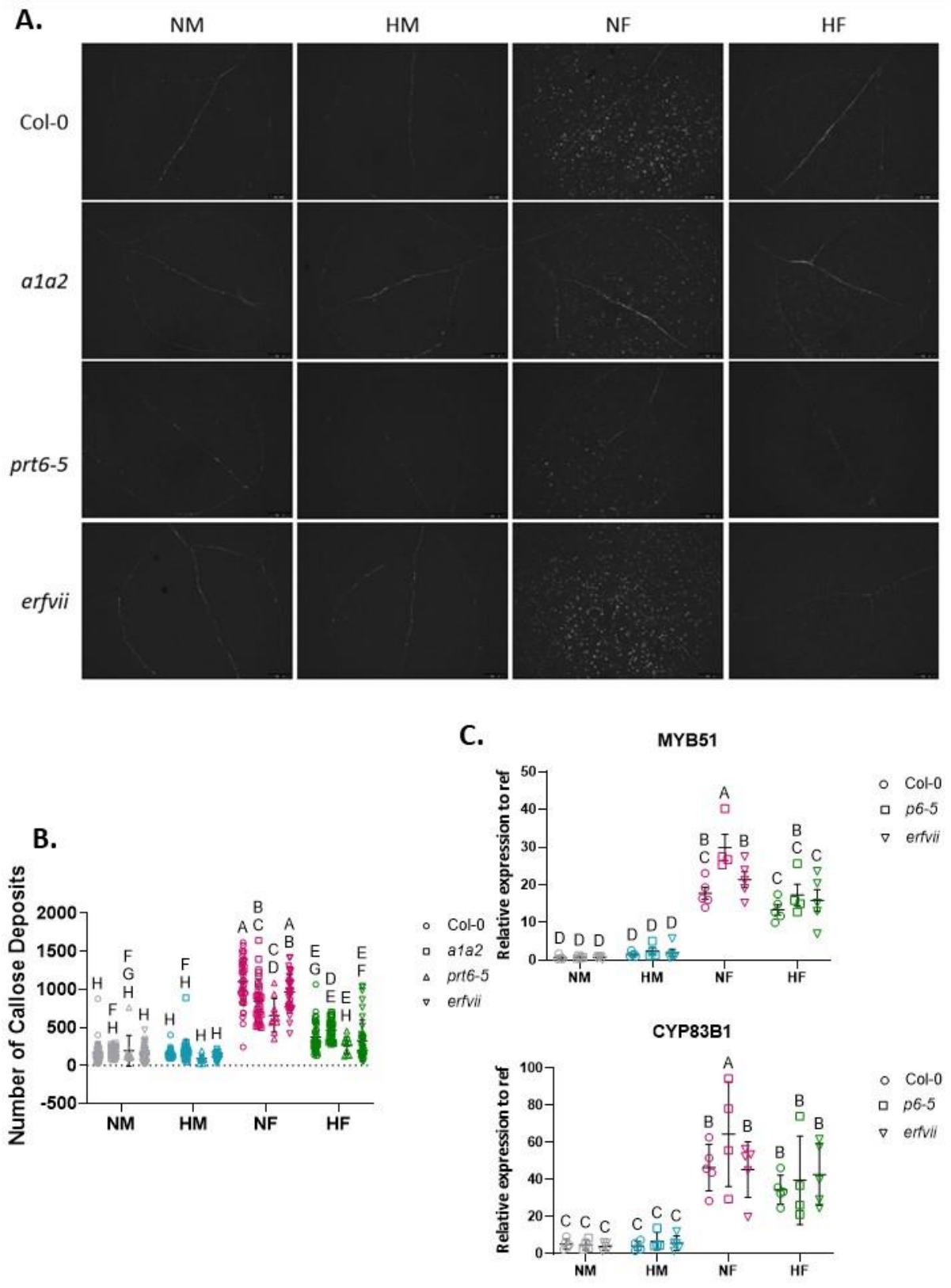

Figure 3.15. Impact of hypoxia and function of N-degron pathway in flg22 induced callose deposition. A. Representative images of callose deposition in 10-day old Col-0, *ate1ate2, prt6-5* and *erfVII* treated to +/- hypoxia (5% oxygen) +/- 1 µM flg22 for 24 hours, followed by chlorophyll removal and staining with 0.01% aniline blue. **B.** Quantification of A using Fiji image analysis. Mean and standard deviations of four

biological replicates with five seedlings/genotype/condition in each biological replicate are shown. The results of statistical tests (two-way ANOVA with Tukey test) are represented in CLD format. **C.** RT-qPCR analysis of *MYB51* and *CYP83B1* expression for Col-0*, prt6-5* and *erfVII* treated with 100 nM flg22 for 1 hour. Means and SEMs are shown for five biological replicates for Col-0 and *erfVII* and four biological replicates for *prt6-5*. A two-way ANOVA with Fisher's test was conducted, and results are depicted in CLD format.

To investigate whether the ERFVIIs and/or their N-degron dependent degradation could be involved in the repression of callose deposition during combined hypoxia/flg22 treatment, callose deposition was also monitored in the *ate1 ate2, prt6-5* and *erfVII* mutant seedlings. These assays showed that the *erfVII* quintuple mutant behaved similarly to the wild type, suggesting that the reduction of callose deposition may not be ERFVII dependent. In contrast, the *ate1 ate2* and *prt6-5* mutants were negatively affected for callose deposition in response to flg22 treatment alone (Figure 3.15A and 3.15B). This suggests that the constitutive activation of hypoxia response in these mutants dampens the deposition of callose in response to flg22 even under normoxic conditions. This may be due to the accumulation of the ERFVII transcription factors in these mutants. To test whether ERFVIIs are responsible for the reduced callose deposition upon flg22 treatment in N-degron pathway mutants and have a rescuing effect, higher order mutants (e.g. *ate1 ate2 erfVII* or *prt6-5 erfVII*) would need to be used. Alternatively, the effects observed in *ate1 ate2* and *prt6-5* mutant seedlings could be linked to the accumulation of other N-degron pathway substrates whose degradation is also oxygen dependent and that play a role in hypoxia response (e.g. VRN2 (Gibbs et al., 2018)).

Expression of important genes for the biosynthesis of callose *MYB DOMAIN PROTEIN 51 (MYB51)* and *CYTOCHROME P450 FAMILY 83 SUBFAMILY B (CYP83B1)* (Figure 3.15C) were monitored in Col-0, *prt6-5* and *erfVII* seedlings through RT-qPCR. MYB51 is required for flg22-induced callose deposition. It was previously shown to be involved in regulating the expression of indolic glucosinolate biosynthesis genes including *CYP83B1*. This could be relevant to the callose deposition defects observed, as the indole glucosinolate, 4-methoxy-I3G, is necessary for callose deposition (Clay et al., 2009). NF and HF treatments both resulted in increased expression of these two genes in the three genotypes tested. However, there were differences between *prt6-5* and the Col-0 and *erfVII* seedlings, both of which behaved similarly to each other. Indeed, in the *prt6-5* mutant, there was significantly higher expression of *MYB51* upon flg22 treatment alone compared to the Col-0 or *erfVII* seedlings. This went against the observation that prt6-5 seedlings have reduced callose deposition. While it appeared that there was reduced expression

in combined hypoxia/flg22 compared to flg22 treatment, this was only significant in *prt6-5* for *MYB51* and *CYP83B1* and in *erfVII* for *MYB51*. Combined hypoxia/flg22 resulted in similar levels of expression for both genes in all three genotypes. Altogether, these findings suggest that the expression level of *MYB51* and *CYP83B1* do not correlate with the levels of callose deposition.

1,3 ß-glucanases are responsible for the degradation of callose. Out of the fifty 1,3 ß-glucanases encoded in the Arabidopsis genome (Doxey et al., 2007), four were differentially expressed in the HF v NM RNA-Seq dataset (AT2G27500; AT3G55430; AT4G18340; AT4G34480). While some of these DEGs are expressed at higher levels upon combined hypoxia/flg22 compared to flg22 treatment (Figure 3.16, the differences are not statistically significant. Thus, it is possible that the repression of callose deposition upon combined hypoxia/flg22 may result from post-translational regulatory mechanisms, such as protein degradation or post-translational modifications.

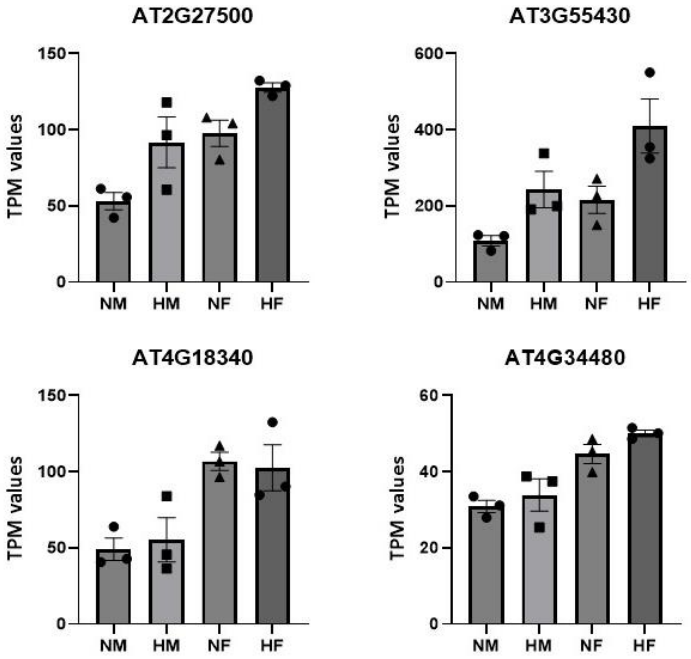

Figure 3.16. Hypoxia/flg22 induced expression of 1,3 ß-glucanases. TPM values from RNA-seq analysis of the 1,3 ß-glucanases (*AT2G27500; AT3G55430; AT4G18340; AT4G34480*) which are differentially expressed in HF v NM dataset. Mean and SEM are plotted using GraphPad prism.

The role of NO in the repressive effect of hypoxia on callose deposition was also investigated. Due to time constraints only one biological replicate could be performed. The preliminary results of callose deposition assays under normoxic conditions (NF) showed that NO is important for

flg22-dependent callose deposition (in line with previous studies, see discussion), with a significant reduction of callose deposits in *hb1* and *gsnor1-3* seedlings and a near lack of deposition in *noa1* seedlings (Figure 3.17A and 3.17B). The mutants show the same phenotype of lower callose deposition despite some of them having presumed lower or higher NO levels. This could suggest that the correct balance of NO levels may be important in this response. Under combined hypoxia/flg22, the *gsnor1-3* and *hb1* mutants retained a reduction in callose deposition compared to their respective genotypes treated with flg22 alone. Hence, it appears that the reduction of callose deposition under combined hypoxia/flg22 is not NO dependent. The *noa1* mutant kept the near absence of callose under hypoxia/flg22 treatment, as was observed under normoxia/flg22 (Figure 3.17A and 3.17B), so that *NOA1* appears to be necessary for flg22 induced callose under both hypoxic and normoxic conditions. However, caution must be taken as further biological replicates are needed to validate these preliminary conclusions. RT-qPCR results show that expression differences of *MYB51* and *CYP83B1* (Figure 3.17C) are unlikely to be the source of the impact of NO on callose deposition (Figure 3.17C).

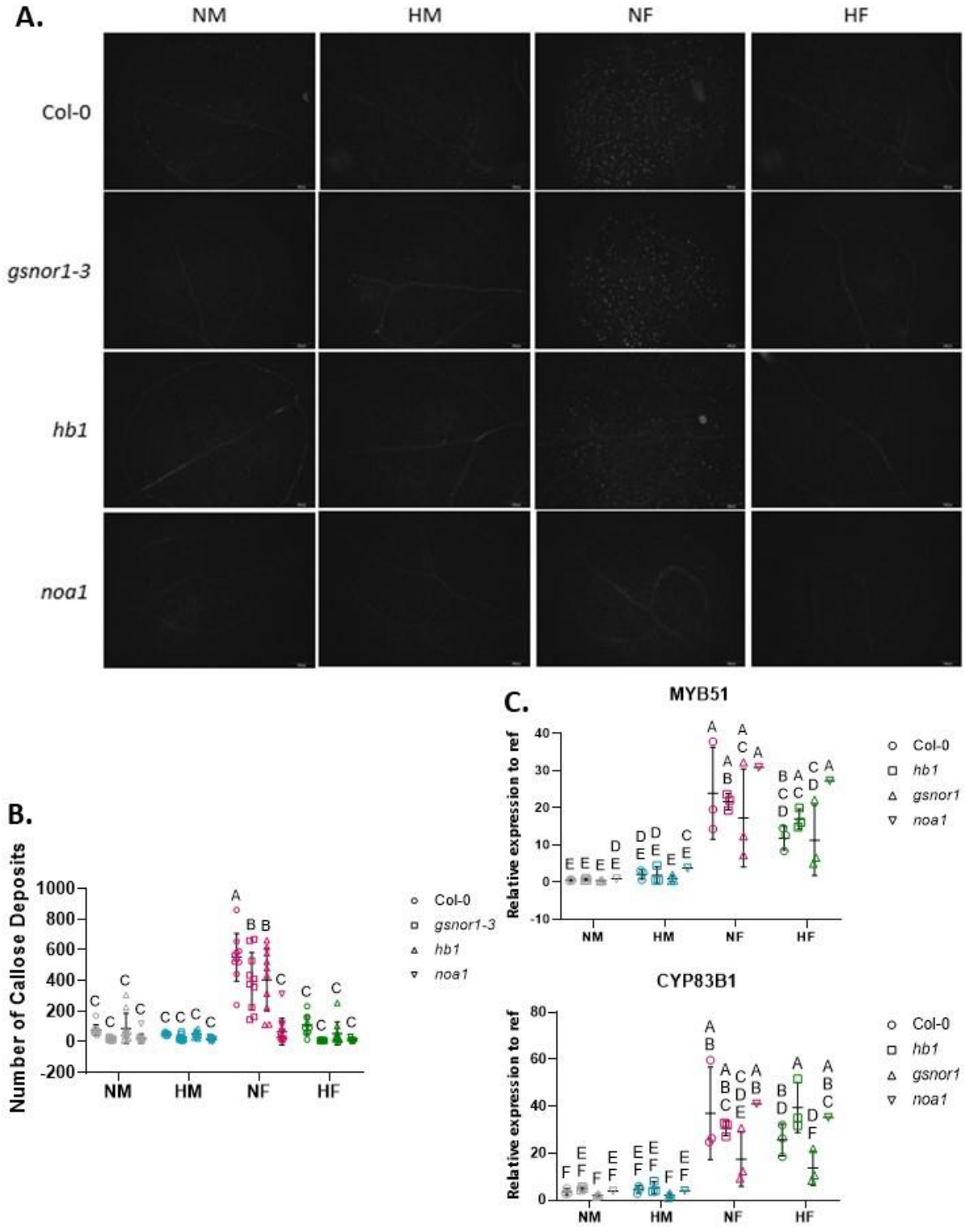

Figure 3.17. Role of hypoxia and NO on flg22 induced callose deposition. A. Representative images of callose deposition in 10-day old Col-0, *gsnor1-3, hb1* and *noa1* treated to +/- hypoxia (5% oxygen) +/- 1 µM flg22 for 24 hours, chlorophyll destaining and staining with 0.01% aniline blue. n = 1 with five seedlings/genotype/condition in each biological replicate. **B.** Quantification of A using Fiji image analysis. Mean and standard deviation are shown. Statistical test (two-way ANOVA with Tukey test) results are

presented in CLD format. **C.** RT-qPCR analysis of *MYB51* and *CYP83B1* for Col-0, *gsnor1-3, hb1* and *noa1*. n = 3 for Col-0, *hb1* and *gsnor1*. n = 1 for *noa1*. Mean and SEM are shown. A two-way ANOVA with Fisher's test was run and results were shown in CLD format.

3.3. Discussion

Transcriptomic analysis was conducted for individual and combined hypoxia and flg22 treatments of wild-type Col-0 Arabidopsis seedlings in order to better understand interactions and crosstalk between these stresses, when experienced simultaneously by plants. The use of metrics developed to answer such questions using transcriptomics datasets (Tan et al., 2023) indicated a repression of flg22 transcriptional responses by hypoxia, as well as a novel transcriptional response to hypoxia/flg22 compared to individual stresses (Figure 6A). Further analysis of the transcriptomics datasets uncovered potential points of intersection for hypoxia and immunity and ruled out others.

Bjornson et al., 2021, highlighted similarities/overlaps in early responses to different PAMPs and abiotic stresses and showed common genes were induced suggesting an early general stress response. However, the extent of this general stress response and the similarities between stress responses was unclear. Here, a set of 59 common DEGs by hypoxia and/or flg22 treatments were identified, which were enriched for genes associated with responses to hypoxia, cell wall modifications and ethylene signalling. In agreement with the small number of genes common to individual and combined treatments, the overall similarity score between the datasets was low. This suggests that while there are common DEGs and pathways targeted by hypoxia and flg22, in general, the responses to these two stresses is quite different showing that by 1 hour, there is already specificity in plant response to low oxygen and flg22.

WRKY transcription factors are known for their roles in development as well as stress responses. Previous studies looking at plant responses to PAMPs, pathogens and different abiotic stresses show an overrepresentation of this transcription factor family (Bjornson et al., 2021). In particular, *WRKY33* is an important regulator of immune responses (detailed in section 1.4.3.), but it has also been shown to upregulate the expression of *RAP2.2* (one of the *ERFVII*s) and has a positive effect on submergence tolerance (Tang et al., 2021). These results suggest a role for this transcription factor in the combination of hypoxia/immune stresses. In line with this idea, *WRKY33* has higher (however not significant) induction in HF compared to NF treated samples

(Figure 3.1C and 3.4E). WRKY transcription factors were also enriched in HF only responses, highlighting their potential protective role in multistress tolerance. WRKYs induced by HF treatment included *WRKY2, WRKY38, WRKY51, WRKY62*, and *WRKY70*. Of interest, WRKY51 and WRKY70 are transcripiton factors which have been shown to inhibit JA response gene expression (Li et al., 2004; Yan et al., 2018), with WRKY70 upregulating SA response genes (Li et al., 2004; Wani et al., 2021). This particular transcription factor could therefore contribute to coordination between phytohormone signalling pathways upon combined stress.

This work highlighted a potentially relevant role for JA signalling in novel aspects of the transcriptional response to combined hypoxia/flg22. MYC2 being significantly induced under hypoxia/flg22 treatment suggests that this transcription factor, which is a master regulator of JA response genes, may act as an integrator of hypoxia and flg22 responses when the 2 treatments are combined. This is reminiscent of results in *Medicago truncatula*, in which the related *MYC3* gene was upregulated by the combination of drought and ozone (Iyer et al., 2013; Suzuki et al, 2014). Hence, the MYC transcription factors may act more generally as regulators of responses to multiple combined stresses, and here, could act as a point of convergence or perhaps integration for plant hypoxia and flg22 responses. MYC2 upregulation under hypoxia/flg22 may also explain some of the dysregulation of flg22 responses, as MYC2 has been shown to downregulate pathogen responses in favour of responses to wounding and herbivory (Lorenzo et al., 2004; Song et al., 2014). For example, MYC2 negatively regulates indole glucosinolate biosynthesis, which can contribute to callose deposition (Clay et al., 2009). Hence the upregulation of MYC2 correlates well with the observed decreased deposition of callose upon combined hypoxia/flg22 treatment. Beyond the combined treatments used here, the role of JA in hypoxia response has not been fully explored. The ability of MYC2 to bind to the promoter of some hypoxia genes including five core hypoxia response genes (Mustroph et al., 2009), such as *PDC2, ATYPICAL CYS HIS RICH THIOREDOXIN 5 (ACHT5), JAZ3, AT1G74940* and *AT5G10040*, may suggest a direct connection between JA and the regulation of hypoxia response. This link has been explored during my Ph.D. work, with results presented in Chapter 4.

Genes associated with the UPS were enriched among those that are differentially expressed by combined hypoxia/flg22 treatments only, thus suggesting, that the UPS may play an important role in the regulation of plant response to this particular combination of stresses. Considering the important role of the N-degron pathway in the regulation of ERFVII protein stability, and the fact that these transcription factors act as master regulators of hypoxia response while also

having roles during plant/pathogen interactions, I explored whether the N-degron pathway could contribute to the regulation of plant responses to combined hypoxia/flg22. However, the results suggest that this is not the case. I did not have time to follow-up on some of the UPS components identified in this work, but one hypothesis is that they may be of interest to understanding the crosstalk between hypoxia and flg22 responses.

A key finding, from the transcriptional analysis as well as the characterization of PTI-associated responses under combined hypoxia/flg22, is that hypoxia has a negative impact on multiple PTI-related processes, including PRR gene expression, MAPK-phosphorylation and callose deposition (Figure 3.18). Phosphorylation appeared as an enriched GO term in flg22 treated samples only, suggesting that this was dysregulated in combined hypoxia/flg22 treatments. One question was whether hypoxia-mediated repression of PTI responses could be accounted for by this dysregulation of phosphorylation? It was seen that flg22-mediated MAPK-phosphorylation was significantly reduced under hypoxic conditions which may effect the activation of downstream targets. Follow-up experiments could seek to compare the response of a *mpk3 mpk6* double mutant to individual and combined hypoxia/flg22 treatments. The molecular mechanisms resulting in the repression of PRR expression under combined treatment remain to be explored.

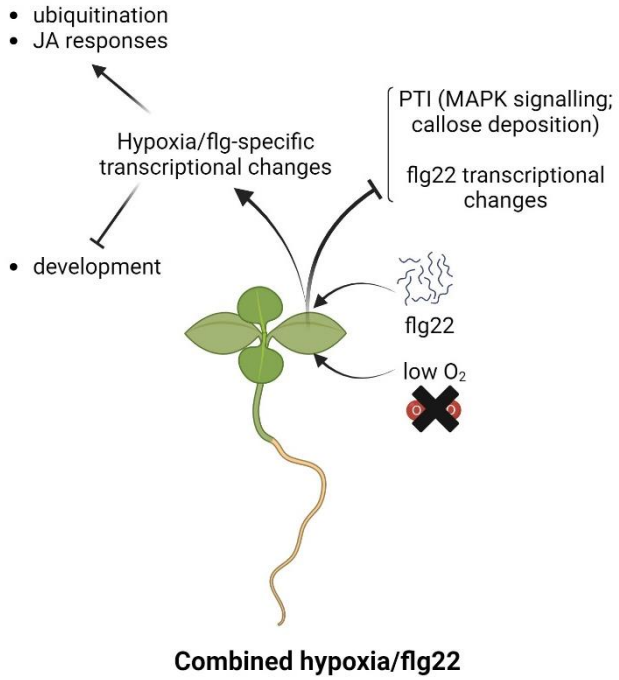

Figure 3.18. Model for results of this chapter. Created with BioRender.com

While the N-degron pathway and NO did not appear to play key roles in hypoxia-induced repression of flg22 response (apart from ERFVIIs having a protective effect against root growth inhibition under combined hypoxia/flg22 treatment), the N-degron pathway and NO were shown to be important for callose deposition. *ate1 ate2* and *prt6-5* mutants exhibit significantly reduced levels of callose deposition in response to flg22 under normoxic conditions. However, this repression does not appear to occur through the repression of callose biosynthesis genes in the mutants, as previous transcriptomics analysis do not suggest such a possibility. Instead, the reduced callose deposition in these mutants could potentially be a consequence of lower glucosinolate levels in these mutants (de Marchi et al., 2016). Alternatively, the constitutive activation of hypoxia response in *ate1 ate2* and *prt6-5* could also contribute to the decreased callose deposition phenotype (*e.g.* callose content changes upon hypoxia treatment of wheat seedlings (Albrecht and Mustroph, 2003; Subbaiah and Sachs, 2001)). In line with this, there was a possible rescuing effect in *erfVII* mutants, suggesting that the reduced callose deposition in N-degron pathway mutants could be ERFVII-dependent. However, the effect of hypoxia treatment further suppresses flg22-induced callose in *ate1 ate2* and *prt6-5* seedlings, suggesting that there are N-degron pathway-independent effects of hypoxia on callose deposition upon combined treatment. As well, *erfVII* mutants showed no statistically significant differences compared to Col-0 for hypoxia/flg22 treatments, suggesting that ERFVIIs are also not responsible for the decreased callose deposition under combined hypoxia/flg22. NO was also shown to be important for callose deposition which is in line with previous studies found that injection of a NO donor (sodium nitroprusside (SNP)) into soybean leaves results in the induction of callose deposits (Xiao et al., 2018). NO was also important for soybean mosaic virus-induction of callose. NO scavengers and NOS and NR inhibitiors delayed the viral induction of callose deposition and subsequently increased susceptibility of the soybean plants to the virus (Xiao et al., 2018). Further, in Arabidopsis, fumegation with the RNS, NO2, increases early induction of PAMP (chitosan)-dependent callose deposition (Mayer et al., 2018). In this study, preliminary results showing that the NO mutants, *gsnor1-3, hb1* and *noa1,* have decreased callose deposits in response to flg22 under normoxia. The fact that these mutants all show inhibition of callose deposition highlights the differences in function of NO and GSNO and highlights the importance of balancing NO levels. Further, *noa1* is shown to be required for flg22-induced callose deposition under both hypoxic and normoxic conditions. Whether the similarities in these results between N-degron pathway and NO mutants is due to NO signalling through the N-degron pathway e.g. NO's role in regulating ERFVII stability will need further study.

Combined hypoxia/flg22 treatment indicates that plants or tissues experiencing acute hypoxia are likely to be more susceptible to pathogens. This has implications in terms of crop production, as it suggests that flooding may have a negative impact on the ability of plants/crops to fight-off pathogens. This could be exacerbated by the fact that flooding also causes an increased risk of pathogen infection, likely as a result of increased dampness and changes to the soil and plants' microbiomes (Gschwend et al., 2020; Hartman and Tringe, 2019). A previous study showed that a submergence pre-treatment was able to increase resistance to *Pst* DC3000 by inducing the expression of *WRKY22* (Hsu et al., 2013), highlighting that the timing of these stresses as well as the plant age/stage, infection and abiotic stress burden can impact combined stress responses (Saijo and Loo, 2020). Hence, the crosstalk between hypoxia and immunity is a new trait to consider in our endeavour to generate more climate resilient crops.

In sum, the findings of this work are that combined hypoxia and flg22 induces hypoxia/flg22 specific transcriptional responses including regulating UPS-related genes and JA response genes, while repressing developmental responses including auxin-related signalling. At the same time, combined hypoxia/flg22 treatments inhibit flg22-induced transcriptional responses, particularly related to phosphorylation and cell-surface receptors, as well as downstream signalling and physiological responses (e.g. MAPK signalling and callose deposition (Figure 3.18)). Identifying the underlying mechanisms for this negative impact of hypoxia on flg22-induced responses requires further work, which could mirror some of the work and findings in the mammalian field of hypoxia/immunity.

Chapter 4: Exploring the connections between the N-degron pathway, JA signalling and hypoxia response

4.1. Introduction

JA is an oxylipin phytohormone involved in a multitude of biological processes from development to response to environmental stresses, both abiotic and biotic. The lipoxygenase pathway mediates the biosynthesis of many development and stress-related metabolites (reviewed in (Feussner and Wasternack, 2002; Viswanath et al., 2020)). Formation of JA and its precursor 12-oxophytodienoic acid (OPDA) from α-linolenic acid makes up one branch of this lipoxygenase pathway (Feussner and Wasternack, 2002; Viswanath et al., 2020; Wasternack and Song, 2017). JA itself can then be enzymatically modified to yield a range of JA derivatives, including the bioactive jasmonyl-L-isoleucine (JA-Ile), as well as JA methyl ester (MeJA), which is used to transport the phytohormone (Wasternack and Song, 2017). JA and its derivatives have been shown to regulate the response to a wide range of (a)biotic stresses and plays a key role in the regulation of the trade-off between growth and defence (Major et al., 2017). Here, I will focus on the role of JA in plant defence, as well as in hypoxia response. I will also detail the regulation of the JA signalling pathway by the UPS.

4.1.1. The JA signalling pathway and its regulation by the UPS

4.1.1.1. JA signalling relies on the degradation of the JAZ repressors

At the core of JA signalling are proteins which act to repress JA-response genes until perception of a specific environmental or developmental cue. These proteins, known as JAZ proteins, act as repressors by interacting with transcription factors that regulate JA-response genes, including one of the master regulators of JA-response gene expression, MYC2 (Chini et al., 2007). The Arabidopsis genome codes for 13 JAZ proteins, which are characterised by an N-terminal ZIM domain and a C-terminal Jas domain (Figure 4.1) (Chini et al., 2007; Howe et al., 2018; Thines et al., 2007; Thireault et al. 2015).

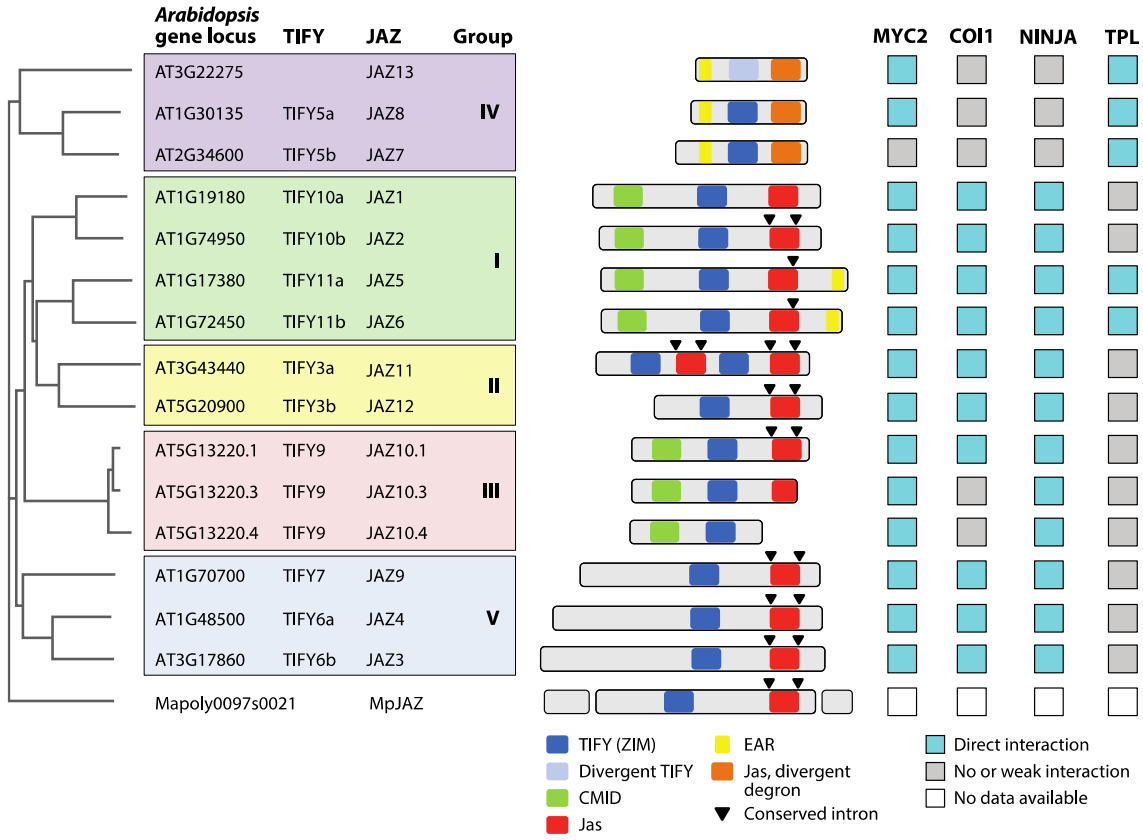

Figure 4.1. Domain architecture of JAZ proteins. In Arabidopsis, the JAZ protein family contains 13 members, defined by the presence of TIFY (ZIM) and Jas domains, some of which are divergent. The 13 JAZ proteins fall into 5 phylogenetic groups, with those in group IV being non-canonical JAZ proteins. Figure from (Howe et al., 2018).

The ZIM domain contains the conserved TIFY motif (TIF[F/Y]XG) which is important for JAZ protein repressor function through the recruitment of the protein NOVEL INTERACTOR OF JAZ (NINJA), which contains an ERF-associated amphiphilic repression (EAR) domain that mediates binding to TOPLESS (TPL) and TPL-like proteins (Howe et al., 2018; Kagale et al., 2010; Pauwels et al., 2010; Shyu et al. 2012). TPL and TPL-like proteins then recruit epigenetic regulators such as the histone deacetylase HDA6, which removes histone acetylation marks, resulting in the repression of transcription (Wu et al., 2008; Zhu et al., 2011) (see also section 4.1.1.2.).

The Jas domain has been shown to be important for protein-protein interactions (Chini et al., 2007; Chini et al., 2009; Chung and Howe, 2009; Sheard et al., 2010; Thines et al., 2007; Thireault et al. 2015) and contains two conserved motifs: 1) the ELPIARR motif in the loop region at the N-terminus (Sheard et al., 2010); and 2) the KRK motif at the C-terminus of the Jas domain (Withers et al., 2012). The latter has been implicated in the interaction with transcription factors such as

the MYC proteins. In contrast, the ELPIARR sequence acts as a degron that is bound by the F-box protein CORONATINE INSENSITIVE1 (COI1) (Sheard et al., 2010), a subunit of the Skp1/Cullin/F-box (SCF)^{COI1} E3 ubiquitin ligase complex. SCF^{COI1} forms a co-receptor for JA-Ile with JAZ proteins. This binding of JAZ proteins to SCF^{COI1} occurs *via* the ELPIARR sequence which forms a loop to keep JA-Ile within the ligand pocket and increases the stability of the complex (Howe et al., 2018; Sheard et al., 2010). The formation of this complex leads to JAZ protein ubiquitination and degradation, thus connecting directly the stability of the JAZ repressors with the perception of JA-Ile (Chini et al., 2007; Sheard et al., 2010; Thines et al., 2007) (Figure 4.2).

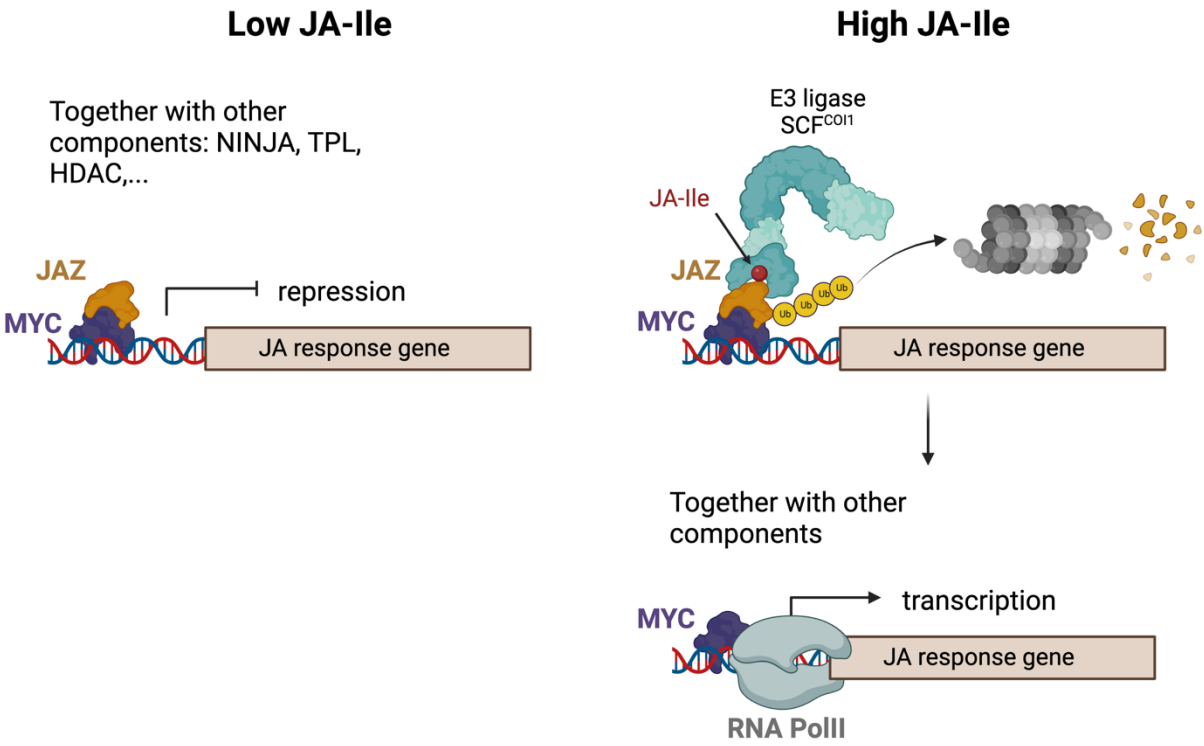

Figure 4.2. Degradation of JAZ proteins by SCF^{COI1}. Under low JA-Ile conditions, JAZ proteins interact with other transcription factors, such as those of the MYC family. JAZ proteins repress the expression of JA response genes through the recruitment of epigenetic regulators that deposit repressive histone marks and by preventing the recruitment of RNA polymerase II. Upon elevated JA-Ile conditions, JAZ proteins can be targeted for degradation by SCF^{COI1} through the UPS, thus allowing the transcription of JA response genes.

While most JAZ proteins have the domains mentioned above, some family members deviate from this consensus (Figure 4.1). For example, the group IV JAZ family members JAZ8 and JAZ13 lack the ELPIARR motif in the Jas domain. This prevents their interaction with SCF^{COI1} E3 ubiquitin ligase and JA-dependent degradation (Shyu et al. 2012; Thireault et al., 2015), and the cellular mechanisms contributing to the regulation of their stability remain unknown. JAZ13 also lacks the TIFY motif in its ZIM domain (Thireault et al., 2015). The absence of this TIFY motif prevents

binding of NINJA to JAZ13 as well as negatively impacting the ability of JAZ13 to form JAZ protein homo- or heterodimers. A yeast-two-hybrid (Y2H) screen showed that JAZ13 was not able to dimerize with itself and only weakly interacted with JAZ3 (Thireault et al., 2015), while JAZ5, JAZ6, JAZ7, JAZ8 and JAZ13 contain an EAR motif which facilitates direct binding to the repressor protein TPL and TPL-like proteins (Causier et al., 2012; Howe et al., 2018; Kagale et al., 2010; Shyu et al., 2012; Thatcher et al., 2016; Thireault et al., 2015).

4.1.1.2. JA signalling results in genome-wide transcriptional changes

Binding of JAZ proteins to target transcription factors leads to transcriptional repression *via* different mechanisms. First, as mentioned above, JAZ proteins recruit either directly (through an EAR domain) or indirectly (through interaction with NINJA) histone deacetylases, which repress transcription (Pauwels et al., 2010). In addition, the polycomb repressive complex 2 (PRC2) and the associated protein LIKE HETEROCHROMATIN PROTEIN 1 (LHP1) are recruited by some JAZ proteins. Specifically, PRC2 and LHP1 were shown to bind to JAZ1, JAZ3, JAZ4, JAZ8, JAZ9, JAZ10 with PRC2 additionally binding JAZ6. PRC2 and LHP1 were shown to deposit the repressive histone 3 lysine 27 tri-methylation (H3K27me3) mark around JA-responsive genes in a JA-dependent manner (Li et al., 2021). The interaction of JAZ proteins with transcription factors such as MYC2, which acts as a master regulator of JA signalling, also prevents the binding of subunits of the mediator complex (e.g. MED25), which is important to recruit RNA polymerase II complex and the up-regulation of JA response genes upon perception of JA-Ile. MED25 in turn is involved in recruiting COI1 to MYC2 in the absence of JA-Ile to facilitate quick activation of JA signalling upon stimuli increasing JA-Ile levels (Zhai and Li, 2019).

Degradation of JAZ proteins culminate in extensive gene expression changes and accounts for the redundancy, specificity, as well as disparate responses to JA (Hickman et al., 2017; Howe et al., 2018; Zander et al., 2020). In general, JAZ proteins bind members of the transcription families: bHLH (e.g. MYC2-5; INDUCER OF CBF EXPRESSION 1 (ICE1); ICE2; INDUCER OF CBF EXPRESSION TRANSPARENT TESTA 8 (TT8); GLABRA 3 *(*GL3); ENHANCER OF GLABRA 3 (EGL3)), MYB (e.g. MYB21, MYB24, MYB75), ERF (e.g. ETHYLENE INSENSITIVE 3 (EIN3); EIN3 LIKE 1 (EIL1); TARGET OF EAT1 (TOE1); TOE2) (Chini et al., 2016; Pauwels and Goossens, 2011) and WRKY transcription factors (WRKY57 and WRKY75) (Chen et al., 2021; Jiang et al., 2014). In Hickman et al., 2017, the timing of JA-induced gene expression changes was dissected using RNA-Seq on 5-week-old Arabidopsis Col-0 plants treated with MeJA for 0.25 – 16 hours. Transcriptional regulators were differentially expressed at early (0.25 and 0.5 hours) and later (2 hours)

timepoints (Figure 4.3). The expression of transcription factor families particularly enriched under MeJA or JA treatments include bHLH, ERF and MYB (Hickman et al., 2017; Zander et al., 2020) which also reflects the main families of transcription factors bound by the JAZs. As expected, the bHLH transcription factor and master regulator of JA responses, MYC2, is upregulated rapidly (0.25 hours) after MeJA treatment. MYC2 in turn is known to regulate a multitude of downstream transcriptional regulators. In Zander et al., 2020, it was shown that MYC2 and MYC3 directly bind the promoters of 268 out of 522 transcription factors differentially expressed in JA-treated etiolated seedlings. MYC2 and other bHLH transcription factors binding motifs were enriched in the promoter regions of multiple different clusters of MeJA response genes, while ERF and MYB motifs were enriched in the promoters of more specific clusters of MeJA-upregulated genes, suggesting that these transcription factors have more targeted roles (Hickman et al., 2017). WRKY transcription factor motifs on the other hand are generally found in the promoters of genes which are downregulated by MeJA treatment (Hickman et al., 2017). These results suggest that the transcriptional response to JA involves a hierarchical cascade of transcriptional events and regulators.

Early responses (within 1 hour) to MeJA treatment include the upregulation of JA biosynthesis genes (Hickman et al., 2017) (Figure 4.3). JA biosynthesis from α-linolenic acid requires the action of a set of enzymes including the family of plant dioxygenases, 13-LIPOXYGENASES (13-LOXs) family, of which four are present in Arabidopsis (LOX2, LOX3, LOX4, LOX6), ALLENE OXIDE SYNTHASE (AOS), ALLENE OXIDE CYCLASES (AOC), OPDA REDUCTASE (OPR3), ACYL-COA-OXIDASE (ACX), THE MULTIFUNCTIONAL PROTEINS (MFPs) and L-3-KETOACYL-COA-THIOLASE (KAT). The resulting JA can then be modified - e.g. isoleucine can be conjugated to JA by JASMONATE RESISTANT 1 (JAR1) to form JA-Ile (Wasternack and Song, 2017).

At later timepoints (>2 hours), genes related to plant defence responses, particularly genes involved in production of secondary metabolites such as glucosinolates and anthocyanin are enriched (Hickman et al., 2017). As stated in section 1.4.2.4., JA promotes defensive responses through the generation of secondary metabolites which possess anti-microbial and anti-herbivory properties. They also have a role in abiotic responses with drought, wounding, temperature, and nutrient deficiencies modulating glucosinolate and anthocyanin levels (del Carmen Martínez-Ballesta et al., 2013; Shan et al., 2009).

Glucosinolates are amino-acid derived sulfur or nitrogen containing compounds and are classified as aliphatic (methionine-derived), indolic (tryptophan-derived) or aromatic (phenylalanine-derived) (Gigolashvili et al., 2009). R2R3 group MYB transcription factors are involved in the induction of glucosinolate biosynthesis enzymes with MYB28, MYB29 and MYB76 inducing genes involved in aliphatic glucosinolate generation, while MYB34, MYB51 and MYB122 are involved in indolic glucosinolate production (Gigolashvili et al., 2009). MeJA treatment induces the expression of aliphatic glucosinolate biosynthesis genes including *MYB29*, *MYB76* and the downstream enzymes *METHYLTHIOALKYLMALATE SYNTHASE 1* (*MAM1*), *GLUCOSINOLATE S-OXYGENASE* (*GS-ox1*) and *ALKENYL HYFROXALKYL PRODUCING 2* (*AOP2*) (Hickman et al., 2017). At the same time, MYC2, which has been shown to negatively regulate indole glucosinolate biosynthesis (Dombrecht et al., 2007), represses *MYB51* at 0.5 hours of MeJA treatment (Hickman et al., 2017) (Figure 4.3).

In a previous study, JA was shown to promote the expression of transcription factors, e.g. *PAP1/MYB75*, *PAP2* and *GL3* which regulate genes involved in anthocyanin biosynthesis, including *DIHYDROFLAVONOL REDUCTASE (DFR), LEUCOANTHOCYANIDIN DIOXYGENASE (LDOX)* and *UDP-GLC:FLAVONOID 2-O-GLUCOSYLTRANSFERASE (UF3GT)* (Shan et al., 2009). In line with this, *LDOX* and *DFR* are upregulated after MeJA treatment as well as *TRANSPARENT TESTA 7* (*TT7*) and *MALONYL-COA:AMTHOCYANIDIN 5-O-GLUCOSIDE-6”-O-MALONYLTRANSFERASE* (*AT5MAT*) (Hickman et al., 2017) (Figure 4.3).

JA has been associated with the regulation of the growth/defence trade-off. This trade-off accounts for observations where young plants and plants prioritizing growth (e.g. during germination and shade avoidance) are more susceptible to infection, while induction of defensive responses comes at the cost of growth, resulting in smaller plants (Figueroa-Macías et al., 2021; He et al., 2022) In line with JA’s role in this switch, growth-related primary metabolites have been shown to be downregulated by jasmonates in favour of secondary metabolites associated with defence (reviewed in Savchenko et al., 2019). This is observed from the transcriptomic analysis in Hickman et al., 2017 as genes responsible for secondary metabolite biosynthesis are upregulated while genes involved in primary metabolism are repressed (Figure 4.3). Crosstalk between phytohormones is also important in the growth/defence trade-off, which is reflected in this RNA-Seq dataset with SA and auxin-related genes being downregulated by MeJA treatments (Hickman et al., 2017) (Figure 4.3).

Important for maintaining sensitivity and regulating trade-offs, JA signalling leads to negative feedback loops. This is shown in this study and previous studies, where expression of multiple members of the JAZ proteins are rapidly increased at the transcriptional level as early as 0.25 hours after MeJA treatment (Hickman et al., 2017; Howe et al., 2018). JA signalling is also regulated by the bHLH transcription factors, JASMONATE-ASSOCIATED MYC2-LIKE 1 (JAM1), JAM2 and JAM3 which inhibit MYC-induced gene expression by competitively binding to the same promoter sequences (Howe et al., 2018). JAM1 and JAM2 were shown to be upregulated early upon MeJA treatment (Hickman et al., 2017).

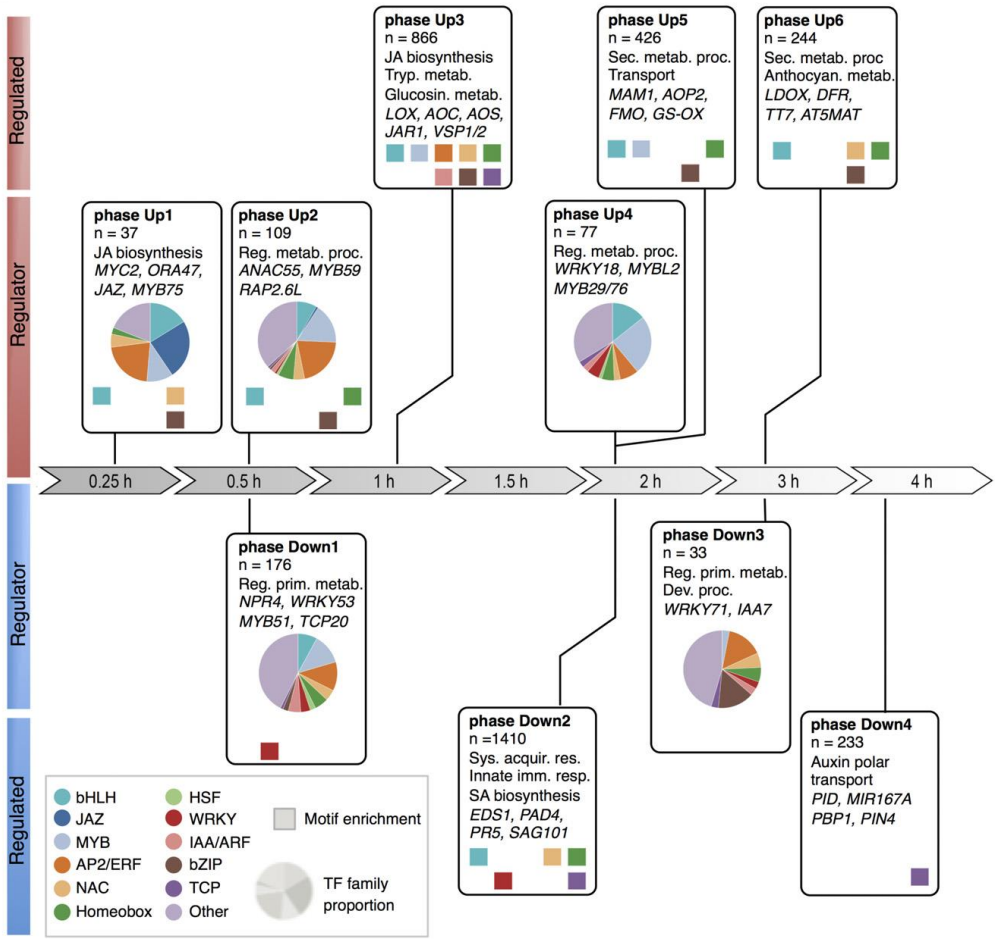

Figure 4.3. Summary of the time-dependent transcriptional regulation of the JA response programme. Early and late JA response genes are involved in different aspects of JA response, with early JA response genes contributing to further increasing JA levels and later genes being involved in the regulation of other processes such as the biosynthesis of secondary metabolites, including glucosinolates. Figure from Hickman et al., 2017.

4.1.1.3. JA signalling is regulated by additional components of the UPS

The canonical pathway for the degradation of JAZ proteins relies on the activity of the SCF^{COI1} E3 ubiquitin ligase, as outlined above. However, JAZ proteins can be targeted for degradation via other E3 ubiquitin ligases. For example, the F-box protein, S PHASE KINASE-ASSOCIATED PROTEIN 1-INTERACTING PARTNER 31 (SKIP31), was shown to bind JAZ proteins (JAZ6, JAZ10 and JAZ11), ubiquitinate and promote their degradation independently of JA-Ile (Varshney et al., 2023). In contrast, the RING type E3 ubiquitin ligase KEEP ON GOING (KEG) binds to JAZ12 and leads to its stabilisation (Pauwels et al., 2015).

The UPS also has roles in preventing inappropriate activation of JA response genes by directly targeting the MYC transcription factors. For example, the E3 ubiquitin ligase PLANT U-BOX PROTEIN 10 (PUB10) was shown to co-localize with MYC2 in the nucleus. Through *in vitro* pull-down assays and *in vivo* co-immunoprecipitation (co-IP), a direct interaction between PUB10 and MYC2 was identified, and *pub10* mutants show increased stability of MYC2 (Jung et al., 2015). In addition, MYC2 and the functionally redundant MYC3 and MYC4 transcription factors, are directly bound by BTB/POZ-MATH (BPM) proteins which act as adaptors and provide specificity to Cullin3-based E3 ubiquitin ligases. BPM proteins were found to ubiquitinate MYC transcription factors and target them for degradation. Further, BPM3 levels are induced under JA treatment, suggesting that it may be part of a negative feedback loop for JA signalling (Chico et al., 2020). In the dark, MYC2, MYC3 and MYC4 are also destabilised indirectly by the RING-finger E3 ubiquitin ligase CONSTITUTIVE PHOTOMORPHOGENIC 1 (COP1) in a COI1-independent manner (Chico et al, 2014).

In sum, JA signalling is regulated through a complex interplay between components of the UPS which control the stability of transcriptional regulators of JA response genes. The reprogramming of transcription following perception of JA is complex, changes over time and results in the regulation of multiple pathways, which contribute to plant responses to biotic and abiotic stresses.

4.1.2. Branches of JA signalling

Two branches of JA signalling have been identified and characterised. One branch, named the MYC branch, is controlled by the related bHLH transcription factors MYC2, MYC3, MYC4 and MYC5 and plays roles in response to wounding and herbivory (Lorenzo et al., 2004; Verhage et

al., 2011) (Figure 4.4). *Pieris rapae* (*P. rapae*) larvae herbivory on Arabidopsis Col-0 plants increase the expression of *MYC2* and downstream MYC branch- and wounding/herbivory-associated gene, *VEGETATIVE STORAGE PROTEIN 2* (*VSP2*). As well, loss of MYC transcription factors lead to an increased incidence of insect attack. This was illustrated by *P. rapae* having a preference for the MYC2 mutant, *jin1*, over Col-0 for feeding (Verhage et al., 2011) as well as *Spodoptera exigua* (*S. exigua*) larvae being heavier when grown on *myc2 myc3 myc4* (myc2/3/4*)* triple mutant plants (Song et al., 2014).

On the other hand, the ERF branch is regulated by the AP2/ERF transcription factors, ERF1 and OCTADECANOID-RESPONSIVE ARABIDOPSIS AP2/ERF 59 (ORA59) which induce expression of their target genes (e.g. *PLANT DEFENSIN 1.2* (*PDF1.2*)) (Zhu, 2014; Zhu et al., 2011) (Figure 4.4). *ERF1* and *ORA59* are regulated by the transcription factors EIN3 and EIL1 which integrate both JA and ethylene signals (Figure 4.4), with *ein3 eil1* mutants being deficient in responses to both phytohormones (Zhu, 2014; Zhu et al., 2011). Ethylene signalling promotes the stability of EIN3 and EIN1 through the activation of EIN2, while JA signalling derepresses EIN3 and EIN1 through the degradation of JAZ proteins (Zhu, 2014) (Figure 4.4). Hence, targets of this branch are synergistically induced by and dependent on both JA and ethylene signalling (Zhu, 2014; Zhu et al., 2011). The ERF branch plays a particularly important role in the regulation of defences against necrotrophic pathogens not only due to its role in the upregulation of *PDF1.2*, *PATHOGENESIS RELATED 3* (*PR3*) and *PR4* gene expression (Figure 4.4), but also *ein3 eil1* mutants show increased susceptibility to *B. cinerea* (Song et al., 2014; Zhu et al., 2011).

While both the MYC and the ERF branches mediate defence against biotic stresses, they are antagonistic to each other (Zhu, 2014) (Figure 4.4). MYC2 was shown to inhibit the ERF branch by destabilizing the EIN3 and EIL1 transcription factors through the upregulation of the F-box protein *EIN3 BINDING F-BOX PROTEIN 1* (*EBF1*) which forms an SCF^{EBF1} E3 ubiquitin ligase complex that targets EIN3 and EIL1 for degradation (Song et al., 2014; Zhu, 2014) (Figure 4.4). MYC2 has also been shown to physically interact with EIN3 and EIL1 which reduces their transcriptional activity, including repressing downstream *ERF1* expression (Song et al., 2014; Zhu, 2014). EIN3 binding to MYC2 also results in reduced wounding response gene expression (Song et al., 2014; Zhu, 2014). Further, *ein2* mutants show increased expression of MYC-branch related genes (Zhu, 2014). This culminates in MYC2 positively regulating wounding response genes, while inhibiting the expression of genes involved in pathogen resistance (Lorenzo et al., 2004; Song et al., 2014). Thus MYC transcription factors increase susceptibility to pathogens, with *jin1*

and *myc2/3/4* mutants showing increased resistance to *B. cinerea* (Lorenzo et al., 2004; Song et al., 2014). MYC2 also increases susceptibility to the hemi-biotroph, *Pst* DC3000. This bacterium enters plants through stomata by secreting the effector molecule, coronatine, which reopens the stomata after immune-induced stomatal closure in a MYC-dependent way (Gimenez-Ibanez et al., 2017). In contrast, activation of the ERF branch increases the preference for feeding by *P. rapae* larvae in two-choice experiments with the larvae selecting *ORA59* over-expression lines (Verhage et al., 2011). *S. exigua* larvae also displayed reduced larval weight when reared on *ein3 eil1* plants (Song et al., 2014). As well as regulating biotic stress responses, these branches have antagonistic roles in developmental processes such as the formation of the apical hook, with the ERF branch promoting apical hook curvature while the MYC branch inhibits this (Song et al., 2014) (Figure 4.4).

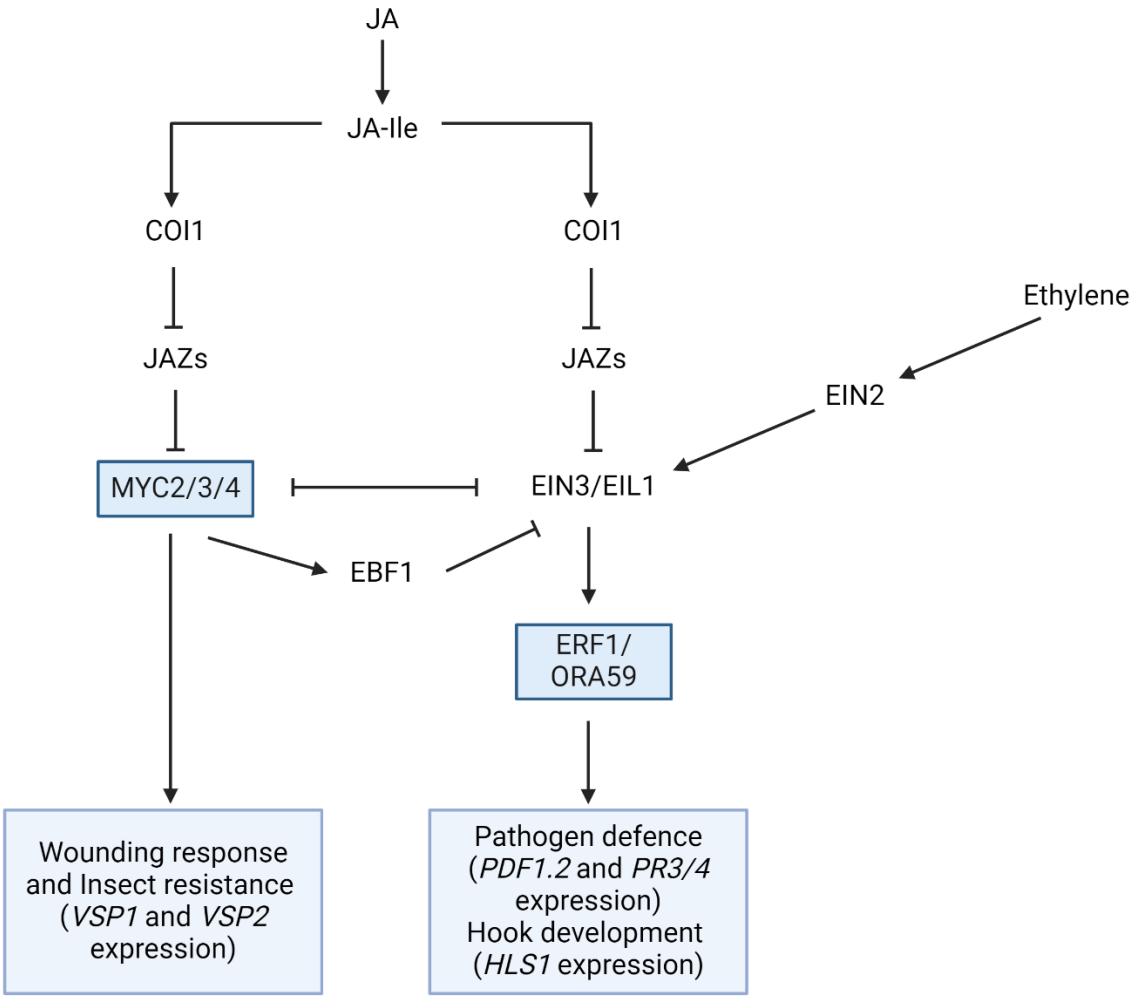

Figure 4.4. The MYC and ERF branches of JA signalling, and their mutually antagonistic relationship. Increased JA-Ile levels leads to derepression of JA signalling which occurs through two main branches. The MYC branch, controlled by MYC2/3/4 transcription factors mediates JA-induced responses to wounding and insect resistance. The ERF branch mediated by ERF1 and ORA59 transcription factors, is regulated by ethylene and JA and leads to induction of pathogen defence (particularly for necrotrophic pathogens) as

well as developmental responses such as apical hook formation. The MYC and ERF branches inhibit each other. Figure based on figure from Zhu, 2014 and was created using BioRender.com.

4.1.3. Role of JA signalling in hypoxia response

JA has been shown to have a role in plant tolerance to numerous abiotic stresses including temperature changes, UV and high light, salinity, water deficit and waterlogging (reviewed in Raza et al., 2021). JA was shown to reduce the impact of waterlogging on agronomic traits such as height, root length, fresh and dry weight and chlorophyll levels on Xinyou No.5 wrinkled skin pepper (referred to as pepper) with MeJA treatment prior to waterlogging having the most significant effect (Ouli-Jun et al., 2017). JA has also been shown to be responsible for hypoxia-induced root growth inhibition (Shukla et al., 2020). Along with this, JA levels increase transiently at early timepoints under hypoxia but decrease at later timepoints across plant species (Arbona and Gómez-Cadenas, 2008; Shukla et al., 2020; Ullah et al., 2017; Yuan et al., 2017). JA levels are also rapidly induced upon reoxygenation with these increased JA levels being important for recovery after hypoxia (Yuan et al., 2017). However, the role of JA in the regulation of hypoxia response and tolerance is not well understood at this stage. Studies looking into the role of JA in mediating tolerance to other abiotic stresses demonstrate its ability to induce physiological, molecular and biochemical changes through the regulation of gene expression changes; modulating soluble sugar and amino acid levels; inducing antioxidants/ROS scavengers; and interacting with other plant phytohormones signalling pathways (e.g. ethylene signalling) (Raza et al., 2021; Sharma et al., 2019). For example, MeJA treatment prior to waterlogging appears to protect pepper *via* some of these mechanisms including increasing soluble sugar and proline levels and upregulating the activity of antioxidant enzymes (e.g. SUPEROXIDE DISMUTASE (SOD) and CATALASE (CAT)) and enzymes involved in anaerobic metabolism (e.g. ADH) (Ouli-Jun et al., 2017). Further studies are required to gain the full scope of JA's role in hypoxia/flooding tolerance and the mechanisms which underly it.

4.1.4. Aims of the work presented in this chapter

As indicated above JA signalling and response is regulated by multiple E3 ubiquitin ligases, with SCF^{COI1} playing a particularly important role as the JA-Ile receptor as well. Previous results obtained by the Graciet lab had shown that mutants for the N-degron pathway had lower JA levels and dampened response to exogenously added MeJA (de Marchi et al., 2016). Specifically, in the absence of any treatment, the *ate1 ate2* double mutant was shown to accumulate lower levels of JA compared to the wild type. In addition, under normal conditions, JA response genes

such as *VSP1*, *VSP2*, *LOX2* or *AOS* were expressed at lower levels in the *ate1 ate2* mutant compared to the wild type. While the upregulation of these genes occurred upon MeJA treatment, it was dampened in the mutant compared to the wild type. Interestingly, genes coding for glucosinolate biosynthesis enzymes were also expressed at lower levels in *ate1 ate2* seedlings compared to the wild type, and this was accompanied by lower levels of both indole and aliphatic glucosinolates. In parallel to these JA signalling defects, the *ate1 ate2* mutant was also found to be more susceptible to the necrotrophic fungus *Sclerotinia sclerotiorum*. Despite these converging pieces of evidence pointing to a role of the N-degron pathway in the regulation of JA signalling, the molecular mechanisms underlying the range of phenotypes (from lower expression of JA response genes, to defect in glucosinolate biosynthesis and defences to necrotrophs) have not been identified.

The dampened JA signalling in *ate1 ate2* mutants could be due to a number of mechanisms, which are not necessarily mutually exclusive:

(1) The N-degron pathway, specifically the arginyl-transferases ATE1/2 and PRT6 (the E3 ligase that acts downstream of ATE1/2) could directly regulate the stability of transcriptional regulators of JA response genes, for example genes coding for some JAZ proteins or the MYC transcription factors. This mechanism would be independent of the canonical SCF^{COI1} pathway.

(2) The accumulation of N-degron pathway substrates in the *ate1 ate2* mutant could indirectly negatively affect JA signalling in this genotype, as well as in the *prt6* mutant. Considering the links between hypoxia response and JA signalling, the N-degron pathway substrates, ERFVII transcription factors, could play such a role.

The aim of this study was to dissect the link between JA signalling and the N-degron pathway in order to understand the molecular and biochemical mechanisms that underlie the JA signalling defects of the *ate1 ate2* mutant. To this end, I explored the two hypotheses outlined above.

4.2. Results

Considering the dampened JA signalling pathway in N-degron pathway mutants, the central role that JAZ proteins play in the repression of JA response genes, and the multiple roles of the UPS in regulating the stability of JAZ proteins, I first tested whether the N-degron pathway could contribute to targeting JAZ proteins for degradation.

4.2.1. Protein/protein interaction between arginyl-transferases and JAZ8

4.2.1.1. Yeast-2-hybrid (Y2H) screen

The first approach taken was to carry out a Y2H screen to investigate whether the arginyl-transferases ATE1/2 could interact with JAZ1-12. For completeness, an interaction between these N-degron pathway enzymes and MYC2/3/4 was also tested. This work was performed by our collaborator, Prof. Alain Goossens (VIB Ghent, Belgium), and the summary of all the interactions tested and results is presented in Table 4.1.

Table 4.1. Summary of interactions tested and of the Y2H results. All experiments were carried out by the group of Prof. Alain Goossens using unpublished constructs coding for N-degron pathway components previously generated in the Graciet lab. All Y2H constructs coding for JAZ and MYC proteins were previously published (Goossens et al., 2015). Constructs in pGADT7 were expressed as a fusion protein with the GAL4 activation domain, while constructs in pGBKT7 were expressed as fusion proteins with the GAL4 DNA binding domain. Selection plates lacked Trp and Leu (for plasmid selection) as well as His, so that only yeast strains in which the 2 fusion proteins interacted could grow in the absence of His.

pGADT7	pGBKT7	2 days @ 30°C	+ 4 days @ RT
JAZ1	ATE1		
JAZ2	ATE1		
JAZ3	ATE1		
JAZ4	ATE1		
JAZ5	ATE1		
JAZ6	ATE1		
JAZ7	ATE1		
JAZ8	**ATE1**	**+++**	**+++**
JAZ9	ATE1		
JAZ10	ATE1		
JAZ11	ATE1		
JAZ12	ATE1		
MYC2	ATE1		
MYC3	ATE1		
MYC4	ATE1		
EMPTY	ATE1		

pGADT7	pGBKT7	2 days @ 30°C	+ 4 days @ RT
JAZ1	ATE2		
JAZ2	ATE2		
JAZ3	ATE2		
JAZ4	ATE2		
JAZ5	ATE2		
JAZ6	ATE2		
JAZ7	ATE2		
JAZ8	**ATE2**		**weak +++**
JAZ9	ATE2		
JAZ10	ATE2		
JAZ11	ATE2		
JAZ12	ATE2		
MYC2	ATE2		
MYC3	ATE2		
MYC4	ATE2		
EMPTY	ATE2		

In this initial Y2H screen, a potential protein/protein interaction was detected between JAZ8 and the arginyl-transferases ATE1 and ATE2, although it seemed weaker with ATE2 as yeasts needed to be grown for longer for colonies to develop. The Y2H screen was then repeated adding also PRT6, two ERFVIIs (RAP2.3 and RAP2.12), and another component of JA signalling, the NINJA protein. The results confirmed the interaction of ATE1/2 with JAZ8 in Y2H, but did not reveal any other protein/protein interactions (Figure 4.5 and Table 4.2).

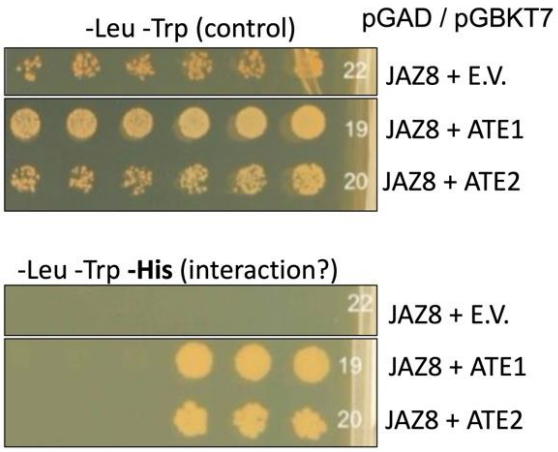

Figure 4.5. Result of Y2H test for interaction between JAZ8 and ATE1/2. Minimal medium -Leu -Trp served as a control for strain growth and plasmid selection. Minimal medium -Leu -Trp -His allowed yeast growth only if the two proteins interacted. A control of JAZ8 with an empty vevtor (E.V.) was also added. pGAD: expression fused to the GAL4 activation domain; pGBKT7: expression as a fusion with the GAL4 DNA binding domain.

Table 4.2. Summary of interactions tested and of results in a second Y2H experiment. All experiments were carried out by the group of Prof. Alain Goossens using unpublished constructs coding for N-degron pathway components and ERFVIIs previously generated in the Graciet lab. All constructs coding for JAZ and NINJA were previously published (Goossens et al., 2015).

pGAD424	pGBKT7	48H/30°C
EMPTY	NINJA	
ATE1	NINJA	
ATE2	NINJA	
PRT6	NINJA	
RAP2.3	NINJA	
RAP2.12	NINJA	
EMPTY	JAZ8	
ATE1	JAZ8	
ATE2	JAZ8	
PRT6	JAZ8	
RAP2.3	JAZ8	
RAP2.12	JAZ8	
JAZ8	ATE1	+++
JAZ8	ATE2	+++
JAZ8	PRT6	
JAZ8	EMPTY	
TIFY8	ATE1	
TIFY8	ATE2	
TIFY8	PRT6	
TIFY8	EMPTY	
NINJA	ATE1	
NINJA	ATE2	
NINJA	PRT6	
NINJA	EMPTY	

In summary, the Y2H experiments suggest that JAZ8 may interact with the two arginyl transferases ATE1 and ATE2.

4.2.1.2. Validation of the interaction between JAZ8 and ATE1/2

To validate the potential interactions using co-IP, transient expression experiments in *N. benthamiana* were carried out using Agrobacterium strains transformed with constructs that allowed expression of epitope-tagged versions of the two proteins (ATE1-HA and JAZ8-myc) under the control of the 35S promoter (constructs pEG345 and pKD29, respectively). A time-course experiment (from 2 days post-infiltration (dpi) to 4 dpi) was first carried out to determine the timepoint at which protein expression was sufficiently high for detection of the epitope tagged proteins by immunoblot. An epitope-tagged version of JAZ1 (JAZ1-myc) was also included as a potential control for subsequent experiments (Figure 4.6). While JAZ1-myc could not be detected, presumably because of its rapid degradation during transient expression, both JAZ8-myc and ATE1-HA accumulated to detectable levels at 2 dpi. ATE1-HA levels remained sufficiently high for detection at 3 and 4 dpi, but these were lower compared to 2 dpi. In contrast, JAZ8-myc became difficult to detect after 2 dpi, which may have been a plant response to the Agrobacterium given the important role of JA signalling in immune responses. Hence, a timepoint of 2 dpi was deemed to be best for the transient expression of *JAZ8-myc* and *ATE1-HA* in *N. benthamiana*. Another interesting result from these preliminary experiments was that the levels of JAZ8-myc appeared to be much lower (below detection) when ATE1-HA and JAZ8-myc were co-expressed together, thus suggesting that ATE1 may contribute to targeting JAZ8 for degradation *in planta* (Figure 4.6; see section 4.2.2.1. for more details). Lastly, when blots were exposed for longer, a higher molecular weight band (>250 kDa) appeared with the anti-HA antibody (Figure A1 in the Appendix), suggesting that ATE1-HA may exist as two forms with different molecular weights (see Discussion).

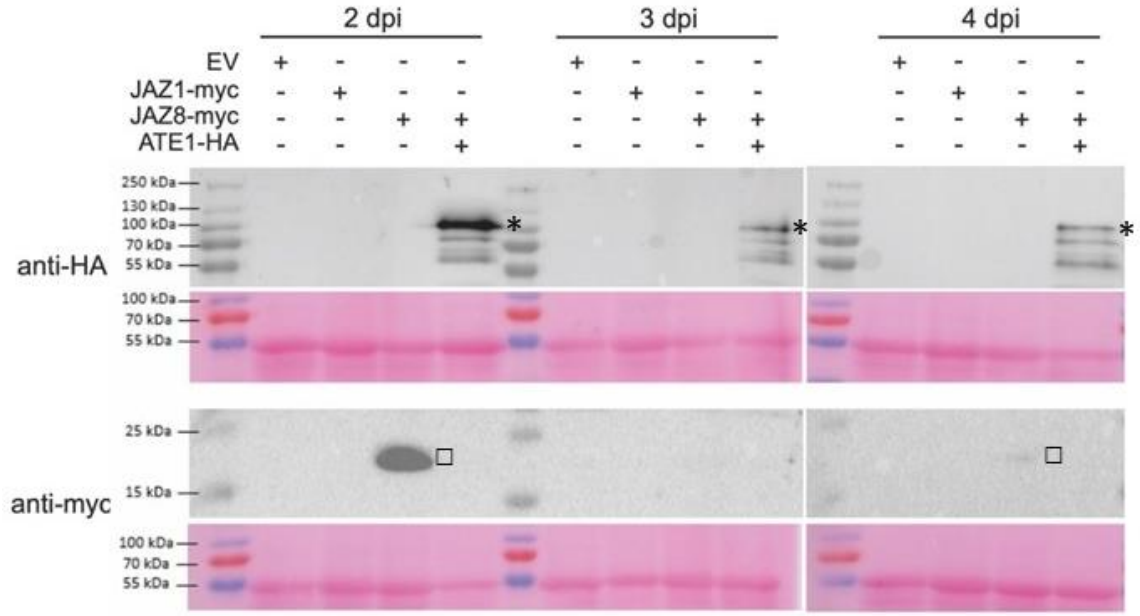

Figure 4.6. Time-course experiment of JAZ8-myc, JAZ1-myc and ATE1-HA transient expression in *N. benthamiana*. At different timepoints after agroinfiltration, leaf tissue was collected, proteins were extracted in SDS loading buffer, amido black protein quantification was performed and 30 µg of protein was loaded per well. Expected molecular weights (MW): ATE1-HA = 78.1 kDa; JAZ8-myc = 16 kDa; JAZ1-myc = 28.8 kDa. Results are representative of one biological replicate. * = ATE1-HA band. □ = JAZ8-myc band.

Next, to confirm the results of the Y2H using Co-IP, I carried out an experiment to allow transient expression of JAZ8-myc and ATE1-HA separately, followed by protein extraction in co-IP buffer (50 mM Tris-Cl, pH 7.5, 100 mM NaCl, 10% [v/v] glycerol, 1 mM PMSF, 0.1% Tween-20 and 1:100 plant protease inhibitor cocktail (PPIC; Merck)). However, using this co-IP buffer, JAZ8-myc was no longer detectable in the soluble protein extracts by immunoblot (data not shown). These problems could be due to the nuclear localization of JAZ8. Hence, in subsequent experiments, ATE1-HA and JAZ8-myc proteins were transiently expressed separately in *N. benthamiana*. The leaf tissue was collected at 2 dpi for nuclei isolation and extraction of nuclear proteins using a ChIP kit (Diagenode). Immunoblot analysis of the different fractions confirmed that (1) JAZ8-myc was indeed nuclear localized, (2) nuclear protein extraction enriched for JAZ8-myc, making it easier to detect it by immunoblot; and (3) ATE1-HA was present both in the cytosolic and in the nuclear fractions, with the latter containing higher levels of ATE1-HA. Thus, ATE1-HA and JAZ8-myc are both present and may co-localize in the nucleus (Figure 4.7).

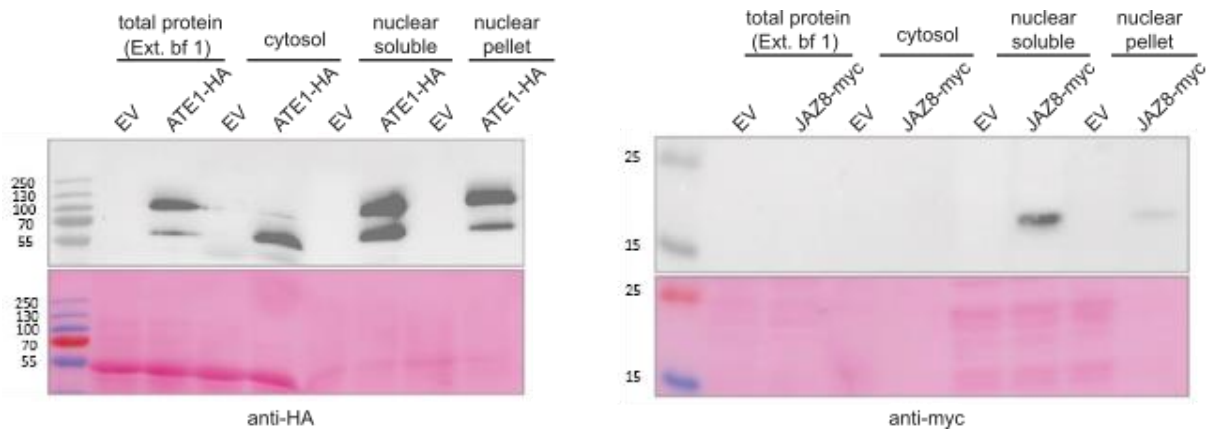

Figure 4.7. Result of nuclear protein extraction experiments. Leaf tissue was collected at 2 dpi. After grinding the tissue in liquid nitrogen, the powder was used to isolate nuclei using a ChIP kit (Diagenode). The fraction directly after grinding in extraction buffer 1 (Ext. bf 1) from the ChIP kit corresponds to total protein. The fraction not containing the nuclei corresponds to cytosolic proteins. The fraction pelleted after sonication corresponds to nuclear pellet.

To perform co-IP experiments, I agroinfiltrated *N. benthamiana* to express ATE1-HA and JAZ8-myc separately, followed by preparation of nuclear protein extracts, each containing ATE1-HA or JAZ8-myc. The two nuclear protein extracts were then mixed together and an anti-HA resin was used to IP ATE1-HA and determine whether JAZ8-myc co-IP'd (Figure 4.8A). The immunoblot analysis of the coIP experiment suggests that JAZ8-myc and ATE1-HA interact with each other (Figure 4.8B).

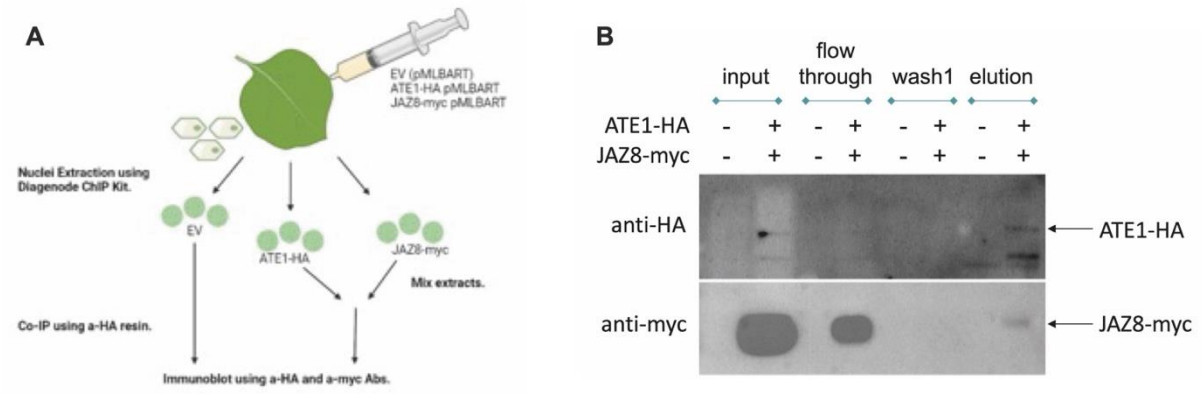

Figure 4.8. Co-IP experiment with ATE1-HA and JAZ8-myc. A. Summary of the co-IP experiment. At 2 dpi, leaf tissue was collected and nuclear proteins were extracted. The ATE1-HA and JAZ8-myc containing nuclear extracts were mixed and incubated for 1 hour on ice. IP was then performed using an anti-HA

resin, followed by immunoblots with anti-HA and anti-myc antibodies. **B.** Immunoblot analysis of the anti-HA IP. Results are representative of 3 biological replicates.

To determine whether JAZ8-myc could potentially bind aspecifically to the anti-HA resin, I carried out one anti-HA IP experiment with a nuclear extract containing only JAZ8-myc. Unfortunately, the resulting immunoblot analysis suggested that JAZ8-myc may be able to bind anti-HA resin (Figure A2 in the Appendix). Because of time constraints, I could not repeat this control experiment or all the co-IP experiments using all relevant samples in one single co-IP experiment. Further work is thus needed to ensure that JAZ8-myc/ATE1-HA interaction detected by co-IP is not due to aspecific binding of JAZ8-myc to the anti-HA resin. This would require optimisation of the co-IP protocol, as well as repeating the IP with an anti-myc resin as opposed to anti-HA. Additionally, validation of the ATE1/JAZ8 interaction would also need to be carried out in Arabidopsis, using for example bimolecular fluorescence complementation (BiFC) experiments in protoplasts or co-IP experiments in protoplasts.

4.2.1.3. Identification of domains involved in the interaction between JAZ8 and ATE1

Y2H experiments were performed to identify the domains involved in the interaction between ATE1 and JAZ8. The crystal structures of the yeasts *K. lactis* ATE1 (KlATE1) and *S. cerevisiae* ATE1 (ScATE1) were recently elucidated. Both papers revealed predicted substrate and arginyl-tRNA binding sites, as well as important amino acid residues (Kim et al., 2022; Van et al., 2022). This protein structure could therefore help to analyse models of Arabidopsis ATE1 (noted AtATE1 here for clarity) generated by AlphaFold (Jumper et al., 2021; https://alphafold.ebi.ac.uk/). Prior to that, a sequence alignment from Kim et al., 2022 which included comparisons of KlATE1, ScATE1, two isoforms of human ATE1 and of mouse ATE1, AtATE1 and AtATE2 was used to identify

common domains and determine whether relevant amino acid residues are conserved across arginyl-transferases (Figure 4.9).

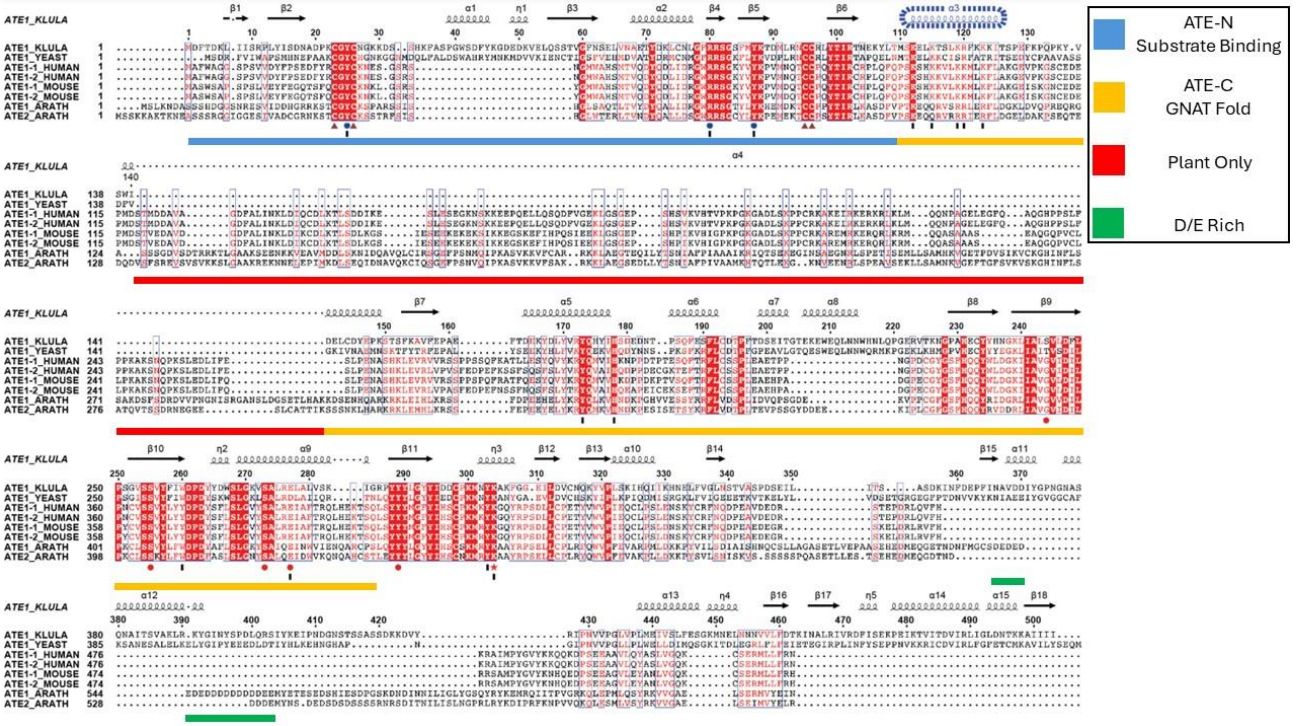

Figure 4.9. protein sequence alignment of arginyltransferases. Translated amino acid sequences for arginyl-transferases from *K. lactis* (ATE1-KLULA), *S. cerevisiae* (ATE1-YEAST), *Homo sapiens* (ATE1-1-HUMAN and ATE1-2-HUMAN), *Mus musculus* (ATE1-1-MOUSE and ATE1-2-MOUSE) and Arabidopsis (ATE1-ARATH and ATE2-ARATH). As well, denoted by blue and red dots underneath the alignment are conserved amino acids involved in forming the positively and negatively charged pockets for the substrate binding site and tRNA binding site, respectively. This figure also shows protein structural elements of KlATE1 above the sequence alignment. Figure from Kim et al., 2022. Blue = ATE-N (Substrate Binding); Orange = ATE-C (GNAT Fold); Red = Plant Only; Green = D/E Rich.

Two main domains, ATE_N (amino acids 1-109, blue; Figure 4.9.) and ATE_C (amino acids 110-285, orange; Figure 4.9.) were detected in KlATE1. Of particular interest, the ATE_C domain contains a GCN5-related N-acetyl transferase (GNAT) fold that has been previously shown to be involved in the transfer of acetyl groups to target substrates and are made up of four conserved motifs A, B, C and D. KlATE1 was found to form two pockets, one positively charged pocket which forms between a motif in the GNAT fold (A motif) and the ATE-N domain while the second pocket is negatively charged and forms between that A and B motif of the GNAT fold in the ATE_C domain. The first pocket is proposed to be the substrate binding site with the positive charge allowing binding to the negatively charged N-terminal D, E and oxidized-C residues of substrate proteins. The negatively-charged second pocket is predicted to bind to the positively-charged Arg-tRNA^{Arg}. Studies using ScATE1 confirmed this bi-lobed structure and different charges of the

pockets. In Arabidopsis ATEs, amino acids involved in binding of the substrate and of the arginyl-tRNA are conserved or replaced by amino acids with similar properties: (1) the arginine residue involved in substrate binding at positions 80 in KlATE1 and 79 in ScATE1 correspond to an arginine at position 65 in AtATE1; (2) the aspartate or glutamate at position 277 in ScATE1 or KlATE1, respectively, which is suggested to be the site of arginyl-tRNA binding, appears to be equivalent to glutamate 428 in AtATE1. Supporting the importance of these residues, as well as the high conservation, mutation of these residues (e.g. R80E and E277A/K) in KlATE1, leads to loss of arginylation activity (Kim et al., 2022). Based on sequencing alignment, AtATE1 was also seen to possess additional regions that are not present in either KlATE1 or ScATE1. This includes a D/E rich region (AtATE1 amino acid residues 539-557) that is present exclusively in AtATE1 (e.g. it is absent in AtATE2) (green; Figure 4.9.).

Considering the sequence similarities of AtATE1 with KlATE1 and ScATE1, the crystal sturctures of fungal ATE1s were compared to the AlphaFold model of AtATE1. This comparison confirmed the conservation of the substrate and arginyl-tRNA binding sites, while also revealing an additional domain in the structure of AtATE1, which protrudes away from the substrate and arginyl-tRNA binding sites (red; Figure 4.10 protein structure) and appears to comprise loops or potentially unstructured regions, as well as alpha-helices and beta-sheets. This corresponds to amino acids 125 to 303, which are not present in either KlATE1 or ScATE1 (red; Figure 4.9.). MmATE1 and HsATE1 also have an additional sequence in this region (Figure 4.9) suggesting that an extra domain may be necessary for function of arginyl-transferases in higher eukaryotes, however there is little sequence or structural similarity between these additional sequences. Further, BLASTp analysis using the amino acid sequence of this region only retrieved matches with arginyl-transferases in other plant species only (Figure A3 in the Appendix), thus suggesting that this domain evolved in the plant lineage and may contribute to the regulation of plant-specific susbtrates or interacting proteins. In addition to this large domain (ref in Figure 4.10), the AtATE1-specific D/E rich region mentioned above appears to be largely unstructured at the C-terminus of the protein (green in Figure 4.10).

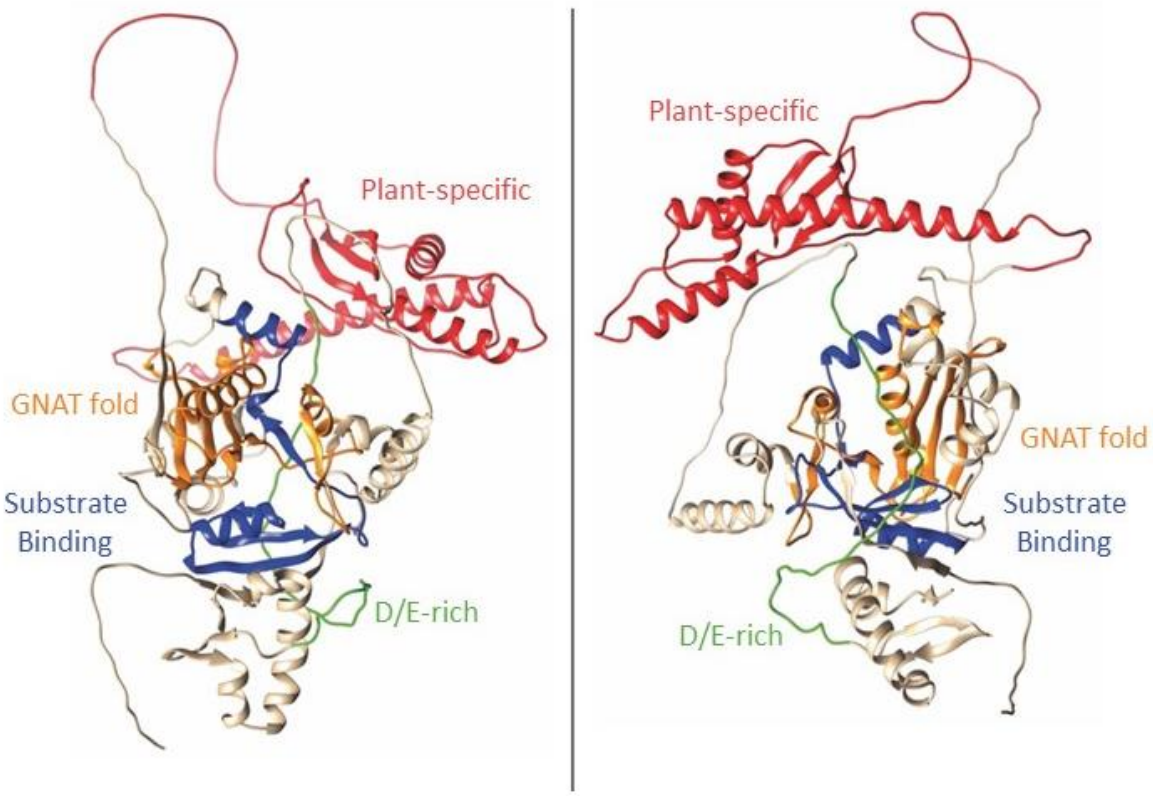

Figure 4.10. AlphaFold model and structural features of AtATE1. The AlphaFold model of AtATE1 (Jumper et al., 2021; https://alphafold.ebi.ac.uk/entry/Q9ZT48) was visualized using Pymol. The image on the left depicts how the substrate binding (blue) and arginyl-tRNA binding (orange) domains come together to form the active site, as found in KlATE1 and ScATE1 (Kim et al., 2022; Van et al., 2022). The image on the right corresponds to the same structure from a different angle, and shows the presence of the additional plant-specific domain (red) that protrudes from the rest of the enzyme. The D/E-rich region, specific to AtATE1 is depicted in green.

Based on this structural analysis, different Y2H pGBKT7 plasmids were generated by our collaborator (Dr. Elia Lacchini (Alain Goossens' lab); unpublished), each coding for specific domains of AtATE1 fused to the GAL4 DNA binding domain (Figure 4.11): (1) the N-terminal half of AtATE1 (amino acids 1 to 310) encompassing the substrate binding domain (blue) and the plant-specific domain (red); (2) the C-terminal half of AtATE1 (amino acids 311 to 632) consisting of the GNAT fold and D/E rich region; (3) The substrate binding domain (amino acids 1 to 115); (4) the plant-specific domain (amino acids 116 to 310); (5) the D/E-rich region; and (6) the GNAT fold. Interaction with full-length JAZ8 expressed as a fusion with the GAL4 activation domain (in pGADT7) was then tested in the absence and presence of 3-amino-1,2,4-triazole (3AT), which increases the stringency of the screen and allows potential autoactivation problems to be overcome from the protein fragments cloned into pGBKT7. The results of these Y2H experiments

confirmed the interaction of ATE1 and JAZ8, and indicated that the ATE1 domains that interact with JAZ8 in yeast includes the substrate binding domain fragment ($ATE1^{1-115}$), as well as the D/E-rich region at the C-terminus ($ATE1^{516-632}$). The latter interaction was detected in the presence of 5 mM 3AT, which was sufficient to inhibit the autoactivation of the $ATE1^{516-632}$ fragment observed when yeast cells were co-transformed with pGBKT7 $ATE1^{516-632}$ and the empty pGADT7 plasmid. All Y2H experiments were performed by Dr. Elia Lacchini (Alain Goossens' group; VIB; Ghent).

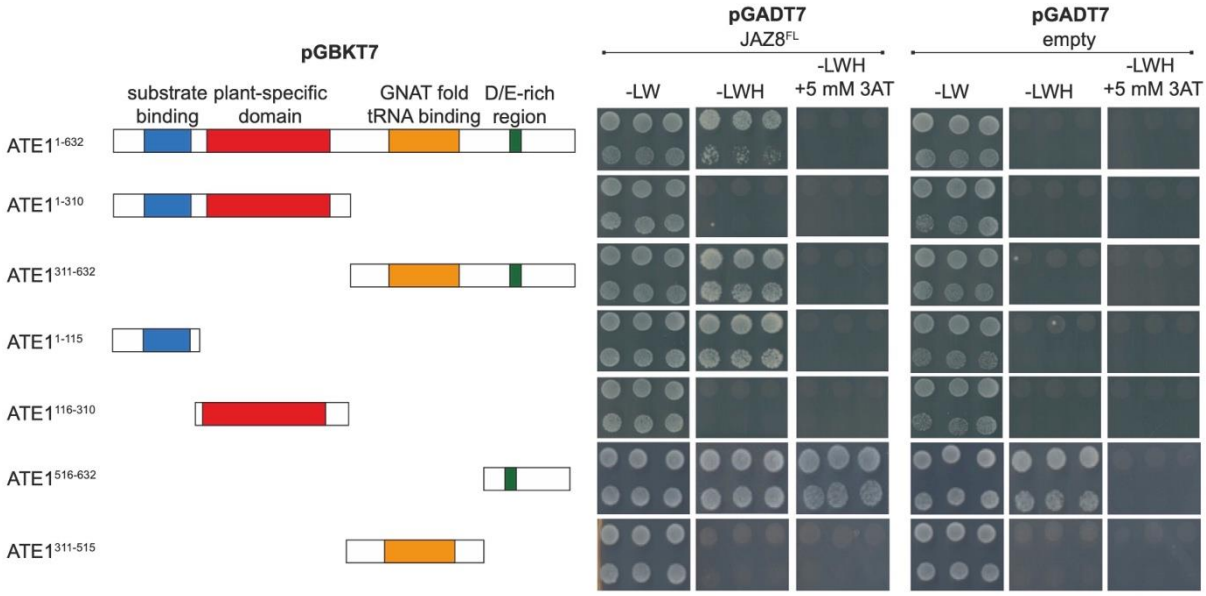

Figure 4.11. Results of Y2H experiments with different domains of ATE1 and full length JAZ8 ($JAZ8^{FL}$). ATE1 domains and full-length protein were cloned into pGBKT7, while JAZ8 was cloned into pGADT7. Growth and plasmid selection were checked on minimum medium minus Leu and Trp (-LW), while interaction was tested on medium minus Leu, Trp and His (-LWH) ± 3AT to remove background growth observed with $ATE1^{516-632}$ and increase stringency of the Y2H assays. Y2H experiments performed by Dr. Elia Lacchini (VIB, Ghent).

Interaction of full-length ATE1 with different domains of JAZ8 was also tested using Y2H. The JAZ8 fragments tested included (1) the N-terminal EAR domain (amino acids 1-34); (2) the TIFY domain in the middle section of the protein (amino acids 35-82); (3) the divergent Jas domain (amino acids 83-131); (4) a combination of the EAR and TIFY domains (amino acids 1-82); and (5) a combination of the TIFY and divergent Jas domains (amino acids 83-131) (Figure 4.12). All Y2H experiments indicated that full length JAZ8 was needed for interaction with ATE1, as none of the shorter JAZ8 fragments appeared to interact with full length ATE1. This may be due to JAZ8 being an inherently disordered protein and the whole protein may be needed for proper folding and interaction with ATE1.

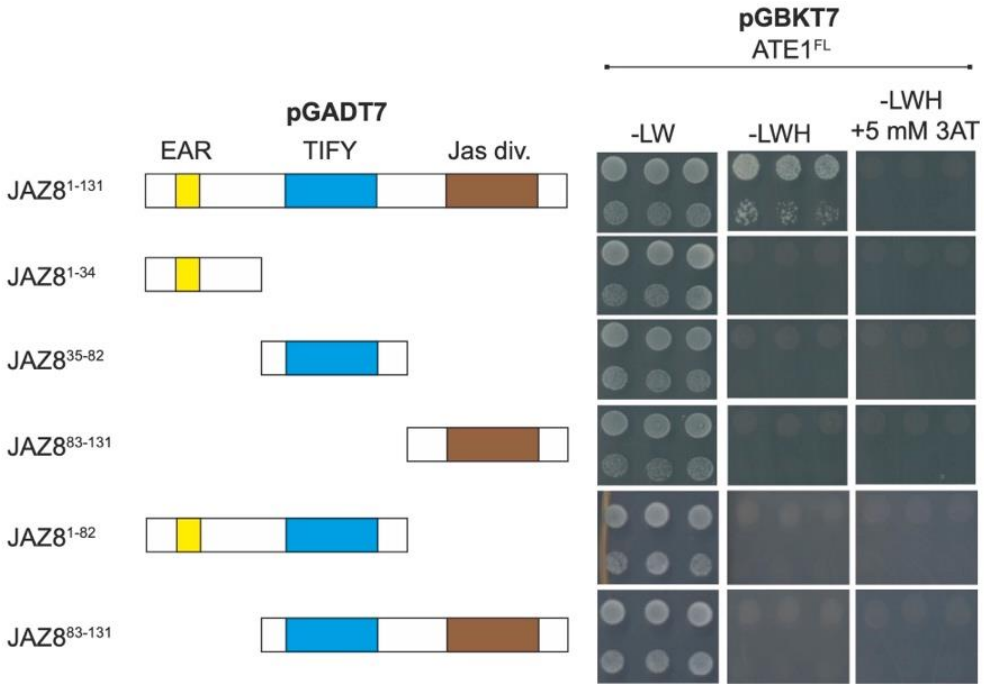

Figure 4.12. Results of Y2H experiments with different domains of JAZ8 and full length ATE1 (ATE1^{FL}). JAZ8 domains and full-length protein were cloned into pGADT7, while ATE1^{FL} was cloned into pGBKT7. Growth and plasmid selection were checked on minimum medium minus Leu and Trp (-LW), while interaction was tested on medium minus Leu, Trp and His (-LWH) ± 3AT to remove background growth observed with ATE1$^{516-632}$ and increase stringency of the Y2H assays. Y2H experiments performed by Dr. Elia Lacchini (VIB, Ghent).

Altogether, the Y2H data suggest that JAZ8 could bind to an interface involving the substrate binding domain of ATE1, as well as the D/E-rich region. The latter, which is negatively charged could serve to strengthen/stabilise the interaction via electrostatic interactions with positively charged sequences of JAZ8. Notably, the C-terminal portion of JAZ8 (amino acid residues 116 to 131) contains a region rich in positively charged residues (KRKIRIQATSPYHSRR). In addition, the lack of JAZ8 interaction with the ATE1$^{1-310}$ fragment could suggest that the plant-specific domain (in red in the structure) may regulate (perhaps inhibit) binding of JAZ8.

4.2.2. Functional connections between JAZ8 and N-degron pathway components

4.2.2.1. ATE1 promotes JAZ8 destabilisation

As indicated in section 4.1.1.1., JAZ8 is a particularly interesting member of the JAZ protein family as it differs from the canonical JAZ proteins by having a divergent Jas domain that carries

mutations in the loop domain, converting the ELPIARR degron motif to PKASMK (Shyu et al., 2012). Loss of this degron motif prevents binding of JAZ8 by the SCF^{COI1} E3 ligase complex and disrupts the JA-dependent degradation of JAZ8 (Shyu et al., 2012). The mechanism by which JAZ8 is targeted for degradation, in the absence or presence of JA, therefore remains an open question. Interaction between JAZ8 and an enzymatic component of the N-degron pathway spurred investigation into whether this protein degradation pathway or its enzymatic components could contribute to the degradation of JAZ8 *in vivo*. The latter could be in agreement with the JA signalling defects of *ate1 ate2* mutant plants, which have dampened regulation of JA signalling (de Marchi et al., 2016) and is hence a phenotype that could be explained by stabilisation of a JAZ repressor protein.

To address this possibility, experiments were performed with the aim of determining whether transient co-expression of ATE1-HA and JAZ8-myc in *N. benthamiana* affected the stability of JAZ8-myc (Figure 4.13A). Immunoblot analysis of protein extracts indicated that transient co-expression reduced JAZ8-myc protein levels compared to expression of JAZ8-myc alone (Figure 4.13B). To rule out potential transcriptional differences between samples, total RNA was extracted from the same samples (Figure 4.13A) for RT-qPCR analysis. In three biological replicates, JAZ8-myc accumulated to lower levels when co-expressed with ATE1-HA in a manner that was not related to potential mRNA abundance differences when co-expressing both transgenes (Figure 4.13C). Other replicates (Figure A4 in Appendix) also show reduced JAZ8 protein abundance in the presence of ATE1-HA, however, these also show lower mRNA abundance. Lastly, one replicate, Figure A4C, shows no difference between levels of JAZ8-MYC and ATE1-HA + JAZ8-MYC. This showcases the variability involved in the transient expression of proteins.

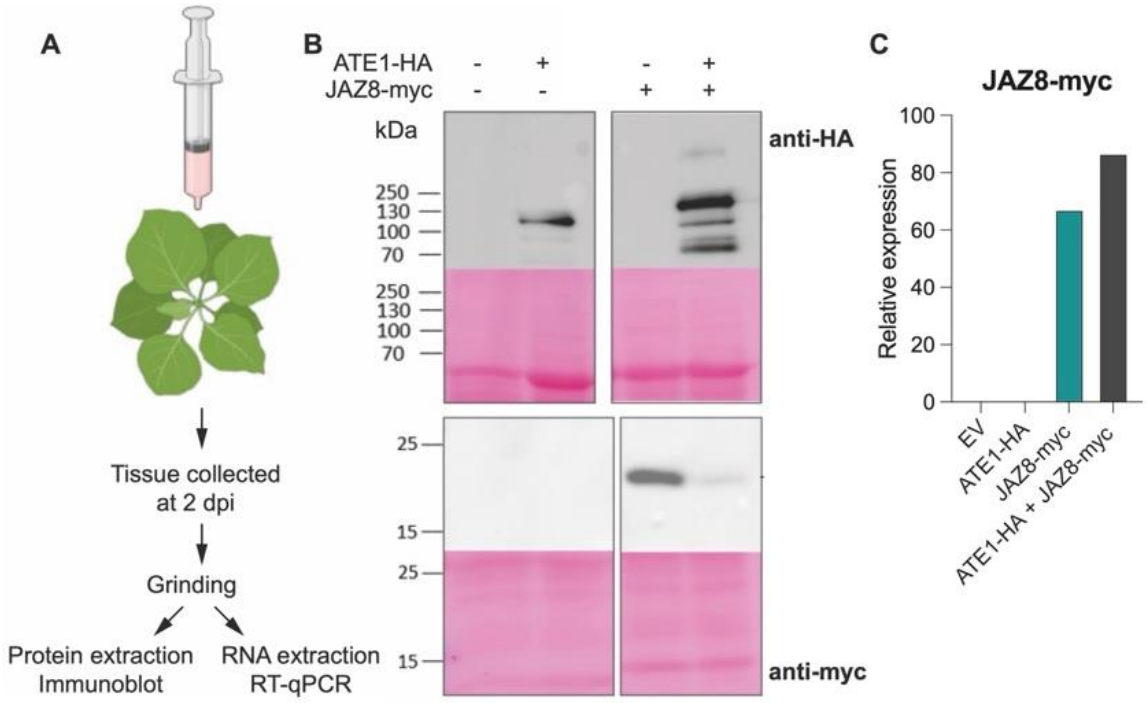

Figure 4.13. Destabilization of JAZ8-myc in the presence of ATE1-HA in *N. benthamiana*. A. Overview of the experiment. At 2 dpi, agroinfiltrated leaf tissue was collected and frozen in liquid nitrogen for protein and RNA extraction from the same samples. **B.** Immunoblot analysis with anti-HA and anti-myc antibodies using tissue co-expressing ATE1-HA and JAZ8-myc, expressing each of the proteins separately, or agroinfiltrated with an Agrobacterium strain that carried an empty pML-BART plasmid (EV) as background control. **C.** Relative expression of JAZ8-myc relative to a *N. benthamiana* reference gene. These data are representative of 3 biological replicates. See Figure A4 in Appendix for other replicates.

Together with the potential interaction of ATE1 and JAZ8, the data obtained suggest that ATE1 may play a role in targetting JAZ8 for degradation in plants.

4.2.2.2. Genetic interaction between arginyl-transferases and *JAZ8*

To further study functional connections between N-degron pathway components and JAZ8, an *ate1 ate2* mutant was crossed with a *jaz8* T-DNA mutant allele (SALK_200208C; Figure 4.14), and an *ate1 ate2 jaz8* triple mutant was obtained. This triple mutant genotype could help determine whether mis-regulation of JAZ8 (its potential accumulation) in *ate1 ate2* might be responsible for the dampened JA signalling pathway in the mutant. A double *prt6-5 jaz8* mutant line was also obtained by crossing *prt6-5* and *jaz8* to assess a potential genetic interaction between *PRT6* and *JAZ8*. It is important to note that additional mutant alleles of JAZ8 are currently being considered to complement the data obtained with SALK_200208, and also that considering the functional

redundancy between JAZ proteins, a single *jaz8* mutant may not be sufficient to detect differences in JA signalling.

First, the expression of JA response genes was monitored in 4-week-old plants after a 3-hour treatment of leaves with 20 µM MeJA or a mock solution containing the same concentration of ethanol. Genes tested included typical target genes of the MYC branch (*VSP2* and *LOX2*) and of the ERF branch (*ORA59* and *PDF1.2a*). Apart from *LOX2*, the MeJA treatment does not result in any statistically different expression changes for these important JA signalling genes (Figure 4.14). This indicates that the treatment did not work and experimental conditions need optimizing. Examples of optimizing would include changing the concentration of MeJA administered or the timing of the treatment. The latter may have some success as VSP2, *ORA59* and *PDF1.2a* typically respond at later timepoints. Hence, future experiments will include (i) a longer treatment of (at least 2 hours); (ii) additional genes of the MYC branch that respond at shorter timepoints (*e.g. MYC2*). It can be seen that there are no statistical differences between any of the genotypes in response to mock or MeJA treatment (Figure 4.14), however, due to the treatments not working in Col-0, conclusions cannot be made for differences between genotypes in response to MeJA treatment and expression of MYC branch vs ERF branch regulated genes.

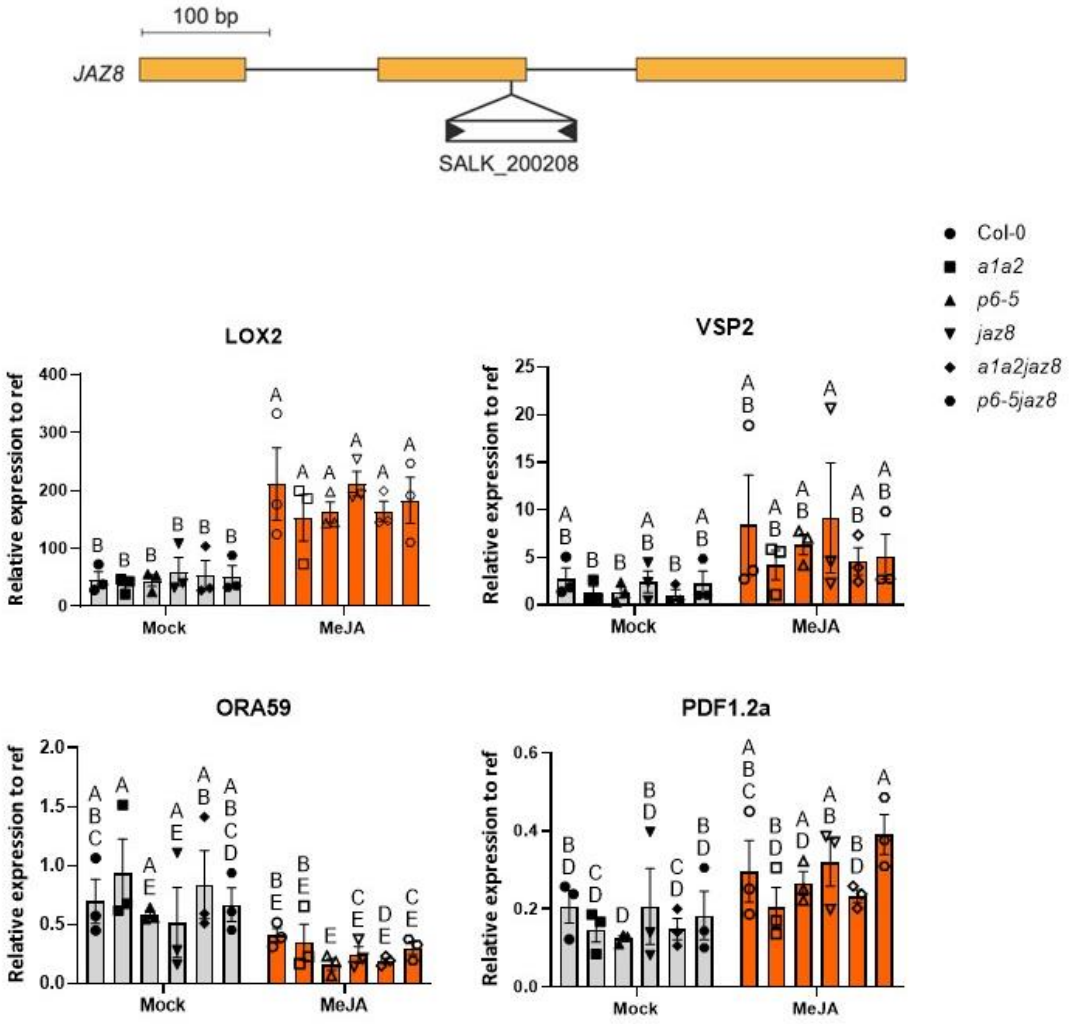

Figure 4.14. Expression of MYC and ERF branch JA-response genes in mock and MeJA treated leaves of different jaz8 mutant combinations. Upper panel: exon structure of the JAZ8 gene, and location of the SALK_200208C T-DNA used in this study. Lower panels: results of RT-qPCR analysis with RNA extracted from leaves of 4-week-old plants treated for 3 hours with 20 µM MeJA or a mock solution. Mean and SEM of the relative expression to a reference gene from 3 biological replicates are shown. Statistical analysis (two-way ANOVA with Fisher's test) was completed and were presented in a CLD format.

JAZ8, together with other JAZ repressors, has been shown to contribute to the regulation of different physiological processes in plants, including anthocyanin production, dark-induced leaf senescence and stamen development. In order to characterise the *ate1 ate2 jaz8* triple mutant, anthocyanin production was induced by growing seedlings for 12 days on plates with 25 µM MeJA or a mock solution (0.12% ethanol), followed by anthocyanin extraction and quantification. The data obtained show that MeJA treatment induced anthocyanin production and accumulation, as expected. Anthocyanin content was lower in *ate1 ate2* and *prt6-5*, but the difference was only statistically significant for *ate1 ate2* (Figure 4.15A). This is in agreement with

results in the community showing that *prt6* mutant alleles have generally a weaker phenotype than *ate1 ate2* mutants. *jaz8* has slightly higher levels of anthocyanin than Col-0, however, the difference is not statistically significant. While there are no statistical differences between Col-0 and the two higher order mutants, *ate1 ate2 jaz8* and *prt6-5 jaz8*, which could potentially suggest a rescue for the *ate1 ate2* phenotype in the presence of *jaz8*, the higher order mutants behave largely like their *ate1 ate2* and *prt6-5* parents, respectively, with there being no statistical differences between *ate1 ate2* and *ate1 ate2 jaz8* (Figure 3.15.A). This suggests that *ate1 ate2* and *prt6-5* are epistatic to *jaz8* and that the potential accumulation of JAZ8 in *ate1 ate2* and *prt6-5* would not be sufficient to explain the defect of *ate1 ate2* and *prt6-5*. One possibility is that the functional redundancy between JAZ proteins poses problem for this analysis. For example, *JAZ1/2/5/6/9/10/11* have been shown to redundantly regulated anthocyanin production with JAZ8 in response to MeJA (Qi et al., 2011).

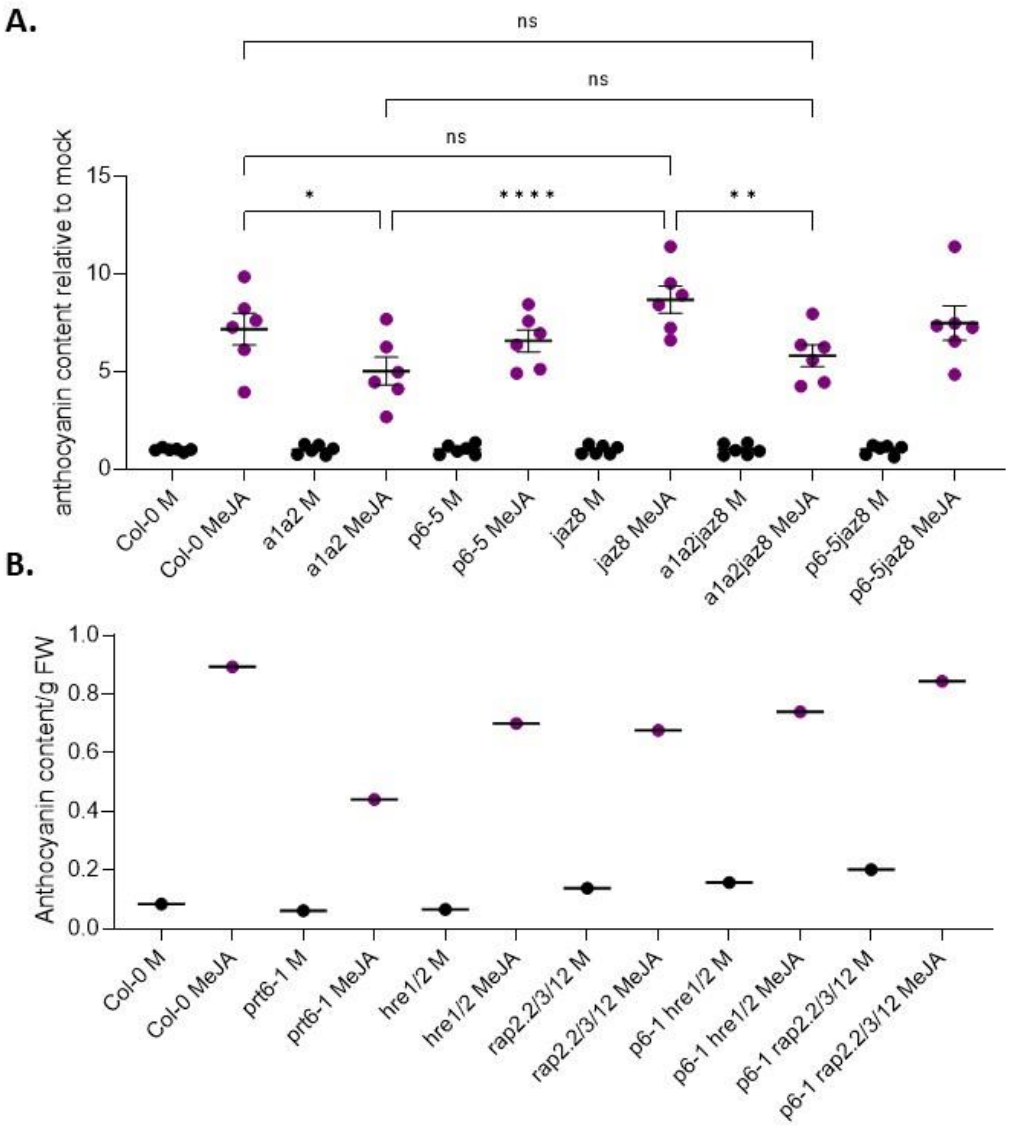

Figure 4.15. MeJA-dependent anthocyanin accumulation in seedlings. Seeds were sown on 0.5xMS plates with 1% sucrose ± 25 µM MeJA, and seedlings grown for 12 days to induce anthocyanin production. **A.** Mean and SEM from 6 biological replicates with, in each replicate, approx. 30 seedlings/genotype and treatment. For each biological replicate, the anthocyanin content per g of fresh weight was normalized for the respective average mock-treated genotype. *ate1ate2*: a1a2; *prt6-5*: p6-5. Statistical analysis conducted using one-way ANOVA with Sidak's multiple comparisons test for the following conditions: Col-0 MeJA to all other MeJA-treated genotypes and comparisons of each MeJA-treated parental genotype to respective higher order mutant (e.g. *ate1ate2* MeJA compared to *ate1ate2jaz8* MeJA and *jaz8* MeJA compared to *ate1ate2jaz8* MeJA) and *jaz8* MeJA to *ate1ate2* MeJA. **B.** Preliminary data for one biological replicate with different combinations of ERFVII mutants (approx. 30 seedlings per genotype and condition). Anthocyanin content is presented per g of fresh weight (FW).

Since accumulation of JAZ8 is not solely responsible for the decreased production of anthocyanins in *ate1 ate2* upon MeJA treatment, preliminary experiments were carried out to explore whether accumulation of ERFVII transcription factors in N-degron pathway mutants could be responsible for the reduced anthocyanin accumulation. Using N-degron pathway (*prt6-1*) and ERFVII (*hre1/2; rap2.2/3/12*) mutants and their combination (*prt6-1hre1/2; prt6-1rap2.2/3/12*), it was seen that *prt6-1* has lower levels of anthocyanins (Figure 4.15B) similar to results using *ate1 ate2* (Figure 4.15A). ERFVII mutants (*hre1/2* and *rap2.2/3/12*) display reduced levels of anthocyanins compared to Col-0 but also appear to partially rescue the *prt6-1* phenotype. This suggests that ERFVIIs have both a positive and negative role on anthocyanin accumulation and that ERFVII stabilization in N-degron pathway mutants is partially responsible for the observed reduced anthocyanin content (Figure 4.15B). This is only one replicate (approx. 30 seedlings per genotype and condition) and additional replicates are needed for statistical analysis and to draw conclusions.

The first function of Arabidopsis *ATE1* was discovered in a genetic screen for delayed leaf senescence. This screen led to the identification of a mutant allele of *ATE1* (*delayed leaf senescence 1* (*dls1*) in the Ws accession, in which *ATE2* is naturally not functional) with delayed leaf senescence (Yoshida et al., 2002). Notably, *jaz8* mutants (CS849856) were shown to senesce faster than wild-type plants upon MeJA treatment. JAZ8 and JAZ4 were also shown to play a role in MeJA-induced leaf senescence via their interaction with the WRKY57 transcription factor (Figure 4.16A), with the latter repressing directly the expression of *SENESCENCE 4* (*SEN4)*, a gene that is induced during senescence (Jiang et al., 2014). JAZ8 and JAZ7 were also shown to be involved in negatively regulating dark-induced senescence with JAZ7-mediated regulation

involving ROS and JA-signalling pathways including COI1 and MYC2 transcription factors (Yu et al., 2016). RT-qPCR was used to monitor the expression of *SEN4* in the N-degron mutant backgrounds, *jaz8* and higher order mutant combinations. Despite the need for additional biological replicates, the data suggest that *SEN4* is expressed at lower levels in *ate1 ate2* and in *prt6-5* compared to the wild type, and that *JAZ8* is not responsible for this differential expression in the N-degron mutants since *SEN4* expression remains lower in the *ate1 ate2 jaz8* and *prt6-5 jaz8* mutants (Figure 4.16B). Additional experiments are needed to monitor the expression of *JAZ8* itself, but also *JAZ4* and *WRKY57*. Furthermore, in our experiments, the expression of *SEN4* was not induced by the MeJA treatment, likely because a longer time is needed to induce the expression of this gene and senescence. For example, Jiang *et al*. (2014) did a time-course over a 3-day period to monitor up-regulation of *SEN4* by MeJA treatment.

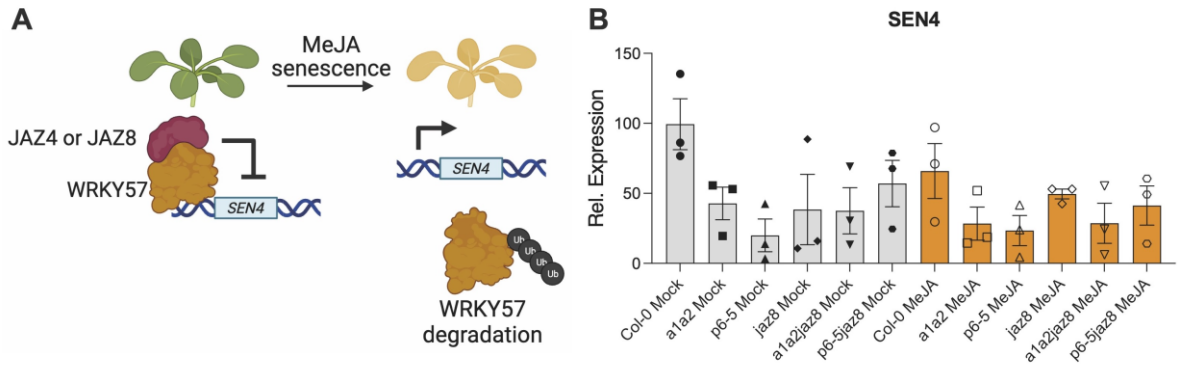

Figure 4.16. Differential expression of *SEN4* in different mutant backgrounds. A. Model summarising the repression of *SEN4* by WRKY57 *via* its interaction with JAZ8 and JAZ4 in the absence of MeJA treatment. Upon addition of MeJA, WRKY57 is targeted for degradation, thus allowing for the up-regulation of *SEN4*. **B.** Results of RT-qPCR analysis with RNA extracted from leaves of 4-week-old plants treated for 3 hours with 20 µM MeJA or a mock solution. Mean and SEM of the relative expression to a reference gene from 3 biological replicates are shown. ANOVA and Tukey's test indicate that the differences are not statistically significant.

To complement these data, defects in dark-induced senescence were tested using 4-week-old plants grown under short-day conditions. However, analysis of the preliminary results indicated that optimisation steps were needed for these experiments. Additional experiments needed include a characterisation of MeJA-induced leaf senescence in the different genetic backgrounds.

In sum, the data presented suggest that *ate1 ate2* and *prt6-5* are epistatic to *jaz8*, and that any potential accumulation of JAZ8 in these N-degron mutant backgrounds is not sufficient to explain the decreased MeJA response of these mutants. It is possible that functional redundancy between JAZ proteins poses a problem for this genetic analysis.

4.2.3. Exploring a potential role of JAZ8 in hypoxia response

Previous studies have shown that JA levels increase during 1, 3 and 6 hours of submergence (Shukla et al., 2020; Yuan et al., 2017), but then decrease at later timepoints (12-, 24- and 36-hours submergence) (Yuan et al., 2017). This decrease may partially be due to the requirement of oxygen for some enzymes of the JA biosynthesis pathway (Feussner and Wasternack, 2002; Iacopino and Licausi, 2020; Wasternack and Song, 2017), but may also be linked to the upregulation of *JAZ* genes by hypoxia, which could then result in the repression of genes coding for enzymes of the JA biosynthesis pathway. Indeed, the same two studies have shown that *JAZ* genes, including *JAZ1* and *JAZ8*, are induced upon hypoxia (Shukla et al., 2020; Yuan et al., 2017). To further explore potential connections between JA signalling and hypoxia response, the overlap between the JA and hypoxia transcriptional response programmes was determined using two published datasets. The first one identified MeJA response genes in 5-week-old plants treated with 0.1 mM MeJA for 14 consecutive timepoints over 16 hours (DEGs defined as having a greater than 2-fold difference in expression in at least one timepoint; minimum of 10 read counts in lowest expressed sample; Bonferroni-corrected p-value ≤ 0.05) (Hickman et al., 2017), while the second dataset contained DEGs identified in 7-day-old seedlings treated with hypoxia for 2 hours (cut-off applied: $|\log_2(FC)|>1.0$ and FDR<0.05) (Lee and Bailey-Serres, 2019). This comparative analysis showed a statistically significant overlap of 235 DEGs common to the JA and hypoxia response programmes (p-value<1.6e-45; gene list in Table B1 in Appendix), suggesting that MeJA and hypoxia regulate a common set of genes (Figure 4.17A). GO analysis of these 235 genes identified an over-representation for genes associated with 'response to hypoxia', 'response to hormone', as well as genes associated with the synthesis of secondary metabolites that are downstream of JA signalling (e.g. 'indole glucosinolate biosynthetic process') (Figure 4.17B). GO terms directly linked to JA signalling were not identified. Among these common DEGs, 111 genes (about 47%) showed the same direction of gene expression change, with 59 DEGs being up-regulated by either treatment, and 52 being down-regulated by MeJA or hypoxia (Figure 4.17C). The former include *PDC2* and *JAZ3*, while the latter include auxin related genes suggesting that both hypoxia and MeJA down-regulate auxin and downstream growth responses. Of the common DEGs, 124 had opposite changes in expression, with 27 DEGs being up-regulated by MeJA but repressed by hypoxia, while 97 DEGs were induced by hypoxia

but repressed by MeJA. The latter observation suggests that JA signalling could repress part of the hypoxia response programme. Notably, important hypoxia response genes such as *HB1*, *HRE1* and *PCO1* appear among the DEGs that are repressed by MeJA treatment (Figure 4.17D).

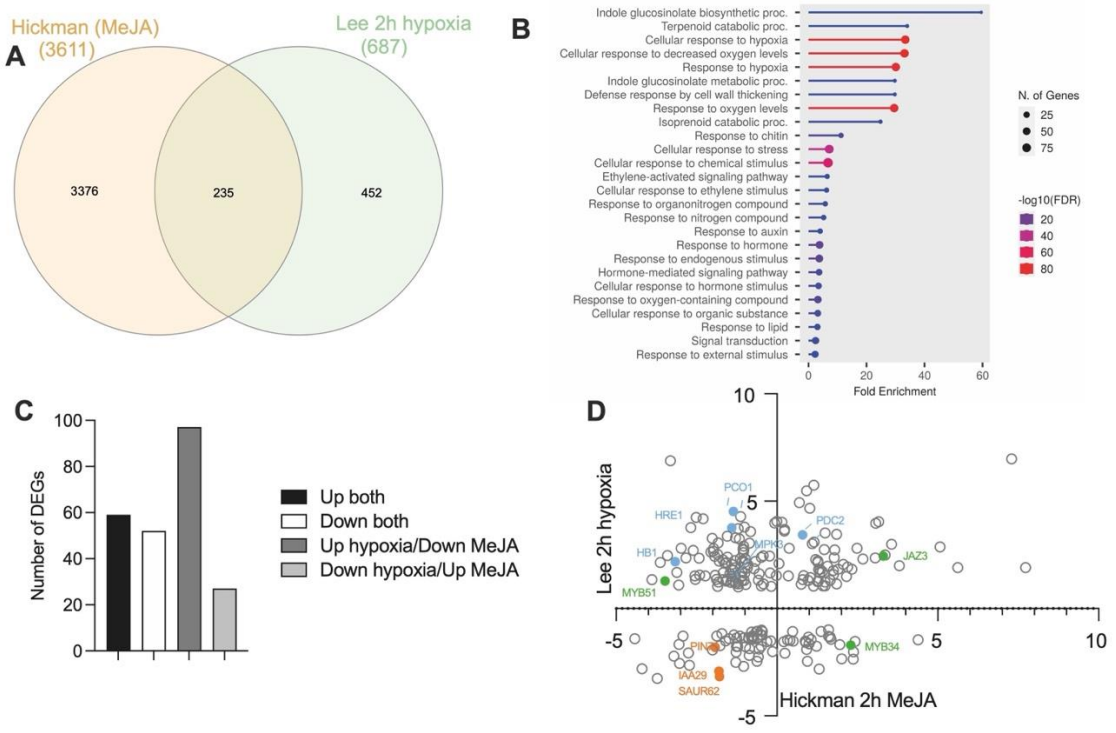

Figure 4.17. Analysis of existing RNA-seq and ChIP-seq datasets. A. Overlap of DEGs between the transcriptional responses to MeJA and to hypoxia. RNA-seq datasets obtained with 5-week-old plants treated with 0.1 mM MeJA for 14 consecutive timepoints over 16 hours (DEGs defined as having a greater than 2-fold difference in expression in at least one timepoint; minimum of 10 read counts in lowest expressed sample; Bonferroni-corrected p-value ≤ 0.05) (Hickman et al., 2017), or with 7-day old seedlings treated with hypoxia for 2 hours (cut-off applied: $|\log_2(FC)|>1.0$ and FDR<0.05) (Lee and Bailey-Serres, 2019) were compared and identified 235 common DEGs. **B.** Top 30 GO terms obtained using the 235 common DEGS to MeJA and hypoxia response. Cut-off: FDR<0.05; obtained using ShinyGO. **C.** Number of common DEGs having similar or opposite changes in gene expression in response to MeJA or hypoxia. **D.** Comparison of the directionality of gene expression change among the 235 DEGs common to MeJA and hypoxia response. The $\log_2$ of fold changes for each dataset are shown. Conserved hypoxia response genes are indicated in blue, JA response genes involved in glucosinolate biosynthesis are indicated in green, and genes associated with auxin response are shown in orange.

In addition, examination of an HRE2 ChIP-seq dataset (Lee and Bailey-Serres, 2019) suggested that this ERFVII transcription factor could potentially directly regulate the expression of some genes involved in JA signalling, including *JAZ8* (Figure 4.18A). Taken together with the observations that ATE1 may target JAZ8 for degradation and that N-degron mutants have

dampened JA signalling, I therefore sought to explore a potential role of *JAZ8* in hypoxia response in connection with the N-degron pathway and the ERFVIIs.

Further analyses of existing datasets indicated an overlap between genes differentially expressed by MeJA treatment (Hickman et al., 2017) and those neighbouring HRE2 binding sites in a ChIP-seq experiment (Lee and Bailey-Serres, 2019) (Figure 4.18A; p-value<1.304e-42). A more specific comparison using only those genes whose promoter region was bound by HRE2 suggested that this TF binds to the promoters of 256 JA response genes (Figure 4.18B; p-value<4.616e-07). Plotting the log_2FC of these genes at 2-hr post MeJA treatment showed that these HRE2 bound genes are both up and downregulated by MeJA treatment (Figure 4.18C). Notable putative targets are *JAZ3*, *JAZ8*, *NINJA* and *ORA59*. Interestingly *JAZ3*, *JAZ8* and *NINJA* are involved in the repression of JA signalling and are all upregulated under 2-hour MeJA treatment. *ORA59* is involved in ERF-branch mediated JA responses and is downregulated during 2-hour MeJA treatment. Next, I sought to determine if some HRE2 bound genes could be responsive to both MeJA and hypoxia, in order to assess whether there could be a link between ERFVIIs, JA signalling and hypoxia response. Overlap analysis of the 3 datasets identified 39 common genes (Figure 4.18D). A heatmap of these 39 genes displaying the log_2FC expression for 2 hours of hypoxia and 2 hours of MeJA treatment (Figure 4.18E) showed in general antagonistic effects of hypoxia and MeJA. Genes which had similar expression under both treatments included *JAZ3*, *MONODEHYDROASCORBATE REDUCTASE 3* (*MDAR3*; also referred to as *MDHAR*), and *EXPANSIN 10* (*EXPA10*). Lastly, a transcription factor binding predictor tool, Plant Promoter Analysis Navigator (PlantPAN4.0) (Chow et al., 2024) predicted binding sites for all five ERFVII members in JAZ8 promoter (Figure 4.18F). For all members, binding was predicted to occur ~365 bp upstream of the transcriptional start site (TSS). While other ERF transcription factor members (e.g. ERF2, ERF5, ERF9, ERF104) were also predicted to bind to this site, it is of interest that the binding site for HRE2 identified in the ChIP-Seq study (Lee and Bailey-Serres, 2019) was 352 bp upstream of the TSS.

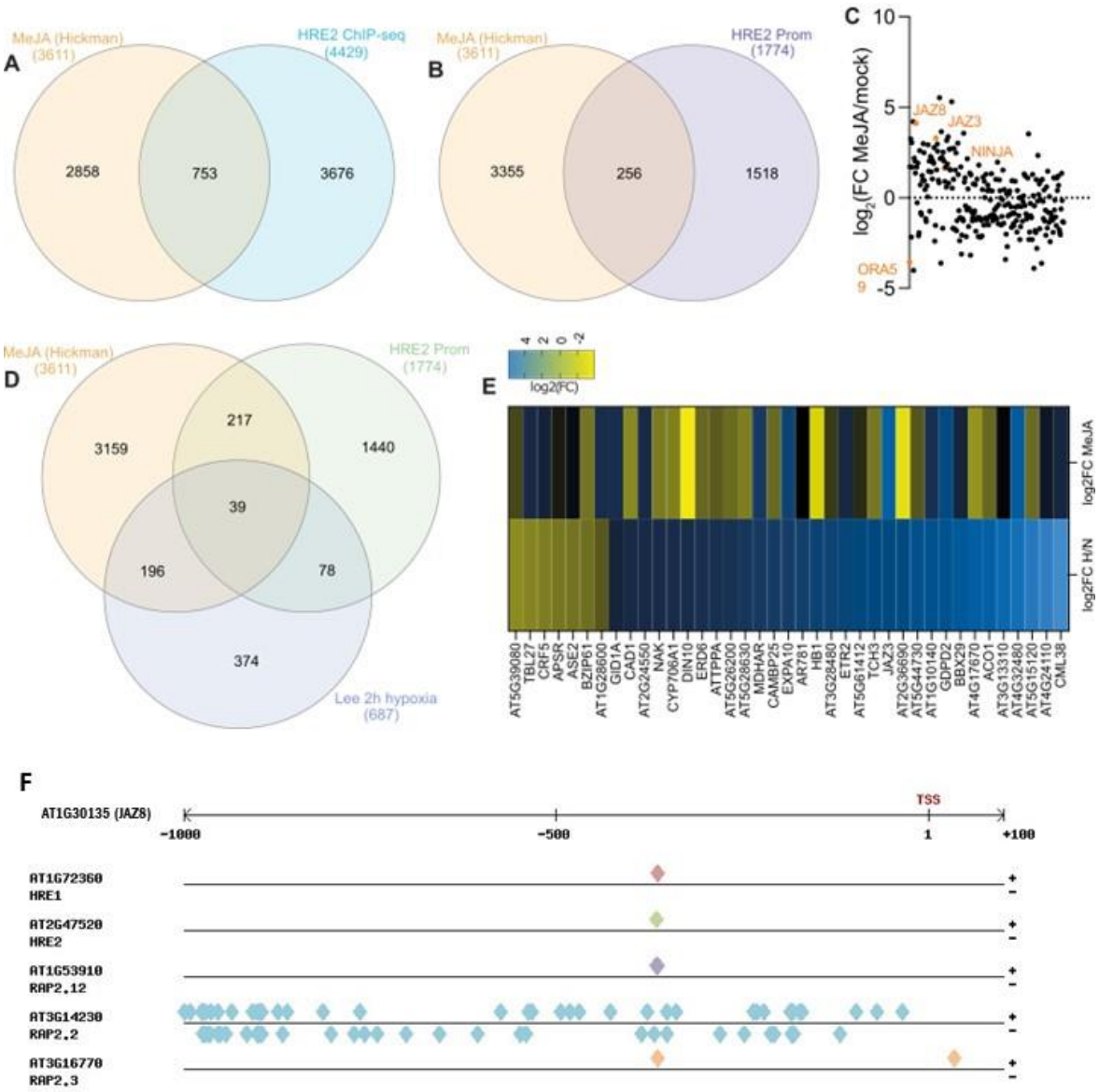

Figure 4.18. Comparison of JA response genes and an HRE2 ChIP-seq dataset. A. Overlap between RNA-Seq results for DEGs upon MeJA treatment of 5-week old plants over a 16 hour time-course (DEGs defined as having a greater than 2-fold difference in expression in at least one timepoint; minimum of 10 read counts in lowest expressed sample; Bonferroni-corrected p-value ≤ 0.05) (Hickman et al., 2017) and ChIP-Seq dataset for HRE2 bound genes for seedlings pretreated to flooding with Calpain inhibitor IV and DMSO followed by hypoxia treatment. Genes identified have at least one significant peak (FDR ≤ 0.01) (Lee and Bailey-Serres, 2019). **B.** Same as A but only genes which are bound by HRE2 at their promoter are considered. **C.** Plot of log_2FC of 256 genes in overlap in B with notable genes labeled. **D.** Overlap between MeJA-mediated DEGs, genes bound by HRE2 at their promoter, and DEGs upon 2 hours of hypoxia in 7-day old seedlings (cut-off applied: |log(FC)|>1.0 and FDR<0.05) (Lee and Bailey-Serres, 2019). **E.** A heatmap showing the 39 genes in overlap in D with log_2FC values for 2 hour MeJA treatment or 2 hour hypoxia treatment. **F.** PlantPAN4.0 analysis of ERFVII transcription factor predicted binding sites in JAZ8 promoter region. Red = HRE1; Green = HRE2; Purple = RAP2.12; Blue = RAP2.2; Orange = RAP2.3.

In sum, HRE2 and potentially other ERFVIIs could be involved in regulating JA response genes with a potential role in hypoxia response. One potential link could be JAZ8, which interacts with ATE1 and could be also targeted for degradation by the N-degron pathway.

4.2.3.1. ERFVII transcription factors regulate *JAZ8* expression

RT-qPCR was used to monitor gene expression levels of *JAZ1* and *JAZ8* in 10-day old N-degron pathway and *erfVII* mutant seedlings under hypoxic or normoxic conditions. *JAZ8* expression appeared to be induced under hypoxia and this induction could be ERFVII dependent. *JAZ1* expression was also induced under hypoxia but unlike *JAZ8*, its up-regulation did not appear to be dependent on ERFVIIs (Figure 4.19). Despite the differences observed, ANOVA and Tukey tests did not retrieve statistically significant differences for comparisons of interest. This could be due to the variation for some of the samples. In other studies, *JAZ2/3/5/6/10* expression was also induced upon hypoxia treatment (Mustroph et al., 2009; Shukla et al., 2020), thus suggesting that the up-regulation of *JAZ* genes could be a feature of the hypoxia response programme.

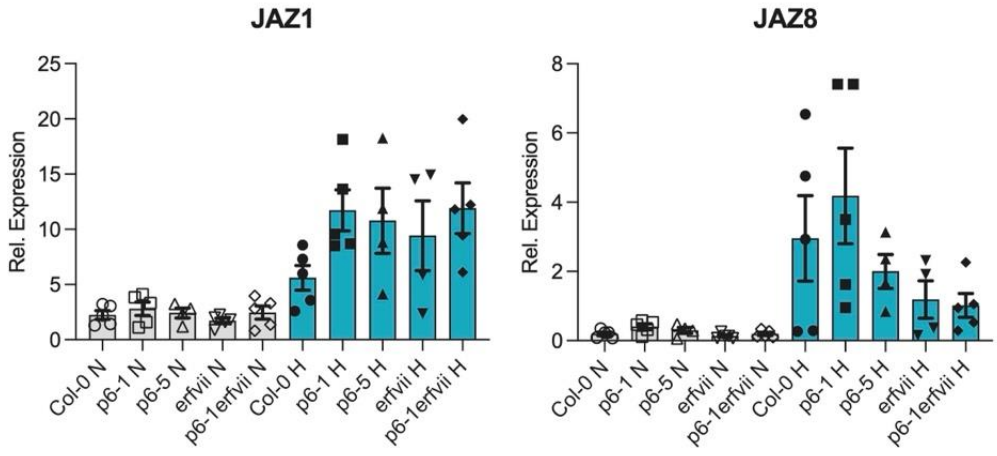

Fig. 4.19. Expression of *JAZ1* and *JAZ8* in response to hypoxia. The expression of JAZ1 and JAZ8 relative to a reference gene was determined using RT-qPCR on total RNA extracted from 10-day old seedlings treated with hypoxia using anaerojars (H) or kept under normoxia (N) for 1 hour. Mean and SEM are shown.

To further dissect which members of the *ERFVII* TF family could be responsible for *JAZ8* induction under hypoxia, different sets of mutants for the *ERFVII* TFs were used, including an *hre1 hre2* (*hre1/2*) double mutant and a *rap2.2 rap2.3 rap2.12* (*rap2.2/3/12*) triple mutant (Gibbs et al., 2014). I also sought to use 35S:*HRE1-FLAG* and 35S:*HRE2-HA* overexpression lines (Gibbs et al., 2011). However, control experiments revealed that while the overexpression lines grew on Basta

selection plates, the transgenes of 35S:*HRE1-FLAG* #1.1 and 35S:*HRE2-HA* lines were silenced (Figure 4.20A), so experiments could only be carried out with two 35S:*HRE1-FLAG* lines (#5.2 and 10.4). These experiments showed that *JAZ1*, *JAZ3* and *JAZ8* were up-regulated by 1 hr hypoxia treatment. This induction was again ERFVII independent for *JAZ1*. For the up-regulation of *JAZ3* under hypoxia, *RAP2.2/3/12* appear to play a more important role than *HRE1/2*, while both *RAP2.2/3/12* and *HRE1/2* are involved in the induction of *JAZ8* expression under hypoxia (Figure 4.20B). Furthermore, the results with the *35S:HRE1-FLAG* overexpression line suggest that both *HRE1* and *HRE2* may regulate *JAZ8* transcription, possibly in a redundant manner. The finding that *RAP2.12* may play a role in the regulation of *JAZ3* and *JAZ8* expression is in agreement with a microarray dataset obtained using seedlings overexpressing a *RAP2.12* variant that had the first 13 amino acid residues truncated (e.g. the resulting ΔRAP2.12 protein is no longer degraded by the N-degron pathway) (Giuntoli et al., 2017). Specifically, this microarray dataset - obtained under normoxic conditions - shows a constitutive induction of *JAZ3* and *JAZ8*, but not of *JAZ1*. Whether RAP2.2/3/12 or HRE1/2 regulate *JAZ8* gene expression directly or indirectly remains to be explored.

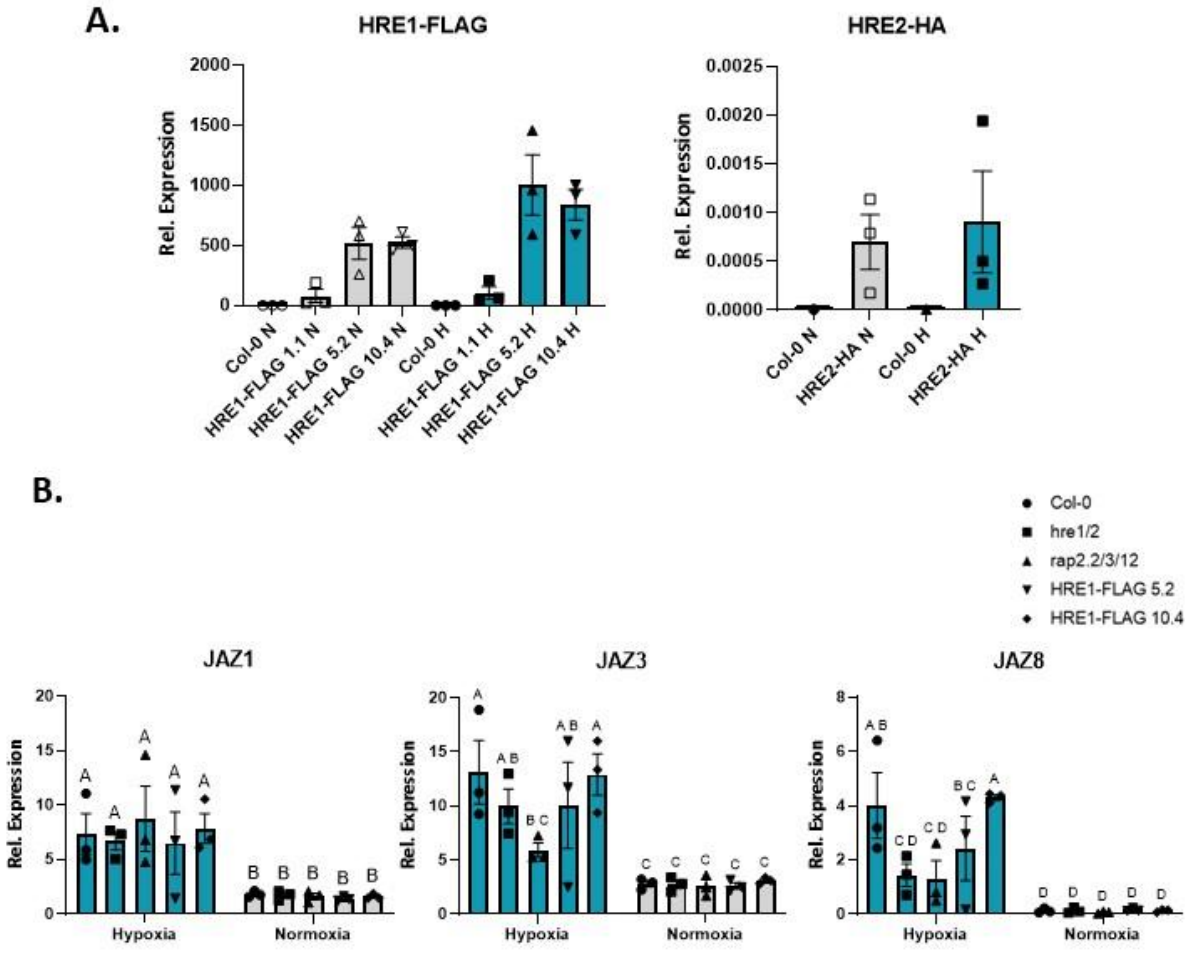

Figure 4.20. Regulation of JAZ8 by ERFVII transcription factors. **A.** RT-qPCR results to determine the expression level of HRE1-FLAG or HRE2-HA in transgenic line expressing these fusions from the 35S promoter. **B.** Relative expression of *JAZ1/3/8* under hypoxia (H) or normoxia (N) in different compbinations of ERFVII mutants and overexpression lines. Mean and SEM of 3 biological replicates are shown. Statistical analysis (two-way ANOVA with Fisher's test) is presented in CLD format.

4.2.3.2. JAZ8 protein levels are regulated by hypoxia

The data obtained indicate that *JAZ8* expression, along with that of a number of other *JAZ* genes, is up-regulated by hypoxia. Here, I explored whether hypoxia could also regulate the stability of JAZ8 at the protein level. To this end, a wild-type Col-0 line expressing JAZ8 fused to YFP from the 35S promoter (*35S:JAZ8-YFP*; (Shyu et al., 2012)) was subjected to hypoxia or normoxia to monitor the effect of hypoxia on JAZ8-YFP protein stability by immunoblot with an anti-GFP antibody (Figure 4.21). The data show that JAZ8-YFP accumulates at a higher level under normoxia compared to hypoxia, starting from one hour and up to at least 6 hours. This suggests that the initial response to hypoxia triggers the degradation of JAZ8-YFP. Interestingly, though, at a later timepoint (24 hours), JAZ8-YFP levels are higher under hypoxia than normoxia. It is therefore possible that the hypoxia-induced degradation of JAZ8-YFP may be transient, and that longer hypoxia treatments result in a stabilization of JAZ8-YFP again.

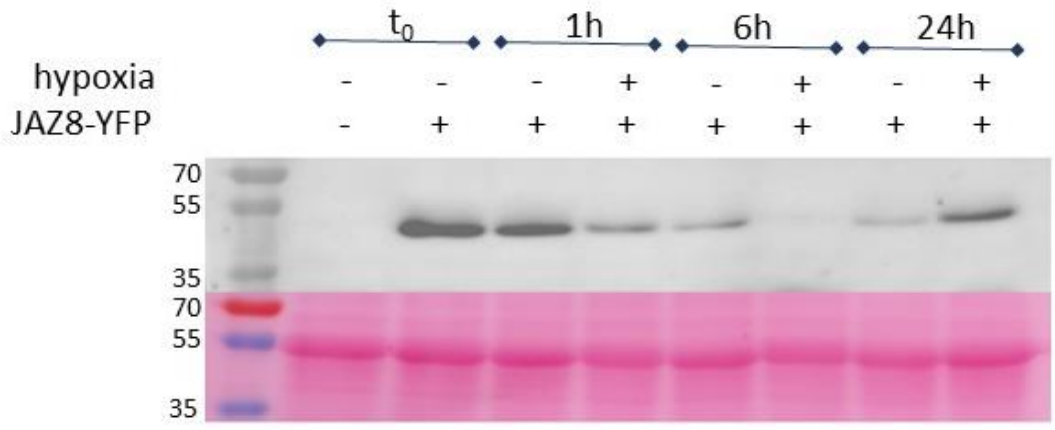

Figure 4.21. Effect of hypoxia on JAZ8 protein levels in Arabidopsis. Col-0 *35S:JAZ8-YFP* seedlings (10-day old) were treated +/- hypoxia using anaerojars for 0, 1, 6 and 24 hours. Protein was extracted in 2xSDS loading dye and quantified using amido black protein quantification method. 30 µg protein was loaded per well and immunoblots were imaged using anti-eGFP/eYFP (Abcam #Ab290) antibody. Blot is representative of 3 biological replicates.

4.2.3.3. Response of *jaz8* and *ate1 ate2 jaz8* mutants to submergence and hypoxia

To further explore a potential role of *JAZ8* during hypoxia, submergence and hypoxia survival assays were performed. First, a 4-day dark submergence treatment was applied to 5-week old plants including wild-type Col-0, *jaz8*, N-degron mutants and their combinations with *jaz8*, followed by a 7-day recovery. To score the response of the plants to dark submergence, the aerial part of the plants were weighed. For each genotype, the comparison of the fresh weight between dark-treated and dark-submerged plants indicated that submerged plants had a reduced fresh weight, indicating that submergence treatment affected plant growth (Figure 4.22A). However, no statistically significant differences in growth were detected between the different genotypes upon dark submergence (Figure 4.22B).

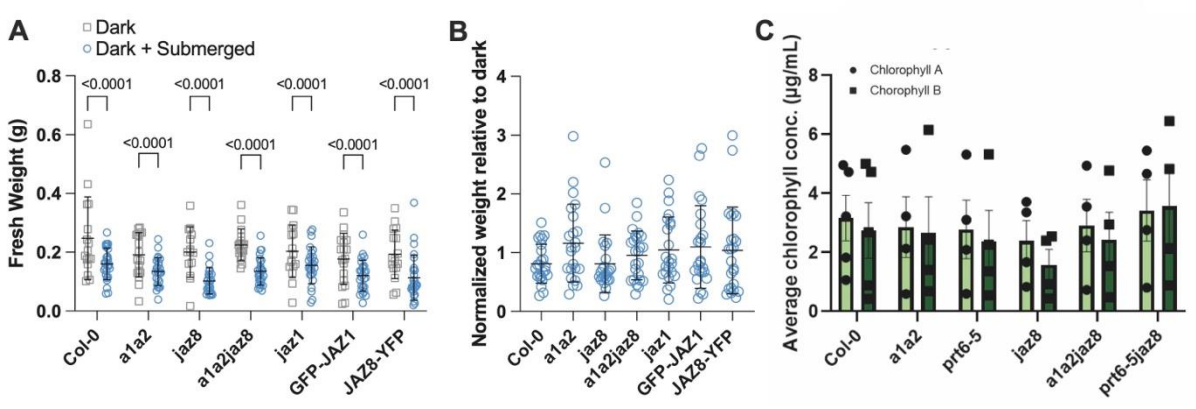

Figure 4.22. Analysis of submergence and hypoxia impact on fresh weight and chlorophyll levels of N-degron pathway and *jaz8* mutant plants. A. Fresh weights (g) of 5-week old plants (Col-0; *ate1ate2; jaz8; ate1ate2jaz8; jaz1*; GFP-JAZ1; JAZ8-YFP) treated to dark submergence after 7 days of recovery. Results of a two-way ANOVA are displayed. **B.** Weights of dark + submerged plants presented in A normalized to the respective genotype kept in the dark (control). **C.** Chlorophyll-A and -B content of 9-day old seedlings (Col-0; *ate1ate2; prt6-5; jaz8; ate1ate2jaz8; prt6-5jaz8*) treated to 16 hours of hypoxia (in anaerojars) in dark period and allowed to recover for 3 days.

To complement these assays, hypoxia survival experiments were also conducted. In this case, 9-day old seedlings were kept overnight (16 hours) in anaerojars in the dark, followed by a 3-day recovery period, after which chlorophyll content was measured. Genotypes exhibiting tolerance to hypoxia treatment would be expected to have higher chlorophyll content. No differences in chlorophyll content were detected between the different genotypes (Figure 4.22C), including *ate1 ate2* and *prt6-5*, suggesting that optimisation steps are needed.

To complete this phenotypic characterisation, the expression of hypoxia response marker genes (*ADH1*, *SUS1*, *HB1* and *HRE2*) was also tested in the different mutant combinations with *jaz8* and their respective parental genotypes, following a 1 hr hypoxia treatment of 10-day old seedlings (Figure 4.23). The results obtained show that under normoxia, *ate1 ate2* and *prt6-5* mutants have higher levels of expression of the 4 hypoxia response marker genes tested. This finding is in agreement with the stabilisation of ERFVIIs and constitutive activation of hypoxia response in these mutants. In addition, in normoxic conditions, the *jaz8* mutant behaves similarly to the wild type, whereas the *ate1 ate2 jaz8* and *prt6-5 jaz8* mutant combinations behave like *ate1 ate2* and *prt6-5*, respectively. *ADH1* is a particularly good marker gene for early hypoxia response, so it can be used as a control to verify that the treatment was sufficient to trigger hypoxia response. While induction is visible for most replicates in most genotypes, 2 biological replicates with Col-0 seedlings have poor induction of *ADH1* expression. This low induction is also visible for *SUS1*, *HB1* and *HRE2*, suggesting a potential problem for two sets of Col-0 biological replicates. While additional replicates are needed to validate the findings, the data obtained for *ADH1* and *SUS1* suggest that there are no strong differences in the expression of these genes under hypoxia. In contrast, for *HB1* and *HRE2*, there are some significant differences. Specifically, expression of these genes in *jaz8* is similar to that of Col-0, while *ate1 ate2* and *prt6-5* have higher expression of these genes. In addition, the *ate1 ate2 jaz8* and *prt6-5 jaz8* mutant combinations behave like *ate1 ate2* and *prt6-5*. This suggests that hypoxia triggers a stronger up-regulation of *HB1* and *HRE2* in N-degron pathway mutant genotypes, either as a result of (i) the constitutive stabilisation of ERVIIs in these backgrounds which could prime the plants to respond faster and more efficiently to hypoxia, or (ii) the stabilisation of other N-degron pathway substrates that could dampen the up-regulation of these genes under hypoxia. The fact that *ate1 ate2 jaz8* and *prt6-5 jaz8* have similar amplitude of gene up-regulation compared to *ate1 ate2* and *prt6-5*, respectively, suggests that *JAZ8* may not be required to control/dampen the level of up-regulation of *HB1* and *HRE2* under hypoxia. It remains possible that other JAZs play a role in this process though.

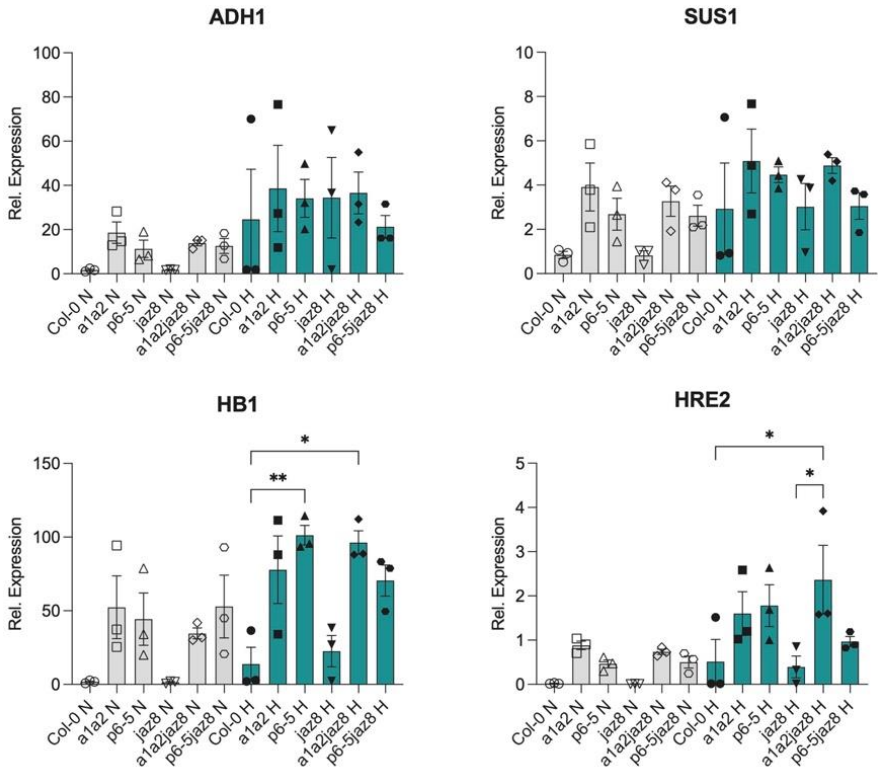

Figure 4.23. Expression of hypoxia response genes in jaz8 mutant combinations and control genotypes. Ten-day old seedlings (Col-0; *ate1 ate2 (a1a2); prt6-5 (p6-5); jaz8; ate1ate2jaz8 (a1a2j8); prt6-5jaz8 (p6-5j8)*) were treated with 1 hr hypoxia (H) in anaerojars or left in normoxia (N). Mean and SEM of relative expression to a reference gene are shown. Statistical analysis: one-way ANOVA with Tukey's post-hoc test. For *ADH1* and *SUS1*, ANOVA results suggest no statistically significant differences. For *HB1* and *HRE2*, ANOVA indicates that there are statistically significant differences. For these 2 genes, only statistically significant differences are shown for the following post-hoc comparisons: Col-0 to all other genotypes in normoxia; Col-0 to all other genotypes in hypoxia; normoxia compared to hypoxia for a given genotype; parental genotypes compared to respective higher order mutants under normoxia or hypoxia.

Altogether, the data obtained show that *JAZ* expression is regulated by hypoxia, with some genes being up-regulated independently of the ERFVIIs (e.g. *JAZ1*), while up-regulation depends on ERFVIIs in other cases (e.g. *JAZ3* and *JAZ8*). In addition, JAZ8 protein stability is regulated by hypoxia, so that it is degraded during the first hours of hypoxia treatment, but becomes stable again for longer treatments (24 hours). This suggests a dynamic regulation of both *JAZ8* expression and protein stability by hypoxia, which appears to be paradoxical (see Discussion below). Despite these effects, hypoxia response gene expression does not appear to be affected in *jaz8* single mutants, and higher order mutant combination of *jaz8* with *ate1 ate2* and *prt6-5* indicate that *jaz8* does not contribute to the phenotype of the N-degron mutants. Submergence

and hypoxia survival assays remain inconclusive regarding a potential role of *JAZ8* in hypoxia, perhaps because of functional redundancy among JAZ proteins.

4.3. Discussion

The work presented in this Chapter aimed to uncover the mechanistic link(s) between the N-degron pathway and JA signalling, which had remained unexplored after the initial finding that N-degron pathway mutants such as *ate1 ate2* and *prt6-5* have dampened MeJA responses (de Marchi et al., 2016). Over the course of this work, both direct (e.g. JAZ8/ATE1 interaction) and indirect (*via* ERFVIIs) links were found. Y2H experiments and preliminary co-IP data suggest a direct protein/protein interaction between JAZ8 and ATE1, involving the ATE1 substrate binding domain and its D/E-rich region (Figure 4.11). The biochemical and biological relevance of the D/E rich region in ATE1 remains to be understood, but such negatively charged sequences have been associated with multiple functions including metal binding (e.g. calcium), or mediating protein/protein interactions. Further work is needed to confirm this ATE1/JAZ8 interaction *in planta* through optimising co-IPs in *N. benthamiana* and using Arabidopsis protoplasts (see Figure 4.24 for a working model). Immunoblot results also identified higher molecular weight forms of ATE1-HA in *N. benthamiana*, which could point to potential (unknown) covalent post-translational modifications of ATE1, that could be relevant to post-translational regulatory mechanisms for the activity of this enzyme.

Transient co-expression of ATE1-HA and JAZ8-myc in *N. benthamiana* provides a potential physiological relevance to this interaction, as JAZ8-myc appears to be targeted for degradation in an ATE1-dependent manner (Figure 4.13). More investigations are needed to establish if ATE1-mediated degradation requires PRT6 and indeed occurs through the N-degron pathway, or if this may be the first case of an N-degron pathway independent function of ATE1 in plants. The latter has been shown to occur in mammals with arginylation of ACTIN, ß-AMYLOID, and CALRETICULIN (Carpio et al., 2010; Karakozova et al., 2006; Pavlyk et al., 2018; Wang et al., 2017b). The following key questions remain to be addressed:

(1) Is JAZ8 a *bona fide* N-degron pathway substrate? For this to be the case, it would be important to determine:

(a) if the destabilisation of JAZ8 is PRT6 dependent. Unfortunately, transient co-expression experiments of JAZ8-myc and PRT6 in *N. benthamiana* could not be carried out because PRT6 containing plasmids are unstable in Agrobacterium (E. Graciet personal

communication). Additional reagents such as a *prt6* mutant expressing tagged JAZ8 are being generated.

(b) whether JAZ8 is proteolytically cleaved prior to binding by ATE1/2. Indeed, N-degrons are typically exposed following cleavage of a protein by a protease, thus resulting in the exposure of a new N-terminal residue, which can serve as a N-degron. Constructs to express a N-terminally and C-terminally tagged version of JAZ8 (*35S:GFP-JAZ8-myc*) have been generated and infiltrated in tobacco to determine if they were cleaved. However, control constructs *35S:GFP-LUC*, which had the same linker sequence between GFP and LUC compared to GFP and JAZ8 showed that there was artefactual cleavage of this linker sequence. I am planning on designing new constructs to address this question.

(2) Does JAZ8 interact with ATE1/2 in Arabidopsis? In order to address this essential question, I have crossed *ate1 ate2* mutants expressing an ATE1-HA fusion protein from the 35S promoter (35S:*ATE1-HA*; E. Graciet (unpublished)) with a wild-type Arabidopsis line expressing JAZ8-YFP from the 35S promoter ($35S_{pro}$:*JAZ8-YFP*). I obtained 35S:*ATE1-HA* 35S:*JAZ8-YFP* plants with segregating *ate1 ate2* in the F2 for co-IP experiments, however, immunoblots showed that the 35S:*ATE1-HA* and 35S:*JAZ8-YFP* transgenes were silenced.

(3) Is JAZ8 also destabilised by ATE1/2 in Arabidopsis? To address this question, I crossed *ate1 ate2* mutants with *35S:JAZ8-YFP* and isolated the *ate1 ate2 35S:JAZ8-YFP* line in the F2. However, *JAZ8-YFP* was also silenced in these lines, so that studies of JAZ8 accumulation in an *ate1 ate2* mutant background compared to the wild type could not be performed.

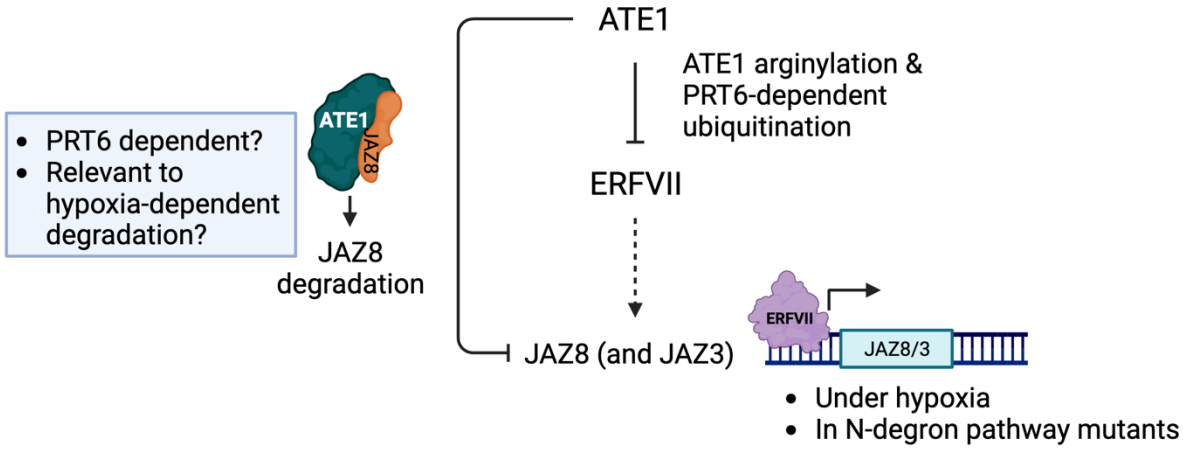

Figure 4.24. Model linking ATE1, ERFVIIs and JAZ8. ATE1 and JAZ8 interact with each other, which could trigger the ATE1-dependent degradation of JAZ8. Links with the N-degron pathway, and in particular with the E3 ubiquitin ligase PRT6 remain to be explored, both under normoxic or hypoxic conditions. One key open question is indeed whether hypoxia-induced degradation of JAZ8 is dependent on ATE1 and PRT6. Under hypoxic conditions and in N-degron pathway mutants, ERFVII transcription factors are stabilised.

HRE2 has been found to bind the promoters of *JAZ8* and *JAZ3* and RT-qPCR results suggest that the up-regulation of these genes under hypoxia could indeed be ERFVII dependent.

Indirect links between N-degron pathway and JA have been previously shown and are primarily mediated through the ERFVII transcription factors, with HRE2 being detected at the promoter of *JAZ8* using a ChIP-Seq dataset (Lee and Bailey-Serres, 2019). The promoter of *ORA59*, mediator of JA signalling through the ERF-branch, is also bound by HRE2 (Lee and Bailey-Serres, 2019) and a protein-protein interaction was found between ORA59 and RAP2.3, which mediates interdependently and additively the resistance to the necrotrophic bacterium *Pectobacterium carotovorum* (Kim et al., 2018). This indirect link is also supported by several observation in the present work: (i) the potential rescue of the reduced MeJA-induced anthocyanin accumulation of N-degron mutants when ERFVIIs are mutated; (ii) both *rap2.2/3/12* and *hre1/2* mutants show reduced *JAZ8* gene expression, while a HRE1-FLAG overexpression line exhibited slightly elevated (not significant) *JAZ8* expression under hypoxia and normoxia. However, due to variation more replicates are needed to confirm this. A previous study presented findings that the ERFVII group transcription factor, SUB1A, in rice delays leaf senescence in part through desensitizing plants to MeJA treatment. SUB1A further limits MeJA-induced expression of senescence response genes, chlorophyll reduction, and shoot growth inhibition as well as dampening dark-induced anthocyanin production (Fukao et al., 2012). This raises the question as to whether the negative regulation of JA signalling by ERFVII transcription factors could be evolutionarily conserved and whether JAZ proteins are at the centre of the underlying molecular mechanisms.

One potential implication of this direct and indirect link between the N-degron pathway and JAZ8, is that in *ate1 ate2* mutant plants, without ATE1-mediated destabilisation of JAZ8, this may lead to an increase in the levels of JAZ8 protein. JAZ8 levels may also accumulate in these mutants as a result of the accumulation of ERFVII transcription factors, which positively regulate JAZ8 transcription (Figure 4.24). While further experiments are needed to validate this, the potential over-accumulation of JAZ8 may explain some N-degron pathway mutant phenotypes including susceptibility to necrotrophic pathogens (de Marchi et al., 2016; Gravot et al., 2016), as *JAZ8* has been shown to reduce resistance to *B. cinerea*. This has been attributed to JAZ8 (as well as JAZ4, JAZ7 and JAZ9) repression of the *WRKY75* transcription factor. WRKY75 promotes tolerance to necrotrophic pathogens with *wrky75* mutants (TDNA lines (*wrky75-1* and *wrky75-25*) and RNAi line) displaying increased susceptibility to *B. cinerea* and *Alternaria brassicicola*. JAZ8 also has roles in suppressing the level of important secondary metabolites involved in

pathogen defence. This includes anthocyanins which JAZ8 regulates along with JAZ1/2/5/6/9/10/11 (Qi et al., 2011) and glucosinolates. The latter is of interest, considering that *ate1 ate2* has been shown to have reduced accumulation of glucosinolates (de Marchi et al., 2016). However, experiments using *ate1 ate2*, *prt6-5*, *jaz8* and their higher order mutants showed little genetic interaction with JA response gene induction in response to MeJA. However, it is possible that longer timepoints are needed for such effects to be detectable, especially considering some of the genes tested, such as SEN4, which would require longer exposures to MeJA to be up-regulated. In contrast, when testing the MeJA-dependent accumulation of anthocyanin, epistatic interactions were found, with *ate1 ate2 jaz8* and *prt6-5 jaz8* mutants generally resembling the *ate1 ate2* and *prt6-5* parents, respectively.

A role of *JAZ8* in hypoxia response was also explored: JAZ8 protein stability was shown to be regulated by hypoxia with JAZ8 being destabilised at 1- and 6-hour treatments but becoming stabilised again by 24 hours. Interestingly, the timing of JAZ8 destabilisation matches previous studies showing increased JA levels at 6 hours of hypoxia treatment. These results suggested a possible role for JAZ8 in the regulation of JA level and signalling during hypoxia (Figure 4.24). The induction of *JAZ8* expression at the mRNA level but destabilisation at the protein level suggests a potential mechanism to allow quick switching off of JA signalling after appropriate responses have been mounted. A genetic approach using a *jaz8* mutant and higher order mutants with N-degron pathway components and comparison with the wild type showed no differences in inducing the expression of key hypoxia response genes and for the ability of these genotypes to tolerate dark submergence or hypoxia treatments. Overall, these genetic results may reflect functional redundancy with other JAZ proteins playing roles in these responses, but may require some experimental optimisation, such as for example the timepoints used. Another hypothesis that would link JAZ8 degradation, hypoxia and immunity is that JAZ8 degradation under low oxygen conditions may be a way of de-repressing responses to necrotrophic pathogens (e.g. through the release of WRKY75) under the hypoxic conditions induced during *B. cinerea* infection, for example. This would require additional experiments to be tested. Finally, as outlined in Chapter 3, multiple JA-response genes are specifically induced under combined hypoxia/flg22 treatment including *JAZ3*, *JAZ8*, *MYC2* and *WRKY51*. The use of combined stresses could potentially help reveal roles of JAZ8 in the context of hypoxia. Indeed, JA plays an important role in regulating growth/defence trade-off, potentially explaining the downregulation of growth-related genes in combined hypoxia/flg22, as outlined in sections 3.2.2.2. and 3.3. This role was also visible when comparing JA and hypoxia response genes, as both MeJA and hypoxia treatments resulted in the repression of a common set of auxin response genes. Taken together,

the results of Chapters 3 and 4 could suggest a role for JA as a possible point of intersection of immunity, N-degron pathway and hypoxia responses.

Chapter 5: Generating an ATE1 deficient macrophage cell line

5.1. Introduction

As outlined in the introduction, one of the aims of this Ph.D. project was to explore potentially conserved roles of the N-degron pathway in immunity in plants and mammals. The fact that ATE1 is a well-defined enzymatic component of the N-degron pathway, encoded by only one gene in mouse, made it a suitable target to KO to study the effects on immune response in a model immunity mouse cell line – RAW264.7 macrophages. Although the work could not be completed, Chapter 5 presents efforts made to generate ATE1 KO RAW264.7 lines using CRISPR/Cas9. This work was carried out in collaboration with Dr. Eoin McNamee (Maynooth University) and Dr. Ailbhe Brazel (Maynooth University).

5.1.1. Role of the N-degron pathway in macrophage function

Macrophages are key immune cells involved in innate immunity. They are phagocytes found in most tissues of the body and are derived from embryo macrophage progenitors and bone marrow derived monocytes. Their ubiquitous nature allows them to be one of the first responders to infection or wounding, and thus form part of the first line of defence. As well as their vital roles in innate immunity, they are important in the activation of adaptive immune responses through production and secretion of cytokines and possessing major histocompatibility complex (MHC) class II molecules which upon phagocytosis of a pathogen, allows them to present antigens on their cell surface. These can then be used to train and activate the adaptive immune B and T cells (Arango Duque and Descoteaux, 2014). Macrophages are also important in homeostasis and thus following infection, macrophages are important in resolving inflammation and in wound healing (Arango Duque and Descoteaux, 2014; Kim and Nair, 2019). The N-degron pathway has been shown to play roles in regulating responses involved in macrophage function.

Inflammation is protective and acts to promote the entry of immune cells into the infection or wound site through production of chemokines and vasodilation of blood vessels (Liu et al., 2017). Binding of PAMPs/DAMPs by macrophage PRRs (e.g. lipopolysaccharide (LPS) binding to TLR4)

results in the induction of an inflammatory response, downstream of the activation of the transcription factor NF-κB, which upregulates expression of pro-inflammatory genes such as pro-inflammatory cytokines. These include tumour necrosis factor (TNF), IL-1ß, IL-6, and IL-12 (Liu et al., 2017). Many pro-inflammatory cytokines are generated in an inactive form and must be activated in response to infection. For example, the cytokine, IL-1ß, is produced in a pro-form. Cleavage by proteases (e.g. caspases) allows for transition from inactive pro-IL-1ß to active IL-1ß. This cytokine is predominantly synthesized and secreted by monocytes and macrophages and is involved in attracting other immune cells (e.g. granulocytes), and mediating differentiation of the adaptive immune cells, CD4+ T cells. IL-1ß is also involved in inducing fever and prostaglandin secretion (Arango Duque and Descoteaux, 2014; Fernández and Lamkanfi, 2015). Caspases (e.g. caspase 1 and caspase 11 in rodents) are activated by important mediators of inflammation called inflammasomes, which are multiprotein complexes that form from the assembly of intracellular receptors (e.g. NLRP1, NLRP3, NLRC4, AIM2, and PYRIN) (Fernández and Lamkanfi, 2015). As well as activating pro-inflammatory cytokines, caspases also promote the activity of a pore-forming protein, known as gasdermin D, which is responsible for an inflammatory form of cell death called pyroptosis (Chui et al., 2019; Sandstrom et al., 2019; Xu et al., 2019). The NF-κB pathway has been shown to be involved in inflammasome formation (Liu et al., 2017) but some NLRs such as NLRP1B form inflammasomes through indirect pathogen recognition by acting as a decoy for pathogen targets during infection (Sandstrom et al., 2019). Activation of cytokines has local and systemic effects.

The N-degron pathway has been shown to have roles in the regulation of inflammation through moderating inflammasome assembly. Anthrax lethal factor (LF) from the bacterium *Bacillus anthracis* activates the NLRP1B inflammasome through a proteasome-dependent mechanism. Addition of LF results in targeting of NLRP1B for degradation. This releases a pro-inflammatory C-terminal fragment which self-assembles and leads to formation of the NLRP1B inflammasome with active caspase 1 (Chui et al., 2019; Sandstrom et al., 2019; Xu et al., 2019). The N-degron pathway was shown to be involved in this mechanism. Indeed, LF acts as a protease which cleaves a short N-terminal fragment of NLRP1B and exposes a N-terminal leucine, a primary destabilising residue. Subsequent proteasomal degradation of NLRP1B through the N-degron pathway removes the inhibitory N-terminal domain and liberates a C-terminal fragment which combines to form the inflammasome. This results in activation of caspase 1 and subsequent inflammatory responses through activation of pro-inflammatory cytokines and pyroptotic cell death in macrophage (Chui et al., 2019; Sandstrom et al., 2019; Xu et al., 2019).

Macrophage migration into and accumulation within tissues is important for inflammation. Notably, ATE1 mediated arginylation of ß-actin is important for proper cell migration, as arginylated ß-actin has been found to predominantly be located to the leading edge of migrating cells (Pavlyk et al., 2018). Specifically, ATE1 KO MEFs, which lack arginylation, exhibit ß-actin aggregates and a range of phenotypes such as smaller cells that spread less, move more slowly, and do not produce proper lamellae – cell protrusions which are formed at the cell edge and drive migration. Addition of antibodies targeting ATE1 in wild type cells confirmed the importance of arginylation in the migration speed and distance. While arginylation of unknown proteins which interact and regulate actin may account for some of these phenotypes, direct arginylation of ß-actin was needed for lamellae formation and proper actin polymerization, as expression of ß-actin that was permanently arginylated in ATE1 KO cells was shown to rescue these phenotypes (Karakozova et al., 2006; Pavlyk et al., 2018). These observations could be relevant to macrophage function but has not been explored so far.

Resolution of inflammation by macrophages involves the inhibition of the activated pro-inflammatory cytokines, secretion of anti-inflammatory cytokines, mainly IL-10, IL-13 and transforming growth factor beta (TGFß), and promotion of wound healing. This requires removal and recycling of cellular debris and of apoptotic cells, as well as remodelling and renewal of the injured tissue (Kim and Nair, 2019). In addition to having roles in the induction of inflammation, the N-degron pathway functions in the sequestration of the inflammatory response through regulating inflammatory caspase activity and stability (Leboeuf et al., 2020a). Inhibition of the N-degron pathway through knock down (KD) of the UBR E3 ubiquitin ligases (UBR1, UBR2, UBR4 and UBR5) resulted in increased inflammatory responses denoted by higher levels of cleaved IL-1ß in the presence, but not absence, of LPS. It was also shown that pro-inflammatory fragments such as those resulting from the cleavage of human but not mouse caspase 1 (resulting in a fragment with N-terminal asparagine) and of granzyme A (which exposed N-terminal isoleucine) were substrates of the N-degron pathway. The exposed N-degrons in the pro-inflammatory peptides were largely conserved across vertebrae, highlighting the importance of these destabilising residues (Leboeuf et al., 2020a).

Macrophages play roles in angiogenesis in part though the generation of VEGF in response to LPS (Ramanathan et al., 2007). In ATE1 KO mice, defects in heart development and angiogenesis are quite prevalent with ATE1 KOs being paler with thinner blood vessels and having frequent haemorrhages and edemas, as well as angiogenic remodelling issues (Kwon et al., 2002). This is

in part attributed to ATE1-mediated degradation of RGS4 and RGS5 through the N-degron pathway. These proteins act as negative regulators of specific G-proteins (Gq and Gi), which are involved in angiogenesis and heart development. Accumulation of these RGS substrates in ATE1 KO mice may contribute to the perturbed cardiac growth, blood vessel defects and remodelling in mouse embryos (Lee et al., 2005; Jin et al., 2009). On the other hand, another N-degron pathway substrate, IL-32, promotes angiogenesis through increasing levels of pro-angiogenic factors such as IL-8, u-plasminogen factor and MATRIX METALLOPEPTIDASE 9 (MMP9) (Nold-Petry et al., 2014).

In summary, murine ATE1 appears to regulate the stability and activity of diverse substrates that control a range of cellular processes that are relevant to macrophage function. However, the role of ATE1 in innate immunity has not been addressed specifically.

5.1.2. The CRISPR/Cas gene editing technology

5.1.2.1. CRISPR/Cas acts as a prokaryotic immune system

CRISPR/Cas were originally reported as prokaryotic nucleotide-based defence mechanisms that confer resistance against foreign DNA in particular that from viruses and conjugative plasmids (Barrangou et al., 2007; Jiang and Doudna, 2017; Mojica et al., 2005). For example, screening for CRISPR sequences in *E. coli* found four CRISPR sequences, with two resembling sequences from plasmids (*RESD* involved in plasmid replication and *TRAI* involved in plasmid transfer), and two other sequences originating from viruses, including the DNA methylase, *DARB*. Bacteria containing CRISPR spacers with similarity to certain plasmids or bacteriophage prevent replication or integration of the plasmid or virus within that cell (Mojica et al., 2005). There are six known CRISPR/Cas systems, of which the type II involves Cas9, a DNA endonuclease, which is guided by a CRISPR RNA (crRNA) and trans-activating crRNA (tracrRNA) to bind and cleave specific sequences, directly upstream of a non-self motif known as a protospacer adjacent motif (PAM) sequence, which for *Streptococcus pyogenes* (*S. pyogenes*) is denoted by a 5'-NGG-3' sequence (Figure 5.1A) (Jiang and Doudna, 2017; Jinek et al., 2012).

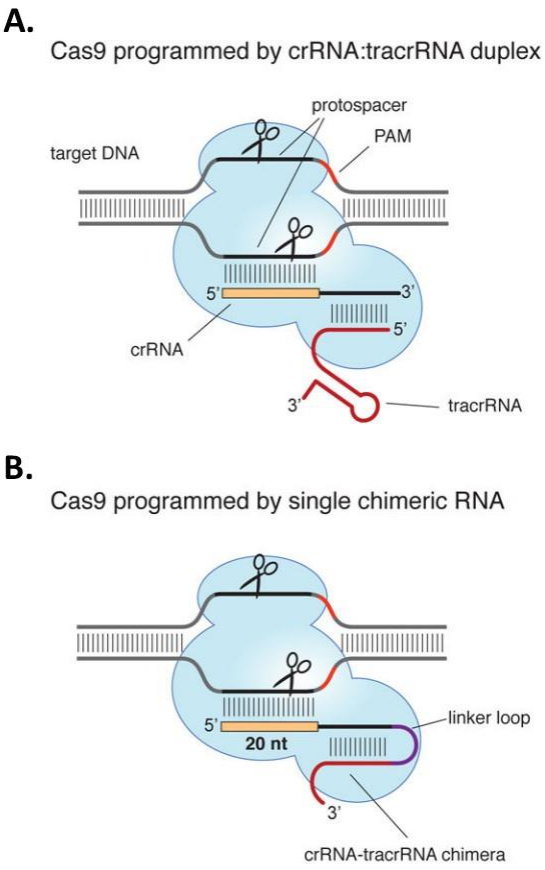

Figure 5.1. The CRISPR/Cas9 system. A. Targeting of Cas9 to target sequence via two RNAs (crRNA and tracrRNA) in prokaryotic immune system. **B.** Application of CRISPR/Cas9 system for genome editing using a single chimeric RNA (gRNA) with properties of both crRNA and tracrRNA. Figure taken from (Jinek et al., 2012).

5.1.2.2. Use of the CRISPR/Cas system as a gene editing technology

Studies in bacteria facilitated the development of the CRISPR/Cas system for genome editing, which led to the 2020 Nobel Prize being awarded to Jennifer Doudna and Emmanuelle Charpentier. This genome editing technology is now widely used in both animals and plants (Tavakoli et al., 2021) and is based on the type II CRISPR/Cas system from *S. pyogenes*. Instead of two RNA molecules acting to bind and guide Cas9 to the target sequence like in *S. pyogenes*, a single guide RNA (gRNA) is used. This gRNA is a chimera of the crRNA and the tracrRNA in that it contains the 20 bp DNA targeting site at its 5' end, a repeat-antirepeat region which forms a hairpin structure and 3' domain that contain other RNA structures which aid with Cas9 recruitment, conformational changes, and activation (Figure 5.1B). This single RNA-guided Cas9 generates double-strand breaks (DSBs) 3 bps upstream of a PAM sequence in the target DNA (Jiang and Doudna, 2017; Jinek et al., 2012). These DSBs are primarily repaired through non-homologous end joining (NHEJ) in an error-prone way which generally results in

insertions/deletions (indels) in the target sequence (Brinkman et al., 2018; Jiang and Doudna, 2017). This RNA-mediated DSB formation is appealing compared to the previous protein-based methods. These previous methods using meganucleases, zinc-finger nucleases, and transcription activator-like effector nucleases have been useful and reliable in generating targeted genome editing in the past but have been difficult to clone or have had context specific uses. The CRISPR-Cas system provides a cheap, easy and accessible method of reverse genetic screening with the caveat that there is some risk of off-target effects (Jiang and Doudna, 2017).

A few studies have successfully used the CRISPR/Cas9 gene editing technology to generate ATE1 KO cell lines. These include ablation of ATE1 from mouse neuroblastoma cells (N2a) (Kasu et al., 2018), human neuroblastoma cells (SH-SY5Y) (Masson et al., 2019), human embryonic kidney cells (HEK293T) (Timms et al., 2019), and C3H mouse embryo cells (C3H10T1/2) (Singh et al., 2019). As well as using different cell lines, these studies use a variety of techniques to insert the gRNA and CRISPR/Cas9 machinery into these cells including transfection of plasmid containing gRNA and Cas9 sequences, nucleofection of Cas9/gRNA-RNA-ribonucleoprotein complex and lentiviral transduction.

5.1.3. Aims of the work presented in this chapter

Despite evolving convergently, many of the signalling pathways in plant and mammal innate immunity are conserved including recognition of PAMPs/DAMPs by PRRs; MAPK-phosphorylation signalling; ROS and RNS signalling; calcium signalling; and transcriptional changes. The N-degron pathway which forms part of the UPS is highly conserved across kingdoms (Gonda et al., 1989; Graciet et al., 2006; Graciet et al., 2010), and in plants, it has been implicated in defence against pathogens (de Marchi et al., 2016; Gravot et al., 2016; Till et al., 2019; Vicente et al., 2019), while in mammals, the N-degron pathway and arginylation play roles in inflammation and resistance to infection (Chui et al., 2019; Leboeuf et al., 2020a; Leysath et al., 2013; Macedo-da-silva et al., 2023; Schnupf et al., 2007; Wang et al., 2017c; Xu et al., 2019). Despite this knowledge, further studies are needed to elucidate the mechanistic role of the N-degron pathway in innate immunity.

Here, the aims were to (1) generate stable ATE1 KO cells for the murine macrophage cell line, RAW264.7; (2) explore further the role of the N-degron pathway in macrophage response to PAMPs such as LPS; (3) investigate the overlap with hypoxia and NO signalling to compare with

the work done *in planta*. However, due to technical difficulties and time constraints, the work was only able to be attempted once and was not brought to completion. Instead attempts to generate ATE1 KO lines are presented.

5.2. Results

5.2.1. ATE1 is expressed in murine macrophages

To study the role of the N-degron pathway in mammalian innate immunity, it was decided to KO ATE1 in RAW264.7 murine macrophages. The RAW264.7 cell line is a well-established model to study innate immune responses in mammals. As mentioned in the introduction, there is only one gene that codes for arginyl-transferase in mammals and knocking out this gene leads to inhibition of the N-degron pathway (as well as any non-N-degron pathway functions of ATE1, such as internal arginylation). Qie et al. conducted a study comparing transcriptomic and proteomic levels of genes/proteins in different murine macrophage populations (Qie et al., 2022). Analysis of their datasets confirmed that ATE1 was expressed in RAW264.7 cells, as well as in other macrophage groups. In fact, RAW264.7 cells have one of the highest transcript levels of ATE1 and have moderate ATE1 protein levels (Figure 5.2A and 5.2B).

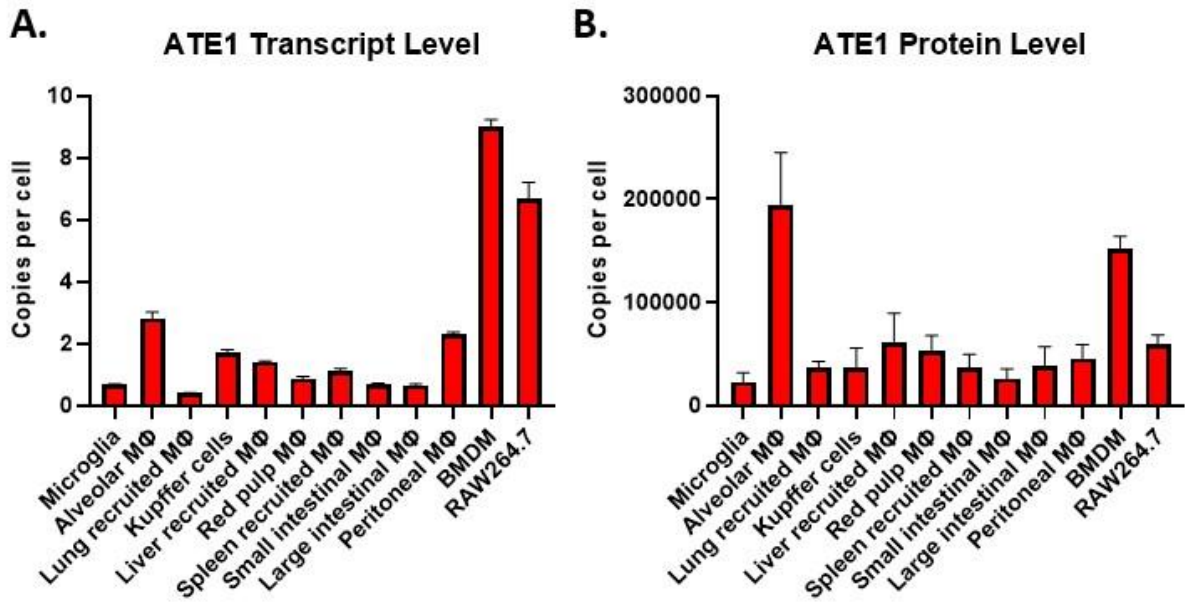

Figure 5.2. ATE1 transcript and protein expression levels in murine macrophage populations. RNA-Seq (**A.**) and mass spectrometry (**B.**) data for mouse ATE1 from transcriptomic and proteomic databases generated by Qie et al., 2022 of 12 different types of murine macrophages (Mϕ): central nervous system

microglia (microglia), primary macrophage populations from lung (alveolar Mϕ; lung recruited Mϕ), liver (Kupffer cells; liver recruited Mϕ), spleen (red pulp Mϕ; spleen recruited Mϕ), intestine (small intestine Mϕ; large intestine Mϕ), and peritoneum (peritoneal Mϕ), bone marrow-derived macrophage (BMDM), and the RAW264.7 macrophage cell line.

5.2.2. Cloning of plasmids for introduction of CRISPR/Cas9 machinery into HEK293T

In Kasu et al., 2018, CRISPR/Cas9-mediated KO of ATE1 in N2a cells was performed to study the role of ATE1 in regulating aggregation of C-terminal fragments of the protein TAR DNA-binding protein 43 (TDP43), which is a hallmark of neurological diseases such as amyotrophic lateral sclerosis (ALS) and frontotemporal lobar dementia (FTLD). The gRNA was designed to target a sequence in exon 2 of the mouse ATE1 (5'-TATCAGGATCTTATAGACCG-3') which is shared across all of the six splice variants of ATE1 (Hu et al., 2006; Kasu et al., 2018) (Figure 5.3) and was cloned into the px330-U6-Chimeric-BB-CHh-hSpCas9 plasmid to allow for transfection into N2a cells. Confirmation of ATE1 KO was conducted via anti-ATE1 immunoblot and an arginylation assay. One of the gRNAs (5'- AGGATCTTATAGACCGAGGA-3') used by Singh et al., 2019 to generate ATE1 KO C3H10T1/2 cells overlaps with this gRNA suggesting that this is a good target sequence to generate ATE1 KOs. Hence, the gRNA designed and utilised in Kasu et al., 2018 was also used for this study. Using the CHOPCHOP tool (Labun et al., 2016; Labun et al., 2019; Montague et al., 2014), it was predicted that the gRNA had good efficiency of 64.89% but also had 6 listed potential off-targets which have 3 mismatches compared to the target sequence in ATE1. Two control non-targeting gRNAs (non-targeting controls (NTCs); noted NTC1 and NTC2) were designed for this study using sequences from the database (Sanjana et al., 2014; addgene.org/pooled-library/zhang-mouse-gecko-v2/), which were predicted not to bind to the mouse genome (experimental strategy based on Giuliano et al., 2019).

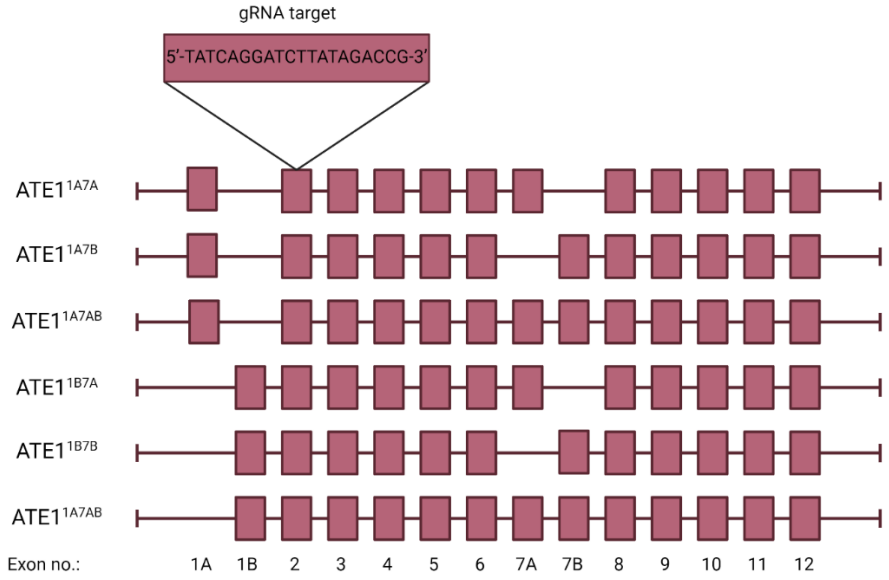

Figure 5.3. Mouse ATE1 isoforms and sequence targeted by gRNA/Cas9. The six splice variants (Hu et al., 2006) are presented with the target sequence in ATE1 exon 2. Created using BioRender.com.

The method chosen to deliver the CRISPR/Cas9 constructs into the RAW264.7 macrophages was through the use of lentiviruses, which are retroviruses that have widespread applications in research and biomedical applications as a mode of gene delivery in mammalian cells. Lentiviral transduction was favoured over transfection as the method is quick, efficient, and cost-effective in generating stable cell lines (Elegheert et al., 2018). In addition, RAW264.7 macrophages are known to be difficult to transfect with non-viral methods, having low transfection efficiencies and shorter times of transgene expression. This may be due to the innate ability of macrophages to recognize foreign DNA and the high levels of nucleases (Burke et al., 2002).

The ATE1 and control gRNAs were cloned upstream of the gRNA scaffold in the LentiCRISPRv2 (Addgene #52961; http://n2t.net/addgene:52961; RRID:Addgene_52961) plasmid. The LentiCRISPRv2 plasmid also contains Cas9 and a puromycin selection marker (Figure 5.4A). Screening and Sanger sequencing of the plasmids generated was carried out to confirm the presence of the gRNAs in the LentiCRISPRv2 plasmids used before the generation of lentiviral particles (Figure 5.4B).

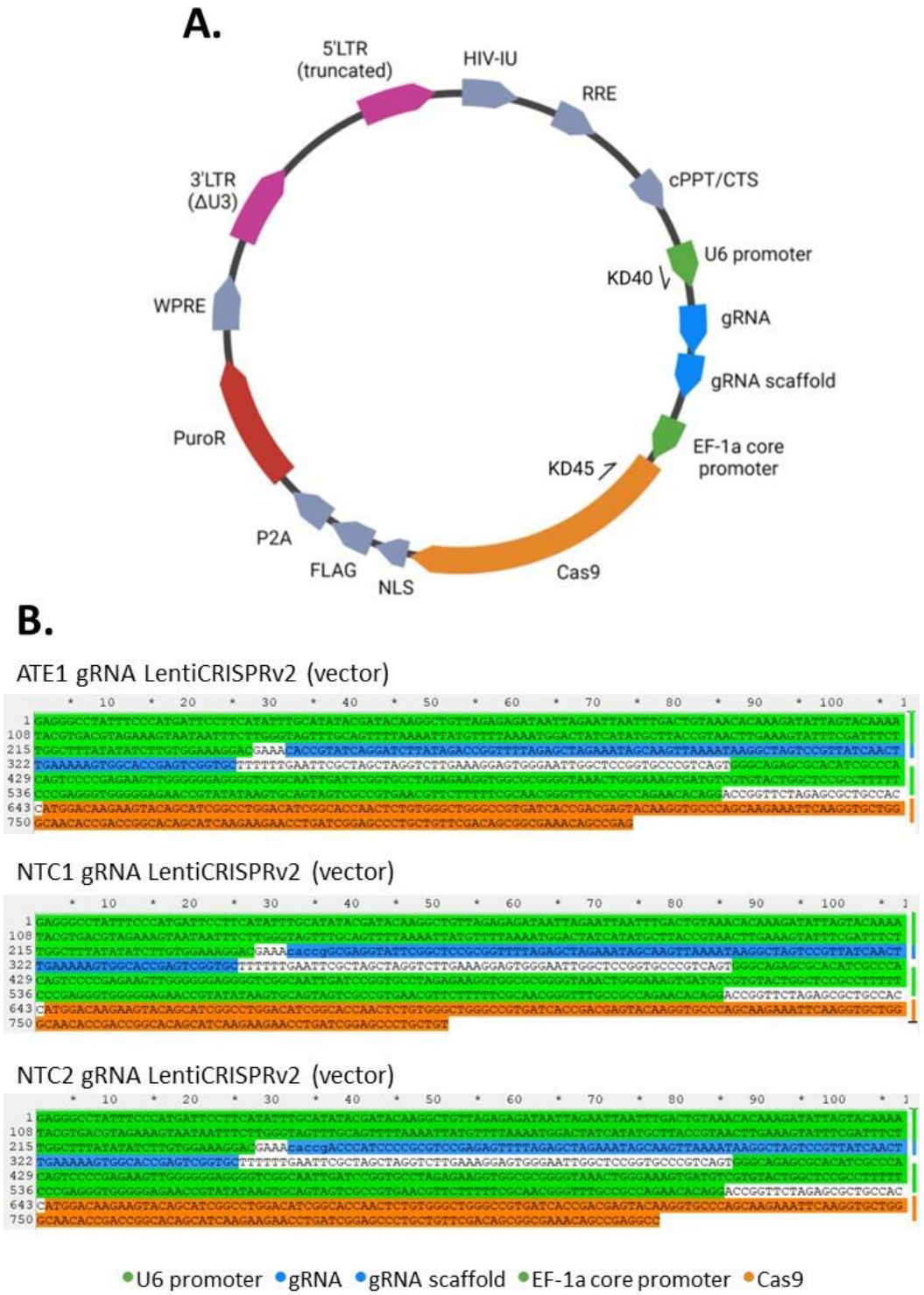

Figure 5.4. Cloning of LentiCRISPRv2 with ATE1 or NTC gRNAs. A. Plasmid map showcasing only the features of LentiCRISPRv2 vector between 5' and 3' LTR. KD40 and KD45 are primers used for sequencing. Created using BioRender.com. **B.** LightRun sequencing results for the LentiCRISPRv2 vectors showing presence of U6 promoter; gRNA target sequence and gRNA scaffold; EF-1α core promoter; and beginning of Cas9 sequence.

5.2.3. Generation of CRISPR/Cas9 containing lentiviral particles and transduction of RAW264.7

To generate the lentiviral particles, HEK293T cells were co-transfected with each of the three LentiCRISPRv2 plasmids with either ATE1 gRNA or the NTC1 and NTC2 gRNAs, together with the plasmid pMD2.G (Addgene plasmid #12259; http://n2t.net/addgene:12259; RRID:Addgene_12259), which contained the genes coding for the viral envelope, and the plasmid psPAX2 (Addgene plasmid #12260; http://n2t.net/addgene:12260; RRID:Addgene_12260) that allows expression of the minimal required genes for packaging and replication of the lentiviral particles (Figure 5.5). After two days, the growth medium containing the lentiviral particles was harvested, HEK293T cells were pelleted, and the viral supernatant was added to 50% confluent RAW264.7 cells. The medium containing the lentiviral particles was diluted 10-fold, 100-fold, 1000-fold and 10,000-fold, and each dilution was used to separately transduce RAW264.7 macrophages. Two wells acted as controls and received no lentiviral particles. After 24 hours of incubation, transduced cells were selected by adding 5 µg/mL puromycin until all cells in the control wells had died. Surviving puromycin-resistant cells from transduced wells were expanded to form a polyclonal pool and stocks were frozen down (Figure 5.5).

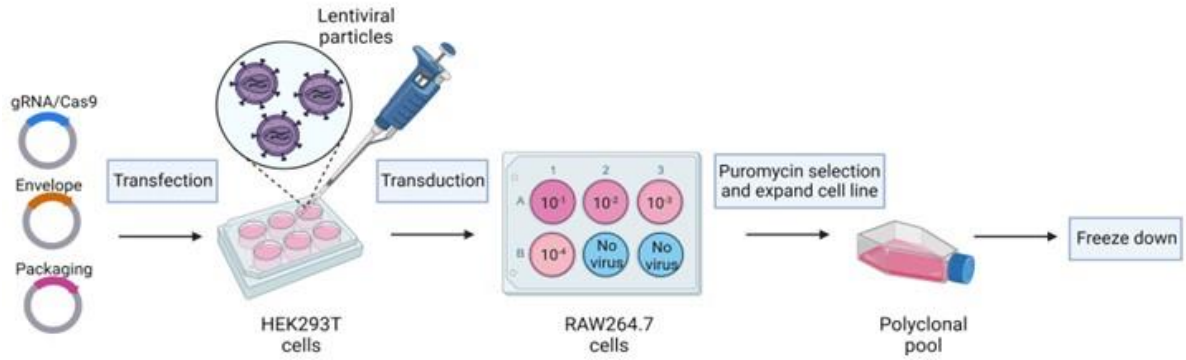

Figure 5.5. Lentiviral transduction and screening of RAW264.7 cells. Graphical overview of the experimental set up and steps for lentiviral transduction for one gRNA. Created using BioRender.com.

5.2.4. CRISPR/Cas mutagenesis of ATE1 was unsuccessful

Successful transduction involves insertion of the region between the 5' and 3' LTRs, shown in Figure 5.4A, into the host cell genome. The presence of puromycin resistant RAW264.7 cells after lentiviral transduction suggests that the procedure was successful. To validate this, genomic DNA (gDNA) was extracted from this pool of cells and PCRs using oligonucleotides (KD40 and KD45) specific to the region of the transgene flanking the gRNA sequence was performed (Figure 5.4.A), followed by Sanger sequencing of the PCR products. This confirmed transgene insertion into the

RAW264.7 macrophage genome. The gRNA and Cas9 sequences were present in the RAW264.7 genome, suggesting stable insertion and efficient transduction for the ATE1 and NTC2 gRNA transgenes (Figure 5.6A and 5.6B). Data could not be obtained with the NTC1 control gRNA because of issues with gDNA extraction for this sample.

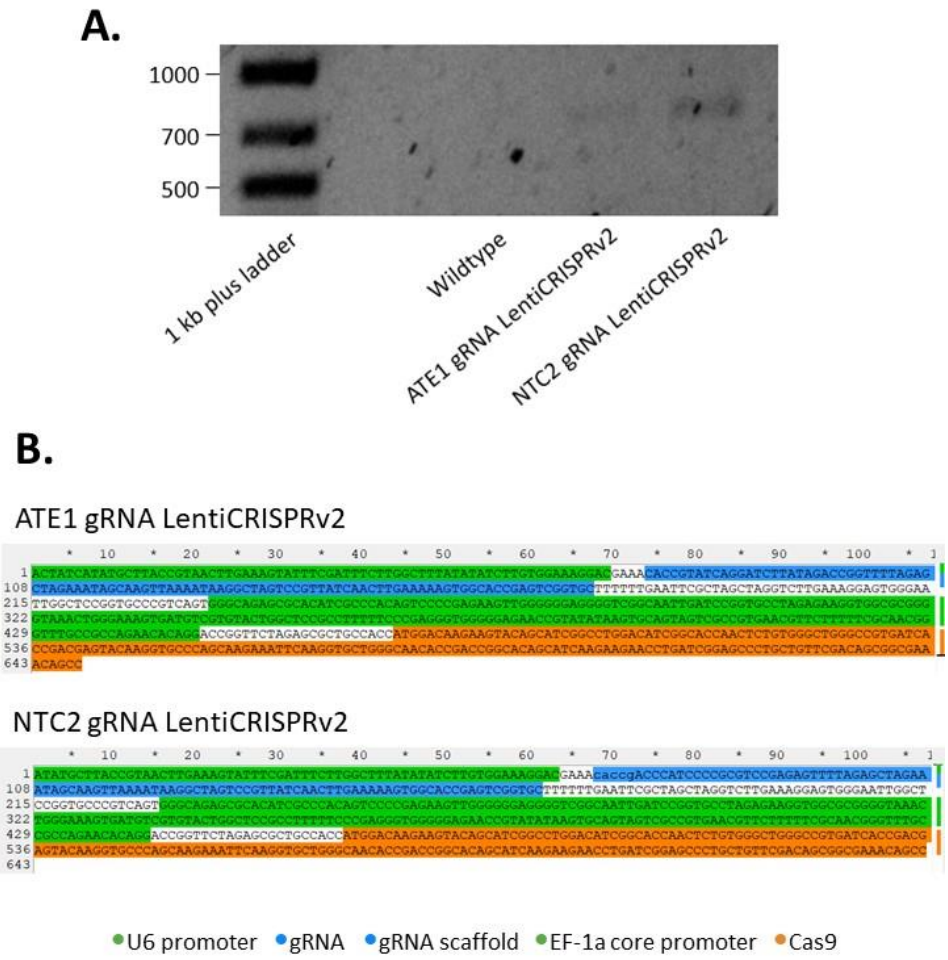

Figure 5.6. Lentiviral transduction and screening of RAW264.7 cells. A. PCR amplifying region flanking gRNA using primers in U6 promoter and Cas9. **B.** LightRun sequencing results for the presence of the gRNA, EF-1α promoter and beginning of Cas9 in the gDNA of transduced RAW264.7 cells.

The ATE1 target region in the transfected cells was then screened for indels using two methods. The first one involved PCR of the target region, Sanger sequencing of the PCR products and analysis using the TIDE (Tracking of Indels by Decomposition) software which compares the CRISPR targeted sequence with the wild type sequence and gives a read out of the efficiency and percentage of insertions or deletions (Brinkman et al., 2014). The TIDE software showed 96.4% of sequences were without indels compared to the wild type (Figure 5.7A). However, 0% aberrant sequences were detected around the expected cut site (denoted by blue dotted line in Figure 5.7A). The only aberrant sequences in the CRISPR/Cas9 targeted sample were detected

100 bp downstream of the predicted cut site, near the end of the PCR fragment where Sanger sequencing becomes unreliable as shown with the high level of aberrant sequences in the control PCR from wild type (non-transduced) RAW 264.7 macrophage genomic DNA (Figure 5.7A). The other method involved performing a PCR on the target region, followed by digestion of the PCR product with T7 endonuclease I, which cleaves heteroduplex DNA resulting from NHEJ repair (Vouillot et al., 2015). Incubation with T7 endonuclease I should yield lower molecular weight bands from cleavage of heteroduplex DNA if mutagenesis has occurred. However, such DNA fragments were absent from the RAW264.7 genomic DNA transduced with the ATE1 gRNA CRISPR-Cas9 construct (Figure 5.7B). These results infer that the CRISPR/Cas9 targeting of ATE1 was likely extremely inefficient (with a reading of 1.6% efficiency according to the TIDE software (Figure 5.6A)), so that it was undetectable in the polyclonal pool of cells or was unsuccessful.

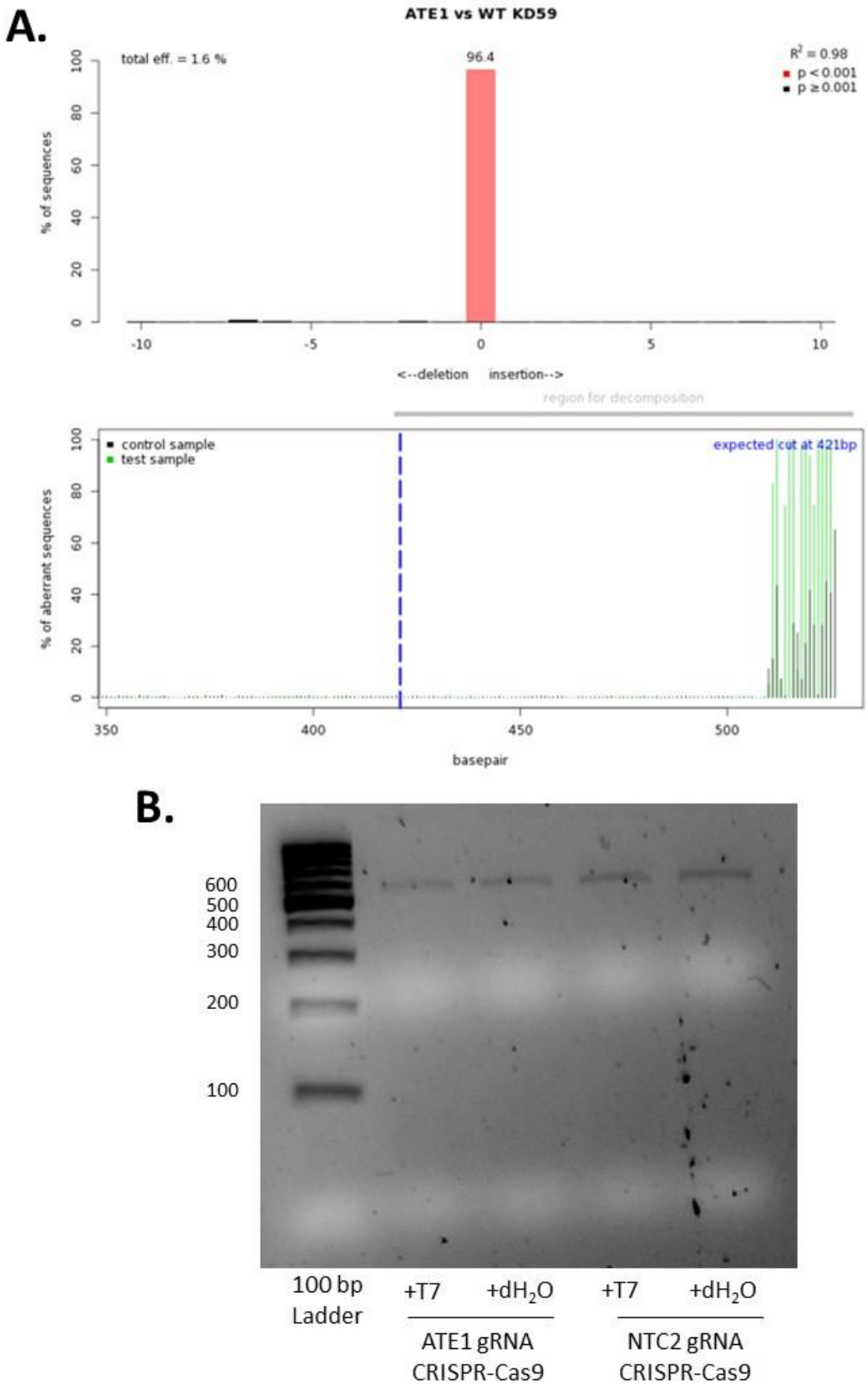

Figure 5.7. Absence of indels in Cas9 targeted region of ATE1. Screening for indels in target region using TIDE analysis (**A.**) and result of T7 endonuclease I assay (**B.**). **A.** The top panel shows the percentage of insertions or deletions in the target region based on a comparison of sequencing files between WT and ATE1 gRNA/Cas9 targeted samples. The bottom panel displays predicted cut site (dotted blue line) and

regions that are different between WT (black) and ATE1 gRNA/Cas9 targeted (green) sequence files. The differences shown here coincide with the end of the PCR template where sequencing accuracy can be impacted. **B.** A ~550 bp region flanking the Cas9 target site in ATE1 was amplified using PCR for ATE1 gRNA/Cas9 targeted and NTC2 samples. PCR products were reannealed and either T7 endonuclease 1 (+T7) or dH_2O ($+dH_2O$) was added to the samples. After stopping the reaction, samples were run on a 3% agarose gel and were analysed for the presence of lower molecular weight bands in the ATE1 gRNA/Cas9 targeted + T7 sample denoting the presence of heteroduplex DNA/mutations. No lower molecular weight bands were seen for any of the samples.

5.3. Discussion

Lentiviral transduction of CRISPR/Cas9 constructs into RAW264.7 macrophages was carried out, followed by selection of puromycin resistant macrophages. Verification that these puromycin-resistant cells carried the gRNA and Cas9 transgenes inserted into the RAW264.7 genome (Figure 5.6A and 5.6B) suggests that the transduction worked efficiently. However, screening of polyclonal cultures of puromycin resistant cells using TIDE and the T7 endonuclease I assays suggest that genome editing did not occur in exon 2 of ATE1 (Figure 5.7A and 5.7B). One explanation for the absence of mutations in the target region is that Cas9 was not present or was expressed at levels that were too low. While genomic DNA isolation and PCR allowed for confirmation of the presence of Cas9 in polyclonal pool (Figure 5.6A), the expression of this gene was not confirmed using RNA extraction and RT-qPCR. However, Cas9 and the puromycin resistance gene were under the control of the same promoter. Hence, considering that the cells were puromycin resistant, this would suggest that Cas9 should also be expressed. Another possible explanation for the absence of indels is that the gRNA was inefficient at targeting the ATE1 region in the RAW264.7 cell line, despite the fact that this gRNA had been used previously to generate ATE1 KO N2a cells (Kasu et al., 2018) with good efficiency. Indeed, multiple experimental factors can influence gRNA targeting efficiencies including its use in different cell lines (Zhong et al., 2023). If the generation of ATE1 KO RAW264.7 cells was to be attempted again, multiple ATE1-specific gRNAs with different target sites in ATE1 should be designed and used in parallel.

However, caution should be taken as no mutagenesis in the targeted region can also suggest that the KO of this gene is lethal to the cell line. While, the generation of ATE1 KO cell lines have been shown to be possible for immortalized MEFs, N2as, SH-SY5Y, HEK293T and C3H10T1/2 cells, as well as ATE1 KD using siRNA-ATE1 in human lung adenocarcinoma cell (Calu-3) (Kasu et al., 2018;

Kwon et al., 2002; Macedo-da-Silva et al., 2023; Masson et al., 2019; Singh et al., 2019; Timms et al., 2019), ATE1 KO mice are embryonic lethal (Kwon et al., 2002). The N-degron pathway functions in proliferation and some studies have suggested that rapidly proliferating cell lines are more sensitive to N-degron pathway mutations (Brower and Varshavsky, 2009; Leboeuf et al., 2020b; Leu et al., 2009). RAW264.7 macrophage cells have fast doubling times and so this may also potentially explain why these cells are more sensitive to ATE1 KO compared to other cell lines. Furthermore, ATE1 was expressed in all murine macrophage cell populations with ATE1 gene expression in RAW264.7 being one of the highest (Qie et al., 2022), suggesting that arginylation and the N-degron pathway may contribute to key processes in these cells. At the same time, ATE1 protein levels in RAW264.7 cells were only moderate with alveolar macrophages having the highest ATE1 levels compared to the other macrophages tested. This suggests that there may be a potential post-transcriptional or post-translational mechanism regulating ATE1 levels in RAW264.7. This is of interest, as regulation of ATE1 abundance and activity is still not well known in eukaryotes in general. The findings in alveolar macrophages may also suggest a potential role for ATE1 in oxygen sensing in these lung-residing macrophages.

Of note, HIF1ß, also known as ARNT, is up-regulated in the RAW264.7 cell line compared with other macrophage populations and this transcription factor is considered to be a cell-type maintenance transcription factor or one which maintains the identity of the different populations (Qie et al., 2022). HIF1ß's role in hypoxia is well known as it works alongside HIF1α to initiate the hypoxia response upon low oxygen conditions (Rosell-Garcia et al., 2023; Semenza, 2007). VHL, the original E3 ubiquitin ligase known to degrade HIF1α under normoxic conditions, is also highly expressed in RAW264.7 cells. A recent study found a direct link between the N-degron pathway and the main HIF1-dependent hypoxia response pathway, with the N-degron pathway targeting HIF1α for degradation (Moorthy et al., 2022). ATE1 KO MEFs exhibit the Warburg effect with increased glycolysis under aerobic conditions (Moorthy et al., 2022). So, another possibility may be that this type of macrophage may be sensitive to ATE1 KO through activation of constitutive hypoxia response and changes in metabolism.

With the risk of lethality with ATE1 KO macrophages, other possibilities to study the N-degron pathway include KD/KO of the UBR domain E3 ubiquitin ligases. Previous studies have generated individual and double KO mutants of the N-recognins, Ubr2 and Ubr4, in RAW264.7 macrophages (Chui et al., 2019) and KD of all four N-recognins in J774A.1 macrophages (Leboeuf et al., 2020a). The KD and KO of the E3 ubiquitin ligases was tolerated in these studies. This may be due to

there being four N-recognins providing some level of redundancy and the KD lines do not completely ablate UBR expression. In line with this, a study attempting to KO UBR1, UBR2 and UBR4 was unable to isolate the triple KO (Timms et al., 2019). Another way to test the role of the N-degron pathway in immunity may be through targeting a more specific N-degron component, such as the oxygen-dependent ADO. ADO KO in SH-SY5Y and human colon cell line (RKO) was tolerated and was successfully used to uncover ADO's role in the N-degron pathway and its involvement in the oxidation of N-terminal cysteine residues which allows their recognition by ATE1 (Masson et al., 2019). ADO KO may allow the study of the role of particular substrates, as well as oxygen and NO dependent functions of the N-degron pathway in immunity rather than removing the N-degron pathway-dependent and -independent functions associated with arginylation. Options to study ATE1 function include inducible ATE1 KOs/KDs like siRNA for ATE1, or chemical inhibitors of ATE1 (Macedo-da-Silva et al., 2023; Saha et al., 2012). Unfortunately, due to time constraints, these alternative approaches could not be used to complete the work.

Had the CRISPR/Cas9-mediated KO of ATE1 been a success, the experimental plan included a careful characterization of the ATE1 KO RAW264.7 cells including appearance and growth of the cells, as well as a characterization of their ability to migrate and phagocytose. I also would have conducted some immunoassays using LPS treatments examining the induction of key immune response gene expression through RT-qPCRs, investigating ROS/RNS generation and MAPK signalling, and testing for the production of pro- or anti-inflammatory cytokines using ELISAs to examine the role of the N-degron pathway in these immune functions. I would then have attempted similar experiments to those conducted *in planta* (Chapter 3) with individual or combined hypoxia and LPS treatments. Using the immunoassays listed above, I would have investigated the effect of hypoxia on mammalian innate immune responses and whether the N-degron pathway plays a role.

Chapter 6: Conclusions

Plants experience a multitude of environmental factors which have the ability to affect their growth and capacity to thrive. These environmental factors can also impact their susceptibility to biotic stresses. To address the current gap of knowledge in plant responses to multiple stresses and combinations of biotic and abiotic stresses, this Ph.D. work sought out to explore the crosstalk between hypoxia and immune responses in plants through the study of plant transcriptional and physiological responses to individual and combined treatments with hypoxia and flg22 and uncover the potential role of the N-degron pathway in its regulation by comparing wild type, N-degron and NO mutants.

A major finding of this work was that the combined treatment induced responses that differed from either of the individual stresses, similar to previous reports looking into multi-stress responses (Pandey et al., 2015; Prasch and Sonnewald, 2013; Rasmussen et al., 2013; Rizhsky et al., 2004; Shaar-Moshe et al., 2017; Zandalinas et al., 2020; Zandalinas et al., 2021), suggesting that plants respond in novel ways to simultaneous treatment with multiple stresses. One unique response was that hypoxia appeared to suppress flg22-induced responses at the transcriptional level. This was also shown at the signalling and physiological level with flg22-dependent MAPK-signalling and callose deposition also being dampened by hypoxia. The N-degron pathway and NO signalling while important in flg22 responses, do not appear to play a major role in regulating the hypoxia-induced dampening of immune responses.

On the other hand, another novel response to combined hypoxia and flg22 treatment was the induction of the major JA signalling regulators: MYC2, JAZ3, and JAZ8 as well as downstream JA signalling genes. JA's known role in mediating developmental and (a)biotic stress responses and regulating growth-defence trade-offs highlighted the phytohormone as a potential regulator for multi-stress responses. Further, a previous study (de Marchi et al., 2016) showed a link between the N-degron pathway and JA signalling. It was therefore aimed to uncover the regulatory role of the N-degron pathway in JA signalling and explore JA's role in hypoxia. It was found that JA signalling is directly and indirectly regulated by the N-degron pathway with ATE1 directly binding and destabilizing JAZ8 and N-degron pathway substrates, ERFVII transcription factors, regulating JAZ8 gene expression. JAZ8 protein levels were also impacted under short treatments with hypoxia however the role of JAZ8 in hypoxia responses and tolerance requires further study as well as validation of PPI and genetic interactions between JAZ8 and ATE1 and whether degradation does indeed occur through N-degron pathway or through another mechanism.

Attempts at similar studies in mammals was impeded by issues with the isolation of ATE1 KO RAW264.7 cells.

As well as the planned experiments to further validate the interactions between ATE1 and JAZ8 and investigate the potential role of JAZ8 (and other JAZ proteins) in hypoxia tolerance, further dissection of the HF novel responses may provide targets for improved tolerance to both hypoxic and immunogenic stresses. As well, mechanisms underlying the role of the N-degron pathway and NO signalling in key immune responses e.g. callose deposition need resolving.

Chapter 7: References

Abbas, M., Berckhan, S., Rooney, D.J., Gibbs, D.J., Conde, J.V., Correia, C.S., Bassel, G.W., Marín-de la Rosa, N., Leon, J., Alabadí, D. and Blazquez, M.A., 2015. Oxygen sensing coordinates photomorphogenesis to facilitate seedling survival. *Current Biology*, *25*(11), pp.1483-1488.

Abu-Soud, H.M., Ichimori, K., Nakazawa, H. and Stuehr, D.J., 2001. Regulation of inducible nitric oxide synthase by self-generated NO. *Biochemistry*, *40*(23), pp.6876-6881.

Adams, E.H. and Spoel, S.H., 2018. The ubiquitin–proteasome system as a transcriptional regulator of plant immunity. *Journal of experimental botany*, *69*(19), pp.4529-4537.

Agani, F.H., Puchowicz, M., Chavez, J.C., Pichiule, P. and LaManna, J., 2002. Role of nitric oxide in the regulation of HIF-1α expression during hypoxia. *American Journal of Physiology-Cell Physiology*, *283*(1), pp.C178-C186.

Albig, A.R. and Schiemann, W.P., 2005. Identification and characterization of regulator of G protein signaling 4 (RGS4) as a novel inhibitor of tubulogenesis: RGS4 inhibits mitogen-activated protein kinases and vascular endothelial growth factor signaling. *Molecular biology of the cell*, *16*(2), pp.609-625.

Albrecht, G. and Mustroph, A., 2003. Sucrose utilization via invertase and sucrose synthase with respect to accumulation of cellulose and callose synthesis in wheat roots under oxygen deficiency. *Russian Journal of Plant Physiology*, *50*, pp.813-820.

Allegre, A., Silvestre, J., Morard, P., Kallerhoff, J. and Pinelli, E., 2004. Nitrate reductase regulation in tomato roots by exogenous nitrate: a possible role in tolerance to long-term root anoxia. *Journal of Experimental Botany*, *55*(408), pp.2625-2634.

Al-Saharin, R., Hellmann, H. and Mooney, S., 2022. Plant E3 ligases and their role in abiotic stress response. *Cells*, *11*(5), p.890.

Anand, R.J., Gribar, S.C., Li, J., Kohler, J.W., Branca, M.F., Dubowski, T., Sodhi, C.P. and Hackam, D.J., 2007. Hypoxia causes an increase in phagocytosis by macrophages in a HIF-1α-dependent manner. *Journal of Leucocyte Biology*, *82*(5), pp.1257-1265.

Anderson, R., Bayer, P.E. and Edwards, D., 2020. Climate change and the need for agricultural adaptation. *Current opinion in plant biology*, *56*, pp.197-202.

Arango Duque, G. and Descoteaux, A., 2014. Macrophage cytokines: involvement in immunity and infectious diseases. *Frontiers in immunology*, *5*, p.491.

Arbona, V. and Gómez-Cadenas, A., 2008. Hormonal modulation of citrus responses to flooding. *Journal of Plant Growth Regulation*, *27*, pp.241-250.

Arganda-Carreras, I., Kaynig, V., Rueden, C., Eliceiri, K.W., Schindelin, J., Cardona, A. and Sebastian Seung, H., 2017. Trainable Weka Segmentation: a machine learning tool for microscopy pixel classification. *Bioinformatics*, *33*(15), pp.2424-2426.

Astier, J. and Lindermayr, C., 2012. Nitric oxide-dependent posttranslational modification in plants: an update. *International journal of molecular sciences*, *13*(11), pp.15193-15208.

Astier, J., Gross, I. and Durner, J., 2018. Nitric oxide production in plants: an update. *Journal of Experimental Botany*, *69*(14), pp.3401-3411.

Atkinson, N.J. and Urwin, P.E., 2012. The interaction of plant biotic and abiotic stresses: from genes to the field. *Journal of experimental botany*, *63*(10), pp.3523-3543.

Ausubel, F.M., 2005. Are innate immune signaling pathways in plants and animals conserved?. *Nature immunology*, *6*(10), pp.973-979.

Bachmair, A., Becker, F. and Schell, J., 1993. Use of a reporter transgene to generate arabidopsis mutants in ubiquitin-dependent protein degradation. *Proceedings of the National Academy of Sciences*, *90*(2), pp.418-421.

Bachmair, A., Finley, D. and Varshavsky, A., 1986. In vivo half-life of a protein is a function of its amino-terminal residue. *science*, *234*(4773), pp.179-186.

Bailey-Serres, J., Fukao, T., Gibbs, D.J., Holdsworth, M.J., Lee, S.C., Licausi, F., Perata, P., Voesenek, L.A. and van Dongen, J.T., 2012. Making sense of low oxygen sensing. *Trends in plant science*, *17*(3), pp.129-138.

Barrangou, R., Fremaux, C., Deveau, H., Richards, M., Boyaval, P., Moineau, S., Romero, D.A. and Horvath, P., 2007. CRISPR provides acquired resistance against viruses in prokaryotes. *Science*, *315*(5819), pp.1709-1712.

Bebber, D.P., Ramotowski, M.A. and Gurr, S.J., 2013. Crop pests and pathogens move polewards in a warming world. *Nature climate change*, *3*(11), pp.985-988.

Bednarek, P., Pislewska-Bednarek, M., Svatoš, A., Schneider, B., Doubský, J., Mansurova, M., Humphry, M., Consonni, C., Panstruga, R., Sanchez-Vallet, A. and Molina, A., 2009. A glucosinolate metabolism pathway in living plant cells mediates broad-spectrum antifungal defense. *Science*, *323*(5910), pp.101-106.

Benhar, M., 2015. Nitric oxide and the thioredoxin system: a complex interplay in redox regulation. *Biochimica et Biophysica Acta (BBA)-General Subjects*, *1850*(12), pp.2476-2484.

Benhar, M., Forrester, M.T. and Stamler, J.S., 2009. Protein denitrosylation: enzymatic mechanisms and cellular functions. *Nature reviews Molecular cell biology*, *10*(10), pp.721-732.

Ben-Lulu, S., Ziv, T., Admon, A., Weisman-Shomer, P. and Benhar, M., 2014. A substrate trapping approach identifies proteins regulated by reversible S-nitrosylation. *Molecular & cellular proteomics*, *13*(10), pp.2573-2583.

Benn, G., Wang, C.Q., Hicks, D.R., Stein, J., Guthrie, C. and Dehesh, K., 2014. A key general stress response motif is regulated non-uniformly by CAMTA transcription factors. *The Plant Journal*, *80*(1), pp.82-92.

Berezovsky, I.N., Kilosanidze, G.T., Tumanyan, V.G. and Kisselev, L.L., 1999. Amino acid composition of protein termini are biased in different manners. *Protein engineering*, *12*(1), pp.23-30.

Bi, G., Zhou, Z., Wang, W., Li, L., Rao, S., Wu, Y., Zhang, X., Menke, F.L., Chen, S. and Zhou, J.M., 2018. Receptor-like cytoplasmic kinases directly link diverse pattern recognition receptors to

the activation of mitogen-activated protein kinase cascades in Arabidopsis. *The Plant Cell*, *30*(7), pp.1543-1561.

Bjornson, M., Benn, G., Song, X., Comai, L., Franz, A.K., Dandekar, A.M., Drakakaki, G. and Dehesh, K., 2014. Distinct roles for mitogen-activated protein kinase signaling and CALMODULIN-BINDING TRANSCRIPTIONAL ACTIVATOR3 in regulating the peak time and amplitude of the plant general stress response. *Plant physiology*, *166*(2), pp.988-996.

Bjornson, M., Pimprikar, P., Nürnberger, T. and Zipfel, C., 2021. The transcriptional landscape of Arabidopsis thaliana pattern-triggered immunity. Nature plants, 7(5), pp.579-586.

Bleau, J.R. and Spoel, S.H., 2021. Selective redox signaling shapes plant–pathogen interactions. *Plant physiology*, *186*(1), pp.53-65.

Bogdan, C., 2001. Nitric oxide and the regulation of gene expression. *Trends in cell biology*, *11*(2), pp.66-75.

Bogdan, C., 2015. Nitric oxide synthase in innate and adaptive immunity: an update. *Trends in immunology*, *36*(3), pp.161-178.

Bogdan, C., Röllinghoff, M. and Diefenbach, A., 2000. The role of nitric oxide in innate immunity. *Immunological reviews*, *173*, pp.17-26.

Bolt, S., Zuther, E., Zintl, S., Hincha, D.K. and Schmülling, T., 2017. ERF105 is a transcription factor gene of Arabidopsis thaliana required for freezing tolerance and cold acclimation. *Plant, cell & environment*, *40*(1), pp.108-120.

Borrowman, S., Kapuganti, J.G. and Loake, G.J., 2023. Expanding roles for S-nitrosylation in the regulation of plant immunity. *Free Radical Biology and Medicine*, *194*, pp.357-368.

Brinkman, E.K., Chen, T., Amendola, M. and Van Steensel, B., 2014. Easy quantitative assessment of genome editing by sequence trace decomposition. *Nucleic acids research*, *42*(22), pp.e168-e168.

Brinkman, E.K., Chen, T., de Haas, M., Holland, H.A., Akhtar, W. and van Steensel, B., 2018. Kinetics and fidelity of the repair of Cas9-induced double-strand DNA breaks. *Molecular cell*, *70*(5), pp.801-813.

Brower, C.S. and Varshavsky, A., 2009. Ablation of arginylation in the mouse N-end rule pathway: loss of fat, higher metabolic rate, damaged spermatogenesis, and neurological perturbations. *PloS one*, *4*(11), p.e7757.

Brüne, B., von Knethen, A. and Sandau, K.B., 2001. Transcription factors p53 and HIF-1α as targets of nitric oxide. *Cellular signalling*, *13*(8), pp.525-533.

Bui, L.T., Shukla, V., Giorgi, F.M., Trivellini, A., Perata, P., Licausi, F. and Giuntoli, B., 2020. Differential submergence tolerance between juvenile and adult Arabidopsis plants involves the ANAC017 transcription factor. *The Plant Journal*, *104*(4), pp.979-994.

Burdon, J.J. and Zhan, J., 2020. Climate change and disease in plant communities. *PLoS biology*, *18*(11), p.e3000949.

Burke, B., Sumner, S., Maitland, N. and Lewis, C.E., 2002. Macrophages in gene therapy: cellular delivery vehicles and in vivo targets. *Journal of leukocyte biology*, *72*(3), pp.417-428.

Callis, J., 2014. The ubiquitination machinery of the ubiquitin system. *The Arabidopsis Book/American Society of Plant Biologists*, *12*.

Carpio, M.A., López Sambrooks, C., Durand, E.S. and Hallak, M.E., 2010. The arginylation-dependent association of calreticulin with stress granules is regulated by calcium. *Biochemical Journal*, *429*(1), pp.63-72.

Castello, P.R., David, P.S., McClure, T., Crook, Z. and Poyton, R.O., 2006. Mitochondrial cytochrome oxidase produces nitric oxide under hypoxic conditions: implications for oxygen sensing and hypoxic signaling in eukaryotes. *Cell metabolism*, *3*(4), pp.277-287.

Castro, B., Citterico, M., Kimura, S., Stevens, D.M., Wrzaczek, M. and Coaker, G., 2021. Stress-induced reactive oxygen species compartmentalization, perception and signalling. *Nature plants*, *7*(4), pp.403-412.

Causier, B., Ashworth, M., Guo, W. and Davies, B., 2012. The TOPLESS interactome: a framework for gene repression in Arabidopsis. *Plant physiology*, *158*(1), pp.423-438.

Chamizo-Ampudia, A., Sanz-Luque, E., Llamas, A., Galvan, A. and Fernandez, E., 2017. Nitrate reductase regulates plant nitric oxide homeostasis. *Trends in Plant Science*, *22*(2), pp.163-174.

Chen, L., Zhang, L., Xiang, S., Chen, Y., Zhang, H. and Yu, D., 2021. The transcription factor WRKY75 positively regulates jasmonate-mediated plant defense to necrotrophic fungal pathogens. *Journal of Experimental Botany*, *72*(4), pp.1473-1489.

Chen, S.C., Huang, B., Liu, Y.C., Shyu, K.G., Lin, P.Y. and Wang, D.L., 2008. Acute hypoxia enhances proteins' S-nitrosylation in endothelial cells. *Biochemical and biophysical research communications*, *377*(4), pp.1274-1278.

Chen, S.J., Wu, X., Wadas, B., Oh, J.H. and Varshavsky, A., 2017. An N-end rule pathway that recognizes proline and destroys gluconeogenic enzymes. *Science*, *355*(6323), p.eaal3655.

Chico, J.M., Fernández-Barbero, G., Chini, A., Fernández-Calvo, P., Díez-Díaz, M. and Solano, R., 2014. Repression of jasmonate-dependent defenses by shade involves differential regulation of protein stability of MYC transcription factors and their JAZ repressors in Arabidopsis. *The Plant Cell*, *26*(5), pp.1967-1980.

Chico, J.M., Lechner, E., Fernandez-Barbero, G., Canibano, E., García-Casado, G., Franco-Zorrilla, J.M., Hammann, P., Zamarreño, A.M., García-Mina, J.M., Rubio, V. and Genschik, P., 2020. CUL3BPM E3 ubiquitin ligases regulate MYC2, MYC3, and MYC4 stability and JA responses. *Proceedings of the National Academy of Sciences*, *117*(11), pp.6205-6215.

Chinchilla, D., Bauer, Z., Regenass, M., Boller, T. and Felix, G., 2006. The Arabidopsis receptor kinase FLS2 binds flg22 and determines the specificity of flagellin perception. *The Plant Cell*, *18*(2), pp.465-476.

Chinchilla, D., Zipfel, C., Robatzek, S., Kemmerling, B., Nürnberger, T., Jones, J.D., Felix, G. and Boller, T., 2007. A flagellin-induced complex of the receptor FLS2 and BAK1 initiates plant defence. *Nature*, *448*(7152), pp.497-500.

Chini, A., Fonseca, S., Chico, J.M., Fernández-Calvo, P. and Solano, R., 2009. The ZIM domain mediates homo-and heteromeric interactions between Arabidopsis JAZ proteins. *The Plant Journal*, *59*(1), pp.77-87.

Chini, A., Fonseca, S.G.D.C., Fernandez, G., Adie, B., Chico, J.M., Lorenzo, O., García-Casado, G., López-Vidriero, I., Lozano, F.M., Ponce, M.R. and Micol, J.L., 2007. The JAZ family of repressors is the missing link in jasmonate signalling. *Nature*, *448*(7154), pp.666-671.

Chini, A., Gimenez-Ibanez, S., Goossens, A. and Solano, R., 2016. Redundancy and specificity in jasmonate signalling. *Current opinion in plant biology*, *33*, pp.147-156.

Cho, H.Y., Loreti, E., Shih, M.C. and Perata, P., 2021. Energy and sugar signaling during hypoxia. *New Phytologist*, *229*(1), pp.57-63.

Chow, C.N., Yang, C.W., Wu, N.Y., Wang, H.T., Tseng, K.C., Chiu, Y.H., Lee, T.Y. and Chang, W.C., 2024. PlantPAN 4.0: Updated database for identifying conserved non-coding sequences and exploring dynamic transcriptional regulation in plant promoters. *Nucleic acids research*, *52*(D1), pp.D1569-D1578.

Chui, A.J., Okondo, M.C., Rao, S.D., Gai, K., Griswold, A.R., Johnson, D.C., Ball, D.P., Taabazuing, C.Y., Orth, E.L., Vittimberga, B.A. and Bachovchin, D.A., 2019. N-terminal degradation activates the NLRP1B inflammasome. *Science*, *364*(6435), pp.82-85.

Chung, H. and Lee, Y.H., 2020. Hypoxia: a double-edged sword during fungal pathogenesis?. *Frontiers in Microbiology*, *11*, p.1920.

Chung, H.S. and Howe, G.A., 2009. A critical role for the TIFY motif in repression of jasmonate signaling by a stabilized splice variant of the JASMONATE ZIM-domain protein JAZ10 in Arabidopsis. *The Plant Cell*, *21*(1), pp.131-145.

Clay, N.K., Adio, A.M., Denoux, C., Jander, G. and Ausubel, F.M., 2009. Glucosinolate metabolites required for an Arabidopsis innate immune response. *Science*, *323*(5910), pp.95-101.

Corpas, F.J., Palma, J.M., Río, L.A.D. and Barroso, J.B., 2009. Evidence supporting the existence of L-arginine-dependent nitric oxide synthase activity in plants. *New Phytologist*, pp.9-14.

Cramer, T., Yamanishi, Y., Clausen, B.E., Förster, I., Pawlinski, R., Mackman, N., Haase, V.H., Jaenisch, R., Corr, M., Nizet, V. and Firestein, G.S., 2003. HIF-1α is essential for myeloid cell-mediated inflammation. *Cell*, *112*(5), pp.645-657.

Cui, W. and Lee, J.Y., 2016. Arabidopsis callose synthases CalS1/8 regulate plasmodesmal permeability during stress. *Nature plants*, *2*(5), pp.1-9.

De Geyter, N., Gholami, A., Goormachtig, S. and Goossens, A., 2012. Transcriptional machineries in jasmonate-elicited plant secondary metabolism. *Trends in plant science*, *17*(6), pp.349-359.

De Lorenzo, G., Ferrari, S., Cervone, F. and Okun, E., 2018. Extracellular DAMPs in plants and mammals: immunity, tissue damage and repair. *Trends in immunology*, *39*(11), pp.937-950.

De Marchi, R., Sorel, M., Mooney, B., Fudal, I., Goslin, K., Kwaśniewska, K., Ryan, P.T., Pfalz, M., Kroymann, J., Pollmann, S. and Feechan, A., 2016. The N-end rule pathway regulates pathogen responses in plants. *Scientific Reports*, *6*(1), p.26020.

DeFalco, T.A. and Zipfel, C., 2021. Molecular mechanisms of early plant pattern-triggered immune signaling. *Molecular Cell*, *81*(17), pp.3449-3467.

del Carmen Martínez-Ballesta, M., Moreno, D.A. and Carvajal, M., 2013. The physiological importance of glucosinolates on plant response to abiotic stress in Brassica. *International journal of molecular sciences*, *14*(6), pp.11607-11625.

Denoux, C., Galletti, R., Mammarella, N., Gopalan, S., Werck, D., De Lorenzo, G., Ferrari, S., Ausubel, F.M. and Dewdney, J., 2008. Activation of defense response pathways by OGs and Flg22 elicitors in Arabidopsis seedlings. *Molecular plant*, *1*(3), pp.423-445.

Dimmeler, S., Haendeler, J., Nehls, M. and Zeiher, A.M., 1997. Suppression of apoptosis by nitric oxide via inhibition of interleukin-1β–converting enzyme (ice)-like and cysteine protease protein (cpp)-32–like proteases. *The Journal of experimental medicine*, *185*(4), pp.601-608.

Dissmeyer, N., Rivas, S. and Graciet, E., 2018. Life and death of proteins after protease cleavage: protein degradation by the N-end rule pathway. *New Phytologist*, *218*(3), pp.929-935.

Doares, S.H., Syrovets, T., Weiler, E.W. and Ryan, C.A., 1995. Oligogalacturonides and chitosan activate plant defensive genes through the octadecanoid pathway. *Proceedings of the National Academy of Sciences*, *92*(10), pp.4095-4098.

Dombrecht, B., Xue, G.P., Sprague, S.J., Kirkegaard, J.A., Ross, J.J., Reid, J.B., Fitt, G.P., Sewelam, N., Schenk, P.M., Manners, J.M. and Kazan, K., 2007. MYC2 differentially modulates diverse jasmonate-dependent functions in Arabidopsis. *The Plant Cell*, *19*(7), pp.2225-2245.

Domitrovic, T., Fausto, A.K., Silva, T.D.F., Romanel, E. and Vaslin, M.F., 2017. Plant arginyltransferases (ATEs). *Genetics and molecular biology*, *40*, pp.253-260.

Doorly, C.M. and Graciet, E., 2021. Lessons from comparison of hypoxia signaling in plants and mammals. *Plants*, *10*(5), p.993.

Doxey, A.C., Yaish, M.W., Moffatt, B.A., Griffith, M. and McConkey, B.J., 2007. Functional divergence in the Arabidopsis β-1, 3-glucanase gene family inferred by phylogenetic reconstruction of expression states. *Molecular biology and evolution*, *24*(4), pp.1045-1055.

Duan, T., Du, Y., Xing, C., Wang, H.Y. and Wang, R.F., 2022. Toll-like receptor signaling and its role in cell-mediated immunity. *Frontiers in Immunology*, *13*, p.812774.

Dubiella, U., Seybold, H., Durian, G., Komander, E., Lassig, R., Witte, C.P., Schulze, W.X. and Romeis, T., 2013. Calcium-dependent protein kinase/NADPH oxidase activation circuit is required for rapid defense signal propagation. *Proceedings of the National Academy of Sciences*, *110*(21), pp.8744-8749.

DuBridge, R.B., Tang, P., Hsia, H.C., Leong, P.M., Miller, J.H. and Calos, M.P., 1987. Analysis of mutation in human cells by using an Epstein-Barr virus shuttle system. *Molecular and cellular biology*, *7*(1), pp.379-387.

Edwards, K., Johnstone, C. and Thompson, C., 1991. A simple and rapid method for the preparation of plant genomic DNA for PCR analysis. *Nucleic acids research*, *19*(6), p.1349.

Elegheert, J., Behiels, E., Bishop, B., Scott, S., Woolley, R.E., Griffiths, S.C., Byrne, E.F., Chang, V.T., Stuart, D.I., Jones, E.Y. and Siebold, C., 2018. Lentiviral transduction of mammalian cells

for fast, scalable and high-level production of soluble and membrane proteins. *Nature protocols*, *13*(12), pp.2991-3017.

Ellinger, D., Naumann, M., Falter, C., Zwikowics, C., Jamrow, T., Manisseri, C., Somerville, S.C. and Voigt, C.A., 2013. Elevated early callose deposition results in complete penetration resistance to powdery mildew in Arabidopsis. *Plant physiology*, *161*(3), pp.1433-1444.

FAO. 2021. The impact of disasters and crises on agriculture and food security: 2021. Rome.

Feechan, A., Kwon, E., Yun, B.W., Wang, Y., Pallas, J.A. and Loake, G.J., 2005. A central role for S-nitrosothiols in plant disease resistance. *Proceedings of the National Academy of Sciences*, *102*(22), pp.8054-8059.

Felix, G., Duran, J.D., Volko, S. and Boller, T., 1999. Plants have a sensitive perception system for the most conserved domain of bacterial flagellin. *The Plant Journal*, *18*(3), pp.265-276.

Feng, J., Chen, L. and Zuo, J., 2019. Protein S-nitrosylation in plants: current progresses and challenges. *Journal of Integrative Plant Biology*, *61*(12), pp.1206-1223.

Fernández, D.J. and Lamkanfi, M., 2015. Inflammatory caspases: key regulators of inflammation and cell death. *Biological chemistry*, *396*(3), pp.193-203.

Feussner, I. and Wasternack, C., 2002. The lipoxygenase pathway. *Annual review of plant biology*, *53*(1), pp.275-297.

Figueroa-Macías, J.P., García, Y.C., Núñez, M., Díaz, K., Olea, A.F. and Espinoza, L., 2021. Plant growth-defense trade-offs: molecular processes leading to physiological changes. *International journal of molecular sciences*, *22*(2), p.693.

Förstermann, U. and Sessa, W.C., 2012. Nitric oxide synthases: regulation and function. *European heart journal*, *33*(7), pp.829-837.

Fukao, T., Barrera-Figueroa, B.E., Juntawong, P. and Peña-Castro, J.M., 2019. Submergence and waterlogging stress in plants: a review highlighting research opportunities and understudied aspects. *Frontiers in Plant Science*, *10*, p.340.

Fukao, T., Yeung, E. and Bailey-Serres, J., 2012. The submergence tolerance gene SUB1A delays leaf senescence under prolonged darkness through hormonal regulation in rice. *Plant Physiology*, *160*(4), pp.1795-1807.

Garzón, M., Eifler, K., Faust, A., Scheel, H., Hofmann, K., Koncz, C., Yephremov, A. and Bachmair, A., 2007. PRT6/At5g02310 encodes an Arabidopsis ubiquitin ligase of the N-end rule pathway with arginine specificity and is not the CER3 locus. *FEBS letters*, *581*(17), pp.3189-3196.

Gautier, C., van Faassen, E., Mikula, I., Martasek, P. and Slama-Schwok, A., 2006. Endothelial nitric oxide synthase reduces nitrite anions to NO under anoxia. *Biochemical and biophysical research communications*, *341*(3), pp.816-821.

Ge, S.X., Jung, D. and Yao, R., 2020. ShinyGO: a graphical gene-set enrichment tool for animals and plants. *Bioinformatics*, *36*(8), pp.2628-2629.

Gibbs, D.J. and Holdsworth, M.J., 2020. Every breath you take: new insights into plant and animal oxygen sensing. *Cell*, *180*(1), pp.22-24.

Gibbs, D.J., Conde, J.V., Berckhan, S., Prasad, G., Mendiondo, G.M. and Holdsworth, M.J., 2015. Group VII ethylene response factors coordinate oxygen and nitric oxide signal transduction and stress responses in plants. *Plant Physiology*, *169*(1), pp.23-31.

Gibbs, D.J., Isa, N.M., Movahedi, M., Lozano-Juste, J., Mendiondo, G.M., Berckhan, S., Marin-de La Rosa, N., Conde, J.V., Correia, C.S., Pearce, S.P. and Bassel, G.W., 2014. Nitric oxide sensing in plants is mediated by proteolytic control of group VII ERF transcription factors. *Molecular Cell*, *53*(3), pp.369-379.

Gibbs, D.J., Lee, S.C., Md Isa, N., Gramuglia, S., Fukao, T., Bassel, G.W., Correia, C.S., Corbineau, F., Theodoulou, F.L., Bailey-Serres, J. and Holdsworth, M.J., 2011. Homeostatic response to hypoxia is regulated by the N-end rule pathway in plants. *Nature*, *479*(7373), pp.415-418.

Gibbs, D.J., Tedds, H.M., Labandera, A.M., Bailey, M., White, M.D., Hartman, S., Sprigg, C., Mogg, S.L., Osborne, R., Dambire, C. and Boeckx, T., 2018. Oxygen-dependent proteolysis regulates the stability of angiosperm polycomb repressive complex 2 subunit VERNALIZATION 2. *Nature communications*, *9*(1), p.5438.

Gigolashvili, T., Berger, B. and Flügge, U.I., 2009. Specific and coordinated control of indolic and aliphatic glucosinolate biosynthesis by R2R3-MYB transcription factors in Arabidopsis thaliana. *Phytochemistry reviews*, *8*(1), pp.3-13.

Gimenez-Ibanez, S., Boter, M., Ortigosa, A., García-Casado, G., Chini, A., Lewsey, M.G., Ecker, J.R., Ntoukakis, V. and Solano, R., 2017. JAZ 2 controls stomata dynamics during bacterial invasion. *New Phytologist*, *213*(3), pp.1378-1392.

Giuliano, C.J., Lin, A., Girish, V. and Sheltzer, J.M., 2019. Generating single cell–derived knockout clones in mammalian cells with CRISPR/Cas9. *Current protocols in molecular biology*, *128*(1), p.e100.

Giuntoli, B., Shukla, V., Maggiorelli, F., Giorgi, F.M., Lombardi, L., Perata, P. and Licausi, F., 2017. Age-dependent regulation of ERF-VII transcription factor activity in Arabidopsis thaliana. *Plant, Cell & Environment*, *40*(10), pp.2333-2346.

Gómez-Gómez, L. and Boller, T., 2000. FLS2: an LRR receptor–like kinase involved in the perception of the bacterial elicitor flagellin in Arabidopsis. *Molecular cell*, *5*(6), pp.1003-1011.

Gonda, D.K., Bachmair, A., Wünning, I., Tobias, J.W., Lane, W.S. and Varshavsky, A., 1989. Universality and structure of the N-end rule. *Journal of Biological Chemistry*, *264*(28), pp.16700-16712.

Goossens, J., Swinnen, G., Vanden Bossche, R., Pauwels, L. and Goossens, A., 2015. Change of a conserved amino acid in the MYC 2 and MYC 3 transcription factors leads to release of JAZ repression and increased activity. *New Phytologist*, *206*(4), pp.1229-1237.

Goslin, K., 2019. *Characterization of the Ubiquitin N-end Rule Pathway in Arabidopsis* (Doctoral dissertation, National University of Ireland, Maynooth (Ireland)).

Goslin, K., Eschen-Lippold, L., Naumann, C., Linster, E., Sorel, M., Klecker, M., de Marchi, R., Kind, A., Wirtz, M., Lee, J. and Dissmeyer, N., 2019. Differential N-end rule degradation of RIN4/NOI fragments generated by the AvrRpt2 effector protease. *Plant Physiology*, *180*(4), pp.2272-2289.

Graciet, E., Hu, R.G., Piatkov, K., Rhee, J.H., Schwarz, E.M. and Varshavsky, A., 2006. Aminoacyl-transferases and the N-end rule pathway of prokaryotic/eukaryotic specificity in a human pathogen. *Proceedings of the National Academy of Sciences*, *103*(9), pp.3078-3083.

Graciet, E., Mesiti, F. and Wellmer, F., 2010. Structure and evolutionary conservation of the plant N-end rule pathway. *The Plant Journal*, *61*(5), pp.741-751.

Graciet, E., Walter, F., Maoiléidigh, D.Ó., Pollmann, S., Meyerowitz, E.M., Varshavsky, A. and Wellmer, F., 2009. The N-end rule pathway controls multiple functions during Arabidopsis shoot and leaf development. *Proceedings of the National Academy of Sciences*, *106*(32), pp.13618-13623.

Gravot, A., Richard, G., Lime, T., Lemarié, S., Jubault, M., Lariagon, C., Lemoine, J., Vicente, J., Robert-Seilaniantz, A., Holdsworth, M.J. and Manzanares-Dauleux, M.J., 2016. Hypoxia response in Arabidopsis roots infected by Plasmodiophora brassicae supports the development of clubroot. *BMC Plant Biology*, *16*(1), pp.1-10.

Grigoryev, S., Stewart, A.E., Kwon, Y.T., Arfin, S.M., Bradshaw, R.A., Jenkins, N.A., Copeland, N.G. and Varshavsky, A., 1996. A mouse amidase specific for N-terminal asparagine: the gene, the enzyme, and their function in the N-end rule pathway. *Journal of Biological Chemistry*, *271*(45), pp.28521-28532.

Grunewald, W., Vanholme, B., Pauwels, L., Plovie, E., Inze, D., Gheysen, G. and Goossens, A., 2009. Expression of the Arabidopsis jasmonate signalling repressor JAZ1/TIFY10A is stimulated by auxin. *EMBO reports*, *10*(8), pp.923-928.

Gschwend, F., Aregger, K., Gramlich, A., Walter, T. and Widmer, F., 2020. Periodic waterlogging consistently shapes agricultural soil microbiomes by promoting specific taxa. *Applied Soil Ecology*, *155*, p.103623.

Gubina, N., Leboeuf, D., Piatkov, K. and Pyatkov, M., 2020. Novel apoptotic mediators identified by conservation of vertebrate caspase targets. *Biomolecules*, *10*(4), p.612.

Guo, F.Q., Okamoto, M. and Crawford, N.M., 2003. Identification of a plant nitric oxide synthase gene involved in hormonal signaling. *Science*, *302*(5642), pp.100-103.

Gupta, K.J., Mur, L.A., Wany, A., Kumari, A., Fernie, A.R. and Ratcliffe, R.G., 2020. The role of nitrite and nitric oxide under low oxygen conditions in plants. *New Phytologist*, *225*(3), pp.1143-1151.

Gupta, K.J., Stoimenova, M. and Kaiser, W.M., 2005. In higher plants, only root mitochondria, but not leaf mitochondria reduce nitrite to NO, in vitro and in situ. *Journal of Experimental Botany*, *56*(420), pp.2601-2609.

Hagen, T., Taylor, C.T., Lam, F. and Moncada, S., 2003. Redistribution of intracellular oxygen in hypoxia by nitric oxide: effect on HIF1α. *Science*, *302*(5652), pp.1975-1978.

Hailemariam, S., Liao, C.J. and Mengiste, T., 2024. Receptor-like cytoplasmic kinases: orchestrating plant cellular communication. *Trends in Plant Science*.

Hammarlund, E.U., Flashman, E., Mohlin, S. and Licausi, F., 2020. Oxygen-sensing mechanisms across eukaryotic kingdoms and their roles in complex multicellularity. *Science*, *370*(6515), p.eaba3512.

Haney, C.H., Urbach, J. and Ausubel, F.M., 2014. Innate immunity in plants and animals. *Biochemist*, *36*(5), pp.40-44.

Hao, F., Zhao, S., Dong, H., Zhang, H., Sun, L. and Miao, C., 2010. Nia1 and Nia2 are involved in exogenous salicylic acid-induced nitric oxide generation and stomatal closure in Arabidopsis. *Journal of Integrative Plant Biology*, *52*(3), pp.298-307.

Hartman, K. and Tringe, S.G., 2019. Interactions between plants and soil shaping the root microbiome under abiotic stress. *Biochemical Journal*, *476*(19), pp.2705-2724.

Hartman, S., Liu, Z., Van Veen, H., Vicente, J., Reinen, E., Martopawiro, S., Zhang, H., Van Dongen, N., Bosman, F., Bassel, G.W. and Visser, E.J., 2019. Ethylene-mediated nitric oxide depletion pre-adapts plants to hypoxia stress. *Nature Communications*, *10*(1), p.4020.

Hayek, I., Schatz, V., Bogdan, C., Jantsch, J. and Lührmann, A., 2021. Mechanisms controlling bacterial infection in myeloid cells under hypoxic conditions. *Cellular and Molecular Life Sciences*, *78*, pp.1887-1907.

He, Z., Webster, S. and He, S.Y., 2022. Growth–defense trade-offs in plants. *Current Biology*, *32*(12), pp.R634-R639.

Hebelstrup, K.H., van Zanten, M., Mandon, J., Voesenek, L.A., Harren, F.J., Cristescu, S.M., Møller, I.M. and Mur, L.A., 2012. Haemoglobin modulates NO emission and hyponasty under hypoxia-related stress in Arabidopsis thaliana. *Journal of Experimental Botany*, *63*(15), pp.5581-5591.

Heberle, H., Meirelles, G.V., da Silva, F.R., Telles, G.P. and Minghim, R., 2015. InteractiVenn: a web-based tool for the analysis of sets through Venn diagrams. *BMC bioinformatics*, *16*, pp.1-7.

Heo, A.J., Kim, S.B., Kwon, Y.T. and Ji, C.H., 2023. The N-degron pathway: From basic science to therapeutic applications. *Biochimica et Biophysica Acta (BBA)-Gene Regulatory Mechanisms*, p.194934.

Hess, D.T., Matsumoto, A., Kim, S.O., Marshall, H.E. and Stamler, J.S., 2005. Protein S-nitrosylation: purview and parameters. *Nature reviews Molecular cell biology*, *6*(2), pp.150-166.

Hewitson, K.S., McNeill, L.A., Riordan, M.V., Tian, Y.M., Bullock, A.N., Welford, R.W., Elkins, J.M., Oldham, N.J., Bhattacharya, S., Gleadle, J.M. and Ratcliffe, P.J., 2002. Hypoxia-inducible factor (HIF) asparagine hydroxylase is identical to factor inhibiting HIF (FIH) and is related to the cupin structural family. *Journal of Biological Chemistry*, *277*(29), pp.26351-26355.

Hickman, R., Van Verk, M.C., Van Dijken, A.J., Mendes, M.P., Vroegop-Vos, I.A., Caarls, L., Steenbergen, M., Van der Nagel, I., Wesselink, G.J., Jironkin, A. and Talbot, A., 2017. Architecture and dynamics of the jasmonic acid gene regulatory network. *The Plant Cell*, *29*(9), pp.2086-2105.

Holdsworth, M.J. and Gibbs, D.J., 2020. Comparative biology of oxygen sensing in plants and animals. *Current Biology*, *30*(8), pp.R362-R369.

Holdsworth, M.J., Vicente, J., Sharma, G., Abbas, M. and Zubrycka, A., 2020. The plant N-degron pathways of ubiquitin-mediated proteolysis. *Journal of Integrative Plant Biology*, *62*(1), pp.70-89.

Howe, G.A., Major, I.T. and Koo, A.J., 2018. Modularity in jasmonate signaling for multistress resilience. *Annual review of plant biology*, *69*, pp.387-415.

Hsu, F.C., Chou, M.Y., Chou, S.J., Li, Y.R., Peng, H.P. and Shih, M.C., 2013. Submergence confers immunity mediated by the WRKY22 transcription factor in Arabidopsis. *The Plant Cell*, *25*(7), pp.2699-2713.

Hu, R.G., Brower, C.S., Wang, H., Davydov, I.V., Sheng, J., Zhou, J., Kwon, Y.T. and Varshavsky, A., 2006. Arginyltransferase, its specificity, putative substrates, bidirectional promoter, and splicing-derived isoforms. *Journal of Biological Chemistry*, *281*(43), pp.32559-32573.

Hu, R.G., Sheng, J., Qi, X., Xu, Z., Takahashi, T.T. and Varshavsky, A., 2005. The N-end rule pathway as a nitric oxide sensor controlling the levels of multiple regulators. *Nature*, *437*(7061), pp.981-986.

Huang, L.E., Gu, J., Schau, M. and Bunn, H.F., 1998. Regulation of hypoxia-inducible factor 1α is mediated by an O2-dependent degradation domain via the ubiquitin-proteasome pathway. *Proceedings of the National Academy of Sciences*, *95*(14), pp.7987-7992.

Huang, P.Y., Catinot, J. and Zimmerli, L., 2016. Ethylene response factors in Arabidopsis immunity. *Journal of experimental botany, 67*(5), pp.1231-1241.

Hwang, C.S., Shemorry, A. and Varshavsky, A., 2010. N-terminal acetylation of cellular proteins creates specific degradation signals. *Science*, *327*(5968), pp.973-977.

Iacopino, S. and Licausi, F., 2020. The contribution of plant dioxygenases to hypoxia signaling. *Frontiers in Plant Science*, *11*, p.1008.

Iliev, E.A., Xu, W., Polisensky, D.H., Oh, M.H., Torisky, R.S., Clouse, S.D. and Braam, J., 2002. Transcriptional and posttranscriptional regulation of Arabidopsis TCH4 expression by diverse stimuli. Roles of cis regions and brassinosteroids. *Plant Physiology*, *130*(2), pp.770-783.

Inoue, H., Nojima, H. and Okayama, H., 1990. High efficiency transformation of Escherichia coli with plasmids. *Gene*, *96*(1), pp.23-28.

Iqbal, Z., Shariq Iqbal, M., Singh, S.P. and Buaboocha, T., 2020. Ca2+/calmodulin complex triggers CAMTA transcriptional machinery under stress in plants: signaling cascade and molecular regulation. *Frontiers in Plant Science*, *11*, p.598327.

Isono, E. and Nagel, M.K., 2014. Deubiquitylating enzymes and their emerging role in plant biology. *Frontiers in Plant Science*, *5*, p.56.

Ivan, M., Kondo, K., Yang, H., Kim, W., Valiando, J., Ohh, M., Salic, A., Asara, J.M., Lane, W.S. and Kaelin Jr, W.G., 2001. HIFα targeted for VHL-mediated destruction by proline hydroxylation: implications for O2 sensing. *Science*, *292*(5516), pp.464-468.

Iyer, N.J., Tang, Y. and Mahalingam, R., 2013. Physiological, biochemical and molecular responses to a combination of drought and ozone in Medicago truncatula. *Plant, Cell & Environment*, *36*(3), pp.706-720.

Jaakkola, P., Mole, D.R., Tian, Y.M., Wilson, M.I., Gielbert, J., Gaskell, S.J., Kriegsheim, A.V., Hebestreit, H.F., Mukherji, M., Schofield, C.J. and Maxwell, P.H., 2001. Targeting of HIF-α to the von Hippel-Lindau ubiquitylation complex by O2-regulated prolyl hydroxylation. *Science*, *292*(5516), pp.468-472.

Jaba, I.M., Zhuang, Z.W., Li, N., Jiang, Y., Martin, K.A., Sinusas, A.J., Papademetris, X., Simons, M., Sessa, W.C., Young, L.H. and Tirziu, D., 2013. NO triggers RGS4 degradation to coordinate angiogenesis and cardiomyocyte growth. *The Journal of clinical investigation*, *123*(4), pp.1718-1731.

Jansson, E.Å., Huang, L., Malkey, R., Govoni, M., Nihlén, C., Olsson, A., Stensdotter, M., Petersson, J., Holm, L., Weitzberg, E. and Lundberg, J.O., 2008. A mammalian functional nitrate reductase that regulates nitrite and nitric oxide homeostasis. *Nature chemical biology*, *4*(7), pp.411-417.

Jennewein, J., Matuszak, J., Walter, S., Felmy, B., Gendera, K., Schatz, V., Nowottny, M., Liebsch, G., Hensel, M., Hardt, W.D. and Gerlach, R.G., 2015. Low-oxygen tensions found in S almonella-infected gut tissue boost S almonella replication in macrophages by impairing antimicrobial activity and augmenting S almonella virulence. *Cellular microbiology*, *17*(12), pp.1833-1847.

Jeong, S., Volny, M. and Lukowitz, W., 2012. Axis formation in Arabidopsis–transcription factors tell their side of the story. *Current opinion in plant biology*, *15*(1), pp.4-9.

Jiang, F. and Doudna, J.A., 2017. CRISPR–Cas9 structures and mechanisms. *Annual review of biophysics*, *46*, pp.505-529.

Jiang, Y., Liang, G., Yang, S. and Yu, D., 2014. Arabidopsis WRKY57 functions as a node of convergence for jasmonic acid–and auxin-mediated signaling in jasmonic acid–induced leaf senescence. *The Plant Cell*, *26*(1), pp.230-245.

Jin, Y., An, X., Ye, Z., Cully, B., Wu, J. and Li, J., 2009. RGS5, a hypoxia-inducible apoptotic stimulator in endothelial cells. *Journal of Biological Chemistry*, *284*(35), pp.23436-23443.

Jinek, M., Chylinski, K., Fonfara, I., Hauer, M., Doudna, J.A. and Charpentier, E., 2012. A programmable dual-RNA–guided DNA endonuclease in adaptive bacterial immunity. *science*, *337*(6096), pp.816-821.

Jones, J.D. and Dangl, J.L., 2006. The plant immune system. *nature*, *444*(7117), pp.323-329.

Jumper, J., Evans, R., Pritzel, A., Green, T., Figurnov, M., Ronneberger, O., Tunyasuvunakool, K., Bates, R., Žídek, A., Potapenko, A. and Bridgland, A., 2021. Highly accurate protein structure prediction with AlphaFold. *Nature*, *596*(7873), pp.583-589.

Jung, C., Zhao, P., Seo, J.S., Mitsuda, N., Deng, S. and Chua, N.H., 2015. Plant U-box protein10 regulates MYC2 stability in Arabidopsis. *The Plant Cell*, *27*(7), pp.2016-2031.

Kadota, Y., Sklenar, J., Derbyshire, P., Stransfeld, L., Asai, S., Ntoukakis, V., Jones, J.D., Shirasu, K., Menke, F., Jones, A. and Zipfel, C., 2014. Direct regulation of the NADPH oxidase RBOHD by the PRR-associated kinase BIK1 during plant immunity. *Molecular cell*, *54*(1), pp.43-55.

Kagale, S., Links, M.G. and Rozwadowski, K., 2010. Genome-wide analysis of ethylene-responsive element binding factor-associated amphiphilic repression motif-containing transcriptional regulators in Arabidopsis. *Plant physiology*, *152*(3), pp.1109-1134.

Kalapos, B., Hlavová, M., Nádai, T.V., Galiba, G., Bišová, K. and Dóczi, R., 2019. Early evolution of the Mitogen-activated protein kinase family in the plant kingdom. *Scientific Reports*, *9*(1), p.4094.

Kapadia, M.R., Eng, J.W., Jiang, Q., Stoyanovsky, D.A. and Kibbe, M.R., 2009. Nitric oxide regulates the 26S proteasome in vascular smooth muscle cells. *Nitric Oxide*, *20*(4), pp.279-288.

Karakozova, M., Kozak, M., Wong, C.C., Bailey, A.O., Yates III, J.R., Mogilner, A., Zebroski, H. and Kashina, A., 2006. Arginylation of ß-actin regulates actin cytoskeleton and cell motility. *Science*, *313*(5784), pp.192-196.

Kasu, Y.A.T., Alemu, S., Lamari, A., Loew, N. and Brower, C.S., 2018. The N termini of TAR DNA-binding protein 43 (TDP43) C-terminal fragments influence degradation, aggregation propensity, and morphology. *Molecular and Cellular Biology*, *38*(19), pp.e00243-18.

Kempf, V.A., Lebiedziejewski, M., Alitalo, K., Wälzlein, J.H., Ehehalt, U., Fiebig, J., Huber, S., Schütt, B., Sander, C.A., Müller, S. and Grassl, G., 2005. Activation of hypoxia-inducible factor-1 in bacillary angiomatosis: evidence for a role of hypoxia-inducible factor-1 in bacterial infections. *Circulation*, *111*(8), pp.1054-1062.

Kerpen, L., Niccolini, L., Licausi, F., van Dongen, J.T. and Weits, D.A., 2019. Hypoxic conditions in crown galls induce plant anaerobic responses that support tumor proliferation. *Frontiers in Plant Science*, *10*, p.56.

Kim, B.H., Kim, M.K., Oh, S.J., Nguyen, K.T., Kim, J.H., Varshavsky, A., Hwang, C.S. and Song, H.K., 2022. Crystal structure of the Ate1 arginyl-tRNA-protein transferase and arginylation of N-degron substrates. *Proceedings of the National Academy of Sciences*, *119*(31), p.e2209597119.

Kim, D.Y., Scalf, M., Smith, L.M. and Vierstra, R.D., 2013. Advanced proteomic analyses yield a deep catalog of ubiquitylation targets in Arabidopsis. *The Plant Cell*, *25*(5), pp.1523-1540.

Kim, J.S., Yoon, S.J., Park, Y.J., Kim, S.Y. and Ryu, C.M., 2020. Crossing the kingdom border: Human diseases caused by plant pathogens. *Environmental Microbiology*, *22*(7), pp.2485-2495.

Kim, N.Y., Jang, Y.J. and Park, O.K., 2018. AP2/ERF family transcription factors ORA59 and RAP2. 3 interact in the nucleus and function together in ethylene responses. *Frontiers in plant science*, *9*, p.1675.

Kim, S.Y. and Nair, M.G., 2019. Macrophages in wound healing: activation and plasticity. *Immunology and cell biology*, *97*(3), pp.258-267.

Kneeshaw, S., Gelineau, S., Tada, Y., Loake, G.J. and Spoel, S.H., 2014. Selective protein denitrosylation activity of thioredoxin-h5 modulates plant immunity. *Molecular cell*, *56*(1), pp.153-162.

Kocmánková, E., Trnka, M., Juroch, J., Dubrovský, M., Semerádová, D., Možný, M. and Žalud, Z., 2009. Impact of climate change on the occurrence and activity of harmful organisms. *Plant Protection Science*, *45*(Special Issue), pp.Impact-of.

Komander, D. and Rape, M., 2012. The ubiquitin code. *Annual review of biochemistry*, *81*, pp.203-229.

Kong, F.J., Oyanagi, A. and Komatsu, S., 2010. Cell wall proteome of wheat roots under flooding stress using gel-based and LC MS/MS-based proteomics approaches. *Biochimica et Biophysica Acta (BBA)-Proteins and Proteomics*, *1804*(1), pp.124-136.

Kozlov, A.V., Staniek, K. and Nohl, H., 1999. Nitrite reductase activity is a novel function of mammalian mitochondria. *FEBS letters*, *454*(1-2), pp.127-130.

Krishnaswamy, S., Verma, S., Rahman, M.H. and Kav, N.N., 2011. Functional characterization of four APETALA2-family genes (RAP2. 6, RAP2. 6L, DREB19 and DREB26) in Arabidopsis. *Plant molecular biology*, *75*, pp.107-127.

Krumenacker, J.S., Hanafy, K.A. and Murad, F., 2004. Regulation of nitric oxide and soluble guanylyl cyclase. *Brain research bulletin*, *62*(6), pp.505-515.

Kubicek, C.P., Starr, T.L. and Glass, N.L., 2014. Plant cell wall–degrading enzymes and their secretion in plant-pathogenic fungi. *Annual review of phytopathology*, *52*, pp.427-451.

Kwon, Y.T., Kashina, A.S., Davydov, I.V., Hu, R.G., An, J.Y., Seo, J.W., Du, F. and Varshavsky, A., 2002. An essential role of N-terminal arginylation in cardiovascular development. *Science*, *297*(5578), pp.96-99.

Kwon, Y.T., Xia, Z., An, J.Y., Tasaki, T., Davydov, I.V., Seo, J.W., Sheng, J., Xie, Y. and Varshavsky, A., 2003. Female lethality and apoptosis of spermatocytes in mice lacking the UBR2 ubiquitin ligase of the N-end rule pathway. *Molecular and cellular biology*, *23*(22), pp.8255-8271.

Labun, K., Montague, T.G., Gagnon, J.A., Thyme, S.B. and Valen, E., 2016. CHOPCHOP v2: a web tool for the next generation of CRISPR genome engineering. *Nucleic acids research*, *44*(W1), pp.W272-W276.

Labun, K., Montague, T.G., Krause, M., Torres Cleuren, Y.N., Tjeldnes, H. and Valen, E., 2019. CHOPCHOP v3: expanding the CRISPR web toolbox beyond genome editing. *Nucleic acids research*, *47*(W1), pp.W171-W174.

Lacchini, E. and Goossens, A., 2020. Combinatorial control of plant specialized metabolism: mechanisms, functions, and consequences. *Annual Review of Cell and Developmental Biology*, *36*, pp.291-313.

Lando, D., Peet, D.J., Gorman, J.J., Whelan, D.A., Whitelaw, M.L. and Bruick, R.K., 2002a. FIH-1 is an asparaginyl hydroxylase enzyme that regulates the transcriptional activity of hypoxia-inducible factor. *Genes & development*, *16*(12), pp.1466-1471.

Lando, D., Peet, D.J., Whelan, D.A., Gorman, J.J. and Whitelaw, M.L., 2002b. Asparagine hydroxylation of the HIF transactivation domain: a hypoxic switch. *Science*, *295*(5556), pp.858-861.

Lange, P.F., Huesgen, P.F., Nguyen, K. and Overall, C.M., 2014. Annotating N termini for the human proteome project: N termini and Nα-acetylation status differentiate stable cleaved protein species from degradation remnants in the human erythrocyte proteome. *Journal of proteome research*, *13*(4), pp.2028-2044.

Le Gall, H., Philippe, F., Domon, J.M., Gillet, F., Pelloux, J. and Rayon, C., 2015. Cell wall metabolism in response to abiotic stress. *Plants*, *4*(1), pp.112-166.

Leboeuf, D., Abakumova, T., Prikazchikova, T., Rhym, L., Anderson, D.G., Zatsepin, T.S. and Piatkov, K.I., 2020b. Downregulation of the Arg/N-degron pathway sensitizes cancer cells to chemotherapy in vivo. *Molecular therapy*, *28*(4), pp.1092-1104.

Leboeuf, D., Pyatkov, M., Zatsepin, T.S. and Piatkov, K., 2020a. The Arg/N-Degron Pathway—A Potential Running Back in Fine-Tuning the Inflammatory Response?. *Biomolecules*, *10*(6), p.903.

Lee, M.J., Tasaki, T., Moroi, K., An, J.Y., Kimura, S., Davydov, I.V. and Kwon, Y.T., 2005. RGS4 and RGS5 are in vivo substrates of the N-end rule pathway. *Proceedings of the National Academy of Sciences*, *102*(42), pp.15030-15035.

Lee, P., Chandel, N.S. and Simon, M.C., 2020. Cellular adaptation to hypoxia through hypoxia inducible factors and beyond. *Nature reviews Molecular cell biology*, *21*(5), pp.268-283.

Lee, S.C., Mustroph, A., Sasidharan, R., Vashisht, D., Pedersen, O., Oosumi, T., Voesenek, L.A. and Bailey-Serres, J., 2011. Molecular characterization of the submergence response of the Arabidopsis thaliana ecotype Columbia. *New Phytologist*, *190*(2), pp.457-471.

Lee, T.A. and Bailey-Serres, J., 2019. Integrative analysis from the epigenome to translatome uncovers patterns of dominant nuclear regulation during transient stress. *The Plant Cell*, *31*(11), pp.2573-2595.

Lee, U., Wie, C., Fernandez, B.O., Feelisch, M. and Vierling, E., 2008. Modulation of nitrosative stress by S-nitrosoglutathione reductase is critical for thermotolerance and plant growth in Arabidopsis. *The Plant Cell*, *20*(3), pp.786-802.

Lei, W., Li, J., Li, C., Chen, L., Huang, F., Xiao, D., Zhang, J., Zhao, J., Li, G., Qu, T. and Zhou, H., 2021. MARCH5 restores endothelial cell function against ischaemic/hypoxia injury via Akt/eNOS pathway. *Journal of cellular and molecular medicine*, *25*(7), pp.3182-3193.

Leu, N.A., Kurosaka, S. and Kashina, A., 2009. Conditional Tek promoter-driven deletion of arginyltransferase in the germ line causes defects in gametogenesis and early embryonic lethality in mice. *PloS one*, *4*(11), p.e7734.

Lewis, J.S., Lee, J.A., Underwood, J.C.E., Harris, A.L. and Lewis, C.E., 1999. Macrophage responses to hypoxia: relevance to disease mechanisms. *Journal of leukocyte biology*, *66*(6), pp.889-900.

Leysath, C.E., Phillips, D.D., Crown, D., Fattah, R.J., Moayeri, M. and Leppla, S.H., 2013. Anthrax edema factor toxicity is strongly mediated by the N-end rule. *PLoS One*, *8*(8), p.e74474.

Li, B., Meng, X., Shan, L. and He, P., 2016. Transcriptional regulation of pattern-triggered immunity in plants. *Cell host & microbe*, *19*(5), pp.641-650.

Li, J., Billiar, T.R., Talanian, R.V. and Kim, Y.M., 1997. Nitric oxide reversibly inhibits seven members of the caspase family via S-nitrosylation. *Biochemical and biophysical research communications*, *240*(2), pp.419-424.

Li, J., Brader, G. and Palva, E.T., 2004. The WRKY70 transcription factor: a node of convergence for jasmonate-mediated and salicylate-mediated signals in plant defense. *The Plant Cell*, *16*(2), pp.319-331.

Li, Z., Luo, X., Ou, Y., Jiao, H., Peng, L., Fu, X., Macho, A.P., Liu, R. and He, Y., 2021. JASMONATE-ZIM DOMAIN proteins engage Polycomb chromatin modifiers to modulate Jasmonate signaling in Arabidopsis. *Molecular plant*, *14*(5), pp.732-747.

Licausi, F., Kosmacz, M., Weits, D.A., Giuntoli, B., Giorgi, F.M., Voesenek, L.A., Perata, P. and Van Dongen, J.T., 2011a. Oxygen sensing in plants is mediated by an N-end rule pathway for protein destabilization. *Nature*, *479*(7373), pp.419-422.

Licausi, F., Weits, D.A., Pant, B.D., Scheible, W.R., Geigenberger, P. and van Dongen, J.T., 2011b. Hypoxia responsive gene expression is mediated by various subsets of transcription factors and miRNAs that are determined by the actual oxygen availability. *New phytologist*, *190*(2), pp.442-456.

Linden, K.J. and Callis, J., 2020. The ubiquitin system affects agronomic plant traits. *Journal of Biological Chemistry*, *295*(40), pp.13940-13955.

Lindsey III, B.E., Rivero, L., Calhoun, C.S., Grotewold, E. and Brkljacic, J., 2017. Standardized method for high-throughput sterilization of Arabidopsis seeds. *JoVE (Journal of Visualized Experiments)*, (128), p.e56587.

Liu, T., Zhang, L., Joo, D. and Sun, S.C., 2017. NF-κB signaling in inflammation. *Signal transduction and targeted therapy*, *2*(1), pp.1-9.

Lorenzo, O., Chico, J.M., Saénchez-Serrano, J.J. and Solano, R., 2004. JASMONATE-INSENSITIVE1 encodes a MYC transcription factor essential to discriminate between different jasmonate-regulated defense responses in Arabidopsis. *The Plant Cell*, *16*(7), pp.1938-1950.

Lozano-Juste, J. and León, J., 2010. Enhanced abscisic acid-mediated responses in nia1nia2noa1-2 triple mutant impaired in NIA/NR-and AtNOA1-dependent nitric oxide biosynthesis in Arabidopsis. *Plant physiology*, *152*(2), pp.891-903.

Luan, S. and Wang, C., 2021. Calcium signaling mechanisms across kingdoms. *Annual review of cell and developmental biology*, *37*, pp.311-340.

Ma, X., Zhang, C., Kim, D.Y., Huang, Y., Chatt, E., He, P., Vierstra, R.D. and Shan, L., 2021. Ubiquitylome analysis reveals a central role for the ubiquitin-proteasome system in plant innate immunity. *Plant physiology*, *185*(4), pp.1943-1965.

Macedo-da-Silva, J., Fernandes, L.R., Gomes, V.D.M., Santiago, V.F., Santos, D.M., Stanischesk, M.C.M., Barboza, B.R., Souza, E.E.D., Marques, R.F., Boscardin, S.B. and Durigon, E.L., 2023. Protein Arginylation is regulated during SARS-CoV-2 infection. *Viruses*, *15*(2), pp.1-25.

Maere, S., Heymans, K. and Kuiper, M., 2005. BiNGO: a Cytoscape plugin to assess overrepresentation of gene ontology categories in biological networks. *Bioinformatics*, *21*(16), pp.3448-3449.

Major, I.T., Yoshida, Y., Campos, M.L., Kapali, G., Xin, X.F., Sugimoto, K., de Oliveira Ferreira, D., He, S.Y. and Howe, G.A., 2017. Regulation of growth–defense balance by the JASMONATE ZIM-DOMAIN (JAZ)-MYC transcriptional module. *New Phytologist*, *215*(4), pp.1533-1547.

Mao, G., Meng, X., Liu, Y., Zheng, Z., Chen, Z. and Zhang, S., 2011. Phosphorylation of a WRKY transcription factor by two pathogen-responsive MAPKs drives phytoalexin biosynthesis in Arabidopsis. *The Plant Cell*, *23*(4), pp.1639-1653.

Marino, S.M. and Gladyshev, V.N., 2010. Structural analysis of cysteine S-nitrosylation: a modified acid-based motif and the emerging role of trans-nitrosylation. *Journal of molecular biology*, *395*(4), pp.844-859.

Marshall, R.S. and Vierstra, R.D., 2019. Dynamic regulation of the 26S proteasome: from synthesis to degradation. *Frontiers in Molecular Biosciences*, *6*, p.40.

Martínez-Arias, C., Witzell, J., Solla, A., Martin, J.A. and Rodríguez-Calcerrada, J., 2022. Beneficial and pathogenic plant-microbe interactions during flooding stress. *Plant, Cell & Environment*, *45*(10), pp.2875-2897.

Mason, K.N., Ekanayake, G. and Heese, A., 2020. Staining and automated image quantification of callose in Arabidopsis cotyledons and leaves. In *Methods in cell biology* (Vol. 160, pp. 181-199). Academic Press.

Masson, N., Keeley, T.P., Giuntoli, B., White, M.D., Puerta, M.L., Perata, P., Hopkinson, R.J., Flashman, E., Licausi, F. and Ratcliffe, P.J., 2019. Conserved N-terminal cysteine dioxygenases transduce responses to hypoxia in animals and plants. *Science*, *365*(6448), pp.65-69.

Mata-Pérez, C. and Spoel, S.H., 2019. Thioredoxin-mediated redox signalling in plant immunity. *Plant science*, *279*, pp.27-33.

Mateo, J., García-Lecea, M., Cadenas, S., Hernández, C. and Moncada, S., 2003. Regulation of hypoxia-inducible factor-1α by nitric oxide through mitochondria-dependent and-independent pathways. *Biochemical Journal*, *376*(2), pp.537-544.

Matsushima, N., Tanaka, T., Enkhbayar, P., Mikami, T., Taga, M., Yamada, K. and Kuroki, Y., 2007. Comparative sequence analysis of leucine-rich repeats (LRRs) within vertebrate toll-like receptors. *BMC genomics*, *8*, pp.1-20.

Maxwell, P.H., Wiesener, M.S., Chang, G.W., Clifford, S.C., Vaux, E.C., Cockman, M.E., Wykoff, C.C., Pugh, C.W., Maher, E.R. and Ratcliffe, P.J., 1999. The tumour suppressor protein VHL

targets hypoxia-inducible factors for oxygen-dependent proteolysis. *Nature*, *399*(6733), pp.271-275.

Mayer, D., Mithöfer, A., Glawischnig, E., Georgii, E., Ghirardo, A., Kanawati, B., Schmitt-Kopplin, P., Schnitzler, J.P., Durner, J. and Gaupels, F., 2018. Short-term exposure to nitrogen dioxide provides basal pathogen resistance. *Plant physiology*, *178*(1), pp.468-487.

McBride, K.E. and Summerfelt, K.R., 1990. Improved binary vectors for Agrobacterium-mediated plant transformation. *Plant molecular biology*, *14*, pp.269-276.

McCormick, C.C., Li, W.P. and Calero, M., 2000. Oxygen tension limits nitric oxide synthesis by activated macrophages. *Biochemical Journal*, *350*(3), pp.709-716.

McLellan, H., Chen, K., He, Q., Wu, X., Boevink, P.C., Tian, Z. and Birch, P.R., 2020. The ubiquitin E3 ligase PUB17 positively regulates immunity by targeting a negative regulator, KH17, for degradation. *Plant communications*, *1*(4).

McNeill, L.A., Hewitson, K.S., Claridge, T.D., Seibel, J.F., Horsfall, L.E. and Schofield, C.J., 2002. Hypoxia-inducible factor asparaginyl hydroxylase (FIH-1) catalyses hydroxylation at the β-carbon of asparagine-803. *Biochemical Journal*, *367*(3), pp.571-575.

Mikula, I., Durocher, S., Martasek, P., Mutus, B. and Slama-Schwok, A., 2009. Isoform-specific differences in the nitrite reductase activity of nitric oxide synthases under hypoxia. *Biochemical Journal*, *418*(3), pp.673-682.

Millet, Y.A., Danna, C.H., Clay, N.K., Songnuan, W., Simon, M.D., Werck-Reichhart, D. and Ausubel, F.M., 2010. Innate immune responses activated in Arabidopsis roots by microbe-associated molecular patterns. *The Plant Cell*, *22*(3), pp.973-990.

Miricescu, A., Goslin, K. and Graciet, E., 2018. Ubiquitylation in plants: signaling hub for the integration of environmental signals. *Journal of Experimental Botany*, *69*(19), pp.4511-4527.

Miyamoto, T., Uemura, T., Nemoto, K., Daito, M., Nozawa, A., Sawasaki, T. and Arimura, G.I., 2019. Tyrosine kinase-dependent defense responses against herbivory in Arabidopsis. *Frontiers in plant science*, *10*, p.776.

Mizel, S.B., West, A.P. and Hantgan, R.R., 2003. Identification of a sequence in human toll-like receptor 5 required for the binding of Gram-negative flagellin. *Journal of Biological Chemistry*, *278*(26), pp.23624-23629.

Mohanta, T.K., Park, Y.H. and Bae, H., 2016. Novel genomic and evolutionary insight of WRKY transcription factors in plant lineage. *Scientific reports*, *6*(1), p.37309.

Mohn, M.A., Thaqi, B. and Fischer-Schrader, K., 2019. Isoform-specific NO synthesis by Arabidopsis thaliana nitrate reductase. *Plants*, *8*(3), p.67.

Mojica, F.J., Díez-Villaseñor, C.S., García-Martínez, J. and Soria, E., 2005. Intervening sequences of regularly spaced prokaryotic repeats derive from foreign genetic elements. *Journal of molecular evolution*, *60*, pp.174-182.

Montague, T.G., Cruz, J.M., Gagnon, J.A., Church, G.M. and Valen, E., 2014. CHOPCHOP: a CRISPR/Cas9 and TALEN web tool for genome editing. *Nucleic acids research*, *42*(W1), pp.W401-W407.

Mooney, B.C., Doorly, C.M., Mantz, M., García, P., Huesgen, P.F. and Graciet, E., 2024. Hypoxia represses pattern-triggered immune responses in Arabidopsis. *Plant Physiology*, p.kiae432.

Moorthy, B.T., Jiang, C., Patel, D.M., Ban, Y., O'Shea, C.R., Kumar, A., Yuan, T., Birnbaum, M.D., Gomes, A.V., Chen, X. and Fontanesi, F., 2022. The evolutionarily conserved arginyltransferase 1 mediates a pVHL-independent oxygen-sensing pathway in mammalian cells. *Developmental cell*, *57*(5), pp.654-669.

Mugnai, S., Azzarello, E., Baluška, F. and Mancuso, S., 2012. Local root apex hypoxia induces NO-mediated hypoxic acclimation of the entire root. *Plant and Cell Physiology*, *53*(5), pp.912-920.

Mukhopadhyay, D. and Riezman, H., 2007. Proteasome-independent functions of ubiquitin in endocytosis and signaling. *Science*, *315*(5809), pp.201-205.

Mustroph, A., Zanetti, M.E., Jang, C.J., Holtan, H.E., Repetti, P.P., Galbraith, D.W., Girke, T. and Bailey-Serres, J., 2009. Profiling translatomes of discrete cell populations resolves altered

cellular priorities during hypoxia in Arabidopsis. *Proceedings of the National Academy of Sciences*, *106*(44), pp.18843-18848.

Nagels Durand, A., Pauwels, L. and Goossens, A., 2016. The ubiquitin system and jasmonate signaling. *Plants*, *5*(1), p.6.

Nakata, M. and Ohme-Takagi, M., 2014. Quantification of anthocyanin content. *Bio-protocol*, *4*(7), pp.e1098-e1098.

Narayanan, K.B. and Park, H.H., 2015. Toll/interleukin-1 receptor (TIR) domain-mediated cellular signaling pathways. *Apoptosis*, *20*, pp.196-209.

Ngou, B.P.M., Ahn, H.K., Ding, P. and Jones, J.D., 2021. Mutual potentiation of plant immunity by cell-surface and intracellular receptors. *Nature*, *592*(7852), pp.110-115.

Ngou, B.P.M., Ding, P. and Jones, J.D., 2022a. Thirty years of resistance: Zig-zag through the plant immune system. *The Plant Cell*, *34*(5), pp.1447-1478.

Ngou, B.P.M., Jones, J.D. and Ding, P., 2022b. Plant immune networks. *Trends in plant science*, *27*(3), pp.255-273.

Nguyen, N.H., Trotel-Aziz, P., Clément, C., Jeandet, P., Baillieul, F. and Aziz, A., 2022. Camalexin accumulation as a component of plant immunity during interactions with pathogens and beneficial microbes. *Planta*, *255*(6), p.116.

Nold-Petry, C.A., Rudloff, I., Baumer, Y., Ruvo, M., Marasco, D., Botti, P., Farkas, L., Cho, S.X., Zepp, J.A., Azam, T. and Dinkel, H., 2014. IL-32 promotes angiogenesis. *The Journal of Immunology*, *192*(2), pp.589-602.

Novaković, L., Guo, T., Bacic, A., Sampathkumar, A. and Johnson, K.L., 2018. Hitting the wall—Sensing and signaling pathways involved in plant cell wall remodeling in response to abiotic stress. *Plants*, *7*(4), p.89.

Ortoneda, M., Guarro, J., Madrid, M.P., Caracuel, Z., Roncero, M.I.G., Mayayo, E. and Di Pietro, A., 2004. Fusarium oxysporum as a multihost model for the genetic dissection of fungal virulence in plants and mammals. *Infection and immunity*, *72*(3), pp.1760-1766.

Ouli-Jun, Z.C.H., Zhou-Bin, L., Ge, W., Bo-Zhi, Y.A.N.G. and Xue-Xiao, Z., 2017. Mitigation of waterlogging-induced damages to pepper by exogenous MeJA. *Pak. J. Bot*, *49*(3), pp.1127-1135.

Pande, A., Mun, B.G., Khan, M., Rahim, W., Lee, D.S., Lee, G.M., Al Azawi, T.N.I., Hussain, A. and Yun, B.W., 2022. Nitric oxide signaling and its association with ubiquitin-mediated proteasomal degradation in plants. *International journal of molecular sciences*, *23*(3), p.1657.

Pandey, P., Ramegowda, V. and Senthil-Kumar, M., 2015. Shared and unique responses of plants to multiple individual stresses and stress combinations: physiological and molecular mechanisms. *Frontiers in plant science*, *6*, p.723.

Pauwels, L. and Goossens, A., 2011. The JAZ proteins: a crucial interface in the jasmonate signaling cascade. *The Plant Cell*, *23*(9), pp.3089-3100.

Pauwels, L., Barbero, G.F., Geerinck, J., Tilleman, S., Grunewald, W., Pérez, A.C., Chico, J.M., Bossche, R.V., Sewell, J., Gil, E. and Garcia-Casado, G., 2010. NINJA connects the co-repressor TOPLESS to jasmonate signalling. *Nature*, *464*(7289), pp.788-791.

Pauwels, L., Ritter, A., Goossens, J., Durand, A.N., Liu, H., Gu, Y., Geerinck, J., Boter, M., Vanden Bossche, R., De Clercq, R. and Van Leene, J., 2015. The ring e3 ligase keep on going modulates jasmonate zim-domain12 stability. *Plant Physiology*, *169*(2), pp.1405-1417.

Pavlyk, I., Leu, N.A., Vedula, P., Kurosaka, S. and Kashina, A., 2018. Rapid and dynamic arginylation of the leading edge β-actin is required for cell migration. *Traffic*, *19*(4), pp.263-272.

Pegg, T., Edelmann, R.R. and Gladish, D.K., 2020. Immunoprofiling of cell wall carbohydrate modifications during flooding-induced aerenchyma formation in fabaceae roots. *Frontiers in Plant Science*, *10*, p.1805.

Perazzolli, M., Dominici, P., Romero-Puertas, M.C., Zago, E., Zeier, J., Sonoda, M., Lamb, C. and Delledonne, M., 2004. Arabidopsis nonsymbiotic hemoglobin AHb1 modulates nitric oxide bioactivity. *The Plant Cell*, *16*(10), pp.2785-2794.

Piatkov, K.I., Brower, C.S. and Varshavsky, A., 2012. The N-end rule pathway counteracts cell death by destroying proapoptotic protein fragments. *Proceedings of the National Academy of Sciences*, *109*(27), pp.E1839-E1847.

Piatkov, K.I., Vu, T.T., Hwang, C.S. and Varshavsky, A., 2015. Formyl-methionine as a degradation signal at the N-termini of bacterial proteins. *Microbial Cell*, *2*(10), p.376.

Popov, N., Schmitt, M., Schulzeck, S. and Matthies, H., 1975. Reliable micromethod for determination of the protein content in tissue homogenates. *Acta biologica et medica Germanica*, *34*(9), pp.1441-1446.

Potuschak, T., Stary, S., Schlögelhofer, P., Becker, F., Nejinskaia, V. and Bachmair, A., 1998. PRT1 of Arabidopsis thaliana encodes a component of the plant N-end rule pathway. *Proceedings of the National Academy of Sciences*, *95*(14), pp.7904-7908.

Prasch, C.M. and Sonnewald, U., 2013. Simultaneous application of heat, drought, and virus to Arabidopsis plants reveals significant shifts in signaling networks. *Plant physiology*, *162*(4), pp.1849-1866.

Qi, T., Song, S., Ren, Q., Wu, D., Huang, H., Chen, Y., Fan, M., Peng, W., Ren, C. and Xie, D., 2011. The Jasmonate-ZIM-domain proteins interact with the WD-Repeat/bHLH/MYB complexes to regulate Jasmonate-mediated anthocyanin accumulation and trichome initiation in Arabidopsis thaliana. *The Plant Cell*, *23*(5), pp.1795-1814.

Qian, J., Chen, F., Kovalenkov, Y., Pandey, D., Moseley, M.A., Foster, M.W., Black, S.M., Venema, R.C., Stepp, D.W. and Fulton, D.J., 2012. Nitric oxide reduces NADPH oxidase 5 (Nox5) activity by reversible S-nitrosylation. *Free Radical Biology and Medicine*, *52*(9), pp.1806-1819.

Qie, J., Liu, Y., Wang, Y., Zhang, F., Qin, Z., Tian, S., Liu, M., Li, K., Shi, W., Song, L. and Sun, M., 2022. Integrated proteomic and transcriptomic landscape of macrophages in mouse tissues. *Nature Communications*, *13*(1), p.7389.

Rahat, M.A., Bitterman, H. and Lahat, N., 2011. Molecular mechanisms regulating macrophage response to hypoxia. *Frontiers in immunology*, *2*, p.12723.

Rahme, L.G., Ausubel, F.M., Cao, H., Drenkard, E., Goumnerov, B.C., Lau, G.W., Mahajan-Miklos, S., Plotnikova, J., Tan, M.W., Tsongalis, J. and Walendziewicz, C.L., 2000. Plants and animals share functionally common bacterial virulence factors. *Proceedings of the National Academy of Sciences*, *97*(16), pp.8815-8821.

Rahme, L.G., Stevens, E.J., Wolfort, S.F., Shao, J., Tompkins, R.G. and Ausubel, F.M., 1995. Common virulence factors for bacterial pathogenicity in plants and animals. *Science*, *268*(5219), pp.1899-1902.

Rai, R. and Kashina, A., 2005. Identification of mammalian arginyltransferases that modify a specific subset of protein substrates. *Proceedings of the National Academy of Sciences*, *102*(29), pp.10123-10128.

Ramanathan, M., Pinhal-Enfield, G., Hao, I. and Leibovich, S.J., 2007. Synergistic up-regulation of vascular endothelial growth factor (VEGF) expression in macrophages by adenosine A2A receptor agonists and endotoxin involves transcriptional regulation via the hypoxia response element in the VEGF promoter. *Molecular biology of the cell*, *18*(1), pp.14-23.

Rao, S., Zhou, Z., Miao, P., Bi, G., Hu, M., Wu, Y., Feng, F., Zhang, X. and Zhou, J.M., 2018. Roles of receptor-like cytoplasmic kinase VII members in pattern-triggered immune signaling. *Plant physiology*, *177*(4), pp.1679-1690.

Raschke, W.C., Baird, S., Ralph, P. and Nakoinz, I., 1978. Functional macrophage cell lines transformed by Abelson leukemia virus. *Cell*, *15*(1), pp.261-267.

Rasmussen, S., Barah, P., Suarez-Rodriguez, M.C., Bressendorff, S., Friis, P., Costantino, P., Bones, A.M., Nielsen, H.B. and Mundy, J., 2013. Transcriptome responses to combinations of stresses in Arabidopsis. *Plant physiology*, *161*(4), pp.1783-1794.

Raza, A., Charagh, S., Zahid, Z., Mubarik, M.S., Javed, R., Siddiqui, M.H. and Hasanuzzaman, M., 2021. Jasmonic acid: a key frontier in conferring abiotic stress tolerance in plants. *Plant Cell Reports*, *40*(8), pp.1513-1541.

Ren, D., Liu, Y., Yang, K.Y., Han, L., Mao, G., Glazebrook, J. and Zhang, S., 2008. A fungal-responsive MAPK cascade regulates phytoalexin biosynthesis in Arabidopsis. *Proceedings of the National Academy of Sciences*, *105*(14), pp.5638-5643.

Reynaert, N.L., Ckless, K., Korn, S.H., Vos, N., Guala, A.S., Wouters, E.F., van der Vliet, A. and Janssen-Heininger, Y.M., 2004. Nitric oxide represses inhibitory κB kinase through S-nitrosylation. *Proceedings of the National Academy of Sciences*, *101*(24), pp.8945-8950.

Rizhsky, L., Liang, H., Shuman, J., Shulaev, V., Davletova, S. and Mittler, R., 2004. When defense pathways collide. The response of Arabidopsis to a combination of drought and heat stress. *Plant physiology*, *134*(4), pp.1683-1696.

Rizza, S., Montagna, C., Di Giacomo, G., Cirotti, C. and Filomeni, G., 2014. S-nitrosation and ubiquitin-proteasome system interplay in neuromuscular disorders. *International Journal of Cell Biology*, *2014*.

Robatzek, S., Chinchilla, D. and Boller, T., 2006. Ligand-induced endocytosis of the pattern recognition receptor FLS2 in Arabidopsis. *Genes & development*, *20*(5), pp.537-542.

Romero-Barrios, N. and Vert, G., 2018. Proteasome-independent functions of lysine-63 polyubiquitination in plants. *New Phytologist*, *217*(3), pp.995-1011.

Rosell-Garcia, T., Rivas-Muñoz, S., Kin, K., Romero-Albillo, V., Alcaraz, S., Fernandez-Tornero, C. and Rodriguez-Pascual, F., 2023. Multimerization of HIF enhances transcription of target genes containing the hypoxia ancillary sequence. *Biochimica et Biophysica Acta (BBA)-Gene Regulatory Mechanisms*, *1866*(4), p.194963.

Saha, B., Nayak, J., Srivastava, R., Samal, S., Kumar, D., Chanwala, J., Dey, N. and Giri, M.K., 2024. Unraveling the involvement of WRKY TFs in regulating plant disease defense signaling. *Planta*, *259*(1), p.7.

Saha, S., Wang, J., Buckley, B., Wang, Q., Lilly, B., Chernov, M. and Kashina, A., 2012. Small molecule inhibitors of arginyltransferase regulate arginylation-dependent protein degradation, cell motility, and angiogenesis. *Biochemical pharmacology*, *83*(7), pp.866-873.

Saijo, Y. and Loo, E.P.I., 2020. Plant immunity in signal integration between biotic and abiotic stress responses. *New Phytologist*, *225*(1), pp.87-104.

Salim, T., Sershen, C.L. and May, E.E., 2016. Investigating the role of TNF-α and IFN-γ activation on the dynamics of iNOS gene expression in LPS stimulated macrophages. *PloS one*, *11*(6), p.e0153289.

Sandstrom, A., Mitchell, P.S., Goers, L., Mu, E.W., Lesser, C.F. and Vance, R.E., 2019. Functional degradation: A mechanism of NLRP1 inflammasome activation by diverse pathogen enzymes. *Science*, *364*(6435), p.eaau1330.

Sanjana, N.E., Shalem, O. and Zhang, F., 2014. Improved vectors and genome-wide libraries for CRISPR screening. *Nature methods*, *11*(8), pp.783-784.

Sasidharan, R., Hartman, S., Liu, Z., Martopawiro, S., Sajeev, N., van Veen, H., Yeung, E. and Voesenek, L.A., 2018. Signal dynamics and interactions during flooding stress. *Plant physiology*, *176*(2), pp.1106-1117.

Savchenko, T.V., Rolletschek, H. and Dehesh, K., 2019. Jasmonates-mediated rewiring of central metabolism regulates adaptive responses. *Plant and Cell Physiology*, *60*(12), pp.2613-2620.

Schaffner, W. and Weissmann, C., 1973. A rapid, sensitive, and specific method for the determination of protein in dilute solution. *Analytical biochemistry*, *56*(2), pp.502-514.

Schindelin, J., Arganda-Carreras, I., Frise, E., Kaynig, V., Longair, M., Pietzsch, T., Preibisch, S., Rueden, C., Saalfeld, S., Schmid, B. and Tinevez, J.Y., 2012. Fiji: an open-source platform for biological-image analysis. *Nature methods*, *9*(7), pp.676-682.

Schmidt, R.R., Fulda, M., Paul, M.V., Anders, M., Plum, F., Weits, D.A., Kosmacz, M., Larson, T.R., Graham, I.A., Beemster, G.T. and Licausi, F., 2018. Low-oxygen response is triggered by an ATP-dependent shift in oleoyl-CoA in Arabidopsis. *Proceedings of the National Academy of Sciences*, *115*(51), pp.E12101-E12110.

Schneider, C.A., Rasband, W.S. and Eliceiri, K.W., 2012. NIH Image to ImageJ: 25 years of image analysis. *Nature methods*, *9*(7), pp.671-675.

Schnupf, P., Zhou, J., Varshavsky, A. and Portnoy, D.A., 2007. Listeriolysin O secreted by Listeria monocytogenes into the host cell cytosol is degraded by the N-end rule pathway. *Infection and immunity*, *75*(11), pp.5135-5147.

Semenza, G.L., 2007. Hypoxia-inducible factor 1 (HIF-1) pathway. *Science's STKE*, *2007*(407), pp.cm8-cm8.

Sewelam, N., Kazan, K., Thomas-Hall, S.R., Kidd, B.N., Manners, J.M. and Schenk, P.M., 2013. Ethylene response factor 6 is a regulator of reactive oxygen species signaling in Arabidopsis. *PloS one*, *8*(8), p.e70289.

Shaar-Moshe, L., Blumwald, E. and Peleg, Z., 2017. Unique physiological and transcriptional shifts under combinations of salinity, drought, and heat. *Plant physiology*, *174*(1), pp.421-434.

Shan, X., Zhang, Y., Peng, W., Wang, Z. and Xie, D., 2009. Molecular mechanism for jasmonate-induction of anthocyanin accumulation in Arabidopsis. *Journal of experimental botany*, *60*(13), pp.3849-3860.

Shao, H., Wang, H. and Tang, X., 2015. NAC transcription factors in plant multiple abiotic stress responses: progress and prospects. *Frontiers in plant science*, *6*, p.902.

Sharma, A., Shahzad, B., Kumar, V., Kohli, S.K., Sidhu, G.P.S., Bali, A.S., Handa, N., Kapoor, D., Bhardwaj, R. and Zheng, B., 2019. Phytohormones regulate accumulation of osmolytes under abiotic stress. *Biomolecules*, *9*(7), p.285.

Sharma, M., Sharma, M., Jamsheer K, M. and Laxmi, A., 2022. Jasmonic acid coordinates with light, glucose and auxin signalling in regulating branching angle of Arabidopsis lateral roots. *Plant, Cell & Environment*, *45*(5), pp.1554-1572.

Sheard, L.B., Tan, X., Mao, H., Withers, J., Ben-Nissan, G., Hinds, T.R., Kobayashi, Y., Hsu, F.F., Sharon, M., Browse, J. and He, S.Y., 2010. Jasmonate perception by inositol-phosphate-potentiated COI1–JAZ co-receptor. *Nature*, *468*(7322), pp.400-405.

Shukla, V., Lombardi, L., Pencik, A., Novak, O., Weits, D.A., Loreti, E., Perata, P., Giuntoli, B. and Licausi, F., 2020. Jasmonate signalling contributes to primary root inhibition upon oxygen deficiency in Arabidopsis thaliana. *Plants*, *9*(8), p.1046.

Shyu, C., Figueroa, P., DePew, C.L., Cooke, T.F., Sheard, L.B., Moreno, J.E., Katsir, L., Zheng, N., Browse, J. and Howe, G.A., 2012. JAZ8 lacks a canonical degron and has an EAR motif that

mediates transcriptional repression of jasmonate responses in Arabidopsis. *The Plant Cell*, *24*(2), pp.536-550.

Singh, A., Borah, A.K., Deka, K., Gogoi, A.P., Verma, K., Barah, P. and Saha, S., 2019. Arginylation regulates adipogenesis by regulating expression of PPARγ at transcript and protein level. *Biochimica et Biophysica Acta (BBA)-Molecular and Cell Biology of Lipids*, *1864*(4), pp.596-607.

Smith, K.D., Andersen-Nissen, E., Hayashi, F., Strobe, K., Bergman, M.A., Barrett, S.L.R., Cookson, B.T. and Aderem, A., 2003. Toll-like receptor 5 recognizes a conserved site on flagellin required for protofilament formation and bacterial motility. *Nature immunology*, *4*(12), pp.1247-1253.

Song, S., Huang, H., Gao, H., Wang, J., Wu, D., Liu, X., Yang, S., Zhai, Q., Li, C., Qi, T. and Xie, D., 2014. Interaction between MYC2 and ETHYLENE INSENSITIVE3 modulates antagonism between jasmonate and ethylene signaling in Arabidopsis. *The Plant Cell*, *26*(1), pp.263-279.

Stary, S., Yin, X.J., Potuschak, T., Schlögelhofer, P., Nizhynska, V. and Bachmair, A., 2003. PRT1 of Arabidopsis is a ubiquitin protein ligase of the plant N-end rule pathway with specificity for aromatic amino-terminal residues. *Plant physiology*, *133*(3), pp.1360-1366.

Staskawicz, B.J., Mudgett, M.B., Dangl, J.L. and Galan, J.E., 2001. Common and contrasting themes of plant and animal diseases. *Science*, *292*(5525), pp.2285-2289.

Stewart, A.E., Arfin, S.M. and Bradshaw, R.A., 1994. Protein NH2-terminal asparagine deamidase. Isolation and characterization of a new enzyme. *Journal of Biological Chemistry*, *269*(38), pp.23509-23517.

Stöhr, C., Strube, F., Marx, G., Ullrich, W.R. and Rockel, P., 2001. A plasma membrane-bound enzyme of tobacco roots catalyses the formation of nitric oxide from nitrite. *Planta*, *212*, pp.835-841.

Stoimenova, M., Igamberdiev, A.U., Gupta, K.J. and Hill, R.D., 2007. Nitrite-driven anaerobic ATP synthesis in barley and rice root mitochondria. *Planta*, *226*, pp.465-474.

Su, J., Zhang, M., Zhang, L., Sun, T., Liu, Y., Lukowitz, W., Xu, J. and Zhang, S., 2017. Regulation of stomatal immunity by interdependent functions of a pathogen-responsive MPK3/MPK6 cascade and abscisic acid. *The Plant Cell*, *29*(3), pp.526-542.

Subbaiah, C.C. and Sachs, M.M., 2001. Altered patterns of sucrose synthase phosphorylation and localization precede callose induction and root tip death in anoxic maize seedlings. *Plant Physiology*, *125*(2), pp.585-594.

Sugiyama, R. and Hirai, M.Y., 2019. Atypical myrosinase as a mediator of glucosinolate functions in plants. *Frontiers in plant science*, *10*, p.1008.

Sumanta, N., Haque, C.I., Nishika, J. and Suprakash, R., 2014. Spectrophotometric analysis of chlorophylls and carotenoids from commonly grown fern species by using various extracting solvents. *Res J Chem Sci*, *2231*, p.606X.

Sun, L., Qin, J., Wu, X., Zhang, J. and Zhang, J., 2022. TOUCH 3 and CALMODULIN 1/4/6 cooperate with calcium-dependent protein kinases to trigger calcium-dependent activation of CAM-BINDING PROTEIN 60-LIKE G and regulate fungal resistance in plants. *The Plant Cell*, *34*(10), pp.4088-4104.

Sun, T. and Zhang, Y., 2022. MAP kinase cascades in plant development and immune signaling. *EMBO reports*, *23*(2), p.e53817.

Sun, Y., Li, L., Macho, A.P., Han, Z., Hu, Z., Zipfel, C., Zhou, J.M. and Chai, J., 2013. Structural basis for flg22-induced activation of the Arabidopsis FLS2-BAK1 immune complex. *Science*, *342*(6158), pp.624-628.

Suzuki, N., Rivero, R.M., Shulaev, V., Blumwald, E. and Mittler, R., 2014. Abiotic and biotic stress combinations. *New Phytologist*, *203*(1), pp.32-43.

Tada, Y., Spoel, S.H., Pajerowska-Mukhtar, K., Mou, Z., Song, J., Wang, C., Zuo, J. and Dong, X., 2008. Plant immunity requires conformational charges of NPR1 via S-nitrosylation and thioredoxins. *Science*, *321*(5891), pp.952-956.

Tan, Q.W., Lim, P.K., Chen, Z., Pasha, A., Provart, N., Arend, M., Nikoloski, Z. and Mutwil, M., 2023. Cross-stress gene expression atlas of Marchantia polymorpha reveals the hierarchy and regulatory principles of abiotic stress responses. *Nature communications*, *14*(1), p.986.

Tang, H., Bi, H., Liu, B., Lou, S., Song, Y., Tong, S., Chen, N., Jiang, Y., Liu, J. and Liu, H., 2021. WRKY33 interacts with WRKY12 protein to up-regulate RAP2. 2 during submergence induced hypoxia response in Arabidopsis thaliana. *New Phytologist*, *229*(1), pp.106-125.

Tanimoto, K., Makino, Y., Pereira, T. and Poellinger, L., 2000. Mechanism of regulation of the hypoxia-inducible factor-1α by the von Hippel-Lindau tumor suppressor protein. *The EMBO journal*, *19*(16), pp.4298-4309.

Tasaki, T., Mulder, L.C., Iwamatsu, A., Lee, M.J., Davydov, I.V., Varshavsky, A., Muesing, M. and Kwon, Y.T., 2005. A family of mammalian E3 ubiquitin ligases that contain the UBR box motif and recognize N-degrons. *Molecular and cellular biology*, *25*(16), pp.7120-7136.

Tasaki, T., Zakrzewska, A., Dudgeon, D.D., Jiang, Y., Lazo, J.S. and Kwon, Y.T., 2009. The substrate recognition domains of the N-end rule pathway. *Journal of Biological Chemistry*, *284*(3), pp.1884-1895.

Tavakoli, K., Pour-Aboughadareh, A., Kianersi, F., Poczai, P., Etminan, A. and Shooshtari, L., 2021. Applications of CRISPR-Cas9 as an advanced genome editing system in life sciences. *BioTech*, *10*(3), p.14.

Taylor, C.T. and Colgan, S.P., 2017. Regulation of immunity and inflammation by hypoxia in immunological niches. *Nature Reviews Immunology*, *17*(12), pp.774-785.

Thatcher, L.F., Cevik, V., Grant, M., Zhai, B., Jones, J.D., Manners, J.M. and Kazan, K., 2016. Characterization of a JAZ7 activation-tagged Arabidopsis mutant with increased susceptibility to the fungal pathogen Fusarium oxysporum. *Journal of Experimental Botany*, *67*(8), pp.2367-2386.

Thines, B., Katsir, L., Melotto, M., Niu, Y., Mandaokar, A., Liu, G., Nomura, K., He, S.Y., Howe, G.A. and Browse, J., 2007. JAZ repressor proteins are targets of the SCFCOI1 complex during jasmonate signalling. *Nature*, *448*(7154), pp.661-665.

Thireault, C., Shyu, C., Yoshida, Y., St. Aubin, B., Campos, M.L. and Howe, G.A., 2015. Repression of jasmonate signaling by a non-TIFY JAZ protein in Arabidopsis. *The Plant Journal*, *82*(4), pp.669-679.

Thompson, A.R., Dickinson, R.S., Murphy, F., Thomson, J.P., Marriott, H.M., Tavares, A., Willson, J., Williams, L., Lewis, A., Mirchandani, A. and Dos Santos Coelho, P., 2017. Hypoxia determines survival outcomes of bacterial infection through HIF-1α–dependent reprogramming of leukocyte metabolism. *Science Immunology*, *2*(8), p.eaal2861.

Thor, K., Jiang, S., Michard, E., George, J., Scherzer, S., Huang, S., Dindas, J., Derbyshire, P., Leitão, N., DeFalco, T.A. and Koester, P., 2020. The calcium-permeable channel OSCA1. 3 regulates plant stomatal immunity. *Nature*, *585*(7826), pp.569-573.

Till, C.J., Vicente, J., Zhang, H., Oszvald, M., Deery, M.J., Pastor, V., Lilley, K.S., Ray, R.V., Theodoulou, F.L. and Holdsworth, M.J., 2019. The Arabidopsis thaliana N-recognin E3 ligase PROTEOLYSIS1 influences the immune response. *Plant Direct*, *3*(12), p.e00194.

Timms, R.T., Zhang, Z., Rhee, D.Y., Harper, J.W., Koren, I. and Elledge, S.J., 2019. A glycine-specific N-degron pathway mediates the quality control of protein N-myristoylation. *Science*, *365*(6448), p.eaaw4912.

Tobias, J.W., Shrader, T.E., Rocap, G. and Varshavsky, A., 1991. The N-end rule in bacteria. *Science*, *254*(5036), pp.1374-1377.

Torres, M.A. and Dangl, J.L., 2005. Functions of the respiratory burst oxidase in biotic interactions, abiotic stress and development. *Current opinion in plant biology*, *8*(4), pp.397-403.

Truman, W., Bennett, M.H., Kubigsteltig, I., Turnbull, C. and Grant, M., 2007. Arabidopsis systemic immunity uses conserved defense signaling pathways and is mediated by jasmonates. *Proceedings of the national academy of sciences*, *104*(3), pp.1075-1080.

Ullah, I., Waqas, M., Khan, M.A., Lee, I.J. and Kim, W.C., 2017. Exogenous ascorbic acid mitigates flood stress damages of Vigna angularis. *Applied Biological Chemistry*, *60*, pp.603-614.

Urano, K., Maruyama, K., Jikumaru, Y., Kamiya, Y., Yamaguchi-Shinozaki, K. and Shinozaki, K., 2017. Analysis of plant hormone profiles in response to moderate dehydration stress. *The Plant Journal*, *90*(1), pp.17-36.

Valeri, M.C., Novi, G., Weits, D.A., Mensuali, A., Perata, P. and Loreti, E., 2021. Botrytis cinerea induces local hypoxia in Arabidopsis leaves. *New Phytologist*, *229*(1), pp.173-185.

van Dongen, J.T., Fröhlich, A., Ramírez-Aguilar, S.J., Schauer, N., Fernie, A.R., Erban, A., Kopka, J., Clark, J., Langer, A. and Geigenberger, P., 2009. Transcript and metabolite profiling of the adaptive response to mild decreases in oxygen concentration in the roots of Arabidopsis plants. *Annals of botany*, *103*(2), pp.269-280.

Van, V., Ejimogu, N.E., Bui, T.S. and Smith, A.T., 2022. The structure of Saccharomyces cerevisiae arginyltransferase 1 (ATE1). *Journal of Molecular Biology*, *434*(21), p.167816.

Vanin, A.F., Bevers, L.M., Slama-Schwok, A. and Van Faassen, E.E., 2007. Nitric oxide synthase reduces nitrite to NO under anoxia. *Cellular and Molecular Life Sciences*, *64*, pp.96-103.

Varshavsky, A., 2019. N-degron and C-degron pathways of protein degradation. *Proceedings of the National Academy of Sciences*, *116*(2), pp.358-366.

Varshney, V., Hazra, A., Rao, V., Ghosh, S., Kamble, N.U., Achary, R.K., Gautam, S. and Majee, M., 2023. The Arabidopsis F-box protein SKP1-INTERACTING PARTNER 31 modulates seed maturation and seed vigor by targeting JASMONATE ZIM DOMAIN proteins independently of jasmonic acid-isoleucine. *The Plant Cell*, *35*(10), pp.3712-3738.

Velásquez, A.C., Castroverde, C.D.M. and He, S.Y., 2018. Plant–pathogen warfare under changing climate conditions. *Current biology*, *28*(10), pp.R619-R634.

Verhage, A., Vlaardingerbroek, I., Raaymakers, C., Van Dam, N.M., Dicke, M., Van Wees, S.C. and Pieterse, C.M., 2011. Rewiring of the jasmonate signaling pathway in Arabidopsis during insect herbivory. *Frontiers in plant science*, *2*, p.47.

Vicente, J., Mendiondo, G.M., Pauwels, J., Pastor, V., Izquierdo, Y., Naumann, C., Movahedi, M., Rooney, D., Gibbs, D.J., Smart, K. and Bachmair, A., 2019. Distinct branches of the N-end rule pathway modulate the plant immune response. *New Phytologist*, *221*(2), pp.988-1000.

Vierstra, R.D., 2009. The ubiquitin–26S proteasome system at the nexus of plant biology. *Nature Reviews Molecular Cell Biology*, *10*(6), pp.385-397.

Viswanath, K.K., Varakumar, P., Pamuru, R.R., Basha, S.J., Mehta, S. and Rao, A.D., 2020. Plant lipoxygenases and their role in plant physiology. *Journal of Plant Biology*, *63*, pp.83-95.

Vitor, S.C., Duarte, G.T., Saviani, E.E., Vincentz, M.G., Oliveira, H.C. and Salgado, I., 2013. Nitrate reductase is required for the transcriptional modulation and bactericidal activity of nitric oxide during the defense response of Arabidopsis thaliana against Pseudomonas syringae. *Planta*, *238*, pp.475-486.

Voesenek, L.A. and Bailey-Serres, J., 2015. Flood adaptive traits and processes: an overview. *New Phytologist*, *206*(1), pp.57-73.

Vouillot, L., Thélie, A. and Pollet, N., 2015. Comparison of T7E1 and surveyor mismatch cleavage assays to detect mutations triggered by engineered nucleases. *G3: Genes, Genomes, Genetics*, *5*(3), pp.407-415.

Wadas, B., Piatkov, K.I., Brower, C.S. and Varshavsky, A., 2016. Analyzing N-terminal arginylation through the use of peptide arrays and degradation assays. *Journal of Biological Chemistry*, *291*(40), pp.20976-20992.

Wang, H., Piatkov, K.I., Brower, C.S. and Varshavsky, A., 2009. Glutamine-specific N-terminal amidase, a component of the N-end rule pathway. *Molecular cell*, *34*(6), pp.686-695.

Wang, J., Grubb, L.E., Wang, J., Liang, X., Li, L., Gao, C., Ma, M., Feng, F., Li, M., Li, L. and Zhang, X., 2018b. A regulatory module controlling homeostasis of a plant immune kinase. *Molecular cell*, *69*(3), pp.493-504.

Wang, J., Han, X., Leu, N.A., Sterling, S., Kurosaka, S., Fina, M., Lee, V.M., Dong, D.W., Yates III, J.R. and Kashina, A., 2017b. Protein arginylation targets alpha synuclein, facilitates normal brain health, and prevents neurodegeneration. *Scientific reports*, *7*(1), p.11323.

Wang, J., Han, X., Saha, S., Xu, T., Rai, R., Zhang, F., Wolf, Y.I., Wolfson, A., Yates, J.R. and Kashina, A., 2011. Arginyltransferase is an ATP-independent self-regulating enzyme that forms distinct functional complexes in vivo. *Chemistry & biology*, *18*(1), pp.121-130.

Wang, J., Han, X., Wong, C.C., Cheng, H., Aslanian, A., Xu, T., Leavis, P., Roder, H., Hedstrom, L., Yates, J.R. and Kashina, A., 2014. Arginyltransferase ATE1 catalyzes midchain arginylation of proteins at side chain carboxylates in vivo. *Chemistry & biology*, *21*(3), pp.331-337.

Wang, J., Pejaver, V.R., Dann, G.P., Wolf, M.Y., Kellis, M., Huang, Y., Garcia, B.A., Radivojac, P. and Kashina, A., 2018a. Target site specificity and in vivo complexity of the mammalian arginylome. *Scientific reports*, *8*(1), p.16177.

Wang, X., Hou, S., Wu, Q., Lin, M., Acharya, B.R., Wu, D. and Zhang, W., 2017a. IDL 6-HAE/HSL 2 impacts pectin degradation and resistance to Pseudomonas syringae pv tomato DC 3000 in Arabidopsis leaves. *The Plant Journal*, *89*(2), pp.250-263.

Wang, Z., Orosa-Puente, B., Nomoto, M., Grey, H., Potuschak, T., Matsuura, T., Mori, I.C., Tada, Y., Genschik, P. and Spoel, S.H., 2022. Proteasome-associated ubiquitin ligase relays target plant hormone-specific transcriptional activators. *Science Advances*, *8*(42), p.eabn4466.

Wang, Z., Xia, X., Yang, X., Zhang, X., Liu, Y., Wu, D., Fang, Y., Liu, Y., Xu, J., Qiu, Y. and Zhou, X., 2017c. A picorna-like virus suppresses the N-end rule pathway to inhibit apoptosis. *Elife*, *6*, p.e30590.

Wani, S.H., Anand, S., Singh, B., Bohra, A. and Joshi, R., 2021. WRKY transcription factors and plant defense responses: Latest discoveries and future prospects. *Plant Cell Reports*, *40*, pp.1071-1085.

Wany, A., Gupta, A.K., Brotman, Y., Pandey, S., Vishwakarma, A.P., Kumari, A., Singh, P., Pathak, P.K., Igamberdiev, A.U. and Gupta, K.J., 2018. Nitric oxide is important for sensing and survival under hypoxia in Arabidopsis. *bioRxiv*, p.462218.

Wany, A., Kumari, A. and Gupta, K.J., 2017. Nitric oxide is essential for the development of aerenchyma in wheat roots under hypoxic stress. *Plant, Cell & Environment*, *40*(12), pp.3002-3017.

Wasternack, C. and Song, S., 2017. Jasmonates: biosynthesis, metabolism, and signaling by proteins activating and repressing transcription. *Journal of Experimental Botany*, *68*(6), pp.1303-1321.

Wasternack, C. and Strnad, M., 2019. Jasmonates are signals in the biosynthesis of secondary metabolites—Pathways, transcription factors and applied aspects—A brief review. *New biotechnology*, *48*, pp.1-11.

Weits, D.A., Giuntoli, B., Kosmacz, M., Parlanti, S., Hubberten, H.M., Riegler, H., Hoefgen, R., Perata, P., Van Dongen, J.T. and Licausi, F., 2014. Plant cysteine oxidases control the oxygen-dependent branch of the N-end-rule pathway. *Nature communications*, *5*(1), p.3425.

Weits, D.A., Kunkowska, A.B., Kamps, N.C., Portz, K.M., Packbier, N.K., Nemec Venza, Z., Gaillochet, C., Lohmann, J.U., Pedersen, O., van Dongen, J.T. and Licausi, F., 2019. An apical hypoxic niche sets the pace of shoot meristem activity. *Nature*, *569*(7758), pp.714-717.

White, M.D., Kamps, J.J., East, S., Kearney, L.J.T. and Flashman, E., 2018. The plant cysteine oxidases from Arabidopsis thaliana are kinetically tailored to act as oxygen sensors. *Journal of Biological Chemistry*, *293*(30), pp.11786-11795.

White, M.D., Klecker, M., Hopkinson, R.J., Weits, D.A., Mueller, C., Naumann, C., O'Neill, R., Wickens, J., Yang, J., Brooks-Bartlett, J.C. and Garman, E.F., 2017. Plant cysteine oxidases are dioxygenases that directly enable arginyl transferase-catalysed arginylation of N-end rule targets. *Nature communications*, *8*(1), p.14690.

Withers, J., Yao, J., Mecey, C., Howe, G.A., Melotto, M. and He, S.Y., 2012. Transcription factor-dependent nuclear localization of a transcriptional repressor in jasmonate hormone signaling. *Proceedings of the National Academy of Sciences*, *109*(49), pp.20148-20153.

Wong, C.C.L., Xu, T., Rai, R., Bailey, A.O., Yates 3rd, J.R., Wolf, Y.I., Zebroski, H. and Kashina, A., 2007. Global analysis of posttranslational protein arginylation. *PLoS biology*, *5*(10), p.e258.

Wu, K., Zhang, L., Zhou, C., Yu, C.W. and Chaikam, V., 2008. HDA6 is required for jasmonate response, senescence and flowering in Arabidopsis. *Journal of experimental botany*, *59*(2), pp.225-234.

Xiao, D., Duan, X., Zhang, M., Sun, T., Sun, X., Li, F., Liu, N., Zhang, J., Hou, C. and Wang, D., 2018. Changes in nitric oxide levels and their relationship with callose deposition during the interaction between soybean and Soybean mosaic virus. *Plant Biology*, *20*(2), pp.318-326.

Xu, G., Moeder, W., Yoshioka, K. and Shan, L., 2022. A tale of many families: calcium channels in plant immunity. *The Plant Cell*, *34*(5), pp.1551-1567.

Xu, H., Shi, J., Gao, H., Liu, Y., Yang, Z., Shao, F. and Dong, N., 2019. The N-end rule ubiquitin ligase UBR2 mediates NLRP1B inflammasome activation by anthrax lethal toxin. *The EMBO journal*, *38*(13), p.e101996.

Yan, C., Fan, M., Yang, M., Zhao, J., Zhang, W., Su, Y., Xiao, L., Deng, H. and Xie, D., 2018. Injury activates Ca2+/calmodulin-dependent phosphorylation of JAV1-JAZ8-WRKY51 complex for jasmonate biosynthesis. *Molecular Cell*, *70*(1), pp.136-149.

Yoon, S.I., Kurnasov, O., Natarajan, V., Hong, M., Gudkov, A.V., Osterman, A.L. and Wilson, I.A., 2012. Structural basis of TLR5-flagellin recognition and signaling. *Science*, *335*(6070), pp.859-864.

Yoshida, S., Ito, M., Callis, J., Nishida, I. and Watanabe, A., 2002. A delayed leaf senescence mutant is defective in arginyl-tRNA: protein arginyltransferase, a component of the N-end rule pathway in Arabidopsis. *The Plant Journal*, *32*(1), pp.129-137.

Yu, J., Zhang, Y., Di, C., Zhang, Q., Zhang, K., Wang, C., You, Q., Yan, H., Dai, S.Y., Yuan, J.S. and Xu, W., 2016. JAZ7 negatively regulates dark-induced leaf senescence in Arabidopsis. *Journal of experimental botany*, *67*(3), pp.751-762.

Yu, M., Lamattina, L., Spoel, S.H. and Loake, G.J., 2014. Nitric oxide function in plant biology: a redox cue in deconvolution. *New phytologist*, *202*(4), pp.1142-1156.

Yuan, L.B., Dai, Y.S., Xie, L.J., Yu, L.J., Zhou, Y., Lai, Y.X., Yang, Y.C., Xu, L., Chen, Q.F. and Xiao, S., 2017. Jasmonate regulates plant responses to postsubmergence reoxygenation through transcriptional activation of antioxidant synthesis. *Plant Physiology*, *173*(3), pp.1864-1880.

Yuan, M., Jiang, Z., Bi, G., Nomura, K., Liu, M., Wang, Y., Cai, B., Zhou, J.M., He, S.Y. and Xin, X.F., 2021. Pattern-recognition receptors are required for NLR-mediated plant immunity. *Nature*, *592*(7852), pp.105-109.

Yun, B.W., Feechan, A., Yin, M., Saidi, N.B., Le Bihan, T., Yu, M., Moore, J.W., Kang, J.G., Kwon, E., Spoel, S.H. and Pallas, J.A., 2011. S-nitrosylation of NADPH oxidase regulates cell death in plant immunity. *Nature*, *478*(7368), pp.264-268.

Zandalinas, S.I., Fritschi, F.B. and Mittler, R., 2020. Signal transduction networks during stress combination. *Journal of Experimental Botany*, *71*(5), pp.1734-1741.

Zandalinas, S.I., Sengupta, S., Fritschi, F.B., Azad, R.K., Nechushtai, R. and Mittler, R., 2021. The impact of multifactorial stress combination on plant growth and survival. *New Phytologist*, *230*(3), pp.1034-1048.

Zander, M., Lewsey, M.G., Clark, N.M., Yin, L., Bartlett, A., Saldierna Guzmán, J.P., Hann, E., Langford, A.E., Jow, B., Wise, A. and Nery, J.R., 2020. Integrated multi-omics framework of the plant response to jasmonic acid. *Nature plants*, *6*(3), pp.290-302.

Zarban, R., Vogler, M., Wong, A., Eppinger, J., Al-Babili, S. and Gehring, C., 2019. Discovery of a nitric oxide-responsive protein in Arabidopsis thaliana. *Molecules*, *24*(15), p.2691.

Zhai, Q. and Li, C., 2019. The plant Mediator complex and its role in jasmonate signaling. *Journal of Experimental Botany*, *70*(13), pp.3415-3424.

Zhan, N., Wang, C., Chen, L., Yang, H., Feng, J., Gong, X., Ren, B., Wu, R., Mu, J., Li, Y. and Liu, Z., 2018. S-nitrosylation targets GSNO reductase for selective autophagy during hypoxia responses in plants. *Molecular cell*, *71*(1), pp.142-154.

Zhang, H. and Sonnewald, U., 2017. Differences and commonalities of plant responses to single and combined stresses. *The Plant Journal*, *90*(5), pp.839-855.

Zhang, H., Rundle, C., Winter, N., Miricescu, A., Mooney, B.C., Bachmair, A., Graciet, E. and Theodoulou, F.L., 2023. BIG participates in the Arg/N-degron pathways and the hypoxia response in Arabidopsis thaliana. *bioRxiv*, pp.2023-05.

Zhang, M. and Zhang, S., 2022. Mitogen-activated protein kinase cascades in plant signaling. *Journal of integrative plant biology*, *64*(2), pp.301-341.

Zhang, X., Wu, Q., Cui, S., Ren, J., Qian, W., Yang, Y., He, S., Chu, J., Sun, X., Yan, C. and Yu, X., 2015. Hijacking of the jasmonate pathway by the mycotoxin fumonisin B1 (FB1) to initiate programmed cell death in Arabidopsis is modulated by RGLG3 and RGLG4. *Journal of experimental botany*, *66*(9), pp.2709-2721.

Zhang, X., Wu, Q., Ren, J., Qian, W., He, S., Huang, K., Yu, X., Gao, Y., Huang, P. and An, C., 2012. Two novel RING-type ubiquitin ligases, RGLG3 and RGLG4, are essential for jasmonate-mediated responses in Arabidopsis. *Plant physiology*, *160*(2), pp.808-822.

Zhao, C., Cai, S., Wang, Y. and Chen, Z.H., 2016. Loss of nitrate reductases NIA1 and NIA2 impairs stomatal closure by altering genes of core ABA signaling components in Arabidopsis. *Plant Signaling & Behavior*, *11*(6), pp.1456-69.

Zhao, Y., Wei, T., Yin, K.Q., Chen, Z., Gu, H., Qu, L.J. and Qin, G., 2012. Arabidopsis RAP2. 2 plays an important role in plant resistance to Botrytis cinerea and ethylene responses. *New Phytologist*, *195*(2), pp.450-460.

Zhong, Z., Li, Z., Yang, J. and Wang, Q., 2023. Unified Model to Predict gRNA Efficiency across Diverse Cell Lines and CRISPR-Cas9 Systems. *Journal of Chemical Information and Modeling*, *63*(23), pp.7320-7329.

Zhou, J., Mu, Q., Wang, X., Zhang, J., Yu, H., Huang, T., He, Y., Dai, S. and Meng, X., 2022. Multilayered synergistic regulation of phytoalexin biosynthesis by ethylene, jasmonate, and MAPK signaling pathways in Arabidopsis. *The Plant Cell*, *34*(8), pp.3066-3087.

Zhou, J., Wang, X., He, Y., Sang, T., Wang, P., Dai, S., Zhang, S. and Meng, X., 2020. Differential phosphorylation of the transcription factor WRKY33 by the protein kinases CPK5/CPK6 and MPK3/MPK6 cooperatively regulates camalexin biosynthesis in Arabidopsis. *Plant Cell*, *32*(8), pp.2621-2638.

Zhu, Z., 2014. Molecular basis for jasmonate and ethylene signal interactions in Arabidopsis. *Journal of Experimental Botany*, *65*(20), pp.5743-5748.

Zhu, Z., An, F., Feng, Y., Li, P., Xue, L., Jiang, Z., Kim, J.M., To, T.K., Li, W., Zhang, X. and Yu, Q., 2011. Derepression of ethylene-stabilized transcription factors (EIN3/EIL1) mediates jasmonate and ethylene signaling synergy in Arabidopsis. *Proceedings of the National Academy of Sciences*, *108*(30), pp.12539-12544.

Zuin, A., Isasa, M. and Crosas, B., 2014. Ubiquitin signaling: extreme conservation as a source of diversity. *Cells*, *3*(3), pp.690-701.

Appendix A: Supplementary Figures

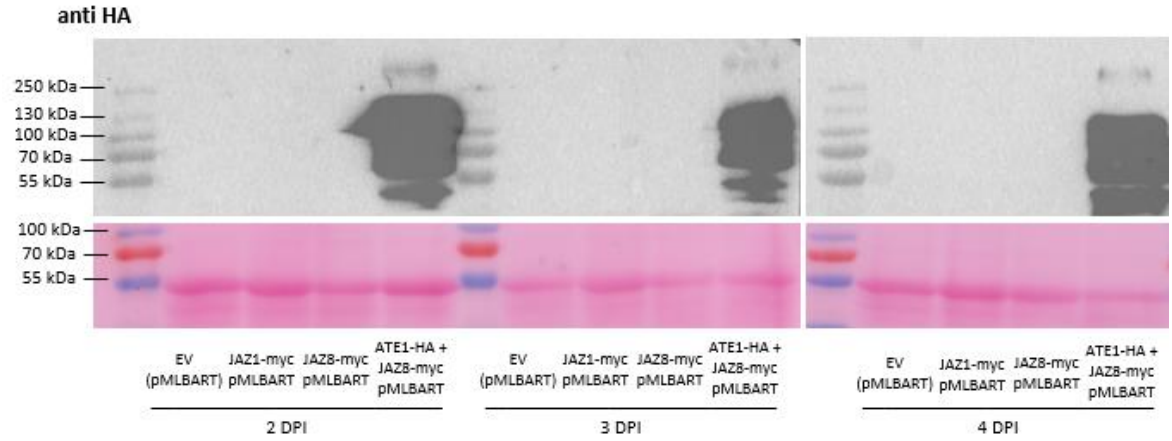

Figure A1. Longer exposure of anti-HA immunoblots from Figure 4.6 showing ATE1 higher molecular weight band.

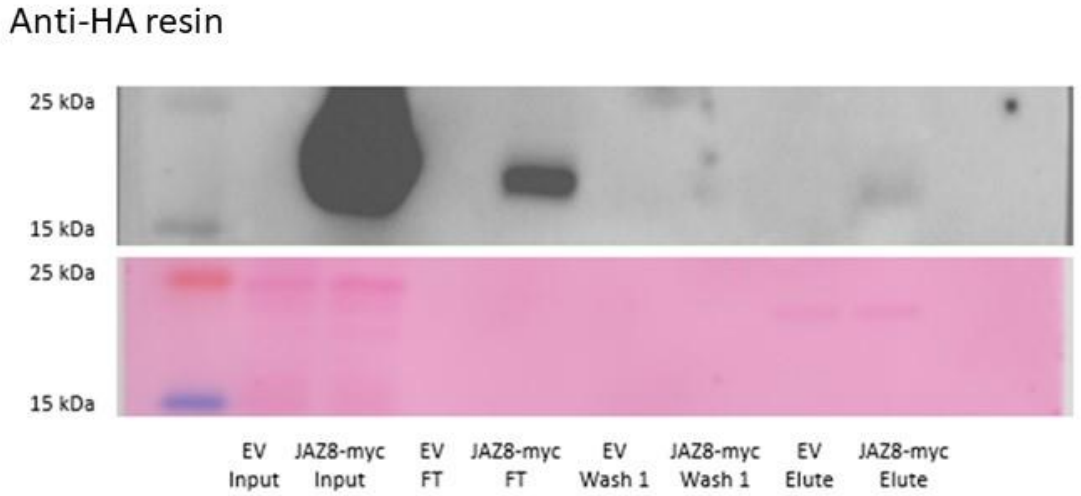

Figure A2. Co-IP control. EV and JAZ8-MYC nuclei extracted proteins IP'd using anti-HA resin and immunoblot analysis done using anti-MYC antibody.

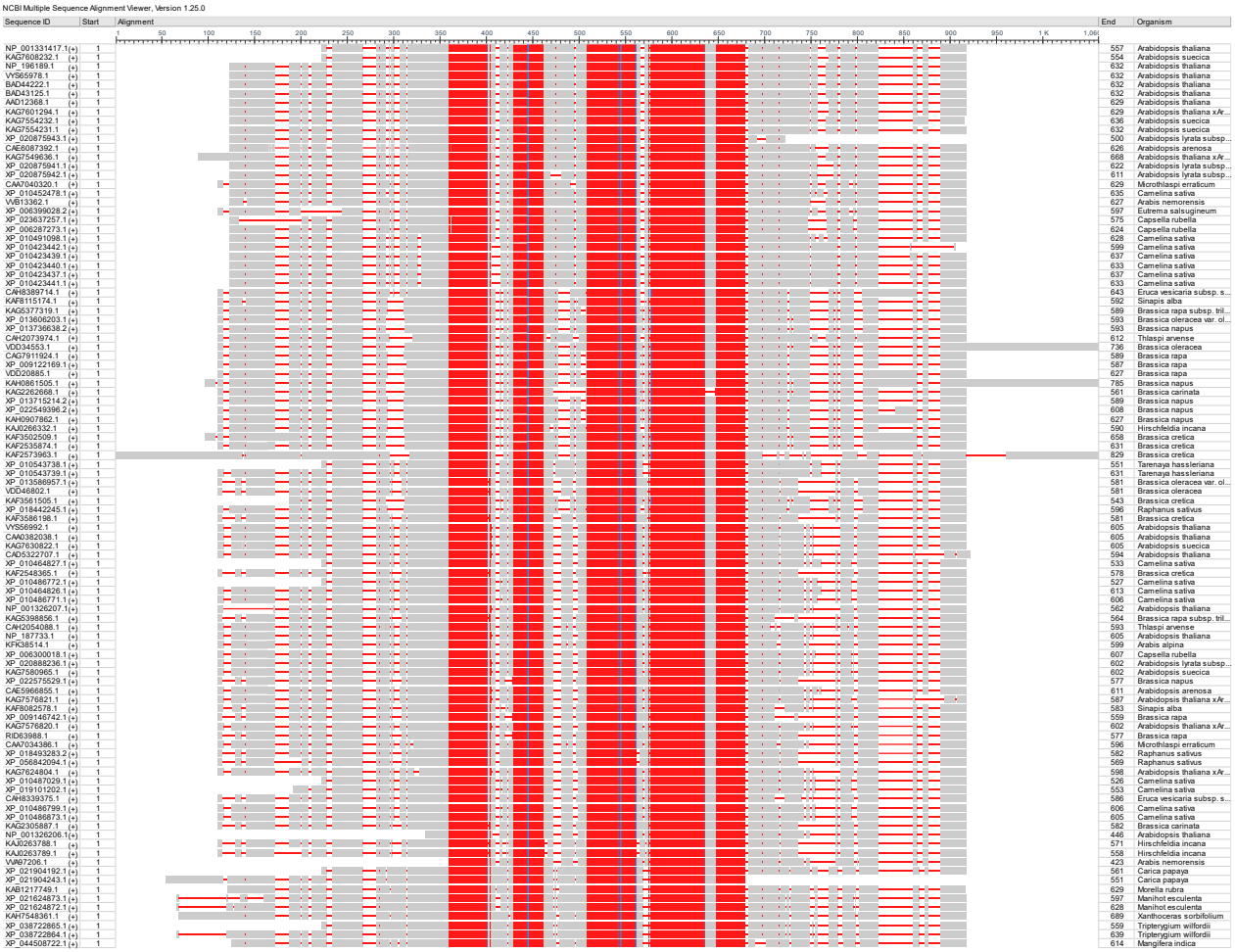

Figure A3. Blastp results for AtATE1 125-303 amino acid sequence.

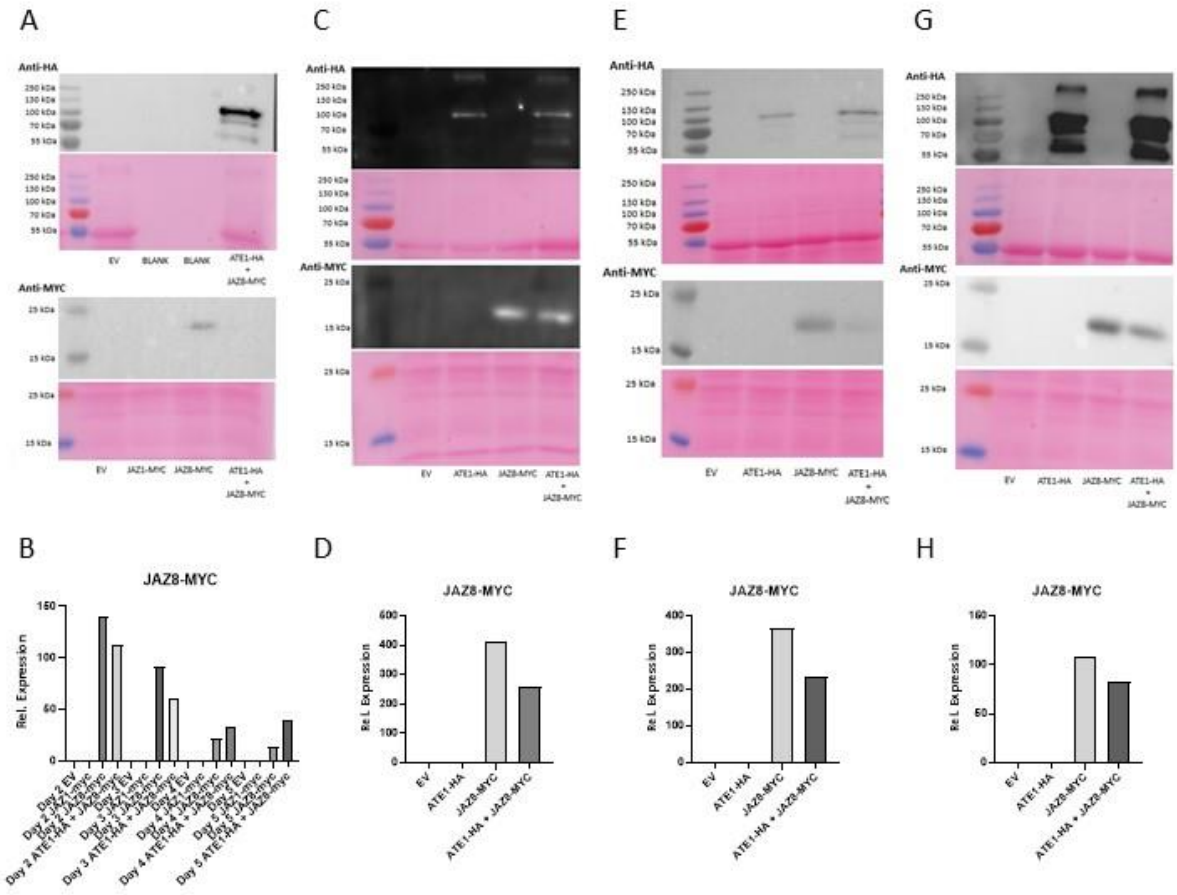

Figure A4. Replicates for ATE1-mediated JAZ8 destabilization. A. At 5 days after agroinfiltration, leaf tissue was collected, proteins were extracted in SDS loading buffer, amido black protein quantification was performed and 30 µg of protein was loaded per well. Expected molecular weights (MW): ATE1-HA = 78.1 kDa; JAZ8-myc = 16 kDa; JAZ1-myc = 28.8 kDa. Results are representative of 1 biological replicate. B. RT-qPCR using same tissue as Figure 4.6 and B. C. E. and G. are immunoblots of proteins extracted from N. benthamiana leaves 2 days after agroinfiltration with ATE1-HA, JAZ8-MYC or the combination, with EV as a control. Proteins were extracted in SDS loading buffer, quantified using amido black, and 30 µg of protein was loaded per well. D. F. and H. is the gene expression level of JAZ8-MYC using the same tissue as B., C., and G., respectively.

Appendix B: Supplementary Tables

Table B1. Gene list for DEGs in corresponding to overlap (Figure 4.17A). Common genes differentially expressed in RNA-Seq datasets from Hickman et al., 2017 and Lee and Bailey-Serres, 2019 which treated Arabidopsis plants to MeJA and hypoxia, respectively. Included in table is Gene ID, Gene Symbol, Protein name, the log2 fold change of DEGs in overlap after 2 hours of MeJA treatment and log 2-fold change of DEGs in overlap after 2 hours of hypoxia treatment.

Gene ID	Gene Symbol	Protein name	log2FC(Hickman 2h MeJA)	log2FC(Lee 2h hypoxia)
828271	MSRB7	methionine sulfoxide reductase B7	7.7281	1.911829
843997	AT1G76640	Calcium-binding EF-hand family protein	7.2934	6.962755
822506	CYP81D11	Cytochrome P450 superfamily protein	5.6204	1.906755
832031	AT5G19110	Eukaryotic aspartyl protease family protein	5.0669	2.868664
829091	AT4G29700	Alkaline-phosphatase-like family protein	4.3897	-1.45843
828460	CORI3	Tyrosine transaminase family protein	3.8006	1.995246
819093	ERF13	ethylene-responsive element binding factor 13	3.5625	2.999176
836797	AT5G66650	calcium uniporter (DUF607)	3.3606	2.495101
821055	JAZ3	jasmonate-zim-domain protein 3	3.3047	2.445207
829383	AT4G32480	sugar phosphate exchanger, putative (DUF506)	3.1634	4.048953
819407	AT2G47950	myelin transcription factor-like protein	3.0711	3.964751
827663	CYP707A1	cytochrome P450, family 707, subfamily A, polypeptide 1	3.0516	2.351982
841843	AT1G54050	HSP20-like chaperones superfamily protein	2.668	2.307615
834110	GDPD2	PLC-like phosphodiesterases superfamily protein	2.4874	2.803586
818640	AT2G40460	Major facilitator superfamily protein	2.4282	-1.53729
822453	AT3G28270	transmembrane protein, putative (DUF677)	2.3803	-2.01943
828683	AT4G25780	CAP (Cysteine-rich secretory proteins, Antigen 5, and Pathogenesis-related 1 protein) superfamily protein	2.3709	-2.35056
836690	bHLH093	beta HLH protein 93	2.3268	1.830298
836210	MYB34	myb domain protein 34	2.2971	-1.71078
839218	EXPA10	expansin A10	2.1944	1.934007
838639	OPCL1	OPC-8:0 CoA ligase1	2.1584	1.495962
838361	AT1G17830	hypothetical protein (DUF789)	2.0609	2.05716
835100	AT5G50335	hypothetical protein AT5G50335	2.0103	-2.34279
829277	CYP83B1	cytochrome P450, family 83, subfamily B, polypeptide 1	1.9536	-1.67637
820155	MDHAR	monodehydroascorbate reductase	1.9044	1.834462
831903	DIP2	E3 ubiquitin-protein ligase	1.8578	3.46114
836547	EXL2	EXORDIUM like 2	1.8504	1.143177

823498	AT3G43850	hypothetical protein AT3G43850	1.7953	2.725857
824168	MYB77	myb domain protein 77	1.7778	2.363554
825220	AT3G60490	Integrase-type DNA-binding superfamily protein	1.7531	1.763026
837701	PMEPCRA	methylesterase PCR A	1.7518	1.582221
836114	ULI3	Cysteine/Histidine-rich C1 domain family protein	1.6819	-1.42791
830003	STY46	ACT-like protein tyrosine kinase family protein	1.6567	1.320731
827912	GT72B1	UDP-Glycosyltransferase superfamily protein	1.6514	-1.33661
829644	AT4G34920	PLC-like phosphodiesterases superfamily protein	1.6035	-1.29541
818333	SLT1	HSP20-like chaperones superfamily protein	1.6007	-0.99803
821495	ZF2	zinc-finger protein 2	1.5716	1.968049
841228	AT1G48100	Pectin lyase-like superfamily protein	1.4946	3.51437
819103	AT2G44940	Integrase-type DNA-binding superfamily protein	1.4946	1.060583
825048	GAUT15	galacturonosyltransferase 15	1.4937	1.237291
837551	AT1G10140	Uncharacterized conserved protein UCP031279	1.4734	2.748346
819674	GID1A	alpha/beta-Hydrolases superfamily protein	1.4274	1.060531
839883	GA2OX2	gibberellin 2-oxidase	1.413	1.723497
839760	AT1G28600	GDSL-like Lipase/Acylhydrolase superfamily protein	1.3732	-1.0709
821826	AT3G22550	NAD(P)H-quinone oxidoreductase subunit, putative (DUF581)	1.3443	1.822975
827435	SCL13	SCARECROW-like 13	1.3403	1.668314
830466	ATL43	RING/U-box superfamily protein	1.3166	-2.81997
819923	AT3G07350	sulfate/thiosulfate import ATP-binding protein, putative (DUF506)	1.2972	1.817777
816991	AT2G24550	major centromere autoantigen B-like protein	1.2906	1.280173
829096	CKX4	cytokinin oxidase 4	1.2711	2.213141
817084	AT2G25460	EEIG1/EHBP1 protein amino-terminal domain protein	1.27	2.151708
	AT4G36648	#N/A	1.2651	1.258971
843359	TBL27	TRICHOME BIREFRINGENCE-LIKE 27	1.2256	-1.7529
821891	ETR2	Signal transduction histidine kinase, hybrid-type, ethylene sensor	1.2023	2.282818
834225	AT5G42200	RING/U-box superfamily protein	1.15	3.098342
843998	CML38	calmodulin-like 38	1.1421	5.747782
835280	AT5G52050	MATE efflux family protein	1.1409	1.046555
835535	BBX29	B-box type zinc finger family protein	1.0938	3.017535
	AT5G07322	#N/A	1.0637	-1.44966
820790	NAC2	NAC domain containing protein 2	1.0353	1.439804
836645	AT5G65207	hypothetical protein AT5G65207	1.0214	4.673897
819239	CRF5	cytokinin response factor 5	0.99849	-1.64295
830591	ST2B	sulfotransferase 2B	0.9766	-1.33598
822833	ERD5	Methylenetetrahydrofolate reductase family protein	0.97431	1.303902
834465	AT5G44390	FAD-binding Berberine family protein	0.94845	-2.45421

819357	AT2G47440	Tetratricopeptide repeat (TPR)-like superfamily protein	0.92134	-1.90903
836455	AT5G63350	von willebrand factor A domain protein	0.92093	5.487162
825793	APR1	APS reductase 1	0.89769	-1.58601
839030	LGT9	Nucleotide-diphospho-sugar transferases superfamily protein	0.87842	-1.51592
824803	AT3G56360	hypothetical protein AT3G56360	0.83182	1.532601
831219	ZIF1	zinc induced facilitator 1	0.80408	1.345964
835587	PDC2	pyruvate decarboxylase-2	0.79326	3.430078
827834	AT4G20860	FAD-binding Berberine family protein	0.7513	1.130639
828511	AT4G24110	NADP-specific glutamate dehydrogenase	0.69287	4.93738
836343	GT18	glycosyltransferase 18	0.5023	-1.52006
844104	AT1G77680	Ribonuclease II/R family protein	0.48761	-1.06595
829626	ASE2	GLN phosphoribosyl pyrophosphate amidotransferase 2	0.40059	-1.47865
843625	AT1G72940	Toll-Interleukin-Resistance (TIR) domain-containing protein	0.37936	2.804218
843197	AT1G68670	myb-like transcription factor family protein	0.35223	1.519635
832119	AT5G19970	GRAS family transcription factor family protein	0.32514	-1.47395
836007	AT5G58900	Homeodomain-like transcriptional regulator	0.24812	-2.08262
842612	PP2-A11	phloem protein 2-A11	0.23961	3.675254
820531	AT3G13310	Chaperone DnaJ-domain superfamily protein	0.22629	3.606182
827655	NCED4	nine-cis-epoxycarotenoid dioxygenase 4	0.21259	-1.54433
843623	AT1G72920	Toll-Interleukin-Resistance (TIR) domain family protein	0.15613	4.024994
817194	AR781	AR781, pheromone receptor-like protein (DUF1645)	0.061511	2.091393
838069	GAT1_2.1	Class I glutamine amidotransferase-like superfamily protein	-0.00249	4.059392
841214	C/VIF1	cell wall / vacuolar inhibitor of fructosidase 1	-0.01778	1.531014
5008138	RTFL12	ROTUNDIFOLIA like 12	-0.07159	3.986323
822185	CRF11	Integrase-type DNA-binding superfamily protein	-0.13577	-2.00992
817925	CRL1	NAD(P)-binding Rossmann-fold superfamily protein	-0.1784	1.026097
830684	AT5G07900	Mitochondrial transcription termination factor family protein	-0.1933	-1.50686
839196	BGLU40	beta glucosidase 40	-0.21589	1.662093
831852	AT5G03390	hypothetical protein (DUF295)	-0.23041	2.440401
842514	APR2	5\\'adenylylphosphosulfate reductase 2	-0.30921	-1.53789
829760	J11	Chaperone DnaJ-domain superfamily protein	-0.41798	1.139904
838066	AT1G15010	mediator of RNA polymerase II transcription subunit	-0.42549	2.452661
837989	PKS2	phytochrome kinase substrate 2	-0.45185	-1.06461
834815	NF-YB2	nuclear factor Y, subunit B2	-0.46608	-1.24577
818390	AUX1	Transmembrane amino acid transporter family protein	-0.48057	-1.00027
825319	BRH1	brassinosteroid-responsive RING-H2	-0.48784	-1.75425
842933	AT1G66180	Eukaryotic aspartyl protease family protein	-0.48982	1.054769

28721283	AT5G61412	hypothetical protein AT5G61412	-0.49113	2.386357
842786	AMT1;2	ammonium transporter 1;2	-0.50574	-1.22165
824140	PSK4	phytosulfokine 4 precursor	-0.55631	1.615628
814670	PIN4	Auxin efflux carrier family protein	-0.55679	-1.8947
5007959	AT2G43445	F-box and associated interaction domains-containing protein	-0.58068	-2.25729
818708	AT2G41090	Calcium-binding EF-hand family protein	-0.58294	1.316147
825887	RFNR1	root FNR 1	-0.60017	-1.05178
823914	MYB94	myb domain protein 94	-0.61019	-1.39404
842184	AT1G58170	Disease resistance-responsive (dirigent-like protein) family protein	-0.62045	-2.46099
818781	AT2G41820	Leucine-rich repeat protein kinase family protein	-0.63561	-1.07095
822478	AT3G28480	Oxoglutarate/iron-dependent oxygenase	-0.67205	2.197758
836610	AT5G64870	SPFH/Band 7/PHB domain-containing membrane-associated protein family	-0.71122	1.862175
816861	MYB70	myb domain protein 70	-0.71736	-1.42449
817382	ARF10	auxin response factor 10	-0.75523	-1.34542
819584	LTL1	Li-tolerant lipase 1	-0.75665	-1.26719
831078	AT5G12050	rho GTPase-activating protein	-0.78019	-1.413
839044	G6PD3	glucose-6-phosphate dehydrogenase 3	-0.78914	-1.09729
844146	AUF1	F-box family protein	-0.79477	-1.31583
819369	AT2G47560	RING/U-box superfamily protein	-0.81743	3.579371
833900	AT5G39080	HXXXD-type acyl-transferase family protein	-0.85254	-1.86737
832044	AT5G19240	Glycoprotein membrane precursor GPI-anchored	-0.8548	3.041062
831373	HB30	homeobox protein 30	-0.86305	-2.1764
834620	MEE62	Leucine-rich repeat protein kinase family protein	-0.87957	-1.42196
828290	sks4	SKU5 similar 4	-0.88076	-1.35978
843833	AT1G74940	cyclin-dependent kinase, putative (DUF581)	-0.91088	2.061393
838515	AT1G19330	histone deacetylase complex subunit	-0.92431	1.887825
818574	AT2G39870	hypothetical protein AT2G39870	-0.96823	1.123946
817868	RLP27	receptor like protein 27	-0.98089	-1.78598
835924	AT5G58120	Disease resistance protein (TIR-NBS-LRR class) family	-0.98467	2.31456
835537	PBP1	pinoid-binding protein 1	-0.98821	2.30767
837980	AT1G14200	RING/U-box superfamily protein	-1.004	2.152603
842105	AT1G56520	Disease resistance protein (TIR-NBS-LRR class) family	-1.0071	1.641953
819250	AT2G46420	helicase with zinc finger protein	-1.0089	-1.35881
828854	AT4G27450	aluminum induced protein with YGL and LRDR motifs	-1.0124	3.799715
825303	AT3G61310	AT hook motif DNA-binding family protein	-1.0172	1.305362
834502	AT5G44730	Haloacid dehalogenase-like hydrolase (HAD) superfamily protein	-1.0275	2.735084

829563	AT4G34150	Calcium-dependent lipid-binding (CaLB domain) family protein	-1.035	2.900293
835502	AT5G54145	hypothetical protein AT5G54145	-1.0396	-2.69082
837226	MAPKKK13	mitogen-activated protein kinase kinase kinase 13	-1.0439	2.602184
843624	TIR	toll/interleukin-1 receptor-like protein	-1.0514	2.774346
823706	MPK3	mitogen-activated protein kinase 3	-1.0817	2.212546
816382	AT2G18670	RING/U-box superfamily protein	-1.0817	1.692499
843236	ACR4	ACT domain repeat 4	-1.086	1.30399
3767624	AT1G63860	Disease resistance protein (TIR-NBS-LRR class) family	-1.0971	1.716962
819386	GSTF8	glutathione S-transferase phi 8	-1.0977	1.479435
835220	ATTPPA	Haloacid dehalogenase-like hydrolase (HAD) superfamily protein	-1.1186	1.465163
839027	AT1G24145	transmembrane protein	-1.1255	4.275906
817155	HSFA2	heat shock transcription factor A2	-1.1391	2.327659
837714	AT1G11700	senescence regulator (Protein of unknown function, DUF584)	-1.1567	-1.2847
828377	ACR7	ACT domain repeat 7	-1.1731	3.247688
829160	AT4G30370	RING/U-box superfamily protein	-1.201	3.714851
818231	AT2G36580	Pyruvate kinase family protein	-1.2014	1.137854
833752	AT5G37740	Calcium-dependent lipid-binding (CaLB domain) family protein	-1.2078	1.005075
834497	AT5G44680	DNA glycosylase superfamily protein	-1.224	-1.77076
839384	FLA9	FASCICLIN-like arabinoogalactan 9	-1.2548	-1.36414
844153	AT1G78170	E3 ubiquitin-protein ligase	-1.2651	-1.76768
834676	FLS2	Leucine-rich receptor-like protein kinase family protein	-1.2688	-2.03219
826853	MYB55	myb domain protein 55	-1.2792	-2.51217
828834	WES1	Auxin-responsive GH3 family protein	-1.2803	1.169686
816478	ACO1	ACC oxidase 1	-1.2858	3.291321
838136	AT1G15670	Galactose oxidase/kelch repeat superfamily protein	-1.2921	1.249942
837414	ERD6	Major facilitator superfamily protein	-1.295	1.456877
843006	AT1G66880	Protein kinase superfamily protein	-1.3111	2.22801
818701	CAMBP25	calmodulin (CAM)-binding protein of 25 kDa	-1.3132	1.896699
819886	AT3G07010	Pectin lyase-like superfamily protein	-1.341	-1.22507
839223	AT1G26800	RING/U-box superfamily protein	-1.3506	1.783315
831364	AT5G15120	2-aminoethanethiol dioxygenase, putative (DUF1637)	-1.3534	4.519622
832689	AT5G26200	Mitochondrial substrate carrier family protein	-1.3585	1.547055
831134	AT5G12940	Leucine-rich repeat (LRR) family protein	-1.361	1.268202
843568	ERF73	Integrase-type DNA-binding superfamily protein	-1.4025	3.761875
842861	AT1G65490	transmembrane protein	-1.4034	2.062084
820355	SYP121	syntaxin of plants 121	-1.4179	1.51008
829301	GDU1	glutamine dumper 1	-1.4195	1.820461

835560	AT5G54710	Ankyrin repeat family protein	-1.4375	1.213588
843216	RAV2	related to ABI3/VP1 2	-1.4648	1.63473
824981	BZIP61	Basic-leucine zipper (bZIP) transcription factor family protein	-1.4897	-1.41051
818709	TCH3	Calcium-binding EF hand family protein	-1.5411	2.398295
830832	FHL	far-red-elongated hypocotyl1-like protein	-1.5445	3.374077
828524	ACBP3	acyl-CoA-binding domain 3	-1.5576	1.342905
820163	AT3G10020	plant/protein	-1.5742	2.148623
831880	NAK	Protein kinase superfamily protein	-1.5755	1.280887
838380	AT1G18000	Major facilitator superfamily protein	-1.5919	-1.50862
824855	AT3G56880	VQ motif-containing protein	-1.6184	2.105263
832966	AT5G28630	glycine-rich protein	-1.6721	1.671683
816085	MEE14	maternal effect embryo arrest 14	-1.6779	2.26646
828365	CYP706A1	cytochrome P450, family 706, subfamily A, polypeptide 1	-1.68	1.337557
825384	AT3G62110	Pectin lyase-like superfamily protein	-1.7138	-1.1681
839540	AT1G04360	RING/U-box superfamily protein	-1.7702	-1.73719
839819	AT1G29430	SAUR-like auxin-responsive protein family	-1.7852	-3.17195
816209	NAC036	NAC domain containing protein 36	-1.7978	2.200646
829361	IAA29	indole-3-acetic acid inducible 29	-1.8062	-2.91847
834430	CAD1	phytochelatin synthase 1 (PCS1)	-1.8174	1.231852
842280	AT1G59860	HSP20-like chaperones superfamily protein	-1.8296	3.056698
844383	AT1G80440	Galactose oxidase/kelch repeat superfamily protein	-1.8433	1.0365
832137	SPX1	SPX domain-containing protein 1	-1.8493	2.52035
839767	ARAB-1	GDSL-like Lipase/Acylhydrolase superfamily protein	-1.8724	-1.28428
828367	CYP706A2	cytochrome P450, family 706, subfamily A, polypeptide 2	-1.8755	1.351986
830651	AT5G07580	ethylene-responsive transcription factor	-1.9212	1.548067
838916	PIN7	Auxin efflux carrier family protein	-1.9223	-1.80736
28717252	AT1G19840	SAUR-like auxin-responsive protein family	-1.9347	2.428297
817159	AT2G26190	calmodulin-binding family protein	-1.9737	2.791022
821667	BBX32	B-box 32	-1.9792	2.663434
828705	CIL	CCT motif family protein	-2.0034	-1.93698
827487	AT4G17670	senescence-associated family protein (DUF581)	-2.0106	3.271547
819014	ARL	ARGOS-like protein	-2.0516	2.634787
2745848	AT1G64065	Late embryogenesis abundant (LEA) hydroxyproline-rich glycoprotein family	-2.2325	1.518705
	AT3G48650	#N/A	-2.2973	4.177379
828417	CRK10	cysteine-rich RLK (RECEPTOR-like protein kinase) 10	-2.4036	1.559701
834770	ERF5	ethylene responsive element binding factor 5	-2.4213	2.341519
834570	CYP707A3	cytochrome P450, family 707, subfamily A, polypeptide 3	-2.5165	4.238133
818598	AT2G40095	Alpha/beta hydrolase related protein	-2.5348	1.354652
828887	OPT6	oligopeptide transporter 1	-2.5537	1.522814

827463	ERF6	ethylene responsive element binding factor 6	-2.6026	2.710765
839523	MPK11	MAP kinase 11	-2.6772	3.773817
819780	AT3G06070	hypothetical protein AT3G06070	-2.7215	-2.64621
832039	AT5G19190	hypothetical protein AT5G19190	-2.756	-2.06523
835353	AT5G52760	Copper transport protein family	-2.832	2.357173
836349	AT5G62280	DUF1442 family protein (DUF1442)	-2.9206	-1.27946
832801	CNI1	carbon/nitrogen insensitive 1	-2.9761	2.803613
835884	AT5G57760	hypothetical protein AT5G57760	-3.0299	-2.55636
831234	AT5G02760	Protein phosphatase 2C family protein	-3.0437	-1.67319
3770304	AT4G18205	Nucleotide-sugar transporter family protein	-3.0532	1.099825
819045	AT2G44380	Cysteine/Histidine-rich C1 domain family protein	-3.1088	1.681868
816103	HB1	hemoglobin 1	-3.1664	2.18458
818626	PYL6	PYR1-like 6	-3.2036	-2.22133
2745837	AT1G59865	transmembrane protein	-3.3155	6.883983
818241	AT2G36690	2-oxoglutarate (2OG) and Fe(II)-dependent oxygenase superfamily protein	-3.407	2.470061
838438	MYB51	myb domain protein 51	-3.4765	1.280862
819044	AT2G44370	Cysteine/Histidine-rich C1 domain family protein	-3.627	2.139785
839180	AT1G26380	FAD-binding Berberine family protein	-3.7237	-3.26117
832147	DIN10	Raffinose synthase family protein	-3.8913	1.347864
843719	BEE3	BR enhanced expression 3	-4.1993	-2.80979
818656	EXPA8	expansin A8	-4.4172	-1.4092